MINERAL DIAGENESIS AND POROSITY EVOLUTION IN

THE HIBERNIA OIL FIELD,

JURASSIC-CRETACEOUS JEANNE D'ARC RIFT GRABEN,

EASTERN GRAND BANKS OF NEWFOUNDLAND, CANADA

by

Iftikhar A. Abid

Department of Geological Sciences

McGill University, Montreal

Quebec, Canada

A thesis submitted to the

Faculty of Graduate Studies and Research

in partial fulfillment of the requirements

for the degree of Master of Science

© 1988, I. A. Abid

Mineral diagenesis and porosity evolution, Hibernia field, Grand Banks

ABSTRACT

Reservoir sandstones and interbedded shales of the Hibernia Oil Field (1000 to 5000 m subsurface depths) were investigated to evaluate the effects of burial diagenesis on reservoir porosity with increasing depth.

Major early to later diagenetic sequences in sandstones are summarized as: thin chlorite rims, siderite, quartz, early pyrite, early ferroan calcite, quartz, dissolution (dominantly of calcite) and generation of secondary porosity, minor grain fracturing, late ferroan calcite/late ferroan dolomite, late quartz, kaolinite, late pyrite and migration of hydrocarbons. Late ferroan dolomite with curved cleavages and sweeping extinction resembles saddle dolomite (common in carbonates) and has not previously been reported from sandstones. The increase in illite, the decrease in kaolinite, the decrease in the percent of smectite in mixed-layers I/S, and the disappearance of discrete smectite with depth are important mineralogical changes observed in shales of the Hibernia and West Ben Nevis fields. The distribution of calcite cements, quartz overgrowths and late ferroan dolomite, and secondary porosity suggests a significant influence of interbedded shales on sandstone diagenesis.

Porosity in the fine-grained, loosely packed diagenetically immature Hauterivian-Albian Avalon Sandstone (2100-2660 m) is mainly primary. The fraction of the total porosity which is secondary in origin increases gradually with depth from 20% in the Avalon Sandstone to >80% in the diagenetically mature

Tithonian Hibernia Sandstone (3480-4100 m). Aggressive pore fluids required for dissolution are inferred (though unproven) to have been provided by multiple complex reactions in organic-matter rich Kimmeridgian shales and shales interbedded in the reservoir sandstones of the Jeanne d' Arc Basin.

RÉSUMÉ

Les grès réservoirs et les schistes argileux interlités du champ Hibernia (de 1,000 à 5,000 m de profondeur en subsurface) furent utilisés pour évaluer les effets de la diagénèse, lors de l'enfouissement, sur la porosité de la roche réservoir et ce en fonction de la profondeur.

Les séquences majeures de la diagénèse précoce et de la diagénèse tardive dans les grès se résument à: de minces couches de chlorite, sidérite, quartz, pyrite précoce, calcite ferrifère précoce, dissolution (surtout la calcite), et la formation d'une porosité secondaire, fracturation mineure des grains, calcite ferrifère/dolomite ferrifère tardives, quartz tardif, kaolinite, pyrite tardive et la migration d'hydrocarbures. La dolomite ferrifère tardive a des clivages recourbés et une extinction ondulante qui ressemblent à ceux de la dolomite en forme de selle (commune dans les carbonates) mais qui n'a jamais été décrite précedemment dans les grès. L'augmentation en illite, les diminutions en kaolinite et du pourcentage en smectite des feuillets mixtes I/S, ainsi que la disparition de la smectite individuelle avec la profondeur sont autant de modifications minéralogiques importantes qui sont observées dans les shales des champs Hibernia et West Ben Nevis. La distribution des ciments de calcite, de quartz d'épitaxie et de dolomite ferrifère tardive, et d'une porosité secondaire suggèrent que les schistes argileux interlités ont eu une influence significative lors de la diagénèse des grès.

La porosité du grès Avalon (2,100-2,600 m), d'âge Hauteri-

iv

vien-Albien, à grains fins et immature, peu consolidé lors de la diagénèse, est en majeure partie d'origine primaire. La fraction de la porosité totale qui est d'origine secondaire augmente graduellement avec la profondeur, de 20 % dans le grès Avalon jusqu'à plus de 80 % dans le grès Hibernia (3,480-4,100 m), d'âge Tithonien, devenu mature lors de la diagénèse. Il est considéré qu'une dissolution par des fluides acides dans les pores de la roche est requise (quoique non-prouvée) et fut provoquée par des réactions complexes et multiples dans les schistes argileux Kimméridgien riches en matières organiques et dans les schistes argileux interlités avec les grès réservoirs du bassin Jeanne d'Arc.

TABLE OF CONTENTS

LIST OF ILLUSTRATION

FIGURES

PLATES

TABLES

ACKNOWLEDGEMENTS

CHAPTER I

INTRODUCTION

The Hibernia Oil Field is located in the Jeanne d'Arc Basin of the eastern Grand Banks, 315 km east of St. John's, Newfoundland, Canada (Fig. 1.1). It was the first major oil discovery in 1979 after more than a decade of exploration along the Canadian East Coast. A preliminary estimate indicates that there are more than 1.8 billion barrels of recoverable oil and 1.6 trillion cubic feet of associated natural gas in the Hibernia and adjacent oil fields (Meneley, 1986). The entrapment of hydrocarbons occurred in a rollover anticline confined to the western periphery of the northern Jeanne d'Arc Basin. Reservoir rocks are mainly Lower Cretaceous fine to medium grained quartz-rich sandstones of the Missisauga Formation. The organic-matter rich Kimmeridgian shales (with up to 8 wt % total organic carbon content) of the Mic Mac Formation are mature enough at their present burial depth (>4000 m) to be the main source for hydrocarbons in the Hibernia field (Creaney and Allison, 1987).

1.1   OBJECTIVES

Sandstones are the main reservoir rocks for hydrocarbons in the Hibernia field. Reservoir quality (porosity and permeability) of deeply buried sandstones are quite variable because of differences in compaction, cementation,

1

and dissolution processes. An understanding of the nature and extent of these processes is necessary to predict reservoir quality and production potential. The major objectives of this investigation are to:

(1) determine the mineralogical composition of sandstones in different reservoir zones;

(2) describe and quantify .authigenic sandstone minerals and to establish paragenetic sequences;

(3) document the mineralogy of interbedded shales ˊ and assess the effect of burial on shale diagenesis;

(4) present results of a detailed petrographic study of porosity development and distribution in the Hibernia field including quantitative estimates and textural characteristics of the different porosity types, and their relationship to compaction, cementation, and dissolution processes with increasing burial depth;

(5) determine the possible role of shale diagenesis for precipitation and dissolution of sandstone minerals, both framework grains and cements, and to trace the sources of the cements.

1.2 METHODS OF STUDY

About 450 m of drill-core (Fig. 1.2 and 1.3) from 5 wells of the Hibernia Field (B-O8, B-27, O-35, K-18, and C-96; ranging from 1700 to 4500 m) were examined during the summers of 1985 and 1986 at Mobil's Core Storage Centre in Calgary and at Canadian Oil and Gas Land Administration's (COGLA'S) Core Storage in Dartmouth, Halifax. All cores were
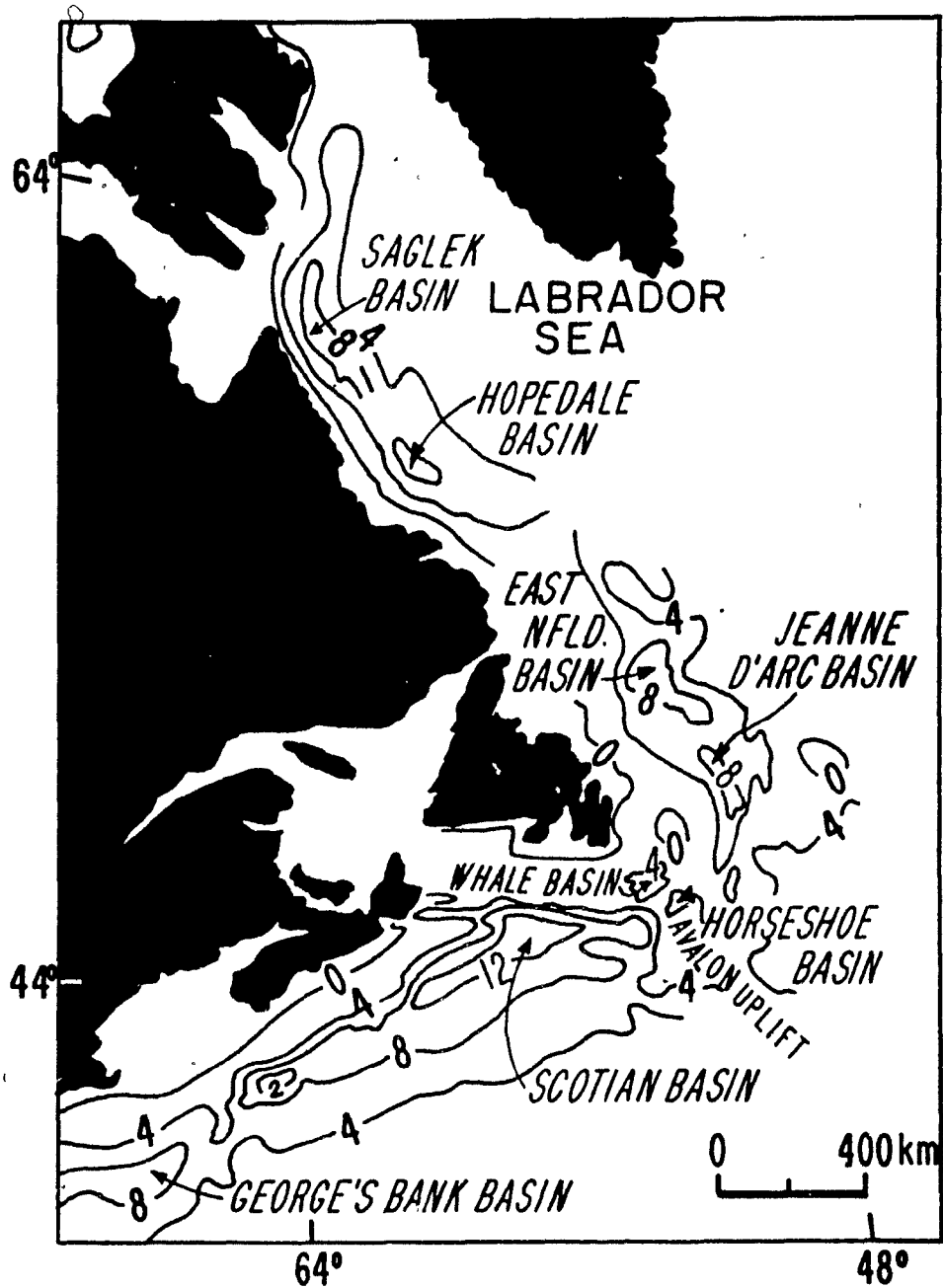
Fig. 1.1 Mesozoic-Cenozoic sedimentary basins along the Canadian
East Coast (from Grant et al., 1986).
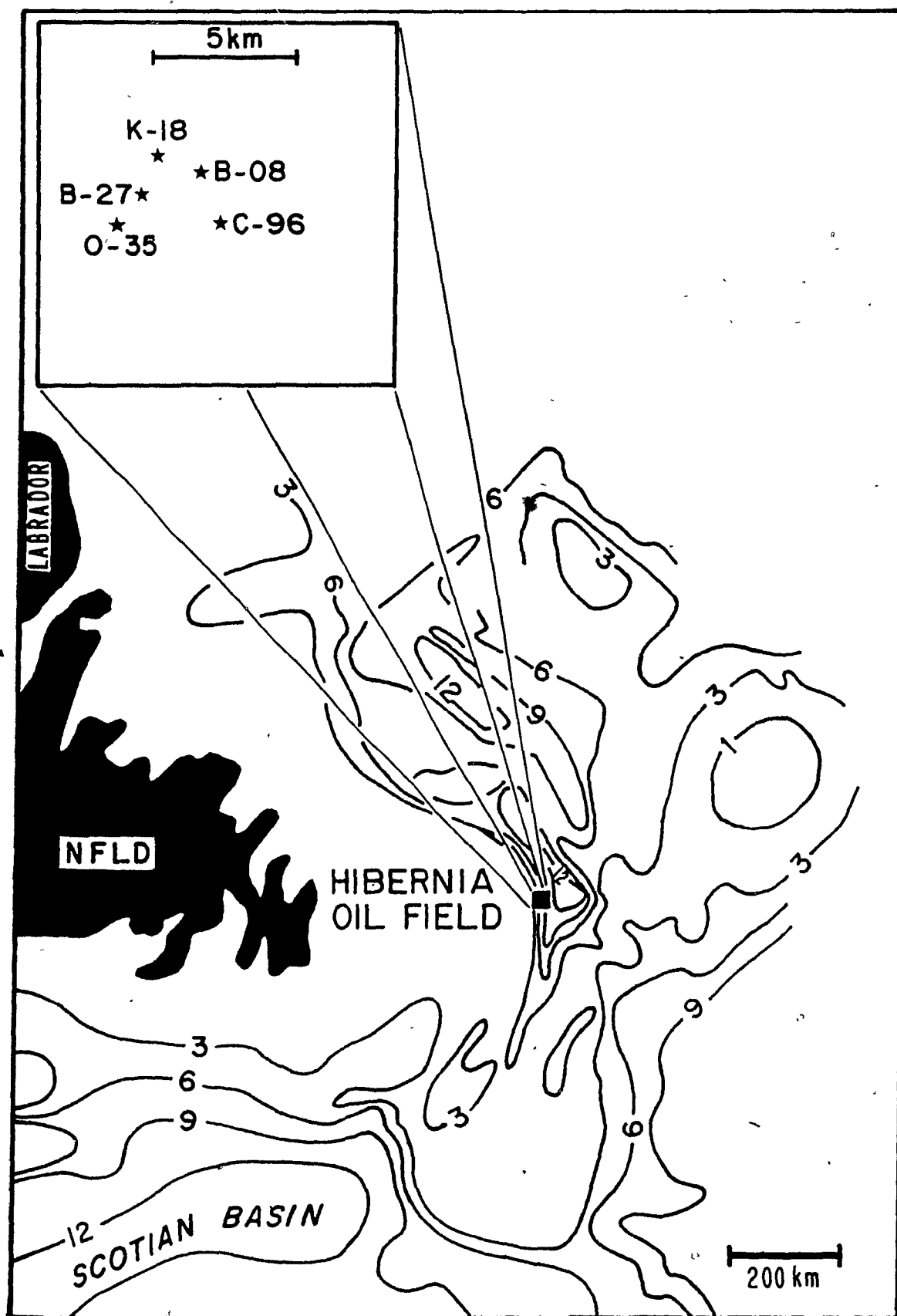
Fig. 1.2 Location of the Hibernia Oil Field and the different
wells studied.   Contours: depths to basement in kilometres
(after Geol. Survey Canada, 1977).

4

logged, recording bed thickness, sedimentary structures, occurrence of fossils, calcite-rich zones, dissolution features, and sample locations (Appendix 1).

More than 70 sandstone and 20 shale core samples were collected at selected locations. Fourty well-cutting shale samples were also collected from the B-08 and B-27 (Hibernia), and B-75 (West Ben Nevis) wells. Samples are numbered by subsurface depth. Carbonate-rich sandstone zones which alternate with porous zones were sampled more closely. All sandstone samples were impregnated with blue-dyed epoxy prior to the preparation of uncovered thin sections. Impregnation with blue-dyed epoxy is the standard method now applied in the oil industry and elswhere for easy recognition and classification of pore spaces. Thin sections were subsequently stained for carbonates (calcite, ferroan-calcite, dolomite, and ferroan-dolomite). Part of each thin section was stained with a mixture of Alizarin-Red and K-ferricyanide and the rest with Alizarin-Red only, following the procedure outlined by Dickson (1965). In addition, numerous stained thin sections were made available for study by Mobil Oil, Toronto. Textural relationships observed under the microscope were used to establish paragenetic sequences of cementing minerals. Criteria of Schmidt and McDonald (1979b), Shanmugam (1985), and Burley and Kantorowicz (1986) were applied to differentiate primary from secondary porosity. On average five hundred points were counted per thin section and secondary pores were classified into different genetic classes.

Fig. 1.3 Simplified lithology in different studied wells from the Hibernia Oil Field. Well-core intervals available for this study are also indicated (modified after Canadian Oil and Gas Land Administration's unpubl. data).
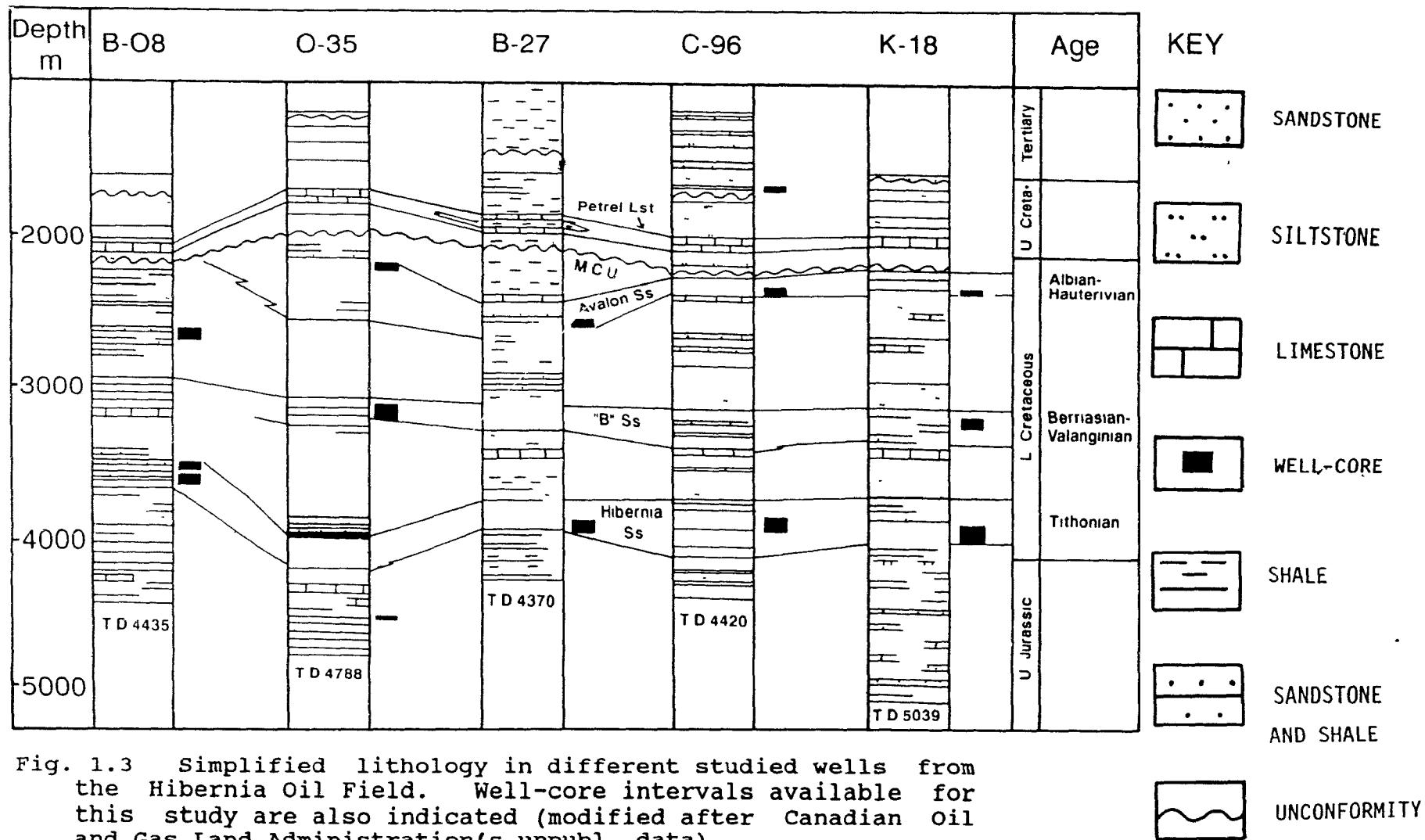
About 40 well-cutting shale samples from three wells (B-08, B-27, Hibernia; and B-75, West Ben Nevis), spanning a subsurface depth from 1000 to 4500 m were analysed by X-ray diffractometry (XRD). Twenty sandstone samples were examined under a JSM-T300 scanning electron microscope (SEM) with an energy dispersive spectrometer (EDS). Disintegrated and ultrasonically cleaned quartz grains from 8 samples were also studied under the SEM. Twenty three shale samples were analysed for total carbon and organic carbon content with a Leco gravimetry method. Twenty-four sandstone samples were analyzed for carbon and oxygen isotopes using a microsampling technique (analyses performed by D. Dettman at the University of Michigan).

1.3 PREVIOUS WORK

Hydrocarbon exploration along the East Coast of Canada began in 1966 (Amoco Imperial Tors Cove D-52 well). However, apart from small oil shows in wells on Sable Island in 1971, no major oil pool was discovered until 1979. This was mainly due to the limited understanding of the nature and distribution of source rocks, basin configuration, and maturation levels in the different basins. However, during these 12 years of exploration, extensive data sets about the stratigraphy, structure, source rock geochemistry and geodynamic evolution of Canada's East Coast offshore area were acquired (Sherwin, 1973; Amoco and Imperial, 1973; Upshaw et al., 1974; Jansa and Wade, 1975; Williams and

Brideaux, 1975; Jansa et al., 1976; Bujak et al., 1977a,b; Purcell et al., 1979; Swift and Williams, 1980; and Rashid et al., 1980).

The first detailed geological history of the East Coast was published by Sherwin (1973). On the Scotian Shelf stratigraphic nomenclature for Mesozoic and Cenozoic sediments was proposed by McIver (1972). This nomenclature was extended, with little modification, to the Grand Banks by Amoco and Imperial (1973) and Jansa and Wade (1975). Results of organic matter studies (Bujak et al., 1977a,b; Purcell et al., 1979; and Swift and Williams, 1980) indicate that Upper Jurassic shales of the Grand Banks are locally rich in oil-prone organic matter (Type II kerogen) and mature enough to generate hydrocarbons, whereas Jurassic shales of the Scotian Shelf are rich in terrestrial organic matter (Type III kerogen) and are gas-prone at their present burial depths (Powell, 1982). The clay mineralogy of shales was not given due attention during previous maturation studies.

The first paper on the Hibernia discovery in 1979 was published by Arthur et al. (1982). Since then, more than 10 papers have been published covering almost every aspect of the geology of Grand Banks, except burial diagenesis. Six of these papers focus on the Jeanne d' Arc Basin where all major oil discoveries have been made so far.

Benteau and Sheppard (1982), and Handyside and Chipman (1983) worked on petrophysical and reservoir simulation studies in the Hibernia field. Depositional environments of reservoir sandstones are briefly mentioned in these

8

publications. Powell (1985) outlined the implications of paleogeography on the distribution of organic matter in the source rocks of the various basins and explained the paucity of organic matter e.g. in the South Jeanne d' Arc Basin. Creaney and Allison (1987) constructed a maturation map for the Kimmridgian shale in the Jeanne d' Arc Basin. However, their data are based only on 5 wells. Meneley (1986) and Grant et al. (1986) published up-to-date summaries about the petroleum geology of the East Coast of Canada, providing numerous cross-sections through different hydrocarbon-bearing sedimentary basins. The structural and geodynamic evolution of these basins is covered in two recent papers by Tankard and Welsink (1987, and in press).

This short summary of previous work reveals that many aspects of the geology of the Hibernia Oil Field have been studied systematically in the past except the diagenesis of the reservoir rocks and their associated shales. It is the first attempt to document the burial diagenesis in the entire stratigraphic interval of the Hibernia Oil Field which contains oil-bearing reservoir rocks from the Upper Jurassic to the top of the Lower Cretaceous (Fig. 1.3). Clearly, the diagenetic study initiated by the present project has been overdue.

CHAPTER II

GEOLOGICAL SETTING, STRATIGRAPHY AND RESERVOIR ROCKS

2.1   STRUCTURE AND GEOTECTONIC ENVIRONMENT

2.1.1   Grand Banks

The continental margin of Eastern Canada is underlain by a series of north and northeast trending Mesozoic-Cenozoic sedimentary basins (Fig. 1.1). Most of these are graben or half-graben structures initiated during different Mesozoic crustal extension and rifting episodes associated with the opening of the North Atlantic Ocean (McMillian, 1982; Tankard and Welsink, in press).

The Late Triassic rifting along the present east coast of North America extended only up to the present Jeanne d' Arc Basin. This rifting episode was followed by sea-floor spreading (175 Ma, Klitgord and Schouten, 1986) which extended northward up to the south of the Grand Banks, where lateral movement was accommodated along the Newfoundland Fracture Zone (NFZ, Fig. 2.1, from Tankard and Welsink, 1987). In the Grand Banks, however, Late Triassic rifting lasted only about 25 Ma and was aborted without the creation of oceanic crust (Tankard and Welsink, in press). A shift in the spreading centre and plate reorganization occurred during Callovian time (Klitgord and Schouten, 1986) with the onset of renewed extension in the present Jeanne d' Arc Basin. This second phase of rifting lasted for a longer period of time (about

50 Ma), until sea floor spreading separated the Grand Banks from the Galicia Bank of the Iberian Peninsula. Separation of the Iberian Peninsula terminated this episode of rifting (Masson and Miles 1984, 1986). Subsequently, Late Cretaceous extensional tectonics dominated in the Orphan Basin of the northeastern Grand Banks (Fig. 2.1) until the beginning of separation of Labrador from Greenland by Labrador sea-floor spreading 80 my ago (Srivastava, 1978).

Along the East Coast of Canada, different rifting episodes and variable amounts of extension were accommodated by major transform faults which divide the region into different extensional terrains (Fig.2.1). These extensional terrains are characterized by different styles of basin formation and sedimentation (Tankard and Welsink, 1987). Figure 2.1 shows the major structural elements of the Grand Banks. The Newfoundland and Charlie Gibbs Fracture Zones separate the Grand Banks from the Scotian Shelf in the south and the Labrador Shelf in the north. The Grand Banks are further divided into a southern, central, and northeastern zones respectively, by relatively small transfer faults (Fig. 2.1). The amount of extension in the central Grand Banks was twice that in the southern Grand Banks. As a result the basins in the central Grand Banks are considerably deeper. The Jeanne d' Arc Basin, for example, is about 16 km deep. The brittle upper crust in the central Grand Banks failed during the extension process (from the Callovian to the Aptian) along a low angle detachment fault which gently dips to the west (Fig. 2.2). Most normal faults in the brittle

11

Fig. 2.1 Sedimentary basins of the Grand Banks separated from the Scotian and Labrador shelves by the Newfoundland and Charlie Gibbs fracture zones, respectively. Division of the Grand Banks into southern (S), central (C), and northern (N) zones is by first-order transfer (or strike-slip) faults (from Tankard and Welsink, 1987).
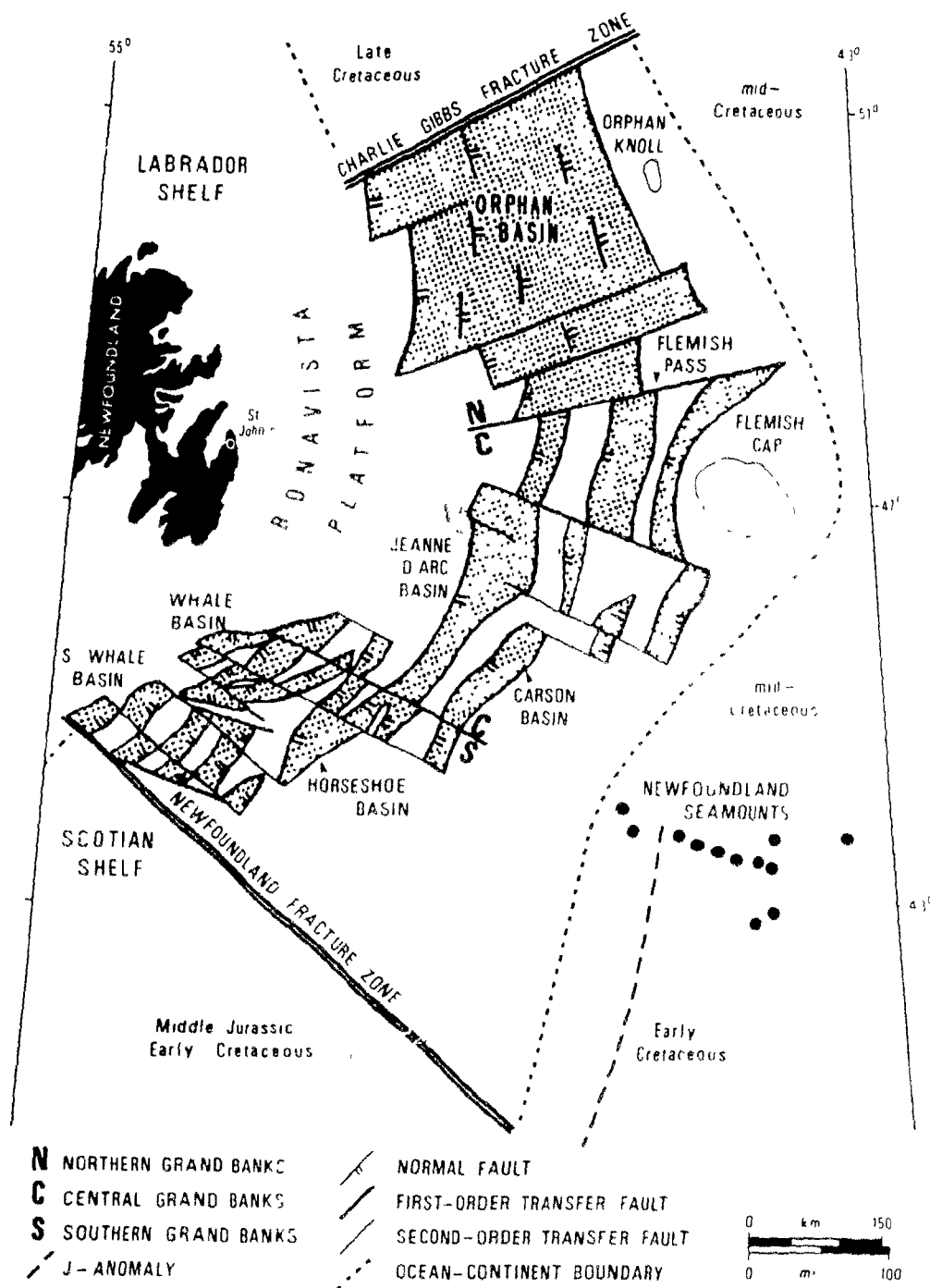
zone terminate along this detachment. Below the Jeanne d' Arc Basin the detachment is inferred to occur at about 26km depth where the Murre Fault soles out into it. Below Flemish Cap, it has risen to 15 to 17 km subsurface depth (Fig. 2.2; Tankard and Welsink, 1987).

The northeast trending basins in the Grand Banks are parallel to the tectono-stratigraphic elements of the Appalachian orogen exposed onshore Newfoundland. It appears that the underlying basement lineaments in the Grand Banks, inherited from Proterozoic and Paleozoic tectonism, have influenced the orientation of Mesozoic rift grabens during the rifting of Pangea (Grant et al., 1986).

2.1.2   The Jeanne d' Arc Basin

The Jeanne d' Arc Basin of the central Grand Banks is a relatively narrow northward plunging trough where all important hydrocarbon discoveries thus far have been made (Fig. 2.3). The present configuration of the basin is the result of two major periods of rifting (Late-Triassic and Callovian to Aptian) and post-rifting thermal subsidence. The western side of the Jeanne d' Arc Basin is mainly bounded by the northeast trending listric-type Murre fault, which strikes parallel to the axis of the basin (Fig. 2.4). The eastern side of the basin is bounded by steep normal faults (Fig. 2.4). These northeast trending basin-boundary faults are intersected by a set of northwest trending oblique transfer faults (Fig. 2.3). Transfer faults separate adjacent

14

km BONAVISTA PLATFORM   JEANNE D ARC   FLEMISH FLEMISH   GALICIA BANK
                            BASIN   PASS   CAP

☐ CENOZOIC   ⊡ MESOZOIC   ▓ CONTINENTAL CRUST   ☐ MANTLE

0   km   200

V.E.= 5:1
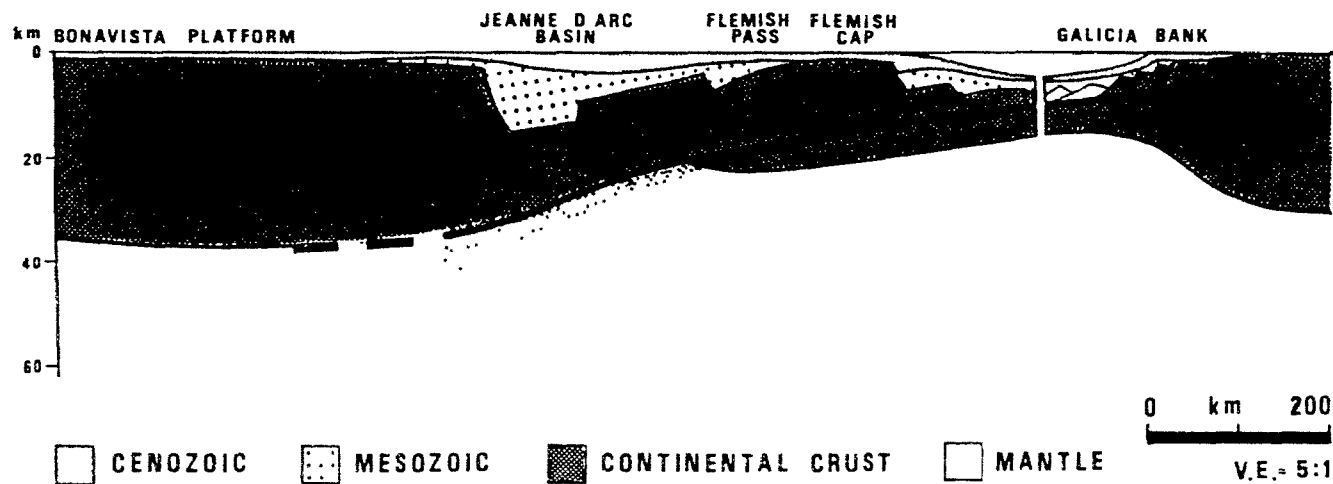
Fig. 2.2   Late Callovian extension along a westward dipping low-angle crustal detachment, showing the Murre-fault as an antithetic fault.   Most normal faults in the brittle zone terminate along the detachment surface   (from Tankard and Welsink, in press).

Fig. 2.3 In the central Grand Banks differential extension
of the Jeanne d'Arc Basin is accomodated along transfer
faults, causing the irregular funnel-shaped geometry of
the basin. Hydrocarbon fields of the Jeanne d'Arc
Basin, including in the Hibernia Oil field, are
indicated (from Tankard & Welsink, in press).

1. Spoonbill

2. Cormorant

3. Murre

4. Egret

5. Terra Nova

6. Hebron

7. Rankin

8. Ben Nevis

9. S. Mara

10. Hibernia P-15

11. Nautilus

12. Mercury

13. Adolphus

14. S. Tempest

FLEMISH PASS

DOMINION HIGH

JEANNE D'ARC BASIN

BONAVISTA PLATFORM

ANSON BASIN

BEOTHUK RIDGE

A

A

N

14

13

12

11

10

9

8

7

6

5

4

3

2

1

CENTRAL RIDGE

CARSON BASIN

Normal Fault

Transfer Fault

Salt Domes

Well Location

0   km   40

0   mi   30

49°   47°   46°
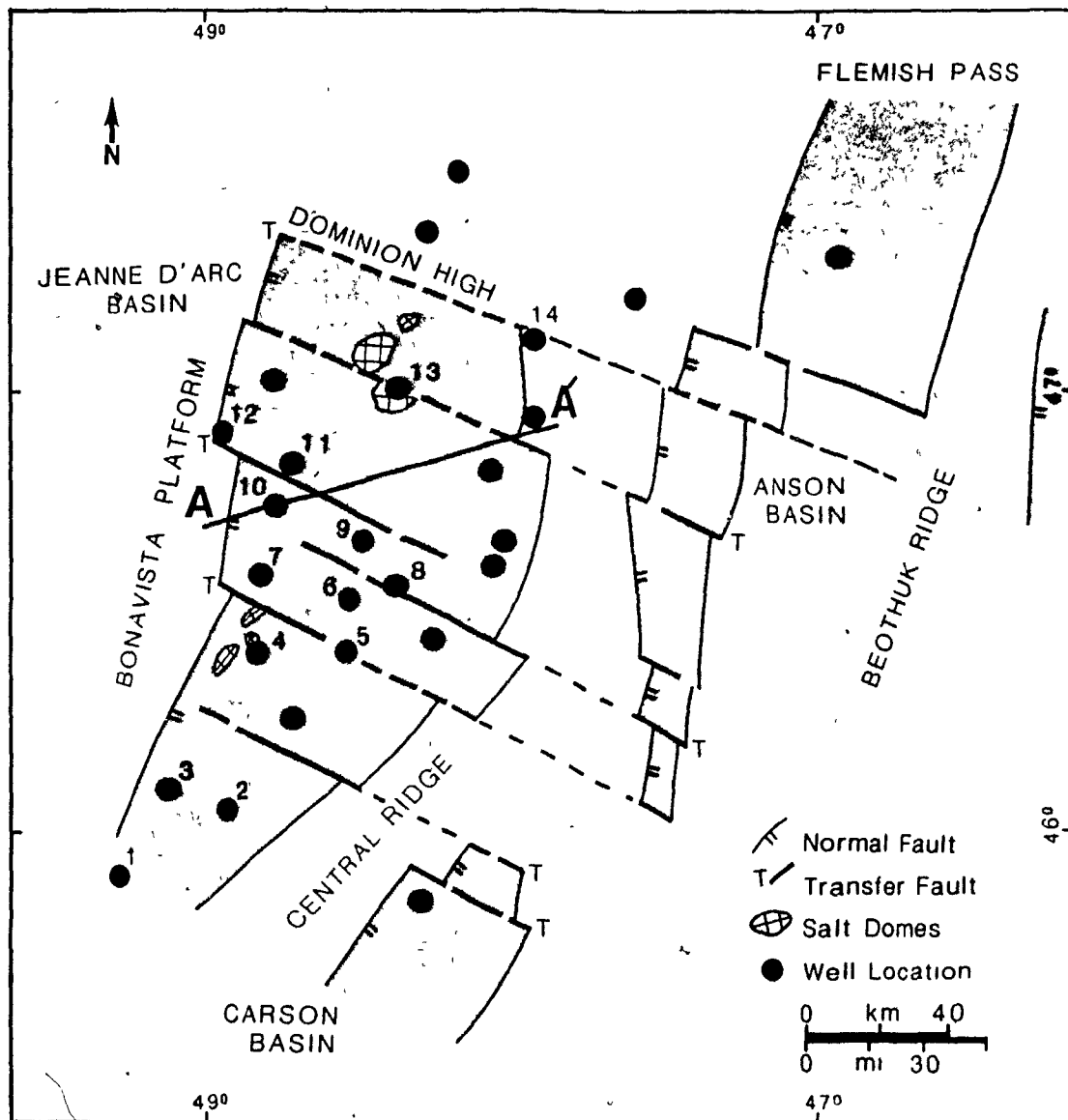
areas subjected to differential amounts of extension. The amount of extension associated with the Jeanne d' Arc Basin increases toward the northeast across a series of transfer faults. and is responsible for the present funnel-shaped geometry of the basin (Fig. 2.3). Some of these transfer faults were reactivated lateron in a normal sence dipping to the northeast and further deepening the Jeanne d' Arc Basin (Tankard and Welsink, 1987).

A schematic cross-section section of the North Jeanne d'Arc Basin reveals the following four segments (Fig. 2.4): (1) a stable shelf (Bonavista Platform in the west) containing a relatively thin cover of Cretaceous-Tertiary sediments which unconformably overlie the Precambrian-Cambrian basement; (2) a highly faulted hinge zone, separated from the stable shelf by the Murre Fault. Active subsidence along this growth fault resulted in the thick reservoir facies of the Avalon and Hibernia Sandstones along the western side of the hinge zone; (3) further eastward, the northward plunging Jeanne d' Arc Basin contains an about 16 km thick sedimentary sequence which, at places, is intruded by salt diapirs; and (4) the Central Ridge, a tilted fault block, where erosion and non-deposition are responsible for a very thin cover of Upper Jurassic and Lower Cretaceous sediments (Terra Nova, Hebron drill holes).

Bonavista   Hinge Zone   Avalon Sub-basin   Ridge Complex
Plateform
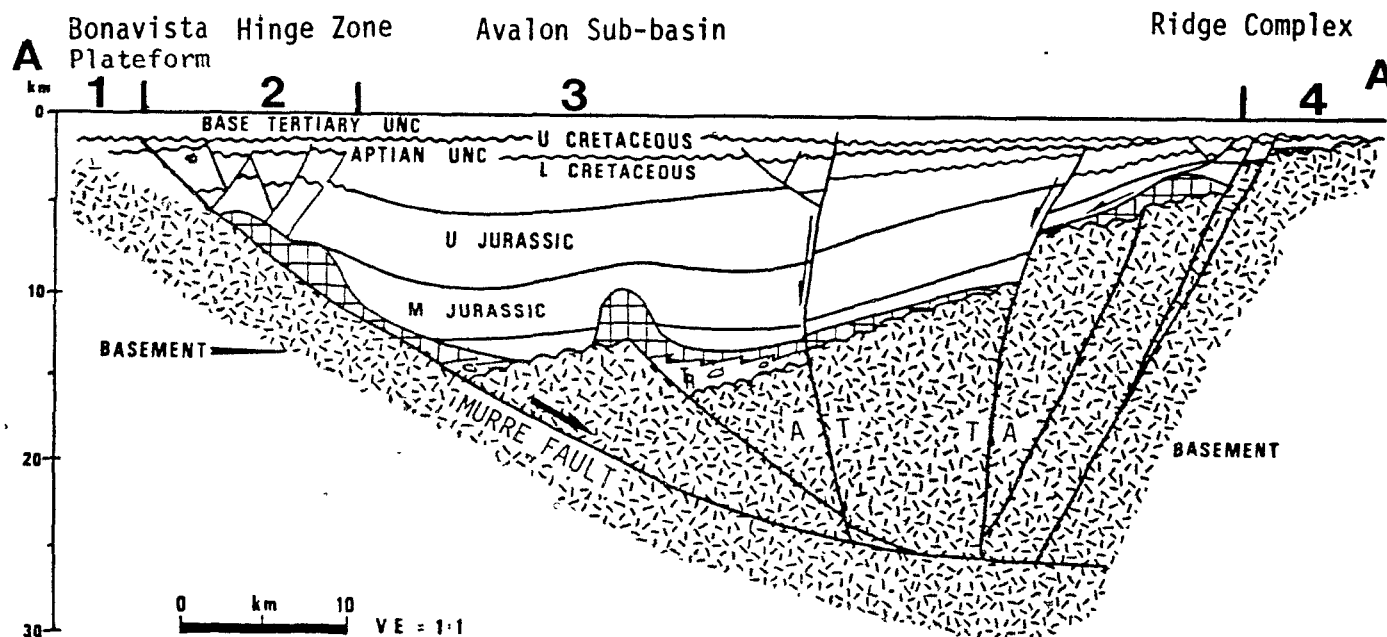
Fig. 2.4 A northeast-southwest cross-section section of the
Jeanne d'Arc Basin showing the following four segments: (1)
Stable shelf (Bonavista Platform), (2) Hinge zone, (3) Central
Jeanne d'Arc Basin, and (4) Central Ridge.   Relative strike-
slip movement along the two transfer faults is indicated as
away from (A) and toward (T) the viewer.   See Figure 2.3 for
the location of the section. (from Tankard & Welsink, 1987).

2.1.3 Hibernia Structure

The Hibernia Oil field is situated in the western hinge zone of the Jeanne d'Arc Basin, just south of the southeast trending Nautilus transbasin fault (Fig. 2.3). The oil field is associated with a large north-northeast trending rollover Hibernia anticline structure (Fig. 2.5) bounded on the west by a major listric growth fault (Murre Fault; Fig. 2.5). Figure 2.6 shows schematic cross-section through the Hibernia field. The Hibernia structure is dissected into a number of separate blocks by small transfer faults (Arthur et al., 1982). Most of these faults have served as a conduit for fluid migration. Until now only one sealing fault has been found between the Murre G-55A and Hibernia O-35 wells (Fig. 2.5). Oil field distribution in the Jeanne d' Arc Basin is closely related to transbasional faults which appear to be an important controlling factor both for trap formation, and hydrocarbon migration and accumulation (Fig. 2.7).

2.2 REGIONAL STRATIGRAPHY

The following information on the general stratigraphy of the Jeanne d' Arc Basin is summarized mainly from Jansa and Wade (1975); Jansa et al. (1976); Barss et al. (1979); Gradstein and Williams (1981); Arthur et al. (1982); Grant et al. (1986); and Tankard and Welsink (1987). The stratigraphic nomenclature used by Grant et al. (1986) was adopted for the present study (Fig. 2.8).

Fig. 2.5 Time seismic structure map on the Lower Cretaceous limestone marker illustrating the basic structural configuration of the Hibernia anticline. Contour interval is 100 msec (from Arthur et al., 1982)

Fig. 2.6 Geological cross-section of the Hibernia Oil Field showing apparent rollover structure into the listric normal Murre Fault. In the Hibernia field, the Hibernia and Avalon sandstones are the major reservoir intervals. See Figure 2.5 for location of the section (after Benteau and Sheppard, 1982).

Map showing Murre Fault with contour lines, coordinates 48° 45', 46° 50', 46° 40', and well locations K-18, B-08A, O-35, P-15, G-55. Scale: 5 km / 5 MILES.

Cross-section A–A' from WEST to EAST showing wells G-55A, J-34, O-35, P-15, K-18, B-08. Labels: SEA LEVEL, 5000 m, AVALON, "B", HIBERNIA, BASEMENT, MURRE FAULT, JURASSIC, MID-CRETACEOUS UNCONFORMITY. Scale: 0 2 4 KILOMETRES.
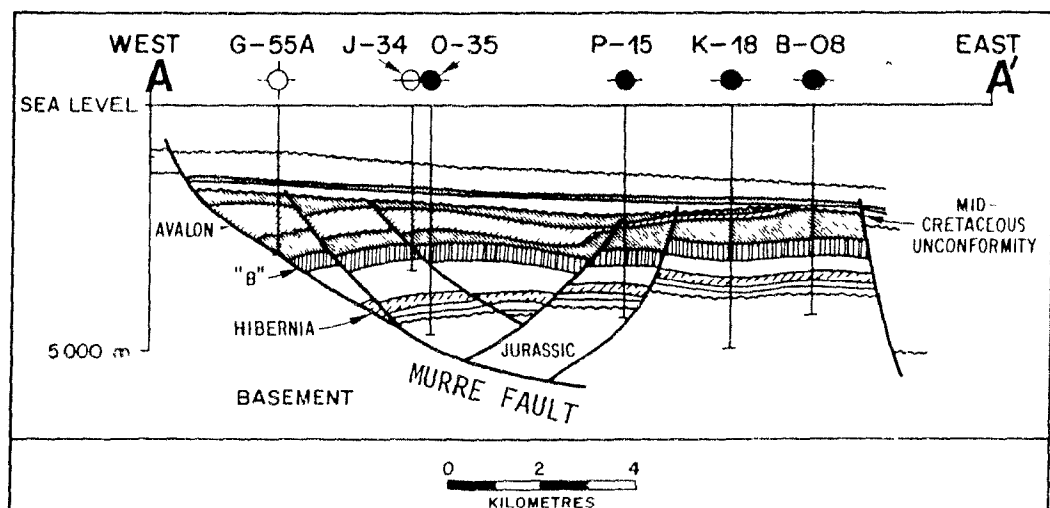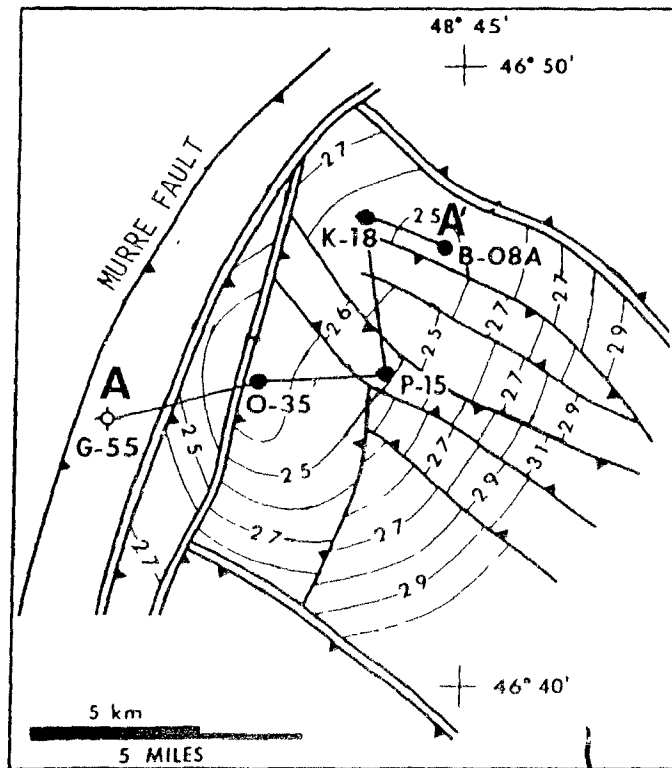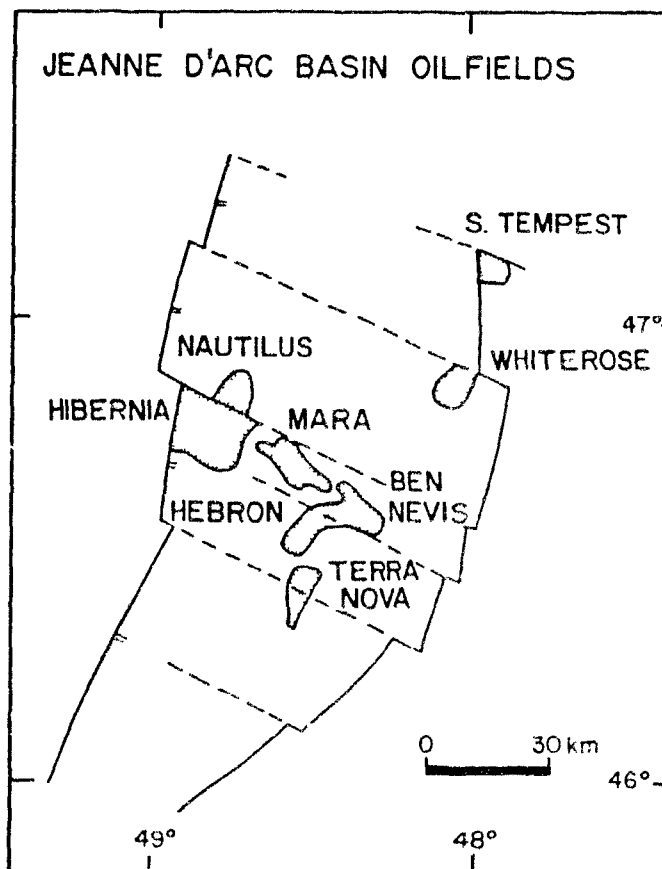
Fig. 2.7 In the Jeanne d'Arc Basin, the location of Oil
fields are closely associated with transfer faults. These
faults appear to be an important controlling factor for
hydrocarbon migration and accumulation (from Tankard and
Welsink, in press).

23

2.2.1   Eurydice Formation

The oldest Mesozoic sediments encountered by drilling in the Jeanne d'Arc Basin (Murre G-67 well) are 60 feet thick continental red beds of the Eurydice Formation. They unconformably overlie metasedimentary rocks of Middle or Late Devonian age. The terrestial red beds record a Late Triassic episode of rifting and basin subsidence on the Grand Banks (Jansa and Wade, 1975; and Jansa et al., 1976). In the G-67 well, an approximately three meter thick layer of conglomerate at the base of the sequence is followed by thick dark reddish-brown silty shales. The upper part of the red bed sequence is anhydritic. These red beds are continental and accumulated under arid climatic conditions. Upper anhydritic beds may have formed in a continental sabkha, or coastal sabkha environment, as no marine fossils were found in this formation. Based on stratigraphic position, a Late Triassic age is suggested for these sediments (Jansa and Wade, 1975).

2.2.2   Argo Formation

The red beds of Late Triassic age underlie wide-spread evaporites of the Argo Formation. The Argo Formation comprises of thick salt deposits under the Scotian Shelf (McIver, 1972 and Emery et al., 1970). Salt deposition was episodic as evidenced by thin argillaceous and sandy zones within the massive salt sequence (Grant et al., 1986). This formation was not encountered in the Jeanne d'Arc Basin, but

24

AGE					FORMATIONS	GENERALIZED LITHOSTRATIGRAPHY	TECTONIC HISTORY
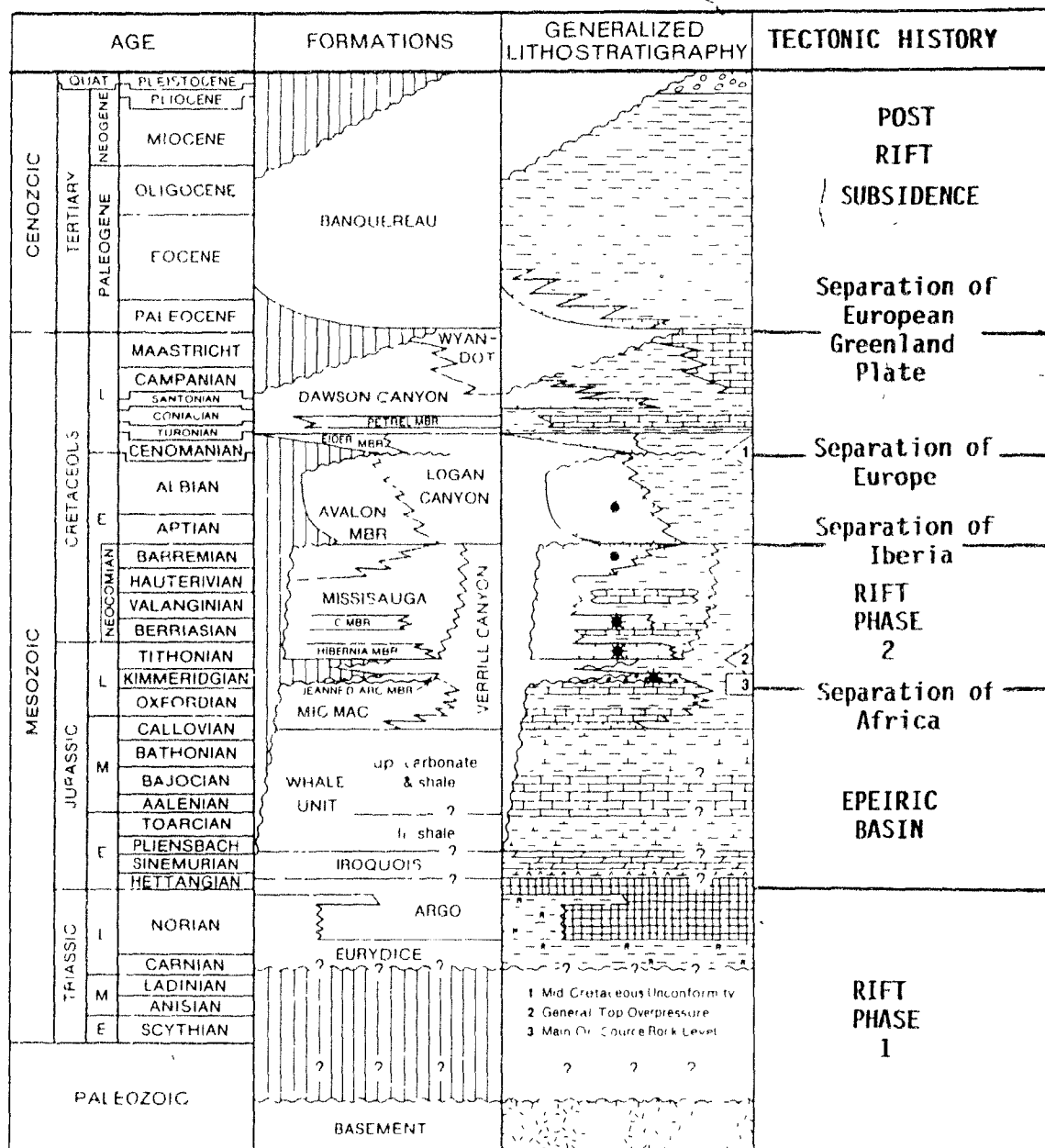
Fig. 2.8 Generalized stratigraphy and tectonic history of the Jeanne d' Arc Basin (modified after Grant et al., 1986; and Tankard and Welsink, 1987)

25

thin salt beds at the base of the Iroquois carbonates (in the Murre G-67 well) probably belong to this formation. Diapiric structures revealed on deep seismic-reflection profiles may also indicate the presence of Argo salt in the Jeanne d'Arc Basin. The Argo salt basin is part of a Late Triassic to Early Jurassic salt basin system, which developed on the periphery of the western extension of the Tethyan Sea (Jansa and Wade, 1975).

2.2.3   Iroquois Formation and Whale Unit

The Early and Middle Jurassic were times characterised by regional thermal subsidence and marine transgression(s) which gradually transformed the Grand Banks into an epicontinental sea (Tankard and Welsink. 1987). The Iroquois Formation and Whale Unit record this progressive change to normal, open marine conditions. The lower part of the Iroquois Formation consists of lagoonal and tidal-flat, microcrystalline dolomite that is yellowish brown and occasionally contains anhydrite. The upper part of the Iroquois Formation is made up of oolitic and skeletal limestones. In the G-67 well (South Jeanne d'Arc Basin) the Iroquois Formation lies directly on the red beds of the Eurydice Formation. The lower shale, and upper carbonate and shale facies of the Whale Unit were deposited in neritic and subtidal environments, respectively (Jansa and Wade, 1975).

2.2.4   Mic Mac Formation and Jeanne d' Arc Member

The Mic Mac   is the oldest formation (Callovian to Tithonian) drilled in the Hibernia oil field.   It has been divided into a Lower and an Upper zone. The Lower Zone consists of limestone, organic matter-rich shales, siltstone and sandstones, representing localized carbonate banks and shallow marine environments. It marks the transition between the preceding epeiric-sea basin and the   Late Kimmeridgian flood of synrift clastic sediments. Interbedded oil-prone organic matter-rich shales of Kimmeridgian age form the principal hydrocarbon source-rocks in the Jeanne d' Arc Basin (Swift and William, 1980). It is probable that transfer faults of the Callovian rift stage have enhanced basin isolation forming source rock depocentres (Tankard and Welsink, 1987).

The   Jeanne d' Arc Member represents the Upper Zone of the Mic Mac Formation (Late Kimmeridgian to Tithonian), and comprises of conglomerate, sandstone and shale beds of fluvial origin. Late Jurassic rifting and brittle failure of the crust generated a rugged relief which contributed a source of coarse clastics to the western margin of the Jeanne d' Arc Basin. Along the Central Ridge, which dips gently to west, the Jeanne d' Arc Member   consists of interbedded mudstone and sandstone facies (e.g. Hebron I-13)

2.2.5   Missisauga Formation and Avalon Sandstone

Throughout the Hibernia Field, the Upper Jurassic and
Lower Cretaceous Missisauga Formation and Avalon Member
represent a thick sequence of clastic rocks, mainly sandstones
and shales with little limestone inter beds.   This major
change in sedimentation to a clastic-dominated   sequence is
attributed to the Mid-Mesozoic rifting episode in the Grand
Banks. Most of the detrital material was supplied from
erosion of : 1) uplifted blocks along the western boundary
(i.e. the Murre Fault) and transbasin faults; 2) unrifted
elevated areas of the Grand Banks present t the West
(Bonavista Platform) and southeast (the Avalon Uplift of Jansa
and Wade, 1975) of the Jeanne d' Arc Basin respectively; and
3) westward tilted and uplifted Central Ridge blocks.   The
detrital material was transported northward and deposited in
deltaic and marine-deltaic environments (Arthur et al., 1982;
Brown, 1985; and Tankard and Welsink, 1987). During Aptian
time the "Avalon Uplift" area was further elevated and deeply
denudated. The Aptian uplift is interpreted as isostatic
rebound which resulted from partial unloading of the
lithospheric plate late in the extensional phases (Tankard
and Welsink, 1987). The reason for the pre-Aptian Avalon
uplift is not clear.

The main reservoir rocks of the Hibernia Field (Hibernia,
"B" and Avalon Sandstones) occur in this stratigraphic
sequence. Because of their significance as hydrocarbon
reservoirs, these rocks will be discussed separately in

section 2.3 below.

2.2.6   Dawson Canyon Formation

Above the Mid-Cretaceous unconformity (or "breakup" unconformity, Fig. 2.7) the Dawson Canyon and Banquereau Formations represent a post-rift sedimentation record. During this time thermal subsidence and relatively shallow shelf seas dominated the Grand Banks.

The Dawson Formation is sandwiched between the Mid-Cretaceous and Cretaceous-Tertiary unconformities and represents a transgressive marine sequence. These undeformed sediments consist mainly of shales and limestones (i.e. Petrel Limestone) with minor siltstone and sandstones.   In the Grand Banks, the microcrystalline Petrel Limestone represents outer-shelf environments (Swift et al., 1975) and serves as a good regional seismic marker.   Only a few faults with small displacements extend upward beyond the Petrel Limestone. Above the Petrel Limestone, the light to medium grey mudstone facies of the Dawson Canyon Formation is calcareous and frequently burrowed.   It contains pelecypods, gastropods, ammonites and foraminiferal tests.   During the Santonian stage, thin intercalated sandstone beds appear in this shale-dominated sequence.   In the axial portion of the basin, time-equivalent rocks include outer neritic chalks and limestones of the Wyandot Formation (Grant et al., 1986).

2.2.7   Banquereau Formation

The Tertiary Banquereau Formation unconformably overlies the Upper Cretaceous sediments. It consists predominantly of marine shale and siltstone with minor sandstone, deposited in the course of a major transgression (Gradstein and Williams, 1981). Its lower part represents a deep marine environment which changed to shallow during Oligocene time. Further up in the stratigraphic column, parts of the Grand Banks may have been exposed subaerially during Middle to Late Miocene time (Grant et al. 1986).

2.3   RESERVOIR ROCKS AND THEIR DEPOSITIONAL ENVIRONMENTS

2.3.1   Jeanne d' Arc Member

The Jeanne d'Arc Member of the Mic Mac Formation is the oldest reservoir rock encountered in the Hibernia Field. It is of Tithonian (Arthur et al., 1982) or Kimmeridgian age (Grant et al., 1986) and shows abnormally high formation pressure (above 10,000 psi) in many Hibernia wells (O-35, B-08, K-18, and P-15) (Grant et al., 1986).

The Jeanne d' Arc Member was deposited by fault controlled streams flowing longitudinally and transversely generating small fan-deltas in the Jeanne d' Arc Basin (Tankard and Welsink, 1987). In the Hibernia oil field, this member was deposited by transversely flowing streams along the Nautilus Fault. It comprises of matrix-supported and clast-supported conglomerate, sandstones, and mudstone. In

30

the O-35 well, conglomerate (> 1 m thick) and sandstone beds (<0.5 m thick) generally show sharp contacts. Here the conglomerates consist of pebbles and cobbles of limestone, schist, quartzite and shale which float in a poorly sorted coarse sandstone matrix. Interbedded coarse grained sandstones are poorly sorted and cross-bedded. These sandstones commonly show broken carbonaceous laminae. In the Hibernia Field, this member contains small amounts of oil (Meneley, 1986).

2.3.2. Hibernia Sandstone of Missisauga Formation

The Hibernia Sandstone of the Missisauga Formation is one of the two major reservoir horizons in the Hibernia area. It has an average thickness of 200 metres, and occurs between 3475 and 4180 m subsurface depth in different wells. It is thickest in the western part of the Hibernia structure and thins out northward (in Hibernia K-18)) and eastward (Fig. 2.5).

Brown (1985) subdivided the Hibernia Sandstone into a Lower and an Upper Zone. The Lower Zone consists of thick-bedded (up to 13 m), medium-to coarse-grained, crossbedded quartz arenite interbedded with siltstone and shales. The sandstone units display both fining-and coarsening-upward sequences. The Upper Zone is characterized by relatively thin (< 2 m) medium- to fine-grained sandstones interbedded with siltstones and mudstones. The sandstone/shale ratio is high in the Lower Zone as compared to the Upper

31

Zone. Siderite nodules (2-3 cm long) are common in the interbedded shales and siltstones. Reworked carbonaceous material is also common in the Hibernia Sandstone. Brown (1985) interpreted the lower part of the Hibernia Sandstone as distributary channel deposits of a deltaic plain, whereas the Upper Zone of the Hibernia Sandstone was assigned to a shallow deltaic-front environment.

2.3.3   B" Sandstone of Missisauga Formation

The "B" Sandstone member of the Missisauga Formation, about 152 m thick, is present between the Hibernia and Avalon Sandstones. It consists of fine to very fine, locally calcareous sandstones. Interbedded shale and siltstones are commonly burrowed. The "B" Sandstone represents marginal marine environments (Meneley, 1986). This sandstone does not contain significant amounts of hydrocarbons.

2.3.4   Avalon Sandstone

The Lower Cretaceous (Hauterivian to Albian) Avalon Sandstone is a very fine to fine-grained, well sorted quartz arenite with variable amounts of calcite cement and fossil fragments. Fossil-rich zones are more common in the B-27 and O-35 wells than in the B-08 well. Many of the fossil fragments (i.e. pelecypods, ostracodes, brachiopods, and foraminfera) show imbricated stacking along bedding planes. The interbedded thin siltstones and shales are commonly burrowed. Reworked shale pebbles (measuring an average 4.5 x 2.5 cm) along erosional surfaces are particularly common in

the B-27 well. Siderite nodules in the siltstone and shale beds are less abundant than in the "B" Sandstone and Hibernia Sandstone.

The Avalon Sandstone represents the uppermost reservoir horizon in the Hibernia area. As a result of rapid subsidence along a fault block and proximity of the sediment source, the Avalon Sandstone attained considerable thickness (790 m in the G-55A well, Fig. 2.5). This sandstone thins out toward the east (313 m in O-35) and north (16 m in B-08) in the Hibernia structure.

Benteau and Sheppard (1982), Handyside and Chipman (1983) and McMillan (1982) considered the Avalon Sandstone as a shallow- water shoreline deposit. Meneley (1986) interpreted it as complex assemblage of delta-front, shore-zone and lagoonal facies.

SANDSTONE PETROGRAPHY AND DIAGENESIS

3.1 SANDSTONE PETROGRAPHY

3.1.1 Introduction

Thin sections of more than 168 sandstone samples from the Hibernia Field (for sample locations see Appendix I) were studied under the petrographic and scanning electron microscope. Thirty six thin sections were point-counted for different components (i.e. framework grains, authigenic minerals, matrix and porosity types). Samples have been selected for thin section analysis if, after megascopic inspection, they appeared interesting from the diagenetic point of view. Based on these 36 analyses, the average sandstone composition is $Q_{87.9}$ $F_{3.6}$ $R_{8.5}$. Following the classification of Folk (1974), most of the sandstones fall in the fields of sublitharenite to quartz arenite (Table 3.1 and Fig.3.1). Five samples plot in the subarkosic field. The majority of the shale clasts probably represents rip-up clasts that were redeposited in deltaic environments (Brown, 1985). If these clasts are excluded, the samples are mineralogically mature and nearly all would be classified as quartzarenite. The detrital constituents of the sandstones are described below.

3.1.2 Quartz

Quartz is the most abundant mineral (average 87.9%) in all samples, ranging from 78% to 99% of the framework grains.

Table 3.1 Percent QFR; Q_p Q_{un} Q_m modes, and percent total detrital and authigenic minerals, and porosity for the Avalon, "B", Hibernia Sandstones, and Jeanne d' Arc Member.

ABBREVIATIONS

AUT   = Authigenic minreals

DET   = Detrital constituents of sandstones

F   = Feldspar

POR   = Porosity

Q   = Quartz

Qm   = Monocrystalline, non-undulose quartz

Qp   = Polycrystalline quartz

Qun   = Undulose quartz

R   = Rock fragments

Depth (m)	% Framework Grains			% Quartz Types			% Whole Rock Volume		
	Q	F	R	Qp	Qun	Qm	DET	AUT	POR

(A) AVALON SANDSTONE

Depth (m)	Q	F	R	Qp	Qun	Qm	DET	AUT	POR
2184.6	77.7	5.3	17.0	4.0	6.8	89.2	79.3	8.2	12.5
2185.8	75.8	5.9	18.3	1.8	2.2	96.0	84.4	6.4	9.2
2190.3	85.6	6.8	7.6	3.3	12.5	84.2	85.8	8.0	6.2
2190.8	87.1	7.5	5.4	4.5	6.2	89.3	85.3	5.5	9.2
2197.5	88.7	3.3	8.0	4.0	4.1	91.9	77.9	4.1	18.0
2197.9	81.6	8.6	9.8	3.5	3.4	93.1	68.6	31.4	0.0
2197.9*	87.3	4.9	7.8	2.3	4.7	93.0	82.2	7.6	10.2
2571.5	85.8	3.4	10.8	3.3	4.0	92.7	70.6	29.4	0.0
2578.8	83.9	2.4	13.6	2.5	8.3	89.2	75.6	3.2	21.2
2659.6	89.8	3.7	6.5	6.0	7.1	86.9	76.4	12.2	11.4
2661.1	81.5	6.5	12.0	3.8	5.7	90.8	69.7	30.3	0.0
Av	84.1	5.3	10.6	3.5	5.9	90.6	77.8	13.3	8.9

(B) "B" SANDSTONE

Depth (m)	Q	F	R	Qp	Qun	Qm	DET	AUT	POR
3174.9	92.0	4.8	3.2	3.5	3.8	92.7	67.6	32.4	0.0
3178.0	89.6	0.8	9.5	9.4	5.5	85.1	79.2	8.2	12.6
3179.1	92.9	2.6	4.5	9.0	8.5	82.5	75.0	14.2	10.8
3180.3	81.7	8.5	9.8	7.4	7.0	85.6	73.7	26.3	0.0
3185.9	89.8	7.0	3.2	1.5	5.6	92.9	66.5	23.8	9.7
3131.5	82.7	6.4	10.9	8.0	6.1	85.9	78.3	12.1	9.6
Av	88.1	5.0	6.9	6.5	6.1	87.4	73.4	19.5	7.1

(C) HIBERNIA SANDSTONE

3481.3	89.7	2.9	7.4	10.7	6.5	82.8	79.4	11.7	8.9
3482.6	93.9	3.3	2.8	9.8	7.4	82.8	80.6	7.3	12.1
3483.4	93.3	1.9	4.8	9.5	8.6	81.9	81.0	12.7	6.3
3555.1	96.8	1.2	2.0	5.1	4.9	90.0	85.9	1.6	12.5
3606.2	98.3	0.0	1.7	14.7	12.0	73.3	95.0	1.6	3.4
3619.4	88.6	6.4	5.0	8.0	7.7	84.3	76.2	11.0	12.8
3622.4	97.8	0.0	2.2	7.1	1.7	91.2	87.8	2.4	9.8
3624.2	86.5	9.7	3.8	6.2	10.4	83.4	79.3	13.0	7.7
3845.8	96.3	1.2	2.5	2.1	4.7	93.2	79.5	9.8	10.7
3846.5	98.2	0.0	1.8	4.6	2.1	93.3	76.6	4.2	19.2
3849.7	95.6	0.5	3.9	5.2	1.9	92.9	73.9	9.2	16.9
3850.3	98.1	0.5	1.4	6.9	2.2	90.9	73.3	4.8	21.9
3850.7	98.6	0.0	1.4	7.4	6.9	85.7	72.7	2.3	25.0
3854.5	96.9	0.0	3.1	6.5	1.6	91.9	80.4	7.0	12.6
3860.8	85.0	5.1	9.9	5.0	7.7	87.3	52.3	47.7	0.0
3879.0	98.4	0.3	1.3	7.1	2.5	90.4	73.0	11.0	16.0
3895.2	99.2	0.3	0.5	7.0	2.7	90.3	84.9	0.9	14.2
Av	94.8	1.9	3.3	7.2	5.4	87.4	78.3	9.3	12.4

(D) JEANNE D' ARC MEMBER

4533.5	89.6	3.0	7.4	7.1	6.5	86.4	85.7	14.3	0.0
4534.0	79.3	1.4	19.3	13.2	6.6	80.2	77.0	23.0	0.0
Av	84.5	2.2	13.3	10.2	6.5	83.3	81.3	18.7	0.0
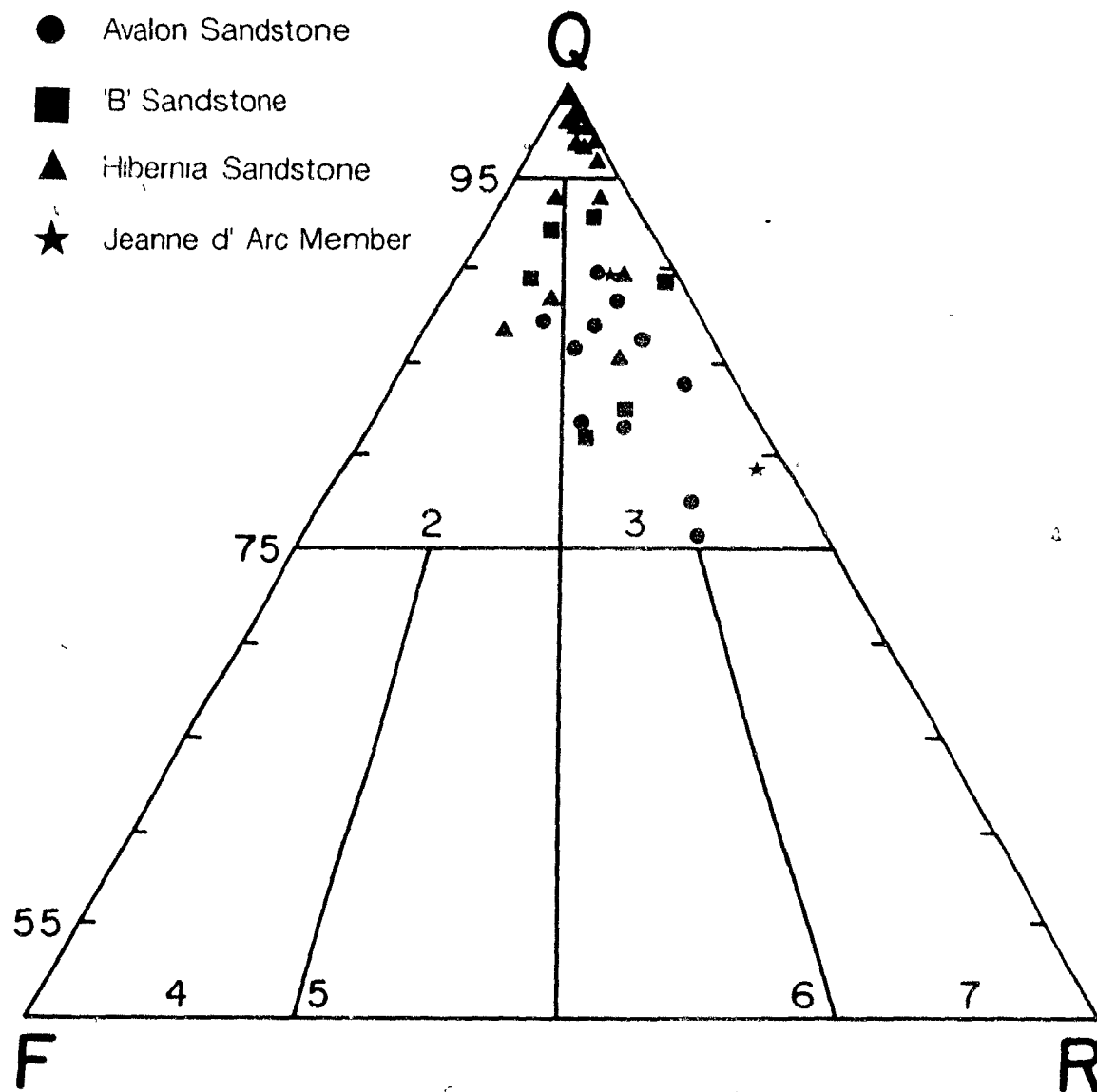
Fig. 3.1 Classification of reservoir sandstones based on major framework components (classification scheme of Folk, 1974).

Monocrystalline quartz is dominant (averaging 87.2%) over polycrystalline quartz (averaging 6.8%). Only 6.0% of the monocrystalline quartz shows undulose extinction (more than 5° rotation for complete grain extinction). Polycrystalline quartz is more abundant in the Hibernia Sandstone (7.2%) than in the Avalon Sandstone (3.5%). Quartz grains are moderately to well sorted; however, some samples show poor sorting. Generally, quartz grains are subrounded to subangular. Roundness increases with stratigraphic depth. At 2100-2600 m depth, the quartz grains are loosely packed having point contacts (Plate 3A). With increasing depth (>3100 m), long concavo-convex and sutured contacts become more common (Plate 3B, 3C, and 3D). In most of the samples, a few quartz grains with zircon inclusions (25-90 um) have been noted. Occasionally, inclusions of apatite, pyrite, muscovite, biotite (average 20 to 40 um) and, rarely of chlorite and sillimanite, are also present in quartz grains.

A triangular plot of monocrystalline, monocrystalline undulose, and polycrystalline quartz (Basu et al., 1975) indicates a plutonic source for most of these quartz grains (Fig. 3.2). However, "water"- clear monocrystalline quartz with straight extinction, straight crystal faces and rare negative inclusions may indicate a minor contribution from volcanic rocks. The presence of elongated and crenulated crystals with deep sutured grain boundaries in polycrystalline quartz aggregates probably indicates a metamorphic source. A minor proportion of the quartz grains has been recycled or reworked. Recycling is indicated by the

Polycrystalline quartz

Medium to High grade
. Metamorphic

Plutonic

Low grade
Metamorphic

Non-
undulose quartz

Undulose
quartz
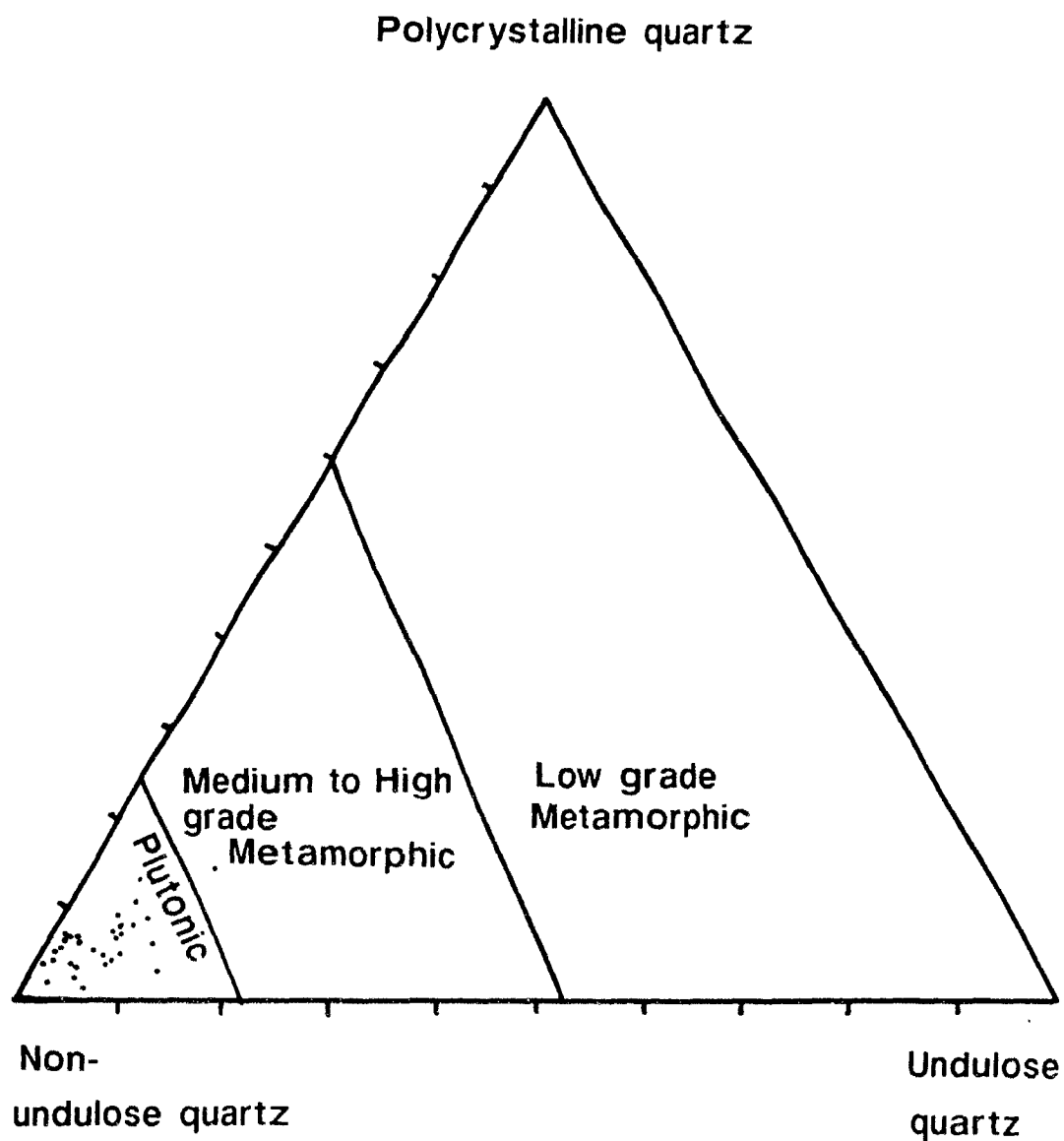
Fig. 3.2 Plots of quartz varieties from the sandstones of the Hibernia
Oil Field on a quartz provenance diagram (after Basu et al., 1975).

40

occurrence of quartz overgrowth on rounded quartz grains that contained a first generation overgrowth. Reworking is assumed for grains with broken calcareous micrite envelopes.

3.1.3 Feldspar

Detrital feldspar content ranges from 0 to 9.7% of the total framework grains with a mean of 3.5%. Plagioclase is the dominant feldspar. Microcline is rarely present. Few grains contain calcareous micrite envelopes. In some thin sections, feldspar exceeds rock fragments in abundance. Most of the feldspar grains show signs of diagenetic alteration and dissolution which will be discussed in section 5.3.4.

The Avalon Sandstone, in which little or no dissolution has occurred, has an average 5.3% feldspar compared to 1.9% in the Hibernia Sandstone. This decrease in feldspar with increasing stratigraphic depth could be the result of: (1) dissolution; (2) increasing grain size; (3) change in the source rocks; or (4) a combination of all of these.

3.1.4 Rock Fragments

Rock fragments follow quartz in order of abundance and constitute an average 8.5% of the framework grains, ranging from 0.5 to 18.3%. These fragments are dominantly sedimentary in origin and include chert, shale, sandstone, siltstone, and limestone, along with negligible amounts of metamorphic, volcanic and igneous fragments. The Avalon Sandstone has, on average, more rock fragments (10.6%) than the Hibernia Sandstone (3.3%). Rather than utilizing a genetic

41

classification, the rock fragments were grouped into four categories based on mineralogy and diagenetic behaviour, i.e. ductile, siliceous, carbonate (non-biogenic), and fossil fragments.

3.1.4.1 Ductile Rock Fragments

Ductile rock fragments range from 0 to 5.7%, with an average 1.3% of the total rock volume. They include rip-up mud clasts, shale fragments and, very rarely, phyllite grains. Among these, mud-clasts are most abundant, and are distinguished from shale clasts by being less consolidated. The amount of silt in mud-clasts is variable. Shale fragments are composed of well-oriented clay minerals, having aggregate birefringence. Their degree of deformation increases with increasing burial depth which results in their being squeezed between detrital grains. This leads to porosity reduction in sandstones with depth. In many depth intervals, carbonaceous wisps are also abundant in the shale clasts.

3.1.4.2 Siliceous Rock Fragments

This class comprises chert grains, sandstone-siltstone, schist (Plate 1A and 1B), siliceous shale, volcanic and other igneous rock fragments. Of these, only chert and sandstone-siltstone are more common. Chert fragments are mostly well rounded, varying from trace amounts to 5.3 % with an average 1.5% of the total rock volume and are present in all samples studied. Sandstone-siltstone fragments average

42

1.3%.

Most of the chert grains consist of microcrystalline quartz. A few of them contain fibrous, radiating chalcedony which appears to be replacing volcanic rock fragments. Replacement of chert by calcite, late dolomite and early pyrite has been noted in many samples. Some of these chert grains comprise both microcrystalline and coarsely crystalline aggregates. In such cases, the coarsely crystalline part is relatively fresh and free of inclusions and appears to be the drusy, pore-filling part of a chert grain.

3.1.4.3 Carbonate Rock Fragments

Carbonate rock fragments (excluding fossil fragments) range from 0 to 8.2%, with an average of 1.5% of the total rock volume. They are relatively common in the Avalon (1.3%) and "B" Sandstones (0.9 %) and less abundant in the Hibernia Sandstone (0.3%). Most of these fragments consist of calcitic micrite, microspar, and sparry calcite. Ferroan carbonate and dolomite are minor. Eight different types of carbonate-rich fragments were recognized: (1) sparry calcite with some quartz grains; (2) sparry calcite with silt-size quartz grains; (3) micritic calcite; (4) sparry calcite; (5) complex carbonate fragments that contain ooids, fossils, micritic and sparry fragments, and micrite coated quartz grains; (6) fine grained dolomite (or siderite) with a few quartz grains; (7) ooids and micritic calcite fragments cemented with tabular and drusy calcite crystals, and (8) ooids. Some sandstone beds (e.g. at 2576-2580.5 m, B-27)

contain   abundant   limestone   fragments   (up   to   10%).   These
limestone   fragments are of uniform size,   well rounded   and a
few of them contain broken fossil fragments.

3.1.4.4   Fossil Fragments

On average,   fossil fragments constitute only 1.2% of the
total   rock volume.   Among them,   fragments   of   pelecypods,
gastropods,   ostracodes and,   less frequently,   foraminfera have
been   noted.   Small amounts of fossil fragments are present in
many samples.   In   fossil-rich zones they may contribute up to
27% to the total framework grains (Plate 1C).   These fragments
are   relatively common   in the Avalon   Sandstone,   but   less
common   in   the   Hibernia Sandstone.   A   few   large   fossil
fragments   contain   holes caused by   boring   organisms.   These
holes are partly filled with calcite cement (Plate 1D).

3.1.5   Heavy Minerals

Heavy   minerals   range from   trace   amounts   to   6.7%,
averaging   1.2%   of   the   framework   grains.   In   order of
abundance,   they include pyrite,   tourmaline, zircon, epidote,
hornblende,   pyroxene, fluorapatite (?) and garnet.

Pyrite   occurs   as   an   interstitial mineral.   It is   also
found   in   calcite   cement,   in   organic   matter   and   as   a
replacement   of   chert,   shale matrix,   dolomite   cement   and
fossil fragments.   In some samples,   pyrite is abundant along
depositional laminae.   Tourmaline (40   to 150 um) and   zircon
(40   um)   are generally   anhedral to subhedral in   the   Avalon
Sandstone   and subrounded to rounded in the   "B"   and   Hibernia
Sandstones.   Fluorapatite   is are only present in the   Avalon

44

PLATE 1

Photographs showing rock and fossil fragments.

(A) Schist fragment containing quartz, chlorite and other argillaceous material. This example shows advanced mechanical compaction between the rigid framework grains. The porosity around the schist fragment is completely occluded. The bedding direction is north-south. Jeanne d' Arc Member, O-35, 4534.82 m. Plane-polarized light. Scale bar: 100 um.

(C) Calcite cemented sandstone rock fragment containing quartz, micrite coated quartz grains and other carbonate fragments. Note differences in the type and size of the clasts within the rock fragment and in the host sandstone itself. The host sandstone is cemented with ferroan dolomite. Jeanne d' Arc Member, O-35, 4534.82 m. Plane-polarized light. Scale bar: 100 um.

(C) Drill-core of a fine-grained, oil-stained thick sandstone showing fossil-rich zone (mostly pelecypods and ostracods). Inspite of abundant fossil fragments the sandstone displays no calcite cementation. Bedding is sub-horizontal. Avalon Sandstone, O-35, 2196.67m. Scale bar in cm.

(D) Large (1.5 cm) mollusk shell fragment perforated by boring organism. The resultant pores (H) are partly filled by ferroan calcite cement. Note marginal pressure solution contacts between fossil fragment and framework quartz grains. Bedding plane is vertical. Avalon Sandstone, B-27, 2582.49 m. Plane-polarized light. Scale bar: 500 um.

45

and "B" Sandstones.

3.1.6 Matrix

Matrix ranges from trace amounts to 11.5% and averages 3.8% of the bulk rock volume. In this study, the term matrix refers to all detrital particles less than 0.03 mm in diameter. It also includes other small rock fragments that have been crushed by compaction between the grains and whose composition has not been identified in detail. These are generally referred to as pseudo-matrix.

3.2   SANDSTONE DIAGENESIS

3.2.1   Introduction

All diagenetic processes (mechanical compaction, dissolution, alteration, precipitation, and recrystallization) that sediments undergo from the time of deposition until metamorphism can significantly modify the reservoir porosity and permeability. Therefore, it is important to understand the timing and extent of diagenetic processes in order to predict porosity distribution in reservoir sandstones. This section presents detailed observations and quantification of mechanical and chemical compaction as well as precipitation of authigenic minerals in the reservoir sandstones of the Hibernia field. The paragenetic sequences of diagenetic events are established using conventional textural relationships visible in thin sections (summarized in Figure 3.8). Dissolution and porosity related features are covered in Chapter 5.

3.2.2   Mechanical Compaction

Mechanical compaction involves re-arrangement and rotation of grains, breakage of brittle components and deformation of ductile grains. The degree of compaction is chiefly dependent on the types framework components and depth of burial (in case where compaction is not inhibited by cementation and/or formation of over-pressure). The net effect of these processes is the reduction of bulk volume, which is accompanied by porosity reduction and ejection of

pore fluids. Figure 3.3 shows pre-cement porosity and the total present porosity versus frequency. The mean pre-cement porosity is 23% and the present mean porosity is 10 %. If we consider 40% a typical value for original porosity in sands at the time of deposition, then around 17% porosity were lost due to mechanical compaction and introduction of detrital matrix prior to cementation. Of the remaining 23%, 13% were lost due to cementation, leaving an average 10% of present porosity in thin sections.

3.2.2.1 Bioturbation

Bioturbation is one of the first processes affecting mechanical compaction. The burrowing activity of benthonic organisms causes mixing of originally distinct sand and mud layers. Two processes reduce intergranular porosity in freshly deposited sands: (1) bioturbation disturbs the original sand grain orientation and adds fine-grained matrix (Plate 2A, 2B, and 2C); (2) as a result of bioturbation, fine-grained, thin sandstone layers in thick silty shale beds are disintegrated into irregular patches (Plate 2D). Pyrite is commonly associated with bioturbated zones. As compared to other wells, the Hibernia Sandstone of the B-27 well shows extensive bioturbation.

3.2.2.2 Avalon Sandstone In the Avalon Sandstone, mechanical compaction is relatively minor. This is indicated by grain-to-grain contact relationships and low packing density (Plate 3A). Quartz grains have pressure solution

49
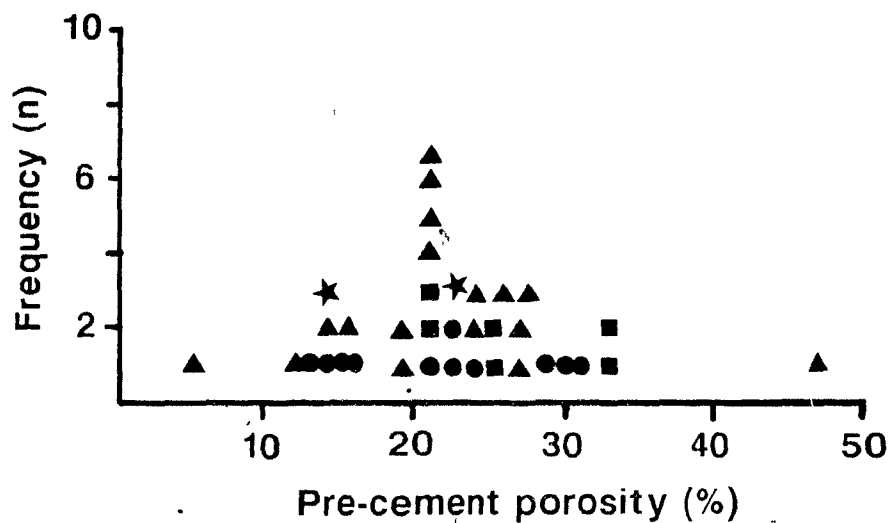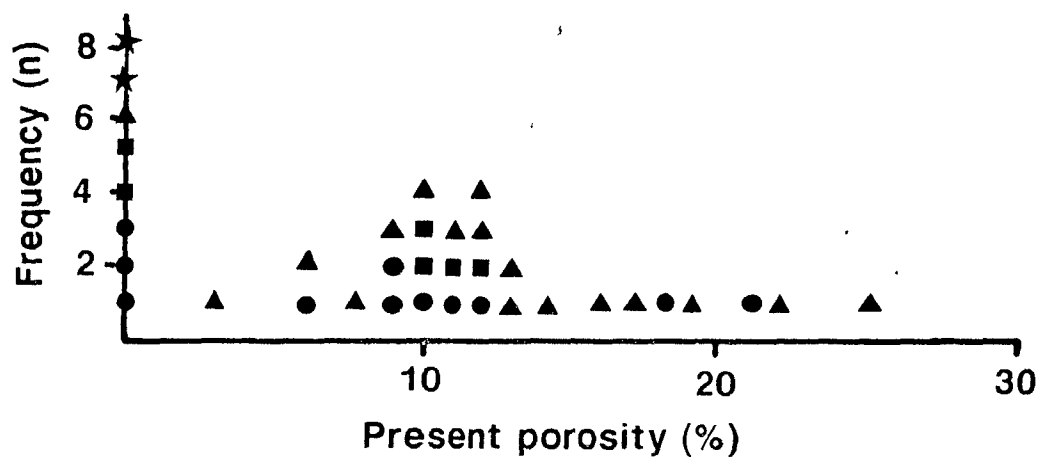
Fig. 3.3 Frequency distribution of pre-cement and present porosity in sandstones of the Hibernia oil field.

PLATE 2

Effects of bioturbation in thin section and drill-core samples.

(A) Spotty distribution of clay material caused by bioturbation which introduced mud into sand layer. In the field of view, the loss of sandstone porosity (upper half of the photograph) is largely due to this process. Note euhedral pyrite crystal in the centre of photograph. Hibernia Sandstone, C-96, 3919.30 m. Plane-polarized light. Scale bar: 100 um.

(B) Mud-clasts (arrow 1) scattered in fine-grained sandstone as a result of bioturbation. Note large mud-lined, sand-filled burrow in the left-centre of photograph (arrow 2). Small sand-filled burrow structures (arrow 3) are probably the casts of chondrites. Small amounts of reworked carbonaceous material are also present (arrow 4). Hibernia Sandstone, B-27, 3862.42 m. Scale bar in cm.

(C) Extensively burrowed fine-grained sandstone. Avalon Sandstone, O-35, 2187.21 m. Scale bar in cm.

(D) Thin, fine-grained sand layers alternating with mud layers were broken and mixed-up. The central part of the photograph shows nearly vertical burrows (arrows a and b). Arrow (c): small mud-filled, sand-lined terebellina (?). In the lower part of the photograph, some of the disturbance might be due to the presence of rip-up clasts. Hibernia Sandstone, B-27, 3885.15 m. (Scale bar in cm.)

A

B

1 4

3

2

1

4

3 362.42

C

D

a c

b

3 885.15
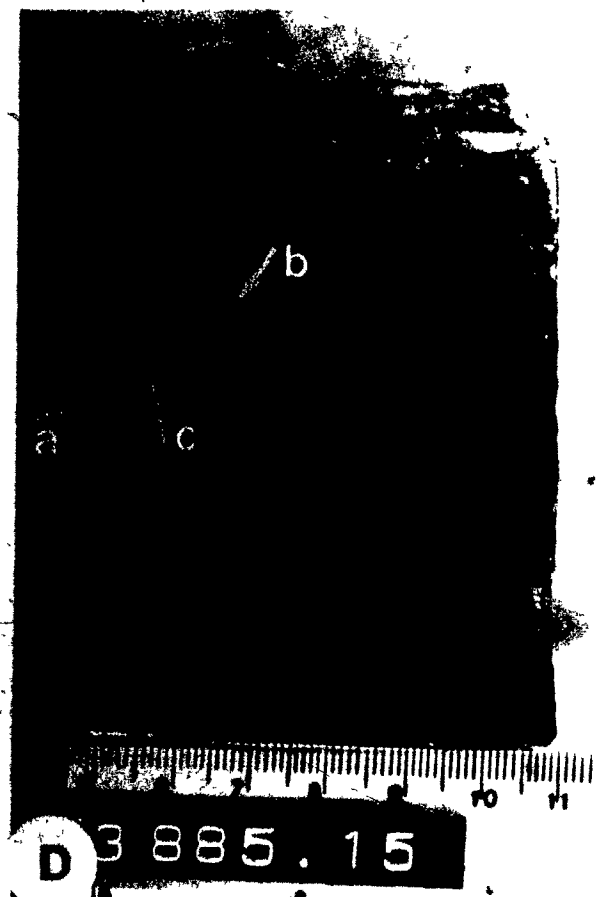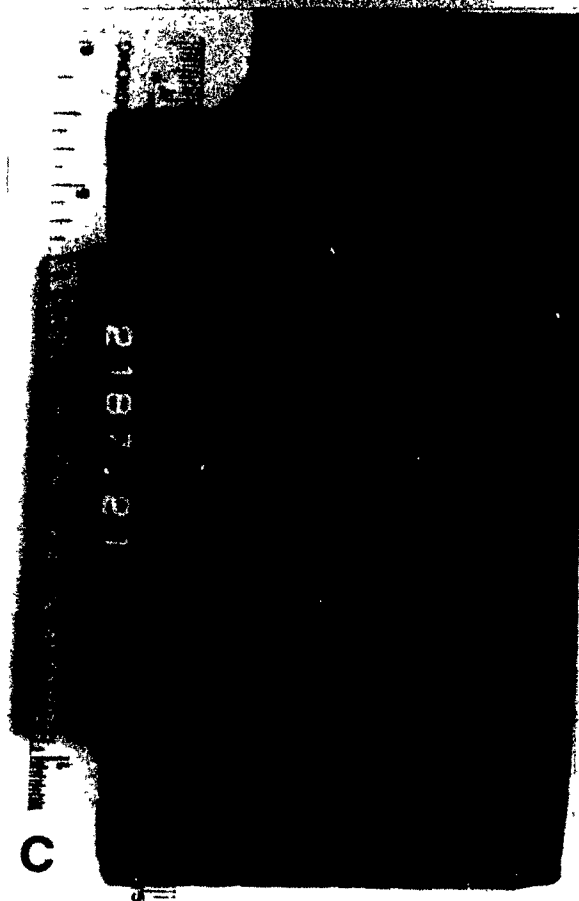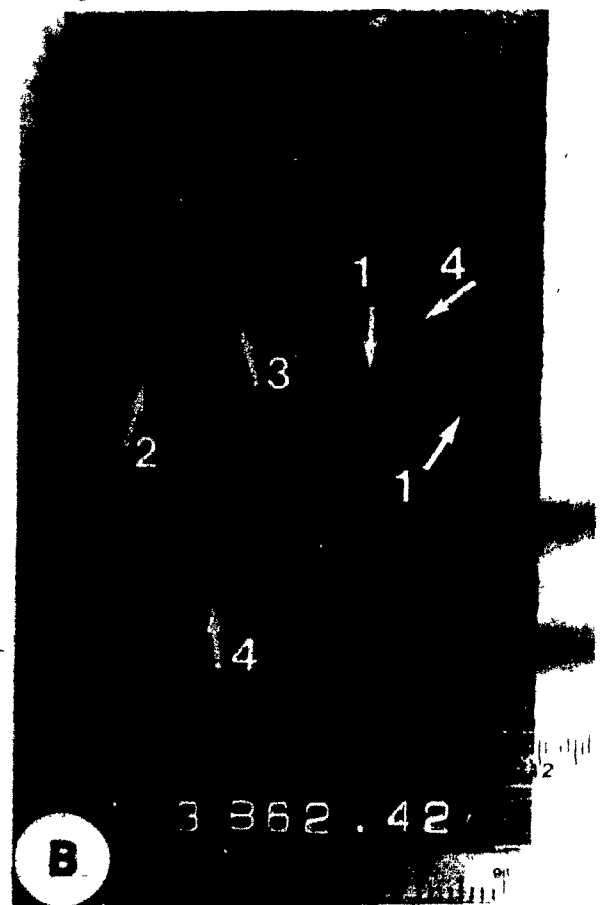
PLATE 3

Mechanical compaction in different reservoir sandstones of the Hibernia field.

(A)   A loosely packed fine-grained sandstone with large fossil fragments (mainly pelecypods). The quartz grains have point contacts among one another; however, with fossil fragments they form pressure solution contacts. The intergranular porosity is interpreted mainly as primary. Bedding direction sub-horizontal. Avalon Sandstone, O-35, 2185.8 m. Plane-polarized light. Scale bar: 500 um.

(B)   Moderately compacted sandstone showing concavo-convex contacts between different framework grains. Note the presence of pyrite in the lower part of photograph. Out of 9.7% of thin-section porosity, 5.3% (54% of total porosity) in this sample is secondary. "B" Sandstone, O-35, 3185.90 m. Plane-polarized light. Scale bar: 500 um.

(C)   Advanced compaction indicated by pressure solution seams (stylolite, arrow) and concavo-convex grain-contacts. Bedding direction vertical. Hibernia Sandstone, B-08, 3606.18 m. Plane-polarized light. Scale bar: 100 um.

(D)   As a result of advanced mechanical compaction the deepest reservoir sandstones of the Hibernia field show reduced intergranular porosity with long concavo-convex contacts among different framework grains (arrow). This sample is cemented with terroan dolomite. Bedding direction vertical. Jeanne d' Arc Member, O-35, 4534.82 m Plane-polarized light. Scale bar: 500 um.
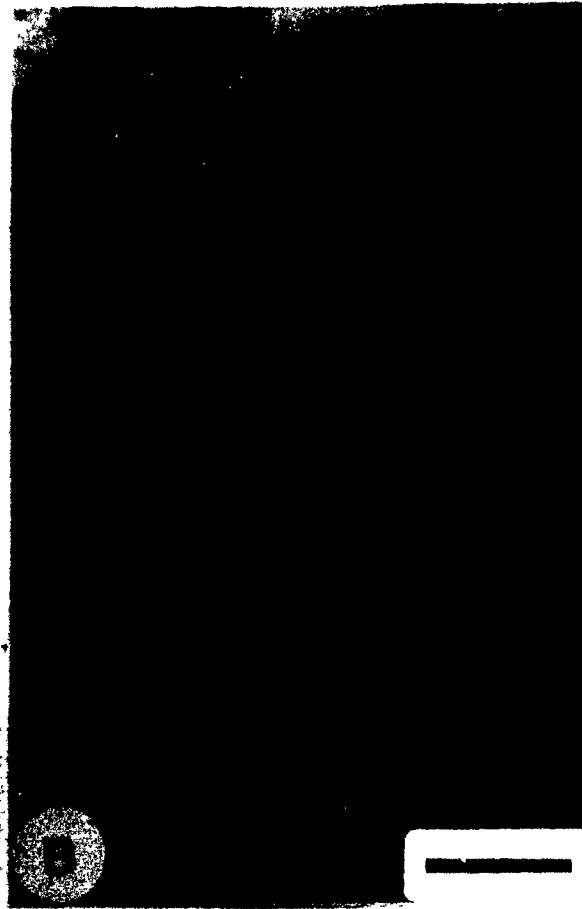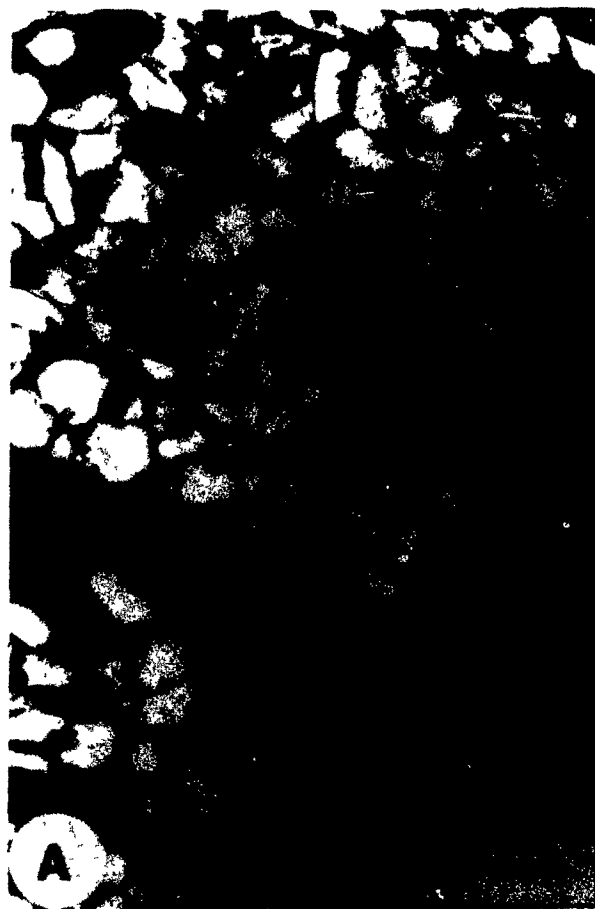
contacts only with some fossil and limestone fragments. As a result of the low level of mechanical compaction, the presence of sedimentary rock fragments (average 10.6%) does not have a major effect in reducing porosity. Sandstones from this zone contain a high percentage of calcite cement ranging from 25% to 30% (in the tight sandstones). With 40% original porosity a minimum of 10 to 15% porosity was lost by mechanical compaction prior to calcite cementation. Calcite precipitation therefore occurred relatively early in the diagenetic history of the Avalon Sandstone.

3.2.2.3 "B" Sandstone   Significant porosity changes due to mechanical compaction occur between 2500 to 3000 m depth. Above 2500 m, sandstones show a fair degree of compaction. Below 3000 m, the effect of overburden is manifested by the development of long concavo-convex grain contacts (Plate 3B), flowage of argillaceous grains around quartz grains, and fracturing of quartz grains. Some of these fractures were developed following calcite dissolution (see Chapter 5). Many of the fractured grains were subsequently healed by calcite, dolomite or pyrite.

3.2.2.4 Hibernia Sandstone   Mechanical compaction in the Hibernia Sandstone is advanced, particularly in horizons which escaped early cementation (e. g. by quartz overgrowth, calcite and siderite cementation, etc.).   Stylolitic structures have been observed in a few samples (Plate 3C). In some thin sections, quartz grains are floating in calcite cement indicating early cementation.   Most of the early

calcite cement, however, was later dissolved, resulting either in framework grain fracturing (due to subsequent compaction) or in a loosely packed fabric.

3.2.2.5   Jeanne d' Arc Member Only a limited number of samples were available from the Jeanne d'Arc member. These indicate an advanced level of compaction (Plate 3D). Advanced pressure solution contacts of quartz grains with schist and limestone fragments are common.

3.2.3 Chemical Diagenesis

Precipitation of authigenic minerals and dissolution/ alteration of sandstone constituents are major effects of chemical diagenesis. Several factors may control chemical diagenesis, i.e. initial composition and depositional environments; pore fluid composition and degree of fluid circulation; temperature/pressure gradients; rate of burial; and sandstone/shale ratio.

In the Hibernia Field, ten authigenic minerals were identified comprising 1.6 to 47.7% (average 15.2 %) of the bulk volume. Only six of them (quartz, calcite, dolomite, kaolinite, siderite, and pyrite) are commonly present (Table 3.2) and are described below.

3.2.3.1 Siderite Precipitation

In general, siderite is a minor authigenic mineral. However, locally it may amount up to 31.8%. It is one of the earliest cement phases. Siderite precipitation continued during the formation of early quartz overgrowths (Plate 5D).

56

Table 3.2 Detrital and authigenic minerals and porosity (in percent) of bulk rock volume for different reservoir sandstones.

ABBREVIATIONS

CAL = Calcite

CRF = Chert rock fragments

DOL = Dolomite

F   = Feldspar

FOS = Fossils

HM   = Heavy minerals (including opaques)

LRF = Limestone rock fragments

MIRF = Metamorphic and igneous rock fragments

MXT = Matrix

PY   = Pyrite

Q   = Quartz

QOV = Quartz overgrowth

SHRF = Shale rock fragments

SID = Siderite

SRF = Sandstone/siltstone rock fragments

TOTϕ= Total porosity

VRF. = Volcanic rock fragments

	% DETRITAL											% AUTHIGENIC MINERALS						
Depth (m)	Q	F	SRF	SHRF	CRF	LRF	FOS	MIRF	VRF	MXT	HM	QOV	CAL	DOL	CLAY	PY	SID	TOTØ

(A) AVALON SANDSTONE

Depth (m)	Q	F	SRF	SHRF	CRF	LRF	FOS	MIRF	VRF	MXT	HM	QOV	CAL	DOL	CLAY	PY	SID	TOTØ
2184.6	55.3	3.7	2.4	5.7	2.5	1.2	2.6	---	---	5.3	0.6	4.2	---	---	4.0	Tr	Tr	12.5
2185.8	43.9	3.4	5.5	2.5	1.2	1.6	23.4	---	---	2.9	--	0.4	2.4	---	3.6	Tr	---	9.2
2190.3	59.8	4.3	0.3	3.1	1.5	---	---	0.2	---	11.5	5.1	3.5	---	---	4.5	---	---	6.2
2190.8	59.1	5.1	1.6	1.6	0.4	---	---	---	---	10.8	6.7	2.0	---	---	3.5	---	Tr	9.2
2197.5	61.4	2.2	1.0	3.1	0.4	0.8	8.0	---	---	---	1.0	2.7	---	---	1.4	Tr	---	18.0
2197.9	59.1	3.6	1.4	1.5	1.0	---	---	0.6	---	1.0	0.4	0.6	30.2	---	0.6	---	---	0.0
2197.9*	70.5	3.0	1.1	3.2	0.8	---	0.4	---	---	1.0	2.2	5.4	0.6	---	1.6	---	---	10.2
2571.5	61.0	2.4	2.2	5.0	Tr	---	---	---	---	Tr	Tr	1.0	28.4	---	---	---	Tr	0.0
2578.8	62.3	1.8	1.4	0.4	Tr	8.2	0.4	0.2	---	0.7	0.2	2.2	0.4	---	0.6	---	---	21.2
2659.6	60.7	2.4	1.1	1.4	1.2	0.5	Tr	0.7	---	7.8	0.6	9.8	1.7	---	0.7	Tr	---	11.4
2661.1	54.7	4.4	1.2	1.7	2.1	2.1	0.3	0.6	Tr	2.1	0.5	0.4	28.9	---	1.0	---	---	0.0
Av	58.9	3.3	1.7	2.7	1.0	1.3	3.2	0.2	Tr	3.9	1.6	2.9	8.4	0.0	2.0	Tr	Tr	8.9

(B) "B" SANDSTONE

Depth (m)	Q	F	SRF	SHRF	CRF	LRF	FOS	MIRF	VRF	MXT	HM	QOV	CAL	DOL	CLAY	PY	SID	TOTØ
3174.9	56.0	3.5	---	0.5	1.4	0.5	---	---	---	0.5	5.2	0.8	31.6	---	---	---	---	0.0
3178.0	67.0	0.6	1.6	0.2	5.3	0.0	0.8	---	0.2	---	3.5	2.7	3.4	0.7	1.4	---	---	12.6
3179.1	65.3	1.6	0.5	0.1	1.9	0.1	Tr	0.1	0.1	5.0	0.3	9.8	3.1	0.3	1.0	---	---	10.3
3180.3	57.9	6.0	0.2	0.4	1.3	2.6	1.5	2.0	---	1.8	Tr	2.7	23.2	---	0.4	---	---	0.0
3185.9	57.2	4.5	0.4	-	1.2	0.4	---	---	---	1.4	1.4	3.5	---	20.3	---	---	---	9.7
3131.5	61.2	4.7	1.6	1.6	2.9	1.9	Tr	---	---	2.3	2.1	8.4	2.4	Tr	1.3	---	---	9.6
Av	60.8	3.5	0.7	0.5	2.3	0.9	0.4	0.4	Tr	1.8	2.1	4.7	10.6	3.5	0.7			7.1

(C) HIBERNIA SANDSTONE

Depth (m)	Q	F	SRF	SHRF	CRF	LRF	FOS	MIRF	VRF	MXT	HM	QOV	CAL	DOL	CLAY	PY	SID	TOTØ
3481.3	67.4	2.1	0.9	2.1	1.7	---	---	0.2	0.5	4.1	0.4	11.4	---	Tr	0.3	---	---	8.9
3482.6	71.9	2.6	0.3	1.0	0.8	---	---	---	---	2.7	1.3	5.8	0.3	1.0	0.2	---	---	12.1
3483.4	67.5	1.4	0.6	1.0	1.8	---	---	Tr	---	7.9	0.8	10.4	---	Tr	2.3	---	---	6.3
3555.1	81.5	1.0	0.6	---	0.6	---	---	0.4	---	1.6	0.2	1.6	---	---	---	---	---	12.5
3606.2	79.0	---	0.3	---	0.8	0.2	---	---	---	13.6	1.1	1.5	---	Tr	0.1	---	---	3.4
3619.4	63.6	4.5	1.3	0.5	1.4	0.1	---	0.1	Tr	4.5	0.2	9.0	0.6	0.2	1.2	---	---	12.9
3622.4	85.3	---	0.2	---	1.7	---	---	---	---	0.6	--	1.2	---	---	1.2	---	---	9.8
3624.2	66.8	7.4	0.9	0.9	0.2	---	---	---	---	1.7	1.4	11.2	0.3	---	1.5	---	---	7.7
3845.8	74.0	0.9	0.3	0.3	1.3	---	---	---	---	2.1	0.6	8.4	---	---	1.4	---	Tr	10.7
3846.5	75.1	---	0.4	---	1.0	---	---	---	---	---	0.1	4.2	---	---	---	---	Tr	19.2
3849.75	69.8	0.4	0.6	1.0	1.3	---	---	---	---	0.7	0.1	9.2	---	---	---	---	Tr	16.9
3850.3	70.2	0.4	0.2	---	0.4	---	---	0.4	---	1.5	0.2	4.3	0.3	---	0.2	---	Tr	21.9
3850.7	71.5	---	0.6	---	0.4	---	---	---	---	0.2	Tr	2.0	0.3	---	0.2	---	---	25.0
3854.5	76.6	---	1.2	---	0.4	---	---	---	---	2.2	Tr	2.9	---	---	---	---	4.1	12.6
3860.8	36.2	2.1	---	---	0.4	3.8	7.6	---	---	0.4	1.8	---	15.9	---	---	---	31.8	0.0
3879.0	71.1	0.2	0.4	---	0.6	---	---	---	---	0.7	Tr	2.1	---	---	---	8.3	---	16.0
3895.2	83.3	0.2	---	---	0.4	---	---	---	---	1.0	--	0.9	---	---	---	---	---	14.2
Av	71.2	1.4	0.5	0.4	0.9	0.3	0.5	0.1	Tr	2.7	0.3	4.9	1.0	0.1	0.5	0.5	2.1	12.4

(D) JEANNE D' ARC MEMBER

Depth (m)	Q	F	SRF	SHRF	CRF	LRF	FOS	MIRF	VRF	MXT	HM	QOV	CAL	DOL	CLAY	PY	SID	TOTØ
4533.5	65.9	2.2	0.2	0.5	1.1	3.5	0.2	---	---	10.8	1.3	4.5	3.4	3.3	3.1	---	---	0.0
4534.0	51.8	1.0	4.2	2.0	2.8	4.0	0.8	1.0	---	2.4	Tr	---	2.9	19.5	0.6	---	---	0.0
Av	58.8	1.6	2.2	1.6	1.9	3.7	0.5	0.5	Tr	6.6	0.6	2.2	3.1	11.4	1.8	0.0	0.0	0.0

Five different types of siderite were observed (Plates 4 and 5): (i) "Wheatseed" siderite, which consists of lenticular crystals with a wheat seed shape and an average length of about 40 um (Plate 4A). Sometimes "wheatseed" siderite shows a radiating pattern in the pores. Some worm-tubes (?) were filled with early siderite which protected them from collapse. (ii) Small euhedral/subhedral siderite crystals (35 um), replacing early ferroan calcite cement (Plate 4B, e.g. at 2560 m in the B-27 well). (iii) Spherulitic siderite occasionally contains pyrite in the central part (Plate 4D) or occurs as grain-rimming cement (Plate 5A and 5B). (iv) Dense siderite-rich laminae occur in fine-grained sandstones (Plate 4C). These siderite-rich sandstones generally occur immediately above shale beds (e.g. at 3854.45 and 3910.45 m, in B-27). (v) Siderite nodules are commonly present in the siltstone-shale facies (Plate 5C). Type 1 to 3 are usually <10% of the bulk rock volume while Type 4 and 5 are commonly associated with shale beds.

3.2.3.2 Quartz Overgrowth

Quartz overgrowth represents the second most abundant type of cement in the Hibernia reservoir sandstones, ranging from trace amounts to 11.2%, with an average 3.7% of the total rock volume. In the Avalon Sandstone, quartz overgrowth is of minor importance (2.9%). However, in the "B" and Hibernia Sandstones, quartz overgrowths become more abundant with depth; about 28% of the sandstone samples contain significant amounts (>8 %) of quartz cement (Fig.

PLATE 4

Photomicrographs of different types of authigenic siderite.

(A) "Wheatseed" siderite crystals (arrow) filling major part of available pore space. Avalon Sandstone, O-35, 2190.81 m. Plane-polarized light. Scale bar: 500 um.

(B) Siderite (S) crystals (40 to 60 um long) replacing early ferroan calcite cement (C). Quartz grains (bottom left) are partly replaced by calcite cement (arrow). Avalon Sandstone B-27, 2562.8 m. Plane-polarized light. Scale bar: 50 um.

(C) A siderite-rich zone with fine-grained quartz. Such zones are usually present above dark gray shales. Note extensive corrosion of quartz grains by siderite. Hibernia Sandstone, B-27, 3910.45 m. Plane-polarized light. Scale bar: 100 um.

(D) Spherulitic siderite (S) containing pyrite (P) in the centre. This type of siderite is rare. Hibernia Sandstone, B-27, 3895.19 m. Plane-polarized light. Scale bar: 50 um.
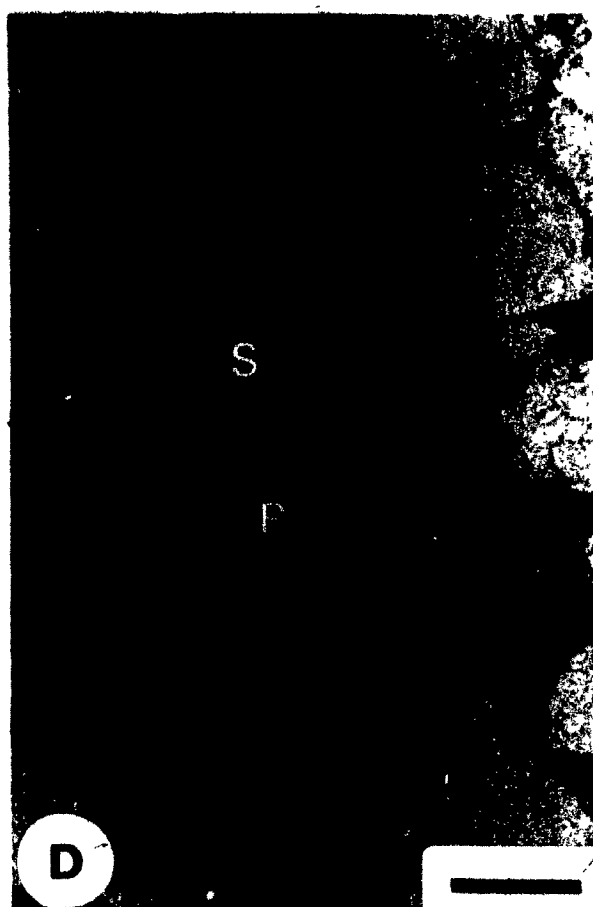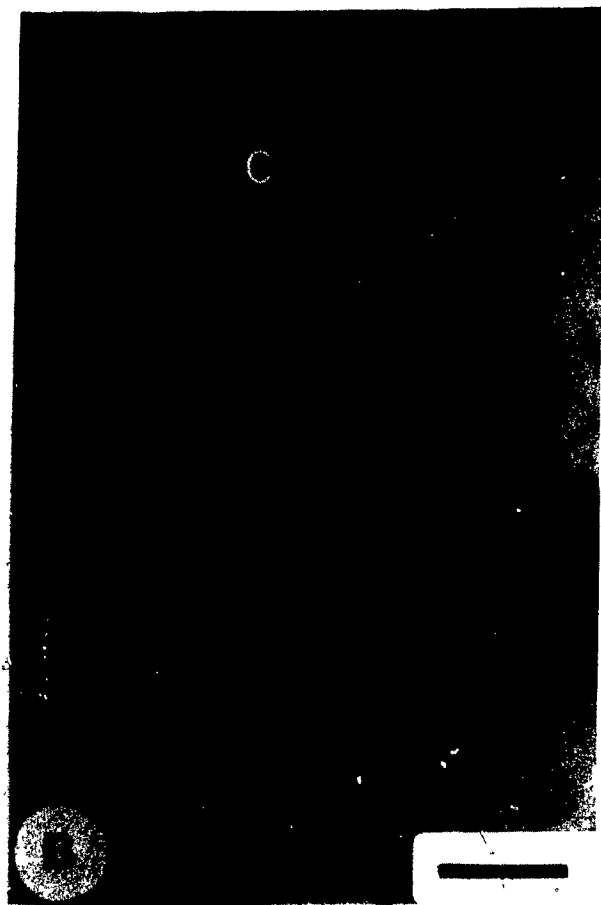
PLATE 5

Different types of siderite in thin sections and drill-core samples (continued).

(A) Authigenic siderite forming grain rimming cement (arrows) around quartz grain. Hibernia Sandstone, B-27, 3854.45 m. Plane-polarized light. Scale bar: 100 um.

(B) Same as above, crossed nicols.

(C) Drill-core of siltstone/shale facies containing siderite nodules (arrows). Bedding direction sub-horizontal. Hibernia Sandstone, K-18, 3882.35 m. Scale bar in cm.

(D) Small crystals of siderite (arrow) encircling outline of detrital quartz grains. Precipitation of siderite occurred mostly prior to the formation of quartz overgrowth but some continued to grow during quartz precipitation. Hibernia Sandstone, B-27, 3854.45 m. Plane-polarized light. Scale bar: 100 um.
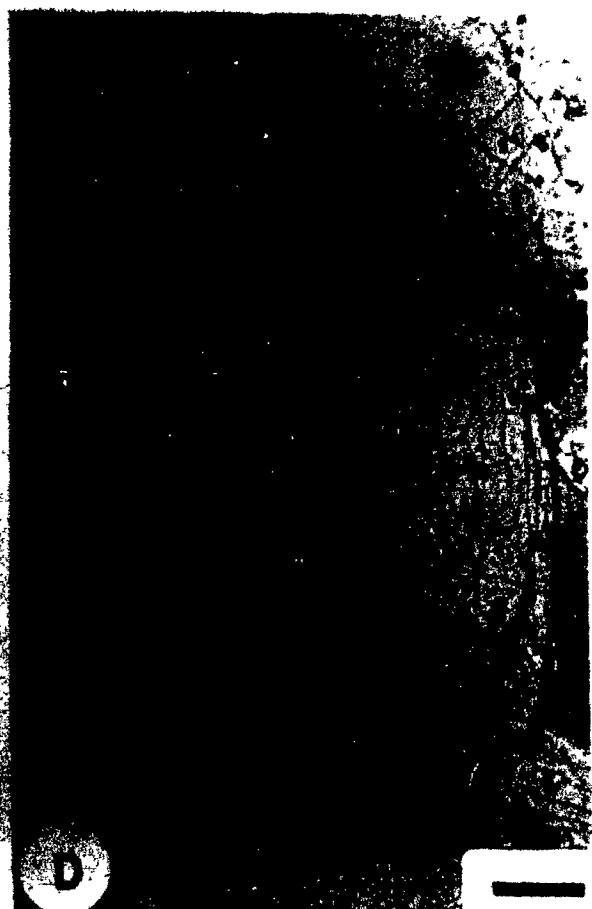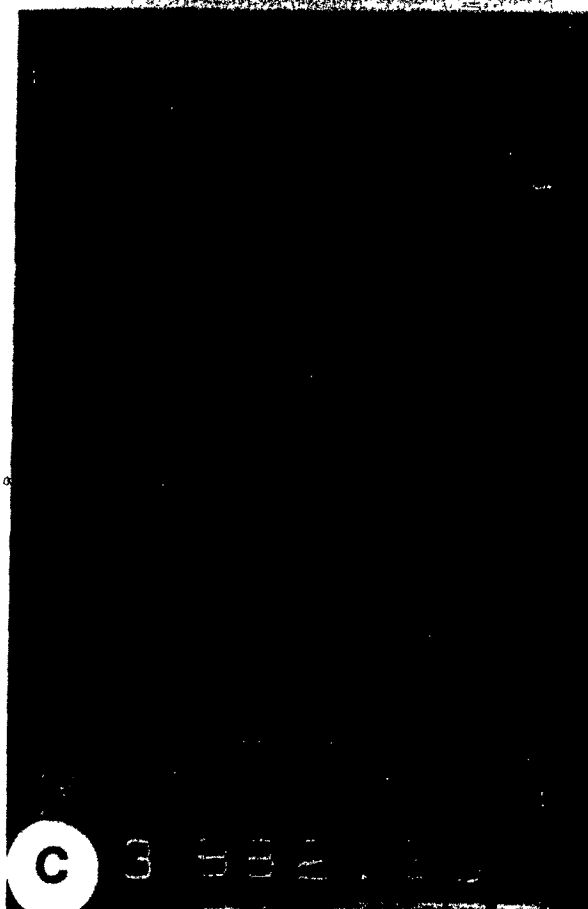
3.4).

Many episodes of quartz cementation have occurred throughout the diagenetic history of the reservoir sandstones in the Hibernia field. It is, therefore, difficult to estimate the depth of quartz precipitation as the present depth of a diagenetic feature does not necessarily indicate its depth of formation. The quartz cements can be grouped into four categories:

(1) Chalcedony cement and opal-CT (?);

(2) Discontinuous (euhedral/subhedral) quartz overgrowths;

(3) Early to middle stage quartz overgrowths (0 to 3000 m); and

(4) Late stage quartz overgrowths (below 3000 m).

3.2.3.2.1 Chalcedony Cement and Opal-CT (?)

Chalcedony cement, Opal-CT (?) and interstitial drusy quartz has been observed in one sandstone sample (1685 m; C-96)./ Most of the intergranular pores in this sample are filled with opal-CT (?) (> 25%) which is partly recrystallized into chalcedony cement and drusy quartz. Chalcedony is characterized by radial fibrous crystals filling pores up to 170 um in size (Plate 7B).

3.2.3.2.2 Discontinuous (euhedral/subhedral) Quartz Overgrowth

The types of quartz vary from small prisms to fully developed continuous overgrowths surrounding the entire grain (Plate 6A, 6B, and 7D). However, some quartz grains show two or more discontinuous small overgrowths of

64
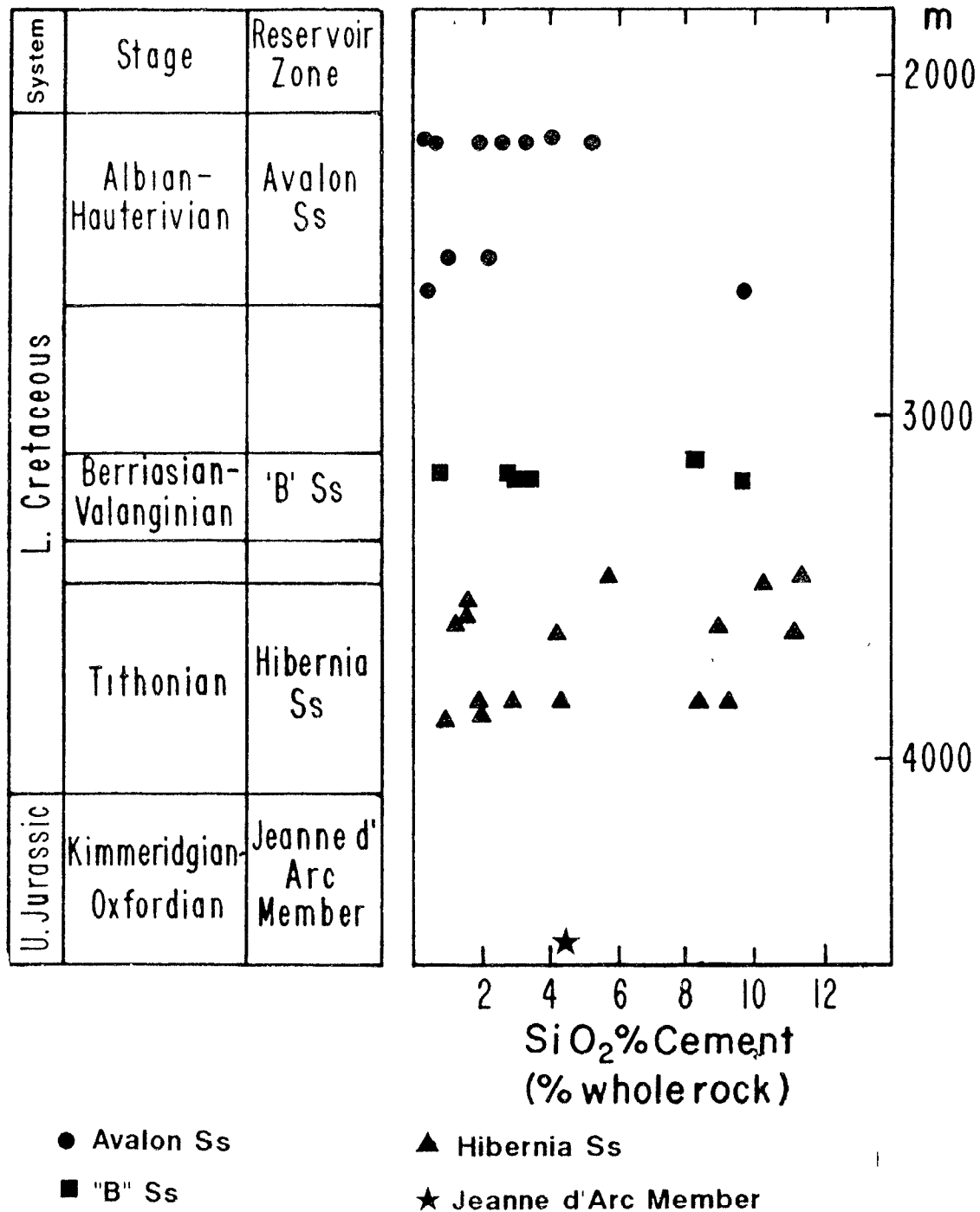
Fig. 3.4 Silica cement versus burial depth in the sandstones of the Hibernia field.

euhedral/subhedral quartz prisms (Plate 6C). Lack of sufficient silica in the pore fluids is most likely the cause of incomplete quartz overgrowth.

3.2.3.2.3   Early to Middle Stage   Quartz Overgrowths (0 to 3000 m)

Petrographic observations indicate that minor quartz overgrowths occurred before early ferroan calcite cement. Early quartz overgrowths have also been reported by other workers (Sibley and Blatt, 1976; Lindquist, 1977; Tillman and Almon, 1979). Where early ferroan calcite did not precipitate and the pore water supplied sufficient amounts of silicon, precipitation of quartz continued to the point where an interlocking mosaic of quartz cements developed, drastically reducing intergranular porosity (Plate 7C). Early to middle stage (from 0 to 3000m depth) quartz cement is corroded and partially replaced by calcite and dolomite. Where these carbonate cements have been dissolved, corroded quartz overgrowths are used as a criterion to recognize secondary porosity (see Chapter 5).

3.2.3.2.4   Late   Quartz Overgrowth (below 3000 m)

In contrast to early quartz overgrowths, late quartz overgrowths are not affected by corrosion (Plate 7D). The substantial size and distinct shape of these overgrowths suggest (but do not prove) a possible late origin. Authigenic kaolinite occurs only below 3100 m. Kaolinite engulfed in quartz overgrowths provides another piece of evidence for late quartz overgrowth. Quartz overgrowths may

PLATE 6

Photomicrographs showing syntaxial quartz overgrowths.

(A) Medium-grained sandstone showing broad syntaxial quartz overgrowths (OV). Pressure solution is not an immediate source of silica in this case. Hibernia Sandstone, B-08, 3481.28 m. Plane-polarized light. Scale bar: 100 um.

(B) Scanning electron micrograph showing advanced quartz overgrowths and their interpenetrations. Hibernia Sandstone, B-08, 3483.43 m. Scale bar: 10 um.

(C) Quartz grain displaying domain overgrowth, i.e. several individual subhedral/euhedral quartz crystals merged to form a continuous overgrowth (OV). Hibernia Sandstone, B-27, 3850.27 m. Plane-polarized light. Scale bar: 50 um.

(D) Advanced quartz overgrowths (OV) showing compromise and "sutured" boundaries between the secondary quartz of different grains. In this sample, boundaries between detrital grains and quartz overgrowths are not always visible, and therefore quartz overgrowths may be misinterpreted as a pressure solution contacts. Hibernia Sandstone, B-08, 3480.83 m. Crossed nicols. Scale bar: 50 um.

PLATE 7

Syntaxial quartz overgrowths (continued) and secondary porosity

(A) Absence of silica cementation inspite of availability of pores and the absence of clay coatings. Porosity (P) in this sample is mainly secondary in origin. Hibernia Sandstone, B-27, 3850.65 m. Plane-polarized light. Scale bar: 500 um.

(B) Intergranular pore space almost completely filled by fibrous chalcedony cement. Late Cretaceous sandstone, C-96, 1670.50 m. Crossed nicols. Scale bar: 50 um.

(C) Interlocking mosaic of quartz overgrowths almost completely filling all available pores. Note thin clay rims (arrows) separating detrital quartz grains from authigenic silica. Hibernia Sandstone, B-08, 3480.83 m. Crossed nicols. Scale bar: 50 um.

(D) Quartz grains with pressure solution contacts (arrows 1) and associated late quartz overgrowths (arrow 2). Hibernia Sandstone, C-96, 3927.20 m. Plane-polarized light. Scale bar: 100 um.

extend into adjacent pores of secondary origin although such quartz is not common. Minor amounts of quartz overgrowths next to pressure solution contacts also appear to indicate a late stage of this cement phase (Plate 7D).

Most of the samples having significant (>8%) quartz cement are from depths below 3000 m. Petrographic evidence shows that this increase in quartz cement is mostly not due to pressure solution in the immediate host sediments. Many samples show advanced quartz overgrowths without any accompanying pressure solution effects (Plate 6A, 6D). On the other hand, many coarser and deeper sandstones do not display any significant quartz overgrowths, in spite of low matrix contents, absence of clay coatings, evidence of pressure solution (concavo-convex contacts), and availability of pore space. In the B-27 well, medium-grained, matrix-free porous Hibernia Sandstone shows only small amounts of quartz overgrowth. These sandstone samples show evidence for significant secondary porosity. It seems that early calcite cementation prevented quartz overgrowths from forming. When the calcite cement was dissolved later on, silica-rich pore fluids were not available (Plate 7A).

3.2.3.3 Feldspar Overgrowths

Feldspar overgrowths (upto 20 um thick) form a very minor authigenic phase. The overgrowth is distinct from the detrital grains due to the lack of inclusions and alteration features (Plate 10A).

3.2.3.4 Clay Minerals

Microscopic and SEM/EDS studies indicate the presence of minor amounts of authigenic clay minerals (kaolinite, chlorite, illite and/or mixed-layer illite/smectite) in several sandstone samples. These authigenic phyllosilicates occur as grain coatings, platelets, as well as fibrous crystals.

3.2.3.4.1 Kaolinite

The amount of authigenic kaolinite is generally less than 1%; however, in a very few samples, it may amount up to 6%. It occurs as small "booklets", several microns in size, which form a mesh-work in secondary and primary pores (Plate 8B, 8C and 9D). Commonly it occupies only a portion of the pores as evidenced by the preserved intercrystalline porosity between the kaolinite flakes (Plate 8B). Occasionally, however, kaolinite completely occludes porosity (Plate 8A, 8C). Kaolinite occurs commonly in sandstones below 3000m subsurface depth, whereas above 3000 m it was not observed. Kaolinite is absent from samples which are completely cemented by carbonate cebments. It is one of the late cements (post-feldspar dissolution) and commonly occupies oversized, irregular and elongated pores.

3.2.3.4.2 Chlorite

Minor amounts of chlorite were observed in the Avalon and "B" Sandstones. This mineral is rarely present in the Hibernia Sandstone and Jeanne d'Arc Member. Chlorite occurs both as a thin grain coatings and as fibrous crystallites

PLATE 8

Authigenic kaolinite in the reservoir sandstones.

(A) Large (50 um) pore-filling crystals of kaolinite (K). Hibernia Sandstone, B-08, 3619.412 m. Crossed nicols. Scale bar: 50 um.

(B) Authigenic booklets of kaolinite (arrow 1), partly filling an elongated secondary pore. Note corroded and irregular outline of quartz grains (arrow 2) which were probably replaced by carbonate cement that itself was dissolved later on (see also Plate 26D). Hibernia Sandstone, B-27, 3849.75 m. Plane-polarized light. Scale bar: 50 um.

(C) Authigenic kaolinite (K) completely filling an intergranular elongated pore. Hibernia Sandstone, B-08, 3555.09 m. Crossed nicols. Scale bar: 50 um.

(D) Scanning electron photomicrograph showing well developed authigenic kaolinite crystals which occur as face-to-face stacks of pseudohexagonal platelets. Note two irregular elongated pores. The left-hand pore (filled with kaolinite) still shows the existence of micropores between the detrital grain boundaries and the pore-filling, and within the pore filling itself. Hibernia Sandstone, B-08, 3483.42 m. Scale bar: 10 um.

around framework grains. Radiating fibrous chlorite cement is rare (Plate 9A, 9B). Most of the authigenic chlorite is pale green to yellow-green. In the Hibernia Sandstone, chlorite inclusions in polycrystalline quartz grains are partly dissolved. This dissolution of chlorite may be either in-situ (by acidic pore fluids, see section 6.3) or may have occurred during sediment transport. The presence of chlorite can inhibit the formation of quartz overgrowth and can also drastically reduce the permeability. In the reservoir sandstones of the Hibernia field, the effect of chlorite on later formation of quartz overgrowths seems negligible.

3.2.3.4.3 Illite and/or Illite/Smectite (I/S) (?)

Illite is recognized under the SEM by its characteristic morphology (bridging pore space between detrital grains) and identified with the help of an energy dispersive spectrometer (EDS, Plate 10B). In a very few samples, substantial amounts (2 to 5%) of illite and/or I/S (?) occur forming rims of uniform thickness around available pores (Plate 9C,). The amount of authigenic illite decreases away from sandstone-shale contacts (i.e. at 2600.64 m, in the B-27 well) and, in general, is negligible.

3.2.3.5 Dead Oil

Dead oil or hydrocarbon residues are diagenetic products which constitute pore-filling materials. They have been observed in a few samples, either as a grain coatings or pore filling material (Plate 10C). Secondary pores resulting

75

PLATE 9

Authigenic clay minerals.

(A) Intergranular pore space completely filled by radiating fibrous pale-green authigenic chlorite cement. Hibernia Sandstone, B-O8, 3483.42 m. Plane-polarized light. Scale bar: 50 um.

(B) Same as above with crossed nicols.

(C) A coarse-grained sandstone showing two authigenic phases, i.e. grain coating with illite/smectite (I/S; arrow), and kaolinite (K). The quartz overgrowth (seems to be reworked) is followed by mixed-layer I/S (or illite) rims around the available pores. The remaining pore space was partly to completely filled by kaolinite. Hibernia Sandstone, C-96, 3908.3 m. Plane-polarized light. Scale bar: 50 um.

(D) Intergranular pore space completely filled with authigenic kaolinite. SEM photomicrograph. Jeanne d' Arc Member, O-35, 4532.48 m. Scale bar: 10 um.
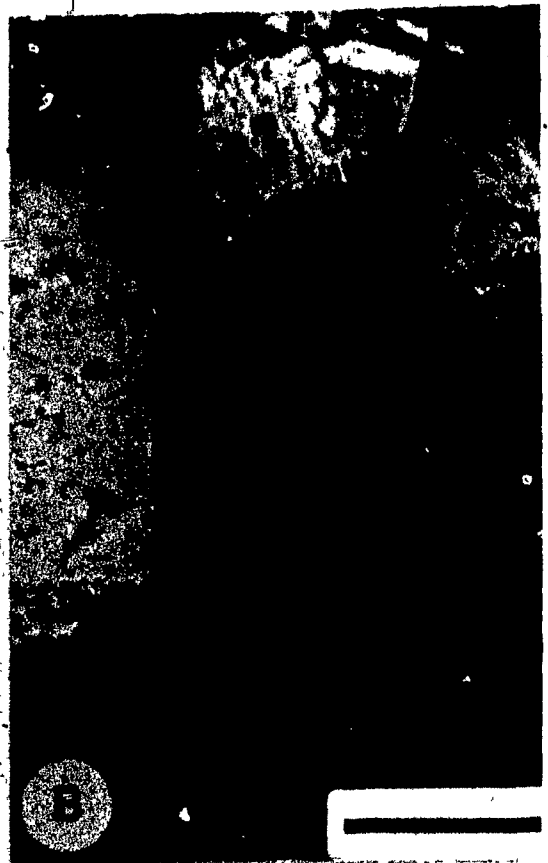
PLATE 10

Authigenic feldspar, illite, and pyrite together with residual hydrocarbons.

(A) Small feldspar overgrowth (arrow) on a plagioclase grain. The altered detrital plagioclase appears turbid while the overgrowth is fresh (arrow). Hibernia Sandstone, B-27, 3849.75 m. Plane-polarized light. Scale bar: 50 um.

(B) Scanning electron micrograph of authigenic illite flakes (arrow) on quartz overgrowths. The illite partly bridges the pore space between different grains. Jeanne d' Arc Member, O-35, 4533.47 m. Scale bar: 10 um.

(C) A pore lined with hydrocarbons (H) indicating oil emplacement prior to the dissolution of a carbonate rock fragment. Small crystals of pyrite denoted by arrows. "B" Sandstone, O-35, 3176.80 m. Plane-polarized light. Scale bar: 50 um.

(D) Early calcite-cemented sandstone containing abundant euhedral pyrite crystals. The pyrite was precipitated before early ferroan calcite cement. "B" Sandstone, O-35, 3174.94 m. Plane-polarized light. Scale bar: 100 um.
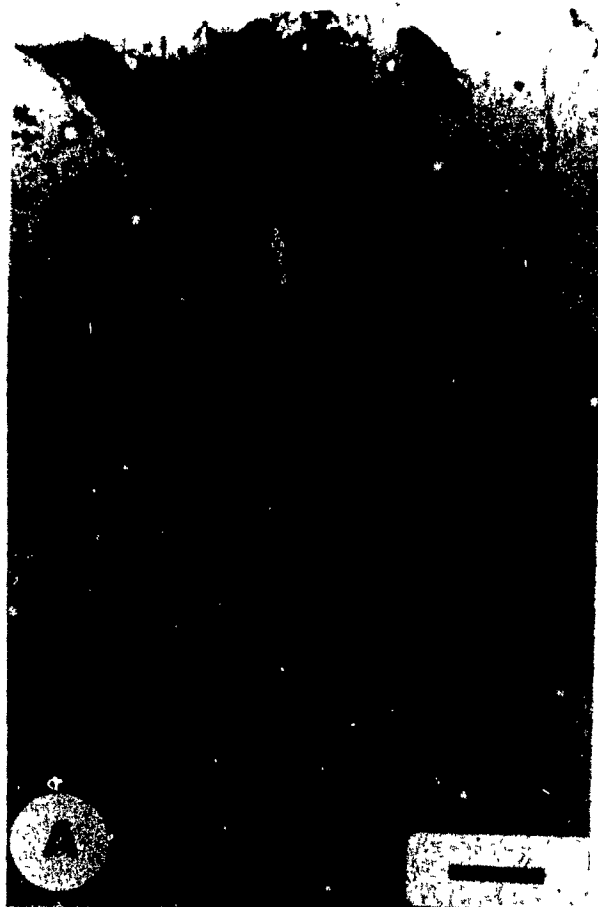
from calcite dissolution (rock fragments and fossils) are partly filled by hydrocarbon residues. In such pores, the presence of authigenic dolomite in the pore centre possibly suggests dolomite precipitation after hydrocarbon migration

3.2.3.6 Pyrite Precipitation
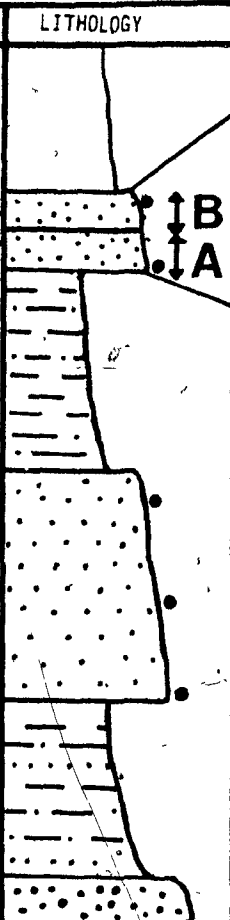
3.2.3.6.1 Early Pyrite

A small amount of pyrite is commonly present in 1) early calcite cement (Plate 10D), 2) fossil fragments, and 3) siderite nodules. It commonly occurs as clusters with crystals of 20 to 80 um diameter. Framboidal pyrite (Brown, 1985) is less common in the sandstones of the Hibernia field.

3.2.3.6.2 Late Pyrite

Late pyrite occurs both as irregular patches and euhedral crystals (averaging 40 um in size) in intergranular pores and fractures. The best example of late pyrite was observed in the Hibernia Sandstone (at 3892 m in the B-27 well). The part of the sandstone which is completely cemented by ferroan-calcite is pyrite-free while a porous zone, only a centimeter away, contains substantial amounts of pyrite (Fig. 3.5). Quartz grain-surfaces studied under SEM from the pyrite-containing porous sandstone zone suggest that it was once cemented with calcite. This relationship suggests precipitation of pyrite after the precipitation and dissolution of ferroan-calcite. The presence of late pyrite has also been substantiated by well-core examination, where late fracture-filling pyrite was

Fig. 3.5 (a): Summary of lithology and petrographic observations from (a) a 5 m long drill-core of the Hibernia Sandstone (B-27). (b) Drill-core photograph at 3892.25 m (marked in Fig. 3.5a). showing contact between calcite-rich (tight-sandstone, upper zone) and calcite-free zones (lower part) (c) Photomicrograph of the same contact. Note presence of pyrite crystals (arrow) only in the lower part of the photograph. The upper half is completely calcite cemented. The bedding direction is horizontal..

DEPTH (m)	LITHOLOGY	CORE OBSERVATIONS	DIAGENETIC FEATURES
3892 (b)		(B) Tight-sandstone	(B) Completely cemented with early ferroan calcite. No pyrite was observed.
	B A	Sharp contact between porous and nonporous sandstone. (A) Oil stained porous sandstone.	(A) Framework grains are more compacted than in (B). 12% secondary porosity. Substantial amounts of pyrite are observed.
		Non-bioturbated and finely laminated shales interbedded with siltstone.	
3894		Fine-grained sandstone with some mudclasts. Pyrite lenses.	Remnants of ferroan calcite cement showing dissolution features. Abundant pyrite crystals. Pyrite crystals are common
3896		Dark gray siltstone and sandstone.	
		• Sample location	

a

BUFFALO 531
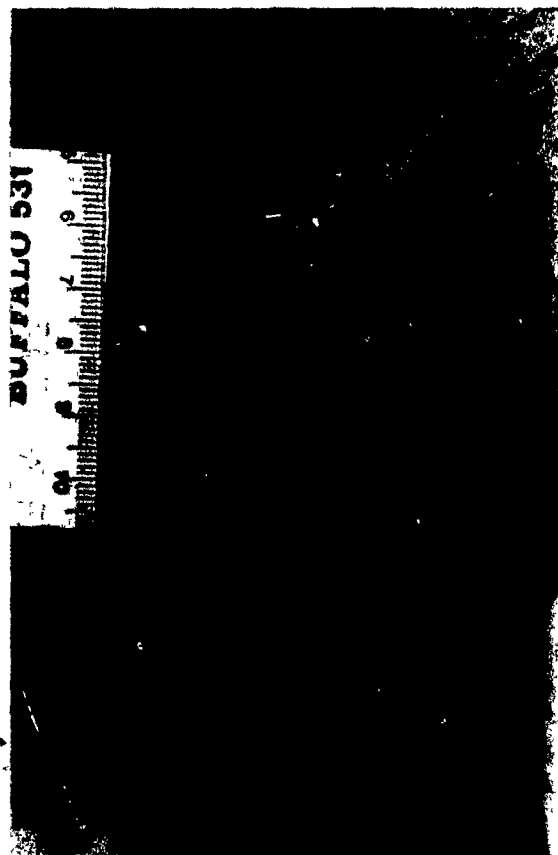
b
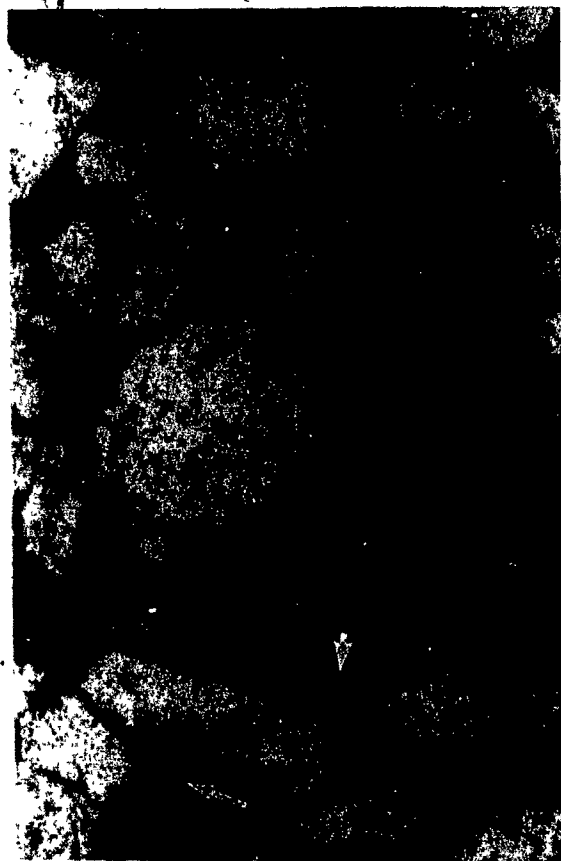
c

observed.

3.2.3.7 · Calcite Cementation

Calcite cement varies in abundance from 0 to 31.6%. Microscopic observations show abundant ferroan calcite cement together with minor iron-free calcite. Thin section staining and textural relationships reveal the presence of three types of calcite cements, i.e. iron-free calcite, early ferroan calcite, and late ferroan calcite.

3.2.3.7.1 Iron-free Calcite Cement (Type 1)

Iron-free calcite cement is usually present near fossil and limestone fragments, which seem an immediate source and/or nucleus for it. In few a samples (i.e. at 2578 m in the B-27 well) syntexial calcite overgrowths on limestone/fossil fragments was also observed. It is not a common cement and was only observed in a few samples.

3.2.3.7.2 Early Ferroan Calcite Cement (Type 2)

Early ferroan-calcite (with variable amounts of iron) following early quartz overgrowths, is the most important carbonate cement in these sandstones. It fills the pores completely and usually forms poikilotopic cements (Plate 11B, 27A). It also occurs as sparry calcite crystals and, less commonly, as granular and prismatic crystals on micritic limestone fragments (Plate 11D). Early fibrous carbonate cement, precipitated around fossil fragments, was also observed but is rare (Plate 11A). Early ferroan calcite cement replaces quartz, feldspar, chert, rock fragments, and

83

PLATE 11

Early calcite cements.

(A) Early fibrous (f) carbonate cement (aragonite?) growing more or less perpendicular to margin of fossil fragment (FR). Avalon Sandstone, O-35, 2197.90 m. Plane-polarized light. Scale bar: 50 um.

(B) Extensive poikilotopic calcite (C) precipitated at shallow burial depth as indicated by framework grains floating in the cement. Note irregular grain boundaries (arrow) of quartz grains replaced by calcite. Hibernia Sandstone, B-08, 3491.36 m. Crossed nicols. Scale bar: 500 um.

(C) Fossil fragment (serpulid worm tube) broken due to mechanical compaction before early calcite (arrow) cementation. Avalon Sandstone, O-35, 2197.90 m. Plane-polarized light. Scale bar: 500 um.

(D) Small granular crystals of calcite (Bathurst, 1958) or orthospar (Wolf and Conolly, 1965) rimming (arrow 1) detrital calcite grain. Large prismatic crystals (arrow 2) continued to grow from the rim crystals into the pores between the detrital quartz grains (Q). Avalon Sandstone, B-27, 2578.84 m. Crossed nicols. Scale bar: 50 um.
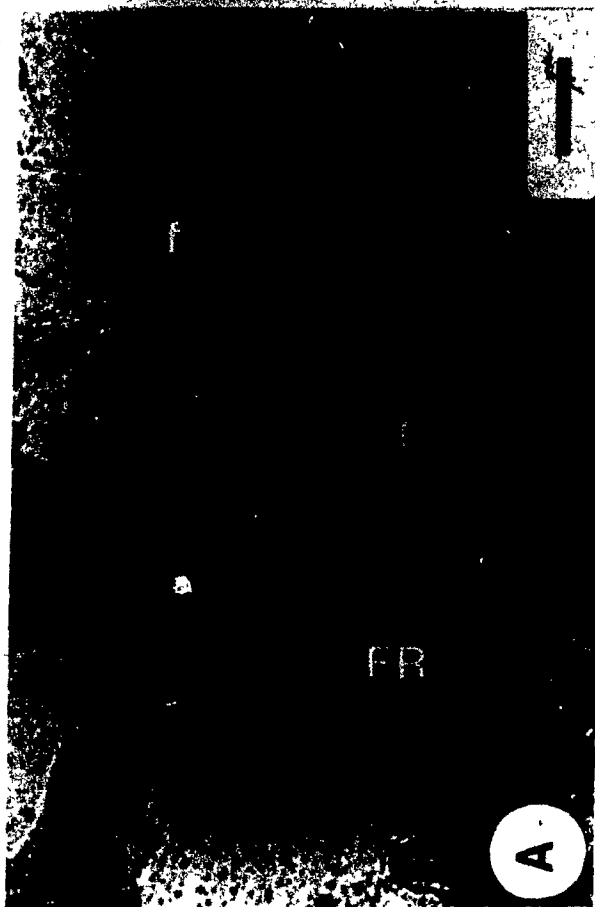
argillaceous matrix. Replacement of plagioclase occurs preferentially along albite twin planes. Grain margin corrosion by early ferroan calcite is common, whereas partial to complete replacement of detrital grains is less frequent. Grains with a thick clay coating are generally not affected by corrosion. In a few samples, early ferroan calcite cement is partly replaced by euhedral siderite (?) crystals (35 µm).

Early precipitation of type 2 calcite cement is indicated by the loose packing of the enclosed grains (Plate 11B, 27A), high (>25%) minus-cement porosity (present porosity plus authigenic cement, including replacement of host grains) and lack of other cements except minor siderite, silica and clay mineral coatings. As a result of early cementation, physical compaction was arrested. Primary pore spaces were completely filled by calcite. Although calcite cementation can occur at or near the surface, petrographic evidence (i.e. minus cement porosity and fractured grains healed with calcite) suggests that in the Hibernia area early ferroan-calcite cementation occurred after some burial (Plate 11C).

Sandstones which are completely cemented by early ferroan calcite (tight-sandstone zones) are quite common in the Avalon and "B" Sandstones, but less abundant in the Hibernia Sandstone. Thin sections covering the contact of tight and porous zones indicate both precipitation (Plate 12) and dissolution (Plate 13) contacts. In the Avalon Sandstone of the B-27 and B-08 wells, such contacts commonly show dissolution features, whereas in the O-35

86

PLATE 12

Contact between the calcite-cemented and calcite-free zone.

(A) Sharp contact (arrow) between calcite-rich (lower) and calcite-free zones. The calcite-free zone is oil stained. The lower part (calcite cemented) has no visible porosity. Avalon Sandstone, 0-35, 2197.90 m. Scale bar in cm.

(B) Photomicrograph from contact of the two zones (upper porous and lower cemented) in Plate 12A. The uncemented porous sandstones contain clay coating which are not present in cemented sandstones. This clay coating at places may give an impression of secondary porosity. Detailed petrographic study at this stratigraphic interval shows mainly primary intergranular porosity. Avalon Sandstone 0-35, 2197.90 m. Plane-polarized light. Scale bar: 100 um .

(C) Close-up of Plate 12B (area outlined by rectangular) showing calcite crystal (C) face pointing towards an open pore (P). This probably indicates a precipitation contact rather than a dissolution boundary. Avalon Sandstone, 0-35, 2197.90 m. Plane-polarized light. Scale bar: 50 um.
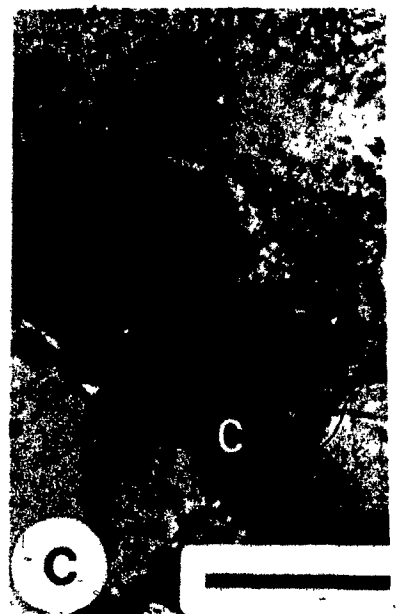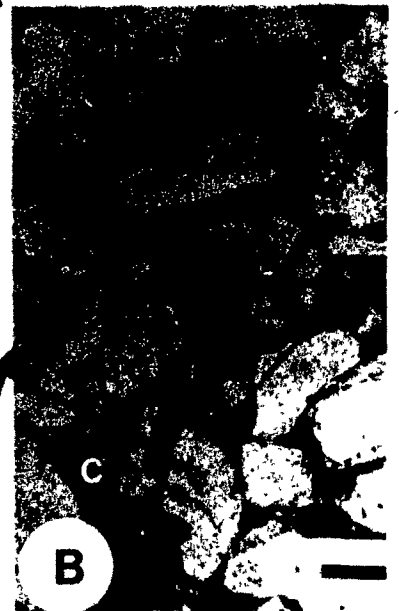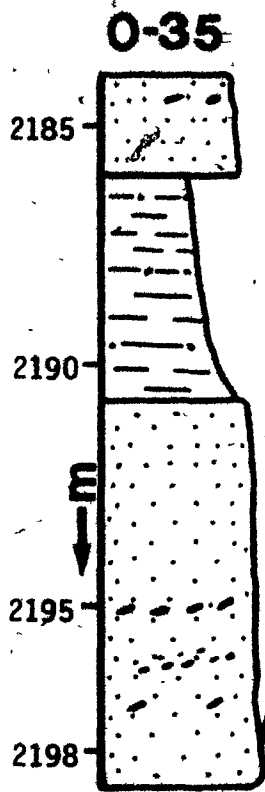
PLATE 13

Dissolution contact between calcite-rich and calcite-free zones.

(A) Within a thick (> 4 m) quartz-rich sandstone a dissolution contact (arrow) occurs between the calcite-cemented (upper) and calcite-free (lower porous) zones. Bedding sub-horizontal. Avalon Sandstone, B-27, 2578.90 m. Scale bar in cm.

(B) Photomicrograph of dissolution contact of calcite cement (Plate 13A). Sandstone in the upper half of the field of view is completely cemented with early ferroan calcite (stained) while in the lower part calcite is partly dissolved generating secondary porosity (arrow). Avalon Sandstone, B-27, 2578.90 m. Plane-polarized light. Scale bar: 100 um.

(C) Fine-grained sandstone with abundant fossil fragments (gastropods) which are partly dissolved producing moldic pores (arrows). Avalon Sandstone, B-27, 2580.85 m. Scale bar in cm.

B-27

2570

2580

2590

2600

2610

A 2578.90

B Q

C 2580.85
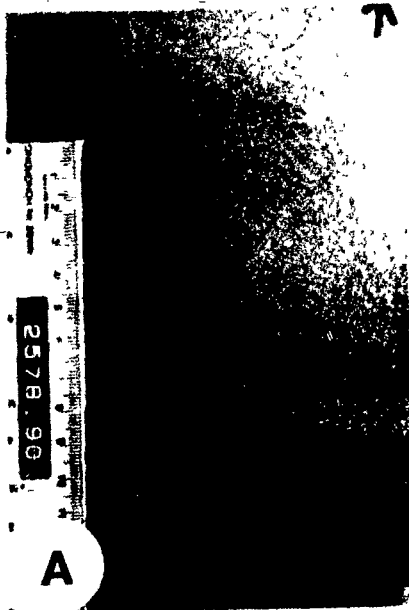
well, these contacts have not been affected by dissolution. The B-27 and B-08 wells are located basinward from the O-35 well. Detailed well-core and microscopic studies of the Avalon Sandstone (O-35, B-27, C-96, and K-18 wells) reveal that these tight-sandstone are the result of localized early calcite cementation rather than partial dissolution of completely cemented sandstones.

3.2.3.7.3   Late Ferroan Calcite Cement (Type 3)

Compared to the early ferroan-calcite, late ferroan-calcite cement is less common. It includes three types: (1) Pervasive sparry calcite, completely filling all reduced intergranular pore spaces. This type was precipitated after significant compaction (Plate 14A) with a minus cement porosity of <15% (i.e. in the K-18 well at 3865 m). (2) Small patches of sparry calcite precipitated between reduced intergranular pores (Plate 14B) or as overgrowth on partly dissolved carbonate fragments. (3) Calcite which dissolved at the site of pressure solution contacts and was reprecipitated on nearby calcite grains in stress free areas. These calcite overgrowths, which are in optical continuity with the host calcite, are iron rich (i.e. in the O-35 at 4534.82 m).

3.2.3.8   Fracture-Filling Ferroan Calcite Cement

Fracture-filling calcite cement has been observed throughout the studied stratigraphic section. It is common in rocks below the Avalon Sandstone. Both grain fractures (within a single grain) and rock fractures (passing through

91

PLATE 14

Late ferroan calcite cement and fracture filling ferroan calcite.

(A) Relatively late ferroan calcite cement (Type 3) precipitated after considerable compaction. Note concavo-convex grain contacts and corroded quartz grain margins (arrow). Hibernia Sandstone, B-27, 3905.00 m. Plan-polarized light. Scale bar: 50 um.

(B) Patches of late sparry calcite cements (pink). Quartz grains facing irregular pores of secondary origin are generally corroded at their margins (arrow 1) whereas in the reduced intergranular primary (?) pores they are not corroded (arrow 2). The relatively large pores (lower centre) were probably formed by dissolution of carbonate cement and/or framework grains. Hibernia Sandstone, B-08, 3482.63 m. Plane-polarized light. Scale bar: 500 um.

(C) Completely shattered quartz grain filled with calcite cement (C). Hibernia Sandstone, B-08, 3496.47 m. Plane-polarized light. Scale bar: 50 um.

(D) Fracture filling ferroan calcite cement subsequently replaced by a few crystals of unknown mineral (arrow). Intergranular brownish siderite represents the earliest cement observed in this sandstone. Note Fe-poor calcite at the top. Hibernia Sandstone, K-18, 3860.32. Plane-polarized light. Scale bar: 50 um.

National Library
of Canada

Bibliothèque nationale
du Canada

Canadian Theses Service

Service des thèses canadiennes

NOTICE

AVIS

THE QUALITY OF THIS MICROFICHE
IS HEAVILY DEPENDENT UPON THE
QUALITY OF THE THESIS SUBMITTED
FOR MICROFILMING.

UNFORTUNATELY THE COLOURED
ILLUSTRATIONS OF THIS THESIS
CAN ONLY YIELD DIFFERENT TONES
OF GREY.

LA QUALITE DE CETTE MICROFICHE
DEPEND GRANDEMENT DE LA QUALITE DE LA
THESE SOUMISE AU MICROFILMAGE.

MALHEUREUSEMENT, LES DIFFERENTES
ILLUSTRATIONS EN COULEURS DE CETTE
THESE NE PEUVENT DONNER QUE DES
TEINTES DE GRIS.
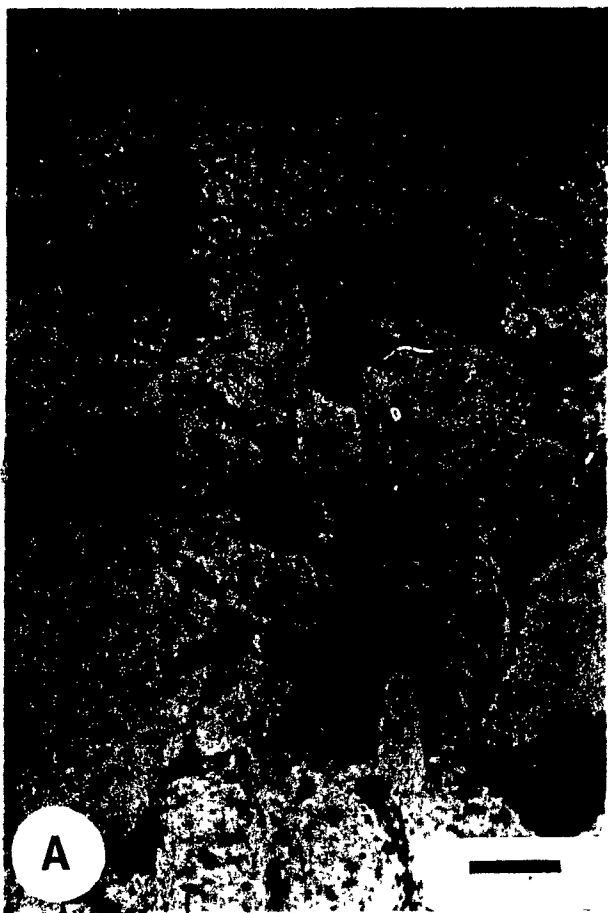
different grains including matrix and cement) have been observed. Some of the quartz grains are partly fractured while others are completely shattered and filled with ferroan calcite (Plate 14C). In a number of samples, fracture-filled ferroan calcite was subsequently replaced by crystals of an unidentifiable mineral. (Plate 14D).

3.2.3.9 Dolomite Cementation

The amount of dolomite cement ranges from 0% to more than 30%. It was observed in the "B" and Hibernia Sandstones and in the Jeanne d' Arc Member but does not occur in the Avalon Sandstone. Four different types of dolomite have been distinguished:

(1) Non-ferroan dolomite;

(2) Early ferroan dolomite;

(3) Late ferroan dolomite; and

(4) Replacement dolomite.

3.2.3.9.1 Non-Ferroan Dolomite (Type 1)

In a very few samples non-ferroan dolomite cement occurs as patches of sparry dolomite between detrital grains. Volumetrically this cement phase is not important.

3.2.3.9.2 Early Ferroan Dolomite (Type 2)

Early ferroan dolomite cement was found in a few samples from a thick (18 m) fine-grained sandstone unit between 3856 and 3874 m in the B-27 well which contains abundant organic-matter fragments. The ferroan nature of the dolomite is revealed by staining. This dolomite is present in thin zones

(less than 1 m thick) where it occludes all available pore spaces and has impeded futher compaction (Plate 15A). It occurs as sparry and granular crystals ranging from approximately 30 to 200um (average 50um). In contrast to late dolomite, it does not show sweeping extinction and curved cleavage, Detrital quartz grains, which are replaced by this dolomite, show irregular grain boundaries. Fossil-like fragments present in these sandstone samples are completely dolomitized. Early precipitation of this dolomite is indicated by the very loose packing of framework grains (minus cement porosity > 30%; e.g. at 3862 m, B-27), and the lack of quartz overgrowths or other cements.

3.2.3.9.3   Late Ferroan Dolomite (Type 3)

Late ferroan dolomite occurs as large granular crystals (Plate 15B), patches of sparry dolomite (Plate 15C) as well as individual euhedral/subhedral rhombs (up to 700 um) usually pointing toward pore spaces (Plate 15D). It generally shows sweeping extinction, rarely with curved cleavage planes, and resembles "saddle dolomite" described in the literature (Plate 16A). Saddle dolomite is commonly reported as a late cement in deeply buried (>2000 m) carbonates (Radke and Mathis, 1980; Mattes and Mountjoy, 1980; and Machel, 1987) and appears to have formed at temperatures between 60 $^{\circ}$C to 150 $^{\circ}$C. A low-temperature (near 25 $^{\circ}$C) origin of saddle dolomite has been suggested by Assereto and Folk (1980) and Morrow et al. (1986). In the

PLATE 15

Dolomite cement in the Hibernia field.

(A) Fine-grained sandstone completely cemented by ferroan dolomite (blue) precipitated before significant compaction. Some quartz grains are replaced by dolomite. Hibernia Sandstone, B-27, 3862.0 m. Plane-polarized light. Scale bar: 100 um.

(B) Large granular crystals of late ferroan dolomite (D). In this sample, framework grains are extensively replaced by ferroan dolomite. Jeanne d' Arc Member, O-35, 4534.0 m. Crossed nicols. Scale bar: 100 um.

(C) Late sparry dolomite (D) precipitated in reduced intergranular pores after considerable compaction (arrow 1) and quartz overgrowths (arrow 2). Section stained with Alizarin-Red only. "B" Sandstone, O-35, 3185.90 m. Crossed nicols. Scale bar: 50 um.

(D) Euhedral ferroan dolomite crystal (D) occupying both primary as well as secondary pores (SP). The secondary pore (SP) was generated by dissolution of a carbonate fragment whose peripheral rim (arrow) is still present. Note presence of quartz overgrowth (ov) in the upper part of photograph. "B" Sandstone, O-35, 3183.7 m. Plane-polarized light. Scale bar: 50 um.
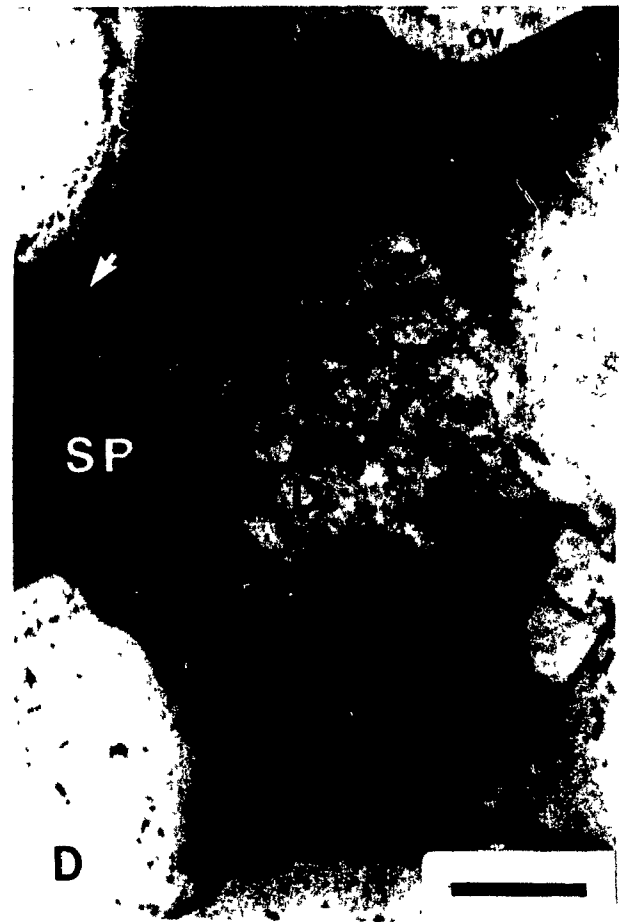
PLATE 16

Dolomite cements (continued).

(A) Late, saddle-shaped, ferroan dolomite (D) with curved cleavages (arrow) and sweeping extinction (dark area). Lower framework grain shows quartz overgrowth. Jeanne d' Arc Member, O-35, 4534.82 m. Crossed nicols. Scale bar: 50 um.

(B) Fractured feldspar grain (F) partly filled by sparry dolomite (D). In the Hibernia field, fractured feldspar grains are only observed below 3000 m depth. This suggest that late dolomite precipitation occurred at relatively great depth (below 2600 m). "B" Sandstone, O-35, 3185.90 m. Crossed nicols. Scale bar: 50 um.

(C) Secondary porosity formed due to partial dissolution of a calcite (C) rock fragment and subsequently occluded by late dolomite (D) cement and hydrocarbon lining. "B" Sandstone, O-35, 3182.82 m. Plane-polarized light. Scale bar: 50 um.

(D) In this section, one of the two secondary pores (SP) caused by dissolution of detrital grains was filled by late dolomite cement (D). These secondary pores (both open and cemented) are lined with hydrocarbons (black). "B" Sandstone, O-35, 3176.00 m. Plane-polarized light. Scale bar: 100 um.
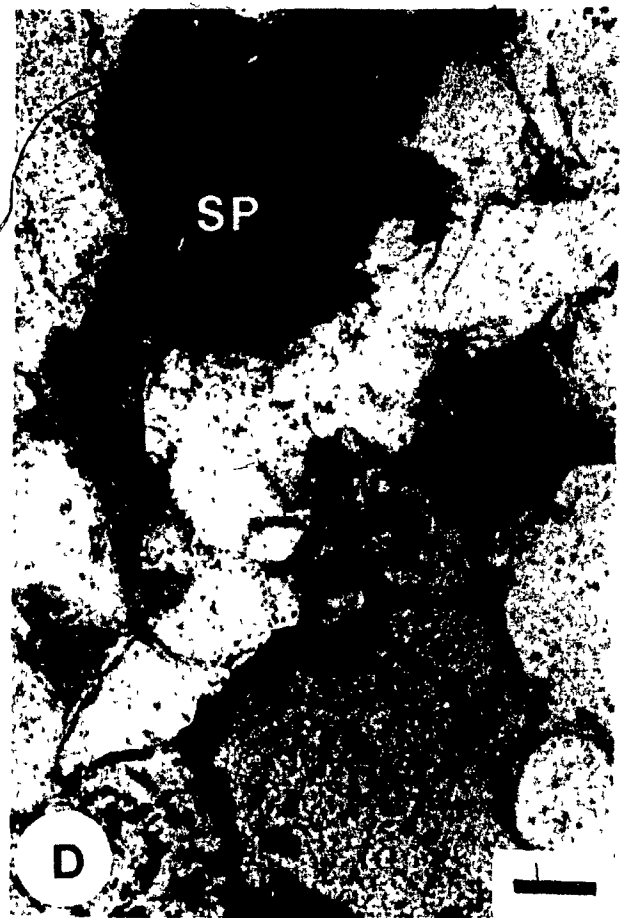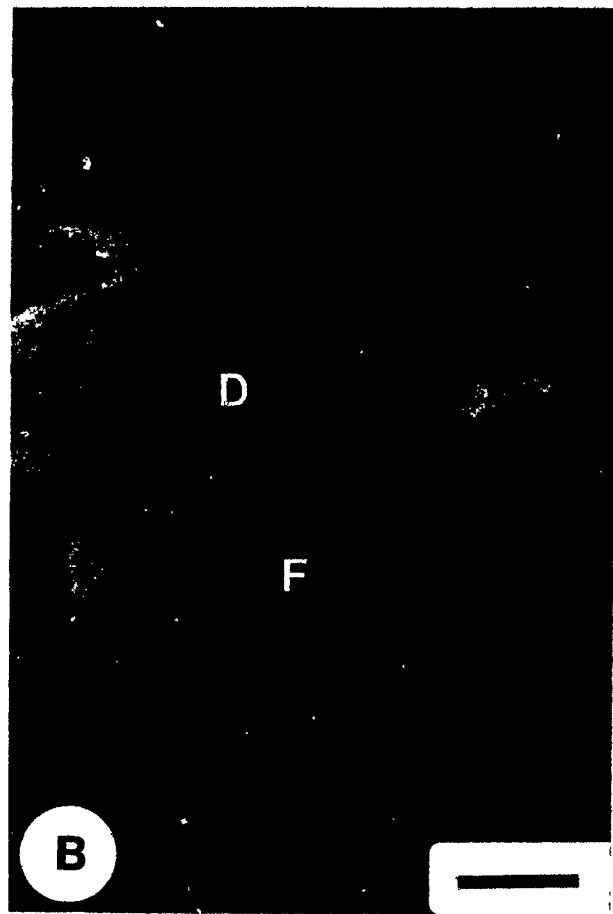
Hibernia field, late ferroan-dolomite (including saddle-shaped dolomite) appears to have precipitated at moderate to deep burial levels (below 2600 m) after significant compaction and dissolution of calcite (Plate 16B, 16C). Figure 3.6 shows a schematic diagenetic history of sandstone containing late dolomite. Several lines of evidence indicate that late dolomite was precipitated after dissolution of carbonates:

(i)   presence of ferroan dolomite in oversized and irregular (Plate 17A) secondary pores including moldic pores (PLate 16D);

(ii) uncorroded smooth crystal faces of late ferroan dolomite pointing toward secondary pores (Plate 15D, 17B); and

(iii) partly dissolved nearby early ferroan calcite cement and calcite rock fragments.

In one sample, a moldic pore lined with heavy oil is filled with dolomite suggesting its precipitation after hydrocarbon migration (Plate 16D).

Late ferroan dolomite was not found in the Avalon Sandstone. However, it is frequently present in the deeper reservoirs ("B" and Hibernia Sandstones, and Jeanne d'Arc Member). Compared to the B-08 and B-27 wells, late ferroan dolomite is most abundand in the O-35 ("B" Sandstone) and K-18 (Hibernia Sandstone) wells. In the C-96 well, ferroan dolomite was not observed.

a   40% porosity

b   Mechanical compaction. Minor early quartz overgrowths. Porosity about 30%.

c   Early calcite cementation. Minus-cement porosity 25-30%.

d   Dissolution of calcite. Secondary porosity (d2).

e   Mechanical compaction continued and grain fracturing (e2). Porosity (e2) = 15%.

f   HYDROCARBONS   LATE DOLOMITE
Porosity (f2) = 8%.
Dolomite cement= 5%.
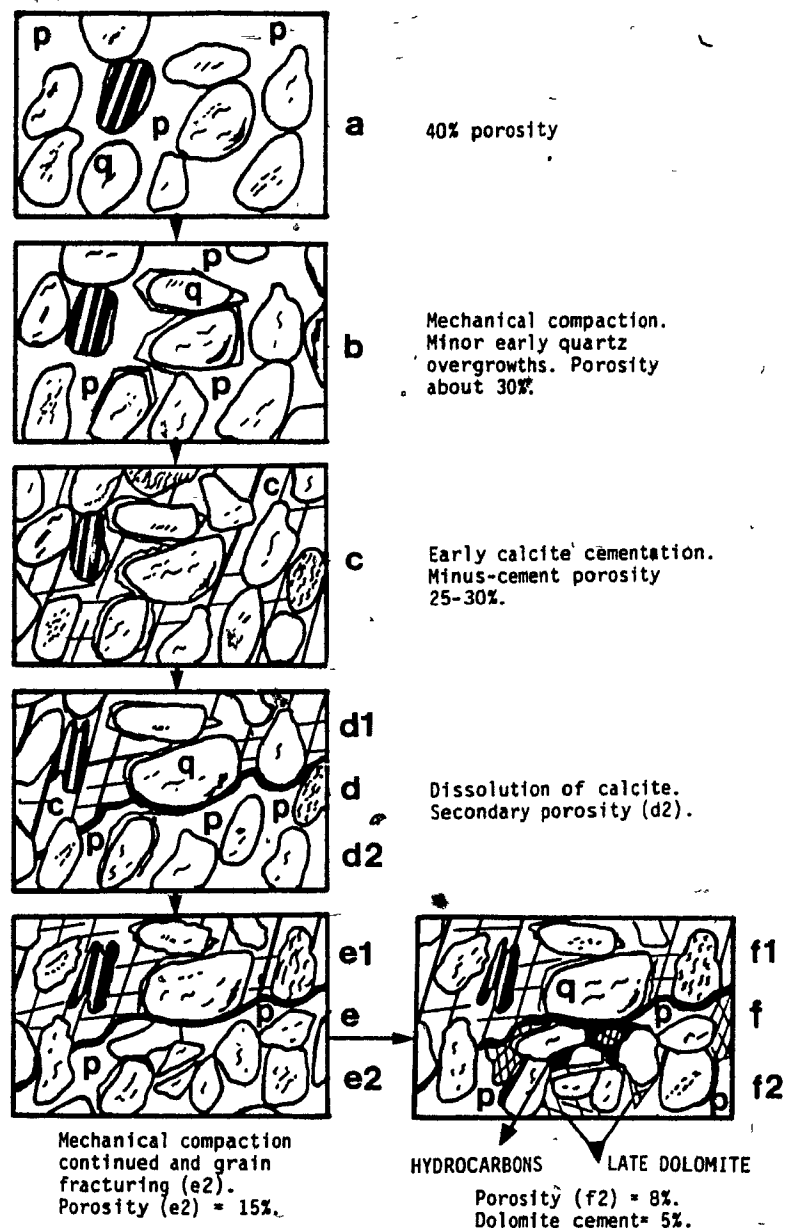
Fig. 3.6   Reconstruction   of   diagenetic   history   from petrographic   relationships   indicating   the precipitation of late   dolomite   after   the dissolution of early calcite.

PLATE 17

Dolomite cement (continued).

(A) Late dolomite (D) cement partly filling an elongated pore (P) at greater depth. Jeanne d' Arc Member O-35, 4534.82 m. Plane-polarized light. Scale bar: 50 um.

(B) Dolomite crystal (D) partly filling a large secondary pore. Note uncorroded crystal face of dolomite. "B" Sandstone, O-35, 3185.90 m. Plane-polarized light. Scale bar: 50 um.

(C) Euhedral to subhedral dolomite (D) crystals replacing clay matrix. Jeanne d' Arc Member, O-35, 4534.82 m. Plane-polarized light. Scale bar: 100 um.

(D) Dolomite rhomb in shale clast. Jeanne d' Arc Member, O-35, 4533.47 m. Crossed nicols. Scale bar: 50 um.
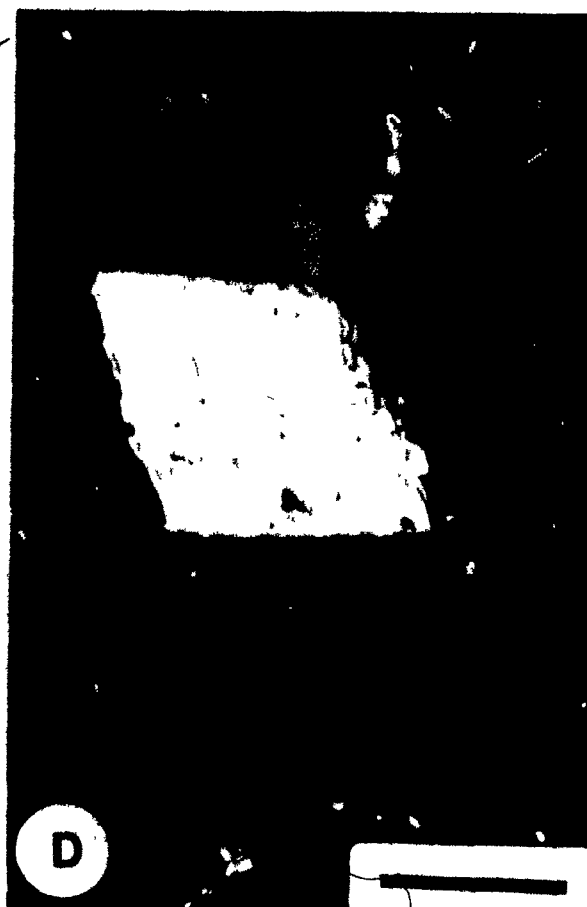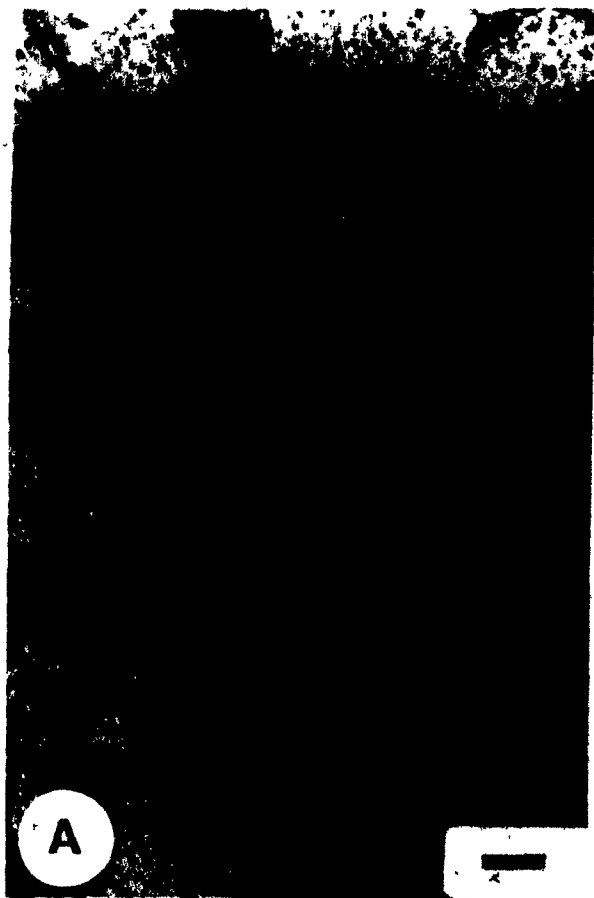
3.2.3.9.4   Replacement Dolomite (Type 4)

Two types of replacement dolomite were observed: (1) euhedral to subhedral dolomite rhombs (up to 85um) replacing shale matrix (Plate 17C, 17D) and having formed in stylolite-like structures; and (2) small dolomite rhombs (40 um) replacing early ferroan calcite cements. Some of the samples were not stained with potassium ferricyanide, therefore, it is not known whether the dolomite is ferroan.

3.2.3.10   Isotope Analyses ($\delta^{18}O$ and $\delta^{13}C$) on Carbonate Cements

3.2.3.10.1   Analytical Procedure

For isotopic analysis polished slabs, opposite to the stained thin sections used in the petrographic study, were examined under a reflected light microscope. In this way particular carbonate phases could be located for the purpose of sampling for isotopic analysis. Samples with abundant detrial carbonate fragments were excluded from analyses.

Micro-samples (0.2 to 0.5 milligrams powder) were extracted at the University of Michigan from polished slabs using a microscope-mounted drill bit of 20 micron to 500 micron diameter. The micro-samples were roasted in vacuum at 380 $^{\circ}$C for one hour. Samples were then reacted with anhydrous phosphoric acid at 55 $^{\circ}$C for approxmately 10 minutes for calcite and about one hour for dolomite. This was done in an on-line gas extraction system connected to an inlet of a VG 602 E ratio mass spectrometer. All analyses were converted to PDB and corrected for ^{17}O as described by

Craig (1957). Precision was monitored by daily analysis of NBS standared-20 and was maintained at a level better than 0.1 permil for both carbon and oxygen (Gonzalez and Lohmann, 1985).

3.2.3.10.2 Results

From 24 sandstone samples, five different types of carbonate cements were analysed for $^{13}C/^{12}C$ and $^{18}O/^{16}O$. The isotopic data of these cments are summarized in Table 3.3 and plotted in Figure 3.7. The results are given in the delta-notation, where

$$\delta^{13}C = \frac{^{13}C/^{12}C \text{ sample} - {}^{13}C/^{12}C \text{ standard}}{^{13}C/^{12}C} \times 1000$$

and in analogous fashion for $^{18}O/^{16}O$. The reference standard used is PDB for both $\delta^{13}C$ and $\delta^{18}O$ vlues.

Each carbonate cement plots in a different field:

(1) Early ferroan calcite cement shows a large variation in $\delta^{18}O$ (-4.3 to -8.6 ‰.; mean -6.66 ‰.) and $\delta^{13}C$ values (+ 2.1 to -5.8 ‰.; mean -1.6).

(2) The isotopic data on late ferroan calcite cement cluster more closely and give the lightest isotopic values: $\delta^{13}C$ values mean -10.9 ‰. (-7.5 to - 12.3 ‰.) and $\delta^{18}O$ mean -8.8 ‰. (-6.9 to -9.5 ‰.). The average $\delta^{13}C$ value of late calcite (-10.9 ‰.) is -9.2 ‰. lighter than the average $\delta^{13}C$ of early calcite (-1.6 ‰.).

(3) Early ferroan dolomite was analysed in only three sandstone samples. The results show only minor isotopic variations. The average $\delta^{18}O$ value is -3.1 ‰.

Table 3.3 Isotopic analyses ($\delta^{18}O$ and $\delta^{13}C$) of carbonate cements.

ABBREVIATIONS

CAL: Calcite

CRF: Sample containing carbonate fragments

FCAL: Ferroan calcite

FDOL: Ferroan dolomite

GR: Granular crystals

POI: Poikilotopic texture

SE: sweeping extinction

SRL: siderite rich laminae

Well No	Reservoir Sandstones	Subserface Depth (m)	$\delta^{18}O$ (PDB)	$\delta^{13}C$ (PDB)	Petrographic Features
A) EARLY CALCITE CEMENT					
O-35	Avalon Sst.	2147.7	−6.07	+2.15	FCAL, POI
O-35	"B" Sst.	3180.2	−8.38	−0.65	CAL, CRF
K-18		3135.6	−5.02	−0.94	FCAL, CRF
K-18		3144.2	−4.33	+0.01	FCAL
K-18	Hibernia Sst.	3814.0	−6.83	−3.23	FCAL, POI
K-14		3861.7	−8.08	−3.33	FCAL, POI
K-14		3872.2	−6.08	−1.31	FCAL
k-14		3932.5	−8.56	−5.89	FCAL
		Mean	−6.66	−1.64	
B) LATE CALCITE CEMENT					
B-27	Hibernia Sst.	3885.4	−9.53	−9.40	FCAL
B-27		3892.3	−9.20	−12.13	FCAL
B-27		3892.4	−9.24	−12.22	FCAL
B-27		3893.6	−9.03	−12.30	FCAL
B-27		3905.0	−9.21	−11.22	FCAL, POI
B-27		3906.0	−8.85	−11.68	FCAL
C-96		3939.1	−6.92	−7.50	FCAL
		Mean	−8.85	−10.92	
C) EARLY DOLOMITE CEMENT					
B-27	Hibernia Sst.	3858.5	−3.62	−3.86	FDOL, GR
B-27		3858.7	−3.20	−4.30	FDOL, GR

B-27		3862.0	−2.51	−2.38	FDOL, GR
	Mean		−3.11	−3.51	

D) LATE DOLOMITE CEMENT

B-08	Hibernia Sst.	3485.6	−9.11	−6.18	FDOL
O-35	J. d'Arc	4533.4	−6.31	−4.55	FDOL, SE
O-35		4534.8	−6.52	−4.45	FDOL, SE
	Mean		−7.31	−5.06	

E) SIDERITE

B-27	Hibernia Sst.	3885.8	−6.49	−5.65	SRL
B-27		3910.4	−3.90	−10.20	SRL
K-18		3860.3	−5.22	−7.13	SRL
	Mean		−5.20	−7.66	

$\delta^{13}C$ (PDB)

+3
+1
-1
-3
-5
-7
-9
-11
-13

$\delta^{18}O$ (PDB)

12   10   8   6   4   2   -1
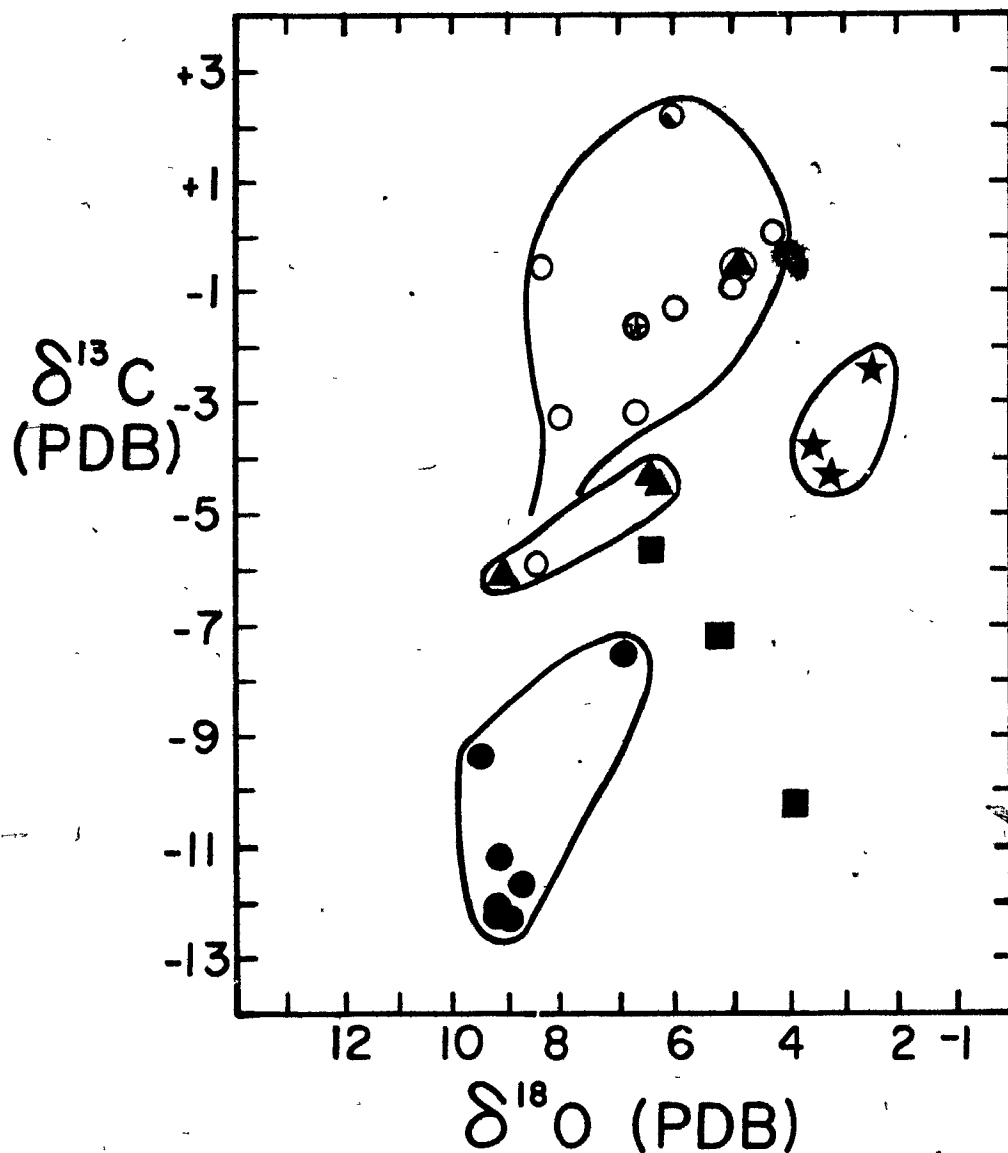
○ Early calcite   ● Late calcite

✶ Early dolomite   ▲ Late dolomite

■ Siderite

Average of Avalon Ss (from Hutcheon et al., 1985) ⊕(triangle)
Average of early calcite cement ⊗

Fig. 3.7 Carbon and oxygen isotope values for the carbonate cements from the reservoir sandstones of the Hibernia field.

(2.5 to 3.6 ‰) which is 4.2 ‰ heavier than that of late ferroan dolomite cement. The average $\delta^{13}C$ for early ferroan dolomite is -3.5 (-2.4 to -4.3 ‰).

(4) The late dolomite shows a mean $\delta^{13}C$ value of -5.0 ‰ (-4.4 to -6.2 ‰) and a mean $\delta^{18}O$ of -7.3 ‰ (-6.3 to -9.1 ‰).

(5) Three samples were analysed from thin siderite-rich laminae. Siderite $\delta^{18}O$ values range from -3.9 to -6.4 ‰ (average -5.2 ‰) with a large range of $\delta^{13}C$ values from -5.6 to -10.2 ‰ (mean -7.6).

(For discussion and interpretations of data see Chapter 6).

3.3 COMPARISON OF HIBERNIA FIELD AND THE U.S. GULF COAST

Diagenesis of the Gulf Coast reservoir sandstones has been particularly well documented (Loucks et al., 1977, 1979, 1984; Franks and Forester, 1984; Land and Milliken, 1981; Land, 1984; Lundegard et al., 1984; Milliken et al., 1985) and is often taken as a standard for the comparison with other petroleun provinces. These Tertiary sandstones (mainly Wilcox and Frio Formations) generally represent deltaic and nearshore coastal-complex environments (Lindquist, 1977). There are some similarities in the diagenesis of the Gulf Coast and the Hibernia Field, which are:

(1) Carbonate cements are volumetrically important in both the Gulf Coast and the Hibernia Field.

(2) Authigenic late ferroan dolomite was observed near or below 3000 m depth in both areas.

(3) $\delta^{18}O$ of calcite decreases with increasing burial depth.

(4) Feldspar dissolution is minor (or absent) at shallow depth in both areas. However, at greater depth (>3000 m in case of the Hibernia Field, about 2500 m in the Gulf Coast) feldspar is partly to completely dissolved;

(5) Precipitation of kaolinite in secondary pores occurs at deeper levels, below the dissolution depth.

(6) In the Gulf Coast, the top of the overpressure zone corresponds to a region of well developed secondary porosity. In the Hibernia Field, the Hibernia Sandstone with well developed secondary porosity also lies above a generally overpressured Kimmridgian shale (Grant et al., 1986).

There are some dissimilarities in the diagenesis between the Gulf Coast and the Hibernia Field. These are:

(1) In the Gulf Coast, quartz overgrowths appear to be limited to intermediate burial depths (Loucks et al., 1984). Contrary to this, in the Hibernia Field quartz overgrowth appears to be progressive and continued during different stages of diagenesis.

(2) The dissolution of feldspars contributes significantly to secondary porosity development in the deep zones of the Gulf Coast. This dissolution has resulted in large amounts of kaolinite cement. Feldspar occurrence and dissolution in the Hibernia Field is minor (average 2.5 % of the bulk rock volume) and, probably for that reason, kaolinite is only a minor authigenic mineral.

(3) Precipitation of late pyrite (following dissolution of

carbonates) was not reported from the Gulf Coast reservoir sandstones in contrast to Hibernia field.

3.4 SEQUENCE OF DIAGENETIC EVENTS IN THE HIBERNIA FIELD

The sequence of diagenetic events in the Hibernia Oil Field, deduced from textural relationships, is summarized in Fig. 3.8 and briefly discussed below. All diagenetic features do not occur in all samples. It is difficult to place textural relationship in an absolute time or burial depth framework as the present depths of various diagenetic features do not necessary indicate their depth of origin.

The chemical diagenesis of these sandstones commenced with the precipitation of minor chlorite coating and siderite precipitation. This was followed by the formatiom of an early quartz overgrowth. However, local precipitation of siderite continued during this early quartz growth. Early quartz overgrowth was followed by an extensive early ferroan calcite cementation (type 2) when 10 % to 15 % of the initial porosity was already reduced by mechanical compaction. Minor amounts of pyrite were also precipitated during or before early calcite cementation. Where early calcite did not precipitated and pore water supplied sufficient amounts of silica, precipitation of silica continued reducing significant amounts of porosity.

A major phase of dissolution (of calcite, rock fragments, feldspar, and matrix) and development of secondary porosity occurred below 3200 m. Minor compaction, late ferroan calcite cement, grain fracturing and late quartz overgrowths occurred

Paragenetic sequences of diagenetic events

Phases (listed in order of first appearance)	Early Diagenesis (<1500m) (I/s with >70%S)	Increasing ——→ burial depth	Base of Middle Diagenesis(>3600m) (I/s with <20%S)
1-Mechanical Compaction			
2 Clay coating of framework grains including early fibrous cement			
3-Siderite			
4-Early quartz overgrowth			
5-Early pyrite			
6-Early Fe-Calcite			
7-Early Fe-dolomite			
8-Quartz overgrowth			
9-Dissolution			
10-Late Calcite			
11-Minor grain fracturing			
12-Quartz overgrowth			
13-Kaolinite			
14-Late Fe-dolomite			
15-Fe-Calcite overgrowth			
16-Late pyrite			
17-Hydrocarbon Migration			

Fig. 3.8 Schematic diagram showing paragenetic sequences of diagenetic events. Stages and relative abundance of diagenetic events are indicated by length and width of bars respectively.

after this porosity enhancing event. Precipitation of
kaolinite and late ferroan-dolomite in secondary, as well
as in remaining primary pores occurred after dissolution.
This was followed by late-pyrite precipitation and
migration of hydrocarbons.

CHAPTER IV

SHALE MINERALOGY AND DIAGENESIS

4.1 INTRODUCTION AND OBJECTIVES

It is not possible to study sandstone diagenesis in an interlayered sandstone/shale sequence without studying shale diagenesis because shales are considered to make available various cations, acidic pore fluids, as well as interlayer-water of clay minerals, capable of explaining various cementation and dissolution processes in nearby sandstones. It is, therefore, significant to investigate mineralogical changes in the interbedded shales while studying sandstone diagenesis. The specific purpose of this Chapter is to:

(1) Identify mineralogical changes in the shales of the Hibernia and West Ben Nevis fields;

(2) Evaluate the effects of diagenesis (and weathering/depositional environments) on the mineralogy of shales with increasing burial depth;

(3) Estimate the percent of illite in mixed-layer I/S;

(4) Measure the illite crystallinity (IC) on different size fractions to assess how other factors (besides diagenesis) may affect IC during early and middle diagenesis.

4.2 SAMPLING AND MATERIAL STUDIED

Sixty subsurface samples were collected from shale cores and well-cuttings of three wells, B-08 and B-27 in Hibernia, and B-75 in West Ben Nevis. From well-cuttings, composite

samples comprising 20 to 50 m stratigraphic intervals were prepared to obtain samples of sufficient size. The well-cuttings were sieved on a 12 mesh sieve (1.7 mm), thoroughly washed to remove drilling mud, and then air dried. Sandstone and siltstone fragments were hand-picked and removed. The shale samples cover a subsurface-depth ranging from 1000 to 4900 m with corresponding temperatures ranging from 40 to 120 °C.

4.3   ANALYTICAL METHODS

From all samples the <2 um size fraction was separated by centrifuging, and pipetted onto a glass slide and air dried. Samples were run on a Siemens X-ray diffractometer (type D-500) using a Cu Kα radiation source set at 20 mA and 40 KV with an aperture of the divergence and scatter slits of 1°. Both glycolated and non-glycolated slides were prepared of each sample, which were scanned from 2° to 33° 2θ. A number of selected samples were scanned after HCl and heat treatments (at 300 and 550 °C for half an hour). Bulk shale samples, 2-16 um, and <0.4 um size fractions were also analysed for selected samples from various subsurface-depths.

The proportion of illite layers in the I/S mixed-layers was estimated according to the method of Reynolds and Hower (1970). For this purpose, <0.4 um size fraction was concentrated by centrifuging and scanned after glycolation from 15° to 18° 2θ at 1/2° 2θ/min. Following Reynolds and Hower (1970) the $I_{(002)}/S_{(003)}$ peak has been used as the most suitable combined diffraction maximum to measure the

percent illite in I/S mixed-layers. This peak is least affected by: (i) domain (crystallite) size distribution, (ii) the proportion of detrital illite, and (iii) type and degree of ordering in I/S mixed-layers.

Semi-quantitative estimates (Biscays, 1965) of the weight percent of smectite, illite (plus mixed-layer I/S), and kaolinite (plus chlorite), in the <2 um fraction of samples from the B-08 (Hibernia), and B-75 (West Ben Nevis) wells are reported in Table 4.1. Due to the low concentration of chlorite, it was not possible to resolve chlorite from kaolinite using the kaolinite-chlorite doublet at 3.5Å.

4.4 MINERALOGY OF THE BULK SHALE

X-ray diffractometry of 16 bulk shale samples, ranging from 1000 to 4900 m sub-surface depth, indicates the presence of quartz, clay minerals (illite, kaolinite, I/S mixed-layer minerals, smectite and chlorite) and calcite with minor amounts of opal-CT, plagioclase, and K-feldspar. Trace amounts of pyrite, siderite and dolomite are also noted in a few samples.

With increasing burial depth the following mineralogical changes were observed. Most of the samples above 3500m contain calcite. However, below this depth calcite is absent in most of the samples. Plagioclase is more abundant than K-feldspar with K-feldspar disappearing below 3600 m (Fig. 4.1). Trace amounts of opal-CT were noted in samples
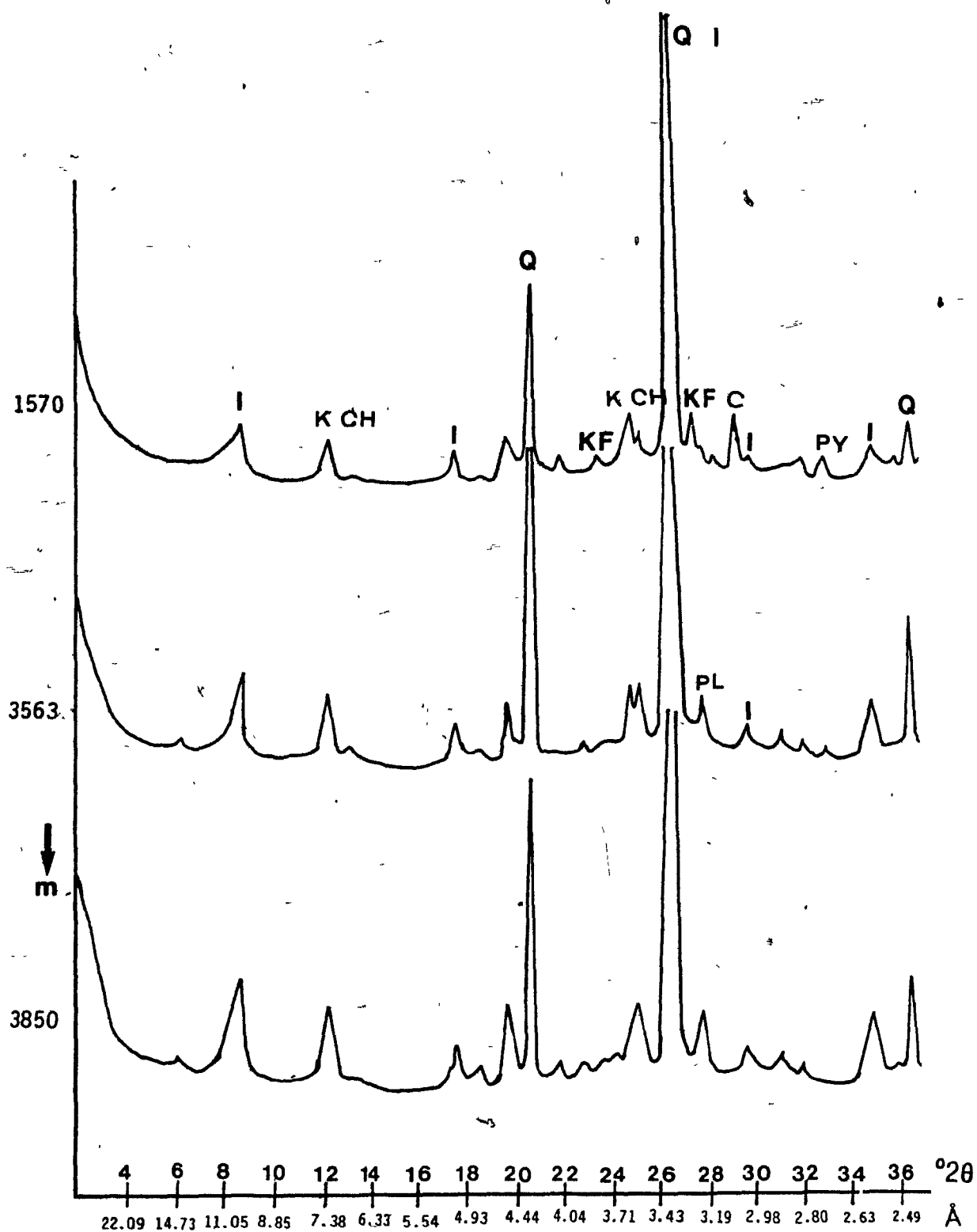
Fig. 4.1 X-ray diffractograms of semi-randomly oriented bulk shale samples. I= illite; Q= quartz; K= kaolinite; P= plagioclase K= potassium feldspar; Cal= calcite.

Table 4.1 Semi-quantitative estimates of clay minerals ($<2 \mu m$) using the method of Biscays (1965).

No	Well	Depth (m)	Illite (+ I/S)	Smectite	Kaolinite (+minor chlorite)
1	B-75	1030	49.0	5.3	45.7
2	B-75	1460	38.6	19.7	41.7
3	B-O8	1540	36.7	15.6	47.7
4	B-75	1635	68.8	12.9	18.3
5	B-O8	1750	29.7	70.3	Tr
6	B-O8	1780	32.8	63.3	3.9
7	B-O8	1840	38.0	32.3	29.7
8	B-O8	1900	24.0	18.0	58.0
9	B-O8	1930	17.0	12.0	71.0
10	B-O8	2115	54.0	0.0	46.0
11	B-O8	2673	74.7	0.0	25.3
12	B-O8	3015	68.2	0.0	31.8
13	B-O8	3130	61.6	0.0	38.4
14	B-O8	3250	68.7	0.0	31.3
15	B-O8	3340	69.4	0.0	30.6
16	B-O8	3460	62.0	0.0	38.0
17	B-O8	3607	71.9	0.0	28.1
18	B-O8	3700	62.2	0.0	34.8
19	B-O8	3820	78.3	0.0	21.7
20	B-O8	3910	86.6	0.0	13.4
21	B-O8	4000	85.0	0.0	15.0
22	B-O8	4120	79.1	0.0	20.9
23	B-O8	4210	80.1	0.0	19.9
24	B-O8	4420	79.0	0.0	21.0

shallower than 2700 m. Only one sample (1455 m) has abundant opal-CT displaying a doublet at 4.25$\overset{o}{A}$ and 4.05$\overset{o}{A}$ (Fig. 4.2).

4.5   CLAY MINERALOGY OF THE <2 μm SIZE FRACTION

4.5.1 Kaolinite

Kaolinite was identified by a first-order basal reflection near 7.1 $\overset{o}{A}$ and corresponding higher-order reflections (Fig. 4.3). It was differentiated from chlorite by HCl treatment and by heating at 550 ^{o} C for 1/2 hour. Except for a few samples, kaolinite is present throughout the wells B-08, B-27 (Hibernia) and B-75 (West Ben Nevis). Samples which do not contain kaolinite are from an unconformity near the Cretaceous/Tertiary boundary. In general, below 3500 m kaolinite decreases with increasing burial depth. Kaolinite peaks show a fairly good crystallinity, however, with depth (below 3600 m) these peaks becom somewhat broader (Table 4.2 and Fig. 4.4).

4.5.2 Smectite

Discrete smectite was found only in samples buried less than 2000 m, a depth which corresponds to temperature of less than about 60 ^{o}C in the subsurface of the Hibernia Oil Field. Above 1500 m, discrete smectite contains little (or no) mixed-layers I/S. However, between 1500 and 2100 m a greater proportion of I/S mixed-layer clays with high smectite contents appears. This is indicated by the presence of a saddle (or jagged tail) on the low-angle side of

120
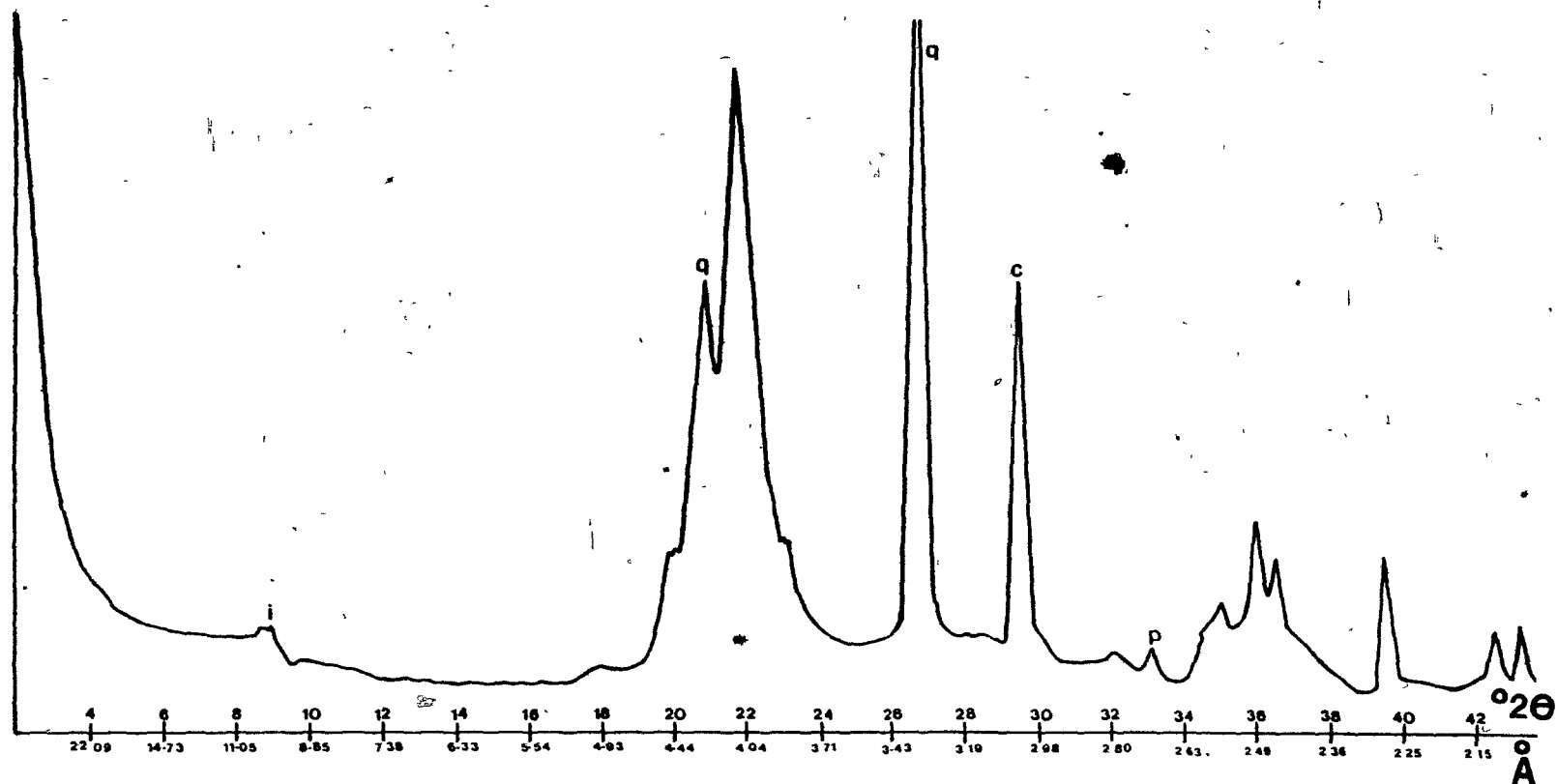
Fig. 4.2 X-ray diffractogram of semi-randomly oriented bulk shale sample showing the presence of a opal-CT doublet at 4.25 and 4.05Å.

Fig. 4.3 X-ray diffractograms of the <2.0 um fraction of selected samples showing the effects of increased burial depth on minerals present. All samples run after glycolation at 40°C for 24 hours. I= illite; I/S= mixed-layer illite/smectite; Ch= chlorite.

S+I/S

A

Ch

B

C

D

E

K+Ch

Ch

Q

K

I+Q

Cal **1540** m

1900

2673

3640

4300

| 4 | 6 | 8 | 10 | 12 | 14 | 16 | 18 | 20 | 22 | 24 | 26 | 28 | 30 | 32 | °2θ |

| 22 09 | 14 73 | 11 05 | 8 85 | 7 38 | 6 33 | 5 54 | 4 93 | 4 44 | 4 04 | 3 71 | 3 43 | 3 19 | 2 96 | 2 80 | Å |
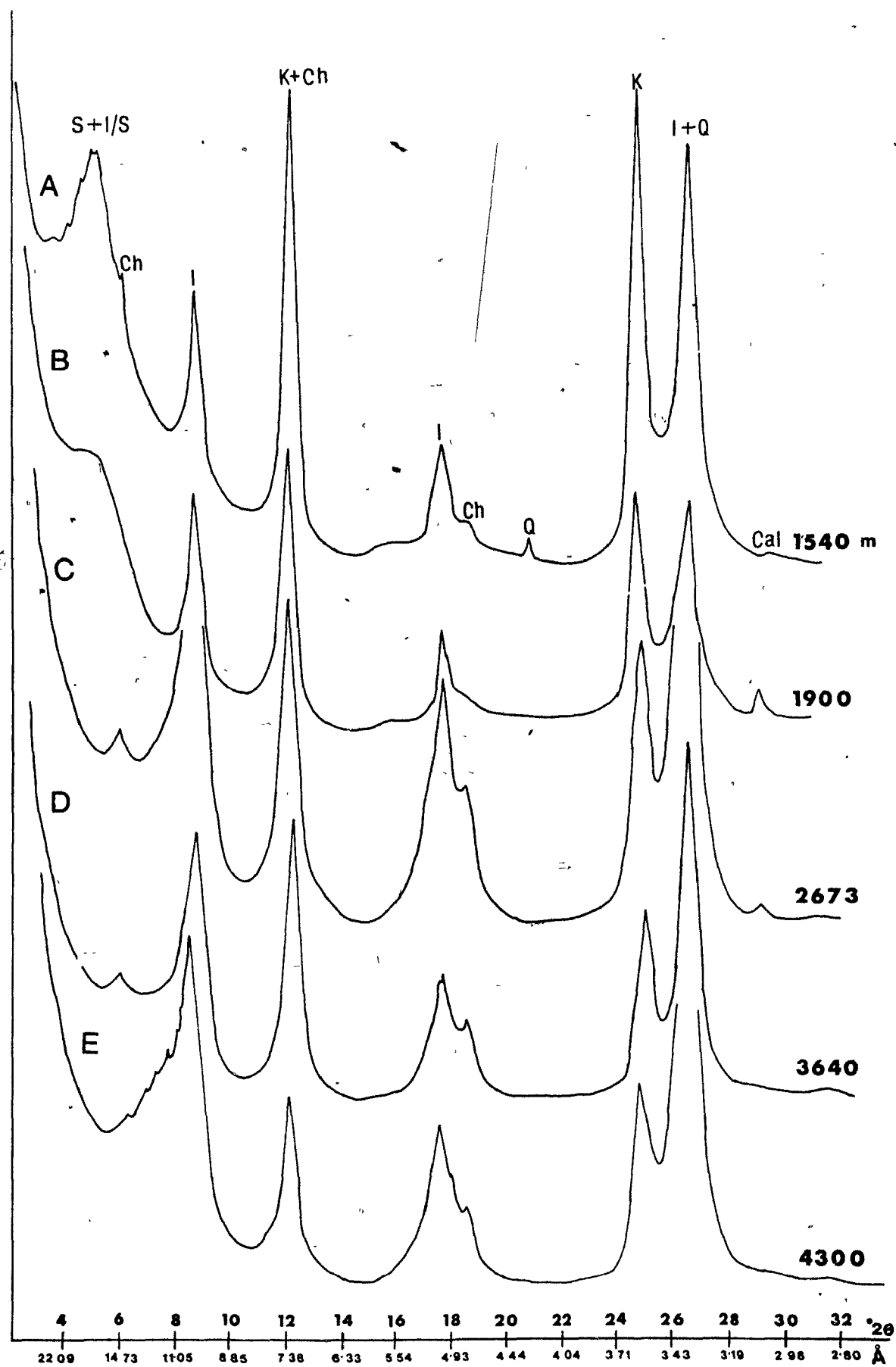
Table 4.2 Crystallinity of kaolinite (area/height) in the <2um size fraction of B-08 (Hibernia) and B-75 West Ben Nevis) fields.

No.	Well	Depth (m)	Area/height ratio
1	B-08	1460	1.27
2	B-08	1540	1.36
3	B-75	1840	1.25
4	B-08	1900	1.48
5	B-75	2115	1.54
6	B-08	2664	1.68
7	B-75	3015	1.69
8	B-08	3250	1.68
9	B-08	3460	1.80
10	B-08	3563	2.13
11	B-08	3607	1.74
12	B-08	3640	1.92
13	B-08	3700	2.12
14	B-08	4000	2.19
15	B-08	4120	2.00
16	B-08	4210	
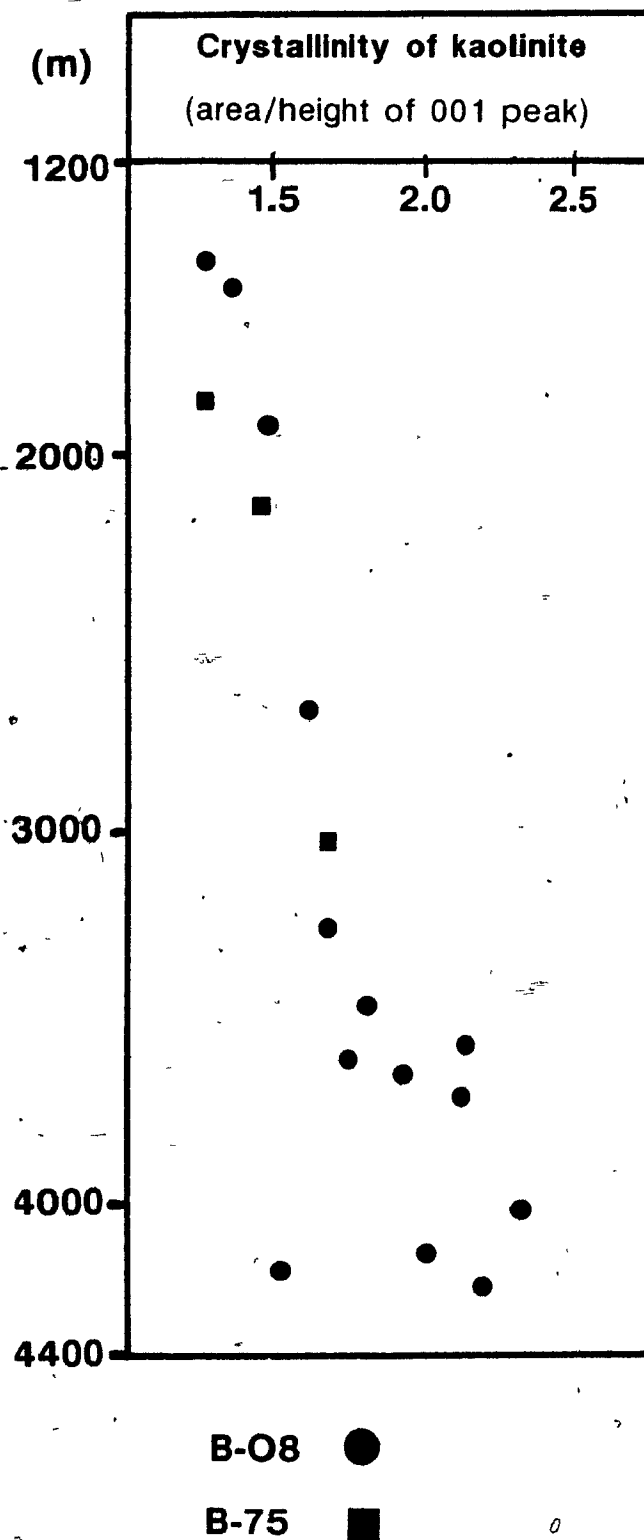
Fig. 4.4 Crystallinity of kaolinite (area/height of 001 peak). The amounts of kaolinite decreases with increasing burial depth.

the glycolated smectite 17Å peak, a feature characteristic of randomly interstratified I/S clay minerals with a high proportion of smectite. Below 2100 m smectite occurs only interstratified with illite.

4.5.3   Interstratified Illite/Smectite

Interstratified I/S is present in all samples below 1500 m. The presence of I/S mixed-layers is confirmed by the asymmetry of the 10Å peak. There is a decrease in expandable smectite layers in I/S mixed-layers from an average 75% S to <10% S from 1000 to 5000 m with the most rapid decrease (to <35% S) occurring above 2500 m subsurface depth (Fig. 4.5).

The mixed-layered I/S is randomly interstratified above 2500 m. Below 2500 m, where illite exceeds 65% in the mixed-layers, I/S is regularly interstratified, as indicated by the low angle plateau between 11Å and 13.8Å (from 2500 m to 3600 m depth) and a small peak between 12.6Å and 13.6Å below 3600 m sub-surface according to Šrodón (1981 and 1984).

5.5.4   Illite

Discrete illite was found in all samples of the <2 um size-fraction and generally constitutes a major part of the clay fraction. Shale samples close to the Cretaceous-Tertiary unconformity contain only small amounts of illite. Illite was identified by a first order basal reflection at approximately 10 Å and corresponding higher-order reflections at 5.0Å and 3.3Å (Fig. 4.3). The amount of illite above 2000 m averages 40%. Upon glycolation, a sharp illite peak

126
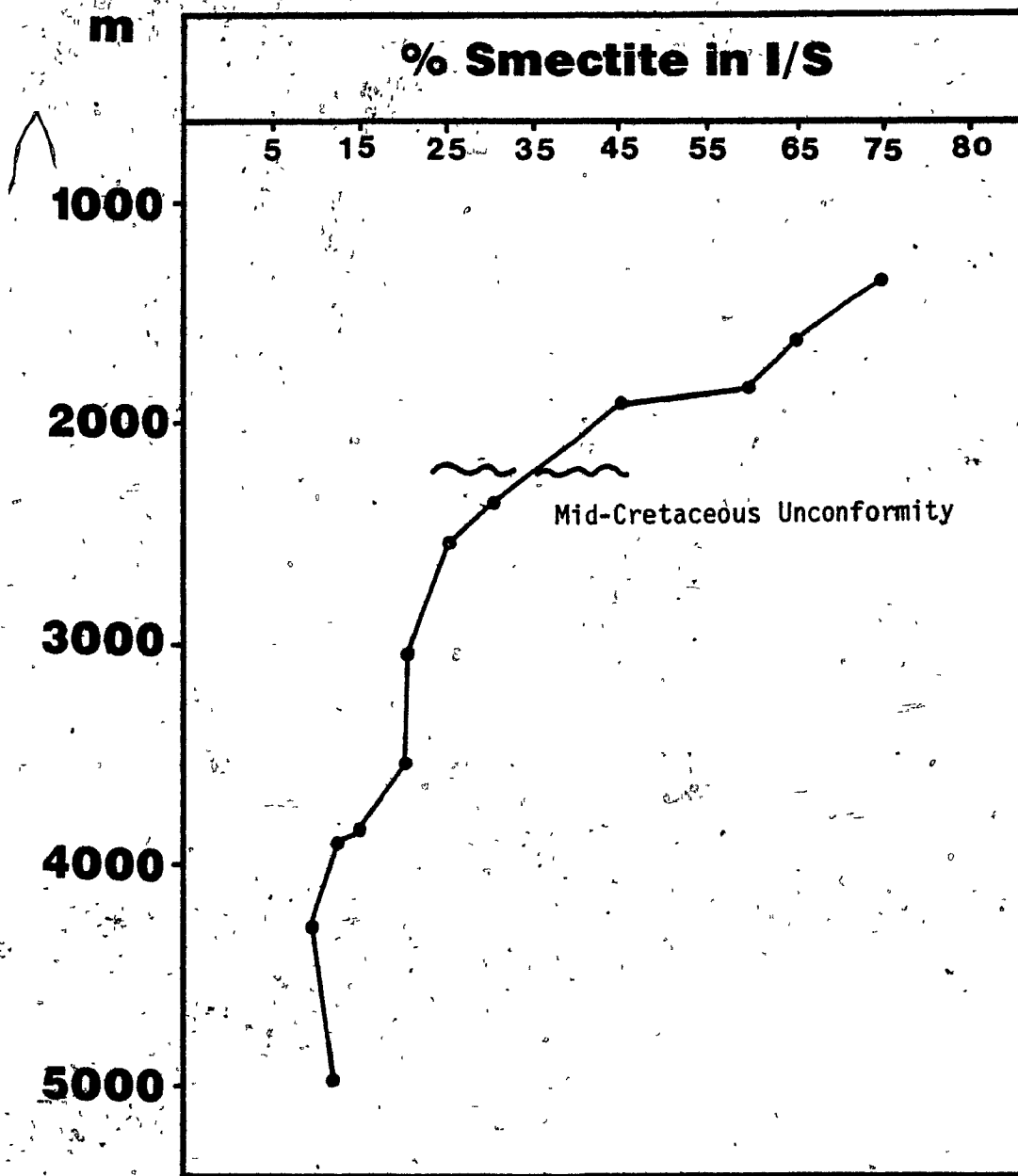
Fig. 4.5 Percent smectite in mixed-layer illite/smectite versus burial depth.

at 10$\overset{o}{A}$ is separated from the broad smectite and I/S reflections. With increasing burial depth the relative amount of illite increases and below 3600m it averages 80%. With increasing depth the 10$\overset{o}{A}$ glycolated peak becomes more asymmetrical towards lower angles. The peak position also moves slightly toward higher d-spacings (from 10.3$\overset{o}{A}$ upto 10.7$\overset{o}{A}$). Heat treatment at 300°C collapses the swelling layers to about 10$\overset{o}{A}$ (Fig. 4.6). This is also reflected by an increase in the intensity of the (001) illite peak.

5.5.5 Chlorite

Small amounts of chlorite are identified in most of the samples by weak (001) and (003) basal reflections at 14.71$\overset{o}{A}$ and 4.71$\overset{o}{A}$ respectively (Fig. 4.3). The strong basal reflections at 7.1$\overset{o}{A}$ and 3.5$\overset{o}{A}$ coincide with the kaolinite peaks. However, kaolinite disappears upon heating at 550 °C. The amount of chlorite relative to other clay minerals increases below 2000 m and decreases below 3600 m depth. In a few samples, the chlorite peak expands upon glycolation from 14.2$\overset{o}{A}$ to 14.9$\overset{o}{A}$, and, when heated up to 550 °C, contracts to a minimum at 13.8$\overset{o}{A}$.

This suggests the presence of minor amounts of expandable chlorite phases (i.e. chlorite/smectite mixed-layers). It is interesting to note that the greatest amount of chlorite occurs in samples which show better illite crystallinity (i.e. around 2500 m depth). A decrease in chlorite concentration below 3600 m corresponds to an overall decrease of illite crystallinity. Below a depth of 3600 m

Fig. 4.6 X-ray diffractograms of clay (<2.0 um) fraction
at 1540 m subserface depth (B-08) showing the effects
of glycolation and thermal treatment.

B-08
1540 m

Air dried

Glycolated

300 ℃

550 ℃
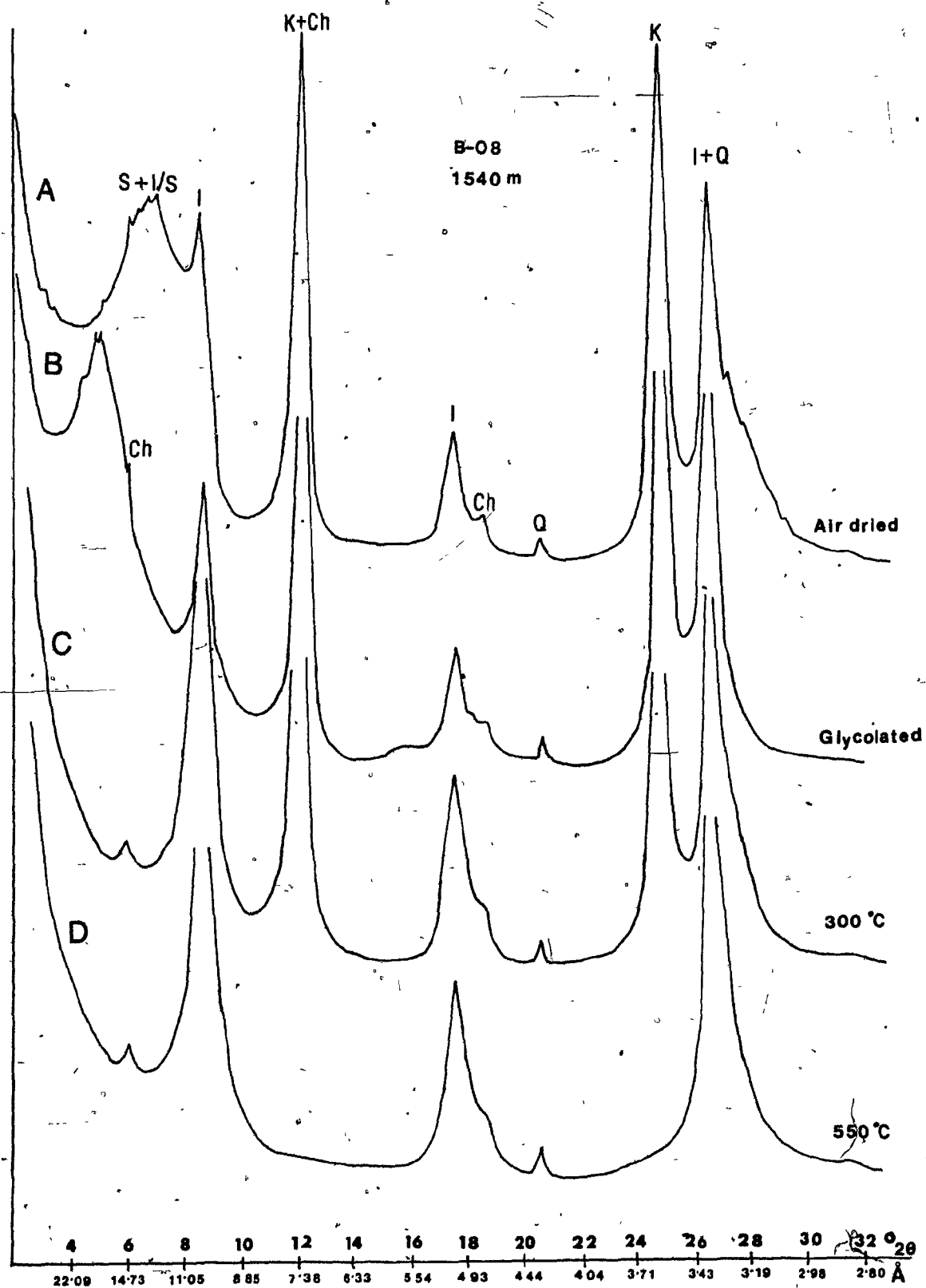
sandstones exhibit high amounts of secondary porosity with chlorite occurring as inclusions of polycrystalline quartz grains, showing signs of dissolution (see section 6.3.5).

4.6 ILLITE CRYSTALLINITY

Illite crystallinity (IC), which is the width of the (001) illite peak at half height expressed as $^{\circ}\triangle 2\theta$ (Kubler, 1967), was measured for shale samples from three wells (B-08, B-27, and B-75, Fig. 4.7).

Illite crystallinity has been used by Kubler (1967), and Foscolos and Stott (1975) and other workers as a diagenetic indicator. This indicator is most valuable at the late stages of diagenesis or the early stages of metamorphism. However, it may also be useful during the middle stages of diagenesis if other diagenetic indicators (such as percent smectite in I/S, and presence or absence of discrete smectite and kaolinite) are also measured for comparison at the same time, as Foscolos and Stott (1975) did for Lower Cretaceous shales of northeastern British Columbia. During middle diagenesis, IC depends on a large number of factors including lithology of shales (e.g. organic matter content), transportation and weathering history, porosity and permeability, pore fluid composition, presence of mixed-layers (i.e. I/S), and poorly crystalline fine-grained authigenic illite. These factors may give rise to anomalous values of IC, therefore, IC alone may not reflect the true degree of diagenesis. Cases of anomalous IC/ depth

trends have been reported by Héroux et al. (1981) and Hiscott (1984) in the Labrador Shelf (Gilbert E-53 and Skolp E-07 wells) and Baffin Shelf (Hekja O-71 well) where IC values increase slightly with increasing burial depth. Hutcheon et al. (1980) also noted a reverse trend of IC in the Kootenay Formation in southeast British Columbia and southwest Alberta. Similar anomalous trends of IC were observed in the Hibernia and West Ben Nevis fields of the Avalon sub-basin (Fig. 4.7). Below 2800 m depth, an overall increase in IC values (i.e. a decrease in crystallinity) is observed in the B-08 and B-75 wells. In the B-27 well, a small jump in IC values (from 0.8 to 1.3 $^{\circ}\triangle 2\theta$) occurs near 3800 m at the top of the Hibernia Sandstone. However, IC then slightly improves at deeper levels. The increase in IC values (or a decrease in crystallinity) is the reverse of what would be expected with increasing burial depth and temperature. Possible causes for this anomalous trend fall into two groups:

(A) Source-rock and/or environment related controls (1 and 2, see below):

    (1) Progressive addition of more poorly crystalline detrital illite at the time of deposition.

    (2) A change in the source environment causing a higher precentage of mixed-layer I/S (and/or smectite) being supplied during the early stages of deposition, followed by a decreasing supply of the mixed-layered I/S (and/or smectite) phase.

(B) Diagenetic and structural controls (3 to 7, see below):

(3) A geothermal anomaly at the level of the Avalon Sandstone which decayed downward.

(4) Juxtaposition or superposition of fault blocks of different maturity.

(5) Increase in the amount of fine-grained authigenic illite with lower IC.

(6) Lack of potassium in the pore fluids.

(7) Increase in organic matter content.

If the observed trends was caused by the first mechanism then coarser fractions (2-16 um), which are expected to be dominated by detrital illite, should also give a similar IC trend (broadening of 001 illite peaks with depth). This possibility is dismissed because no such variation is observed in the coarser fraction (2-16 um) (Fig.4.8).

An increase in IC values with increasing burial depth, noted by Héroux et al. (1981), and Hiscott (1984), has been interpreted as the result of progressive addition of fine-grained authigenic illite. Hutcheon et al., (1980) reported a similar trend of IC (broadening of the 10$\overset{o}{A}$ peak with depth) using the 2-6 um size fraction of shales and sandstones from the Kootenay Formation. They also examined the fabrics of illite under the SEM and noted that although on XRD traces the IC decreases (increase in peak width), the morphological crystallinity (crystal size and shape) of illite improves with increasing depth. On this basis, they concluded that the width of the 10$\overset{o}{A}$ peak probably reflects a combination of detrital (better x-ray crystallinity) and fine-

133

Fig. 4.7 Illite crystallinity (<2.0 um) versus burial
depth for three wells from the Jeanne d' Arc Basin.
Major stratigraphic boundaries and depositional
environments are also given for B-08, B-27 (Hibernia).
For B-75 such data is unavailable.
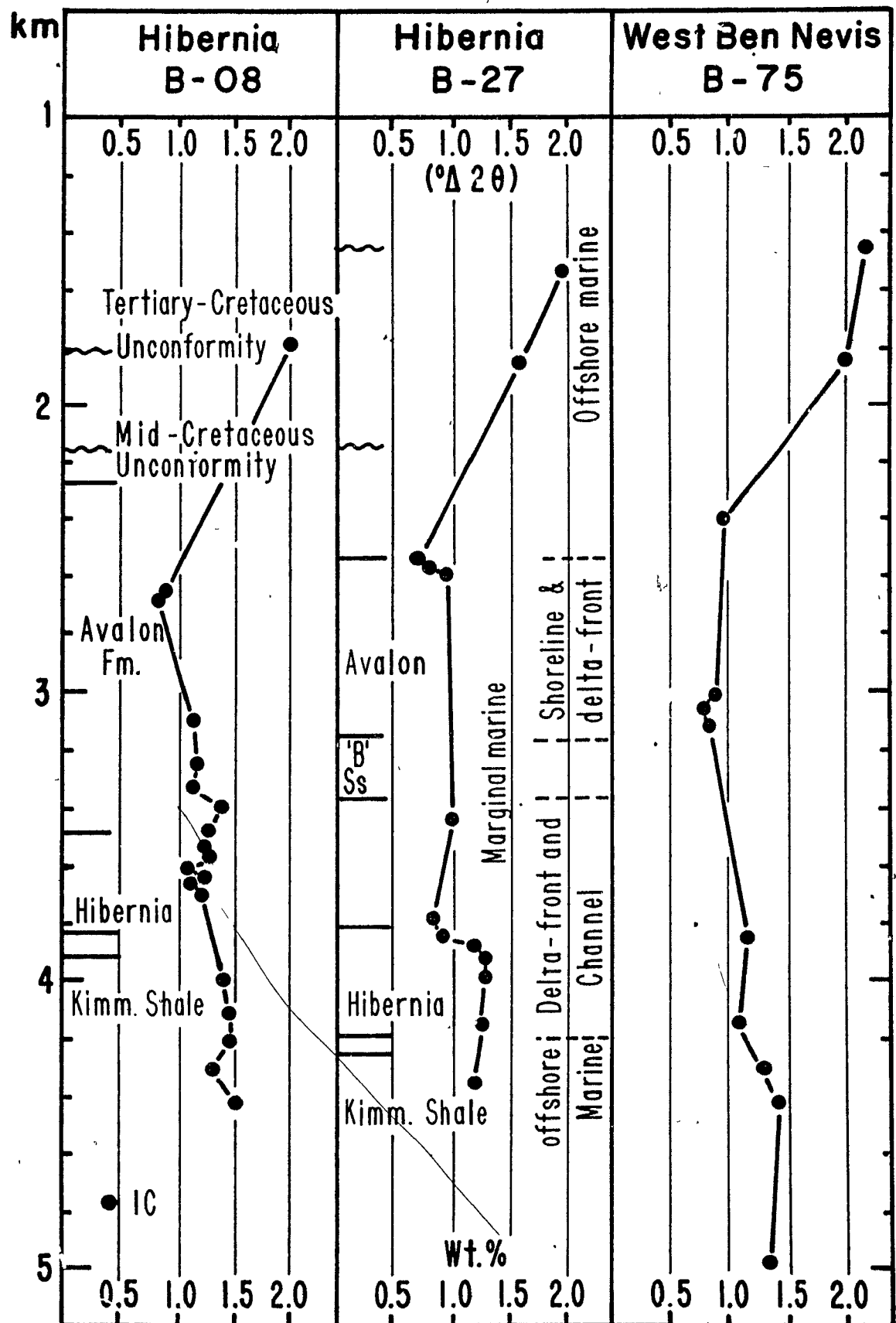
grained authigenic and/or recrystallized detrital illite (poorer x-ray crystallinity). These authors, however, did not analyse the shape and behavior of the 10$\overset{o}{A}$ illite peak with increasing burial depth. If poorly crystalline authigenic illite is the cause of widening of the peak, then this widening should be more or less symmetrical i.e. it should affect both flanks of a peak. In this study it was observed, however, that widening of 10$\overset{o}{A}$ illite peak is mainly due to the opening of low-angle flank of the 10$\overset{o}{A}$ illite peak and that with increasing depth the peak position also moves towards a higher d-spacing (from 10.3 upto 10.7$\overset{o}{A}$). This suggests that widening of tne illite peak might be due to an increase in the amounts of mixed-layer I/S with depth. The finest size-fraction of shales dominantly consists of smectite and mixed-layered I/S. The IC values measured on different size fractions (2-16 um, <2 um, and <0.4 um) indicate that the IC gets poorer with decreasing grain-size (Fig. 4.8). This downward increase in mixed-layer I/S may thus be the result of higher amounts of I/S (and/or smectite) supplied during the early stages of deposition in the basin.

The processes of illitization also depend upon temperature. Higher temperatures enhance the transformation of smectite to illite through the formation of mixed-layer I/S with increasing proportions of illite. Although a paleo-geothermal anomaly can not be ruled out, the well temperatures do not show any geothermal anomalies at present. An abrupt changes in IC may result from faulting which

136
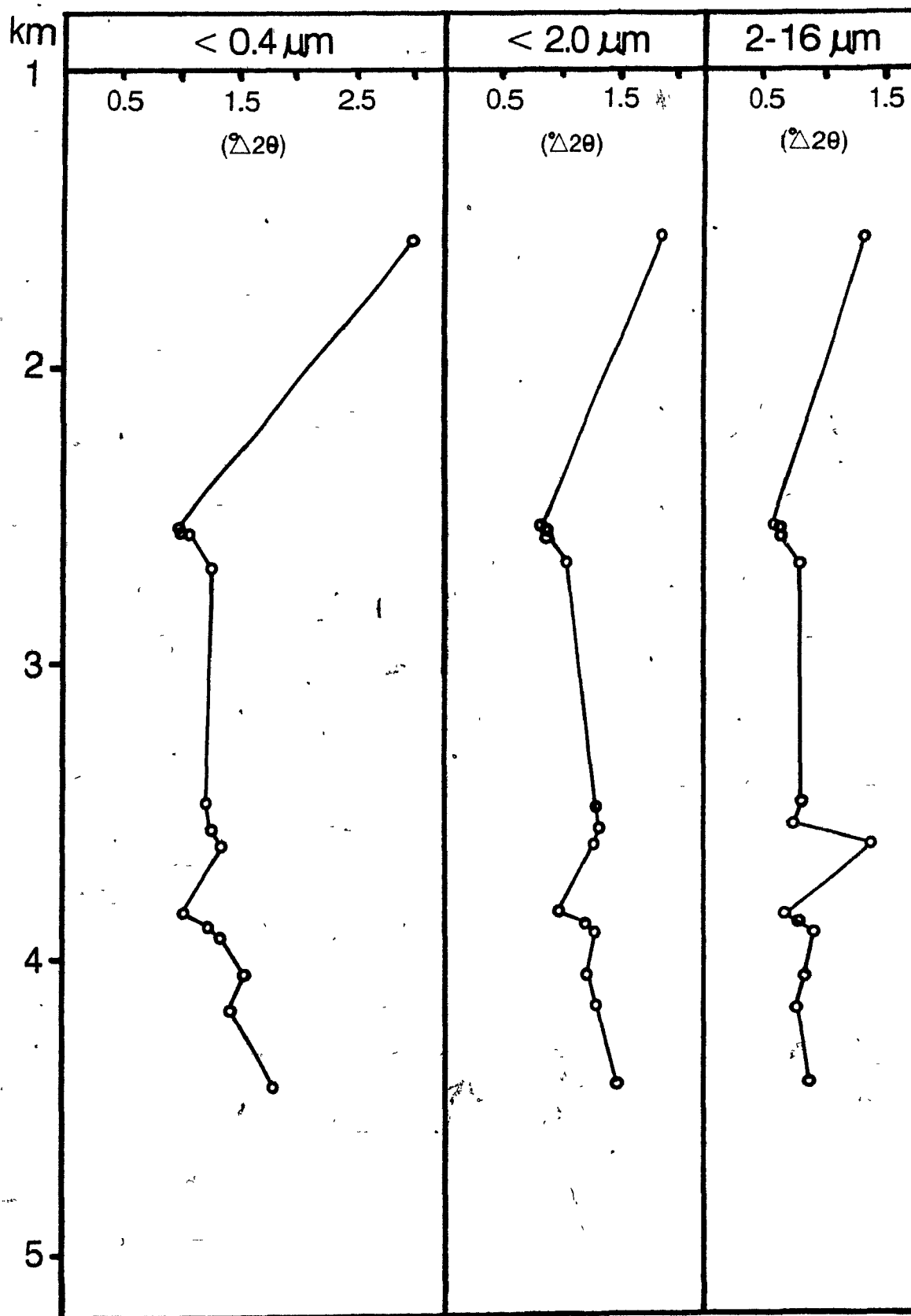
Fig. 4.8 Illite crystallinity versus burial depth for <0.4 um, <2.0 um and 2-16 um size fraction from selected samples.

disrupts a stratigraphic sequence and juxtaposes or superposes fault blocks of different maturity. In the B-08 and B-75 wells, a progressive decrease in IC over a depth interval of about 2 km seems to preclude faulting as a major cause having affected the IC. Small jumps in IC values near 2600 m and 3800 m in the B-27 well, however, might be explained by a thrust fault. However, thrusting does not seem likely in the Jeanne d' Arc Basin because it exhibits an extensional tectonic style with numerous growth faults (Tankard and Welsink, 1987).

Besides temperature, the availability of potassium and the organic matter content of the sediments are considered to be important factors influencing the smectite to illite transformation. Pore water data, presently available from the Canadian Oil and Gas Land Administration (COGLA), are inadeaquate to assess whether or not the availability of potassium was a controlling factor for the observed IC trend. Only 3 water samples are available from the B-08 and B-27 wells. In the B-08 well, the potassium content is low (6 mmole/l at 3900 m). However, in the B-27 well unusually high potassium concentrations (1636 mmole/l at 3300m and 1634 mmole/l at 3950 m) are reported. The dissolution of underlying early Jurassic (Argo Formation) evaporites (i.e. sylvite) could be the source of this high potassium content. Sylvite, however, usually occurs with halite. Sodium content in these two pore water samples is (470 mmole/l, < sea water) much lower than would be expected if dissolution of evaporites had contributed significant

138

amounts of potassium. No authigenic halite was observed in sandstones during this study. Although the source of the elevated potassium content is difficult to constrain from the limited data available, its high levels, however, do not seem to have caused any significant improvement in the IC. Dissolution of feldspars in interbedded sandstones and the disappearance of a small K-feldspar peak from the bulk shale samples were observed near 3600 m (Fig. 4.1). This together with the available pore water data (three samples) suggests that the unavailability of potassium is not the cause of a reverse trend in the IC.

Organic-matter rich black shales are known to show poorer crystallinity than organic-matter poor red and green shales (Ogunyomi et al., 1980). In order to investigate a possible relationship between the observed IC trends and organic matter, the organic carbon content of 22 selected shale samples was analysed. (Fig.4.9 and Appendix 2). The amounts of organic carbon vary from 0.2 to 2.5 wt% and show some positive correlation with the observed IC trends. Particularly in the B-27 well, there is an excellent positive correlation between the organic carbon and IC values. A jump in the IC values from 0.8 to $1.3°\Delta 2\theta$ in the B-27 well corresponds with an increase of organic carbon content. Similarly, a small jump in IC near 2600 m also corresponds with an increase of organic matter (Fig. 4.9). In the B-08 well, some positive correlation is noted below 3600 m, however, above this level there is no correlation.

Fig. 4.9   Weight percent of organic carbon (C_{org}) and
illite crystallinity (<2.0 um fraction) versus burial
depth.
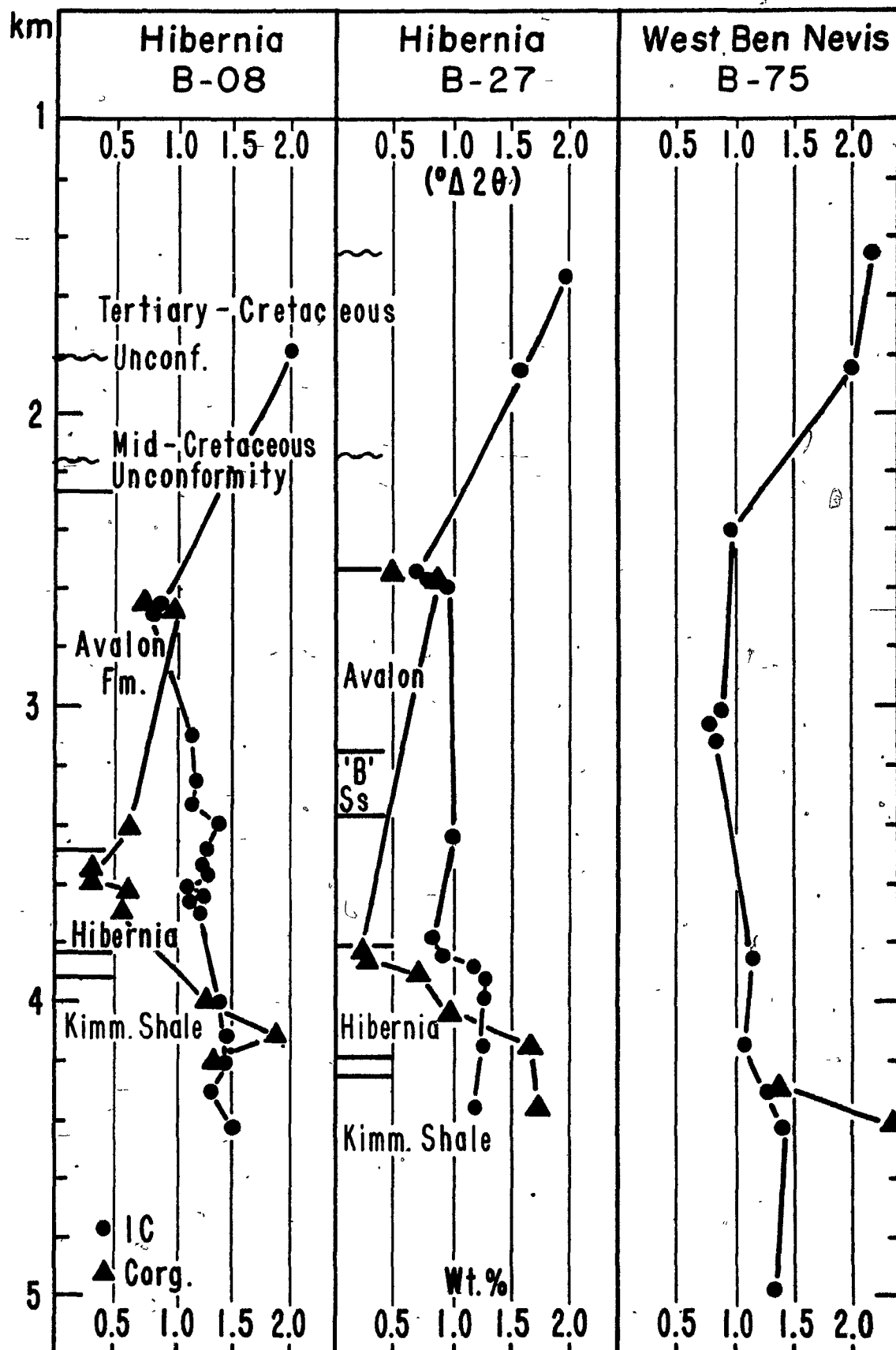
'In the B-75 well, the number of samples analysed (2) is insufficient to establish a correlation. This study, therefore, appears to confirm the well-known effect of organic matter in delaying an improvement in IC during burial diagenesis.

The reversed trend of IC with burial depth, observed in the present study, may be due to several causes: (i) increased organic-matter content; (ii) a higher percentage of mixed-layer I/S (and/or smectite) supplied during the early stages of deposition. The effects of other factors (e.g. authigenic illite) need further evaluation. The use of IC as an indicator of maturation in organic matter-rich source rocks, therefore, requires considerable caution particularly during the middle (and probably also the late) stages of diagenesis.

4.7 DISCUSSION AND SUMMARY

The increase in illite, the decrease in the percentage of smectite in mixed-layered I/S, the decrease in kaolinite and the disappearance of discrete smectite are important mineralogical changes observed in shales of the Hibernia and West Ben Nevis fields.

In the Hibernia and West Ben Nevis areas, a major Middle Cretaceous unconformity is encountered near 2200 m depth. Above the unconformity, the sediments are mainly shales which were deposited in shallow to deep marine environments (Swift et al., 1975). The average mineralogical composition of

142

these shales is 40 weight % illite (plus I/S), 25 weight % -smectite and 35 weight % kaolinite (plus minor chlorite). Below the Middle Cretaceous unconformity, shales interbedded with sandstones were deposited in marine to deltaic to fluvial environments. They contain predominantly illite (75%) and kaolinite (25%). All samples above 1500m subsurface depth show the 17Å peak upon glycolation which disappears near 2000 m depth and shows a shoulder toward higher d-spacing. This reveals that above the unconformity, the disappearance of discrete smectite and a decrease in the smectite content of mixed-layer I/S (from 75% to 45%) are the results of diagenesis. Freed (1981) also observed that significant changes in the shales (i.e. transformation of smectite to illite in mixed-layer I/S) of the Hidalgo County, Texas begin at temperatures between 58 to 69 °C.

Shale samples immediately below the unconformity (near 2500 m) show high amounts of illite with a relatively sharp 10Å illite peak. The mixed-layer I/S content is smaller than in deeper samples. A rapid change below the unconformity (higher amounts of illite with a sharp 10Å peak) appears to be related to a change in the depositional environment and/or in provenance. This change is difficult to explain solely by diagenetic processes. From 2500 m to 4900 m the amount of illite increases and kaolinite decreases. These variations most likely represent diagenetic changes, i.e. the conversion of smectite in I/S mixed layer clays into illite.

The conversion of smectite to illite through mixed-layer

143

I/S is the most widely recognized effect of burial diagenesis (Dunoyer de Segonzac, 1970; Perry and Hower, 1970; Foscolos and Kodama, 1974; and Hower et al., 1976). This conversion involves an increase in net negative layer charge of the expendable layers either due to tetrahedral substitution of Al^{3+} for Si^{4+} or by substitution of Fe^{2+}, Mg^{2+} for Al^{3+} in the octahedral layer. The excess negative layer charge can be balanced by incorporation of K^+ in interlayer positions. These substitutions involves a significant change in the chemical composition of the 2:1 layers (a gain of interlayer potassium; increasing substitution of aluminum for silica in the tetrahedral layers; loss of megnesium; silica; and probably reduction of iron). Such compositional changes lead Hower et al. (1976) and Boles and Franks (1979) to suggest two different reaction mechanisms for the transformation of smectite to illite in mixed-layer I/S clay minerals:

(1) The first mechanism assumes that the original smectite layers remain intact and that the change to illite involves ionic substitution of Al^{3+} for Si^{4+} in the tetrahedral sheet resulting in a net increase in negative charge which is balanced by addition of K^+ to interlayer position (Hower et al., 1976). The overall reaction is:

k-feldspar + smectite ----> illite + quartz
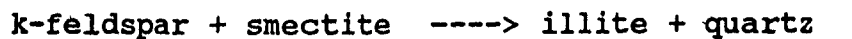
Hower et al. (1976) suggested that the source of alumimum and potassium is K-feldspar in shales which dissolves with depth.

144

(2) The second reaction is based on the assumption of Al^{3+} conservation and requires only the addition of K^+ (Boles and Franks, 1979). According to this reaction some of the original smectite layers in I/S mixed-layer are decomposed to supply Al^{3+} releasing also some other cations (i.e Mg^{2+} Si^{4+} Fe^{2+}). Boles and Franks (1979) also stated that aluminous smectite layers are preferentially converted to illite, leaving behind the more iron- and magnesium-rich smectite layers. These smectite layers are transfered to illite during late diagenesis releasing iron and magnesium to pore fluids. The number of new illite layers in the I/S mixed-layers is smaller than the original number of smectite layers. Some workers (Eberl and Hower, 1976; Eberl, 1978a 1978b; and Lahann and Roberson, 1980) provided experimental support for this model by converting smectite into mixed-layer I/S in the absence of an external source of Al. The overall reaction can be written as:

$$K^+ + \text{smectite} \longrightarrow \text{illite} + \text{quartz} + H^+.$$
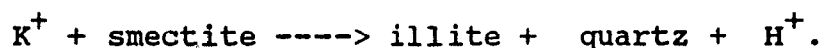
More recently, the use of transmission and analytical electron microscopy (TEM/AEM) have lead to some advances in the understanding of the illitization process although some of conclusions are still controversial. Ahn and Peacor (1986) (using TEM/AEM) studied shale cuttings from the Case Western Reserve University (CWRU) Gulf Coast 6 well. Hower et. al., 1976 had used shale samples from the same well. They suggest that the conversion of smectite into illite

does not necessarily require mixed-layer I/S as an intermediate phase and that illite formation appeared to have started with the growth of small pockets of illite layers within subparallel layers of smectite. Bell's (1986) TEM/AEM study of drill cuttings from the COST 1 well, (east of South Padre Island Texas), however, suggests the presence of interstratified illite smectite layers as originally proposed by Reynolds and Hower (1970). According to this author, the replacement of smectite layers by illite appears to have been the principal transformation mechanism. In this context, it is interesting to note that the conversion of smectite to illite by any of the proposed mechanisms releases a variety of components (Si^{4+}, Mg^{2+}, Fe^{2+}, and Ca^{2+}) to the pore fluids which may then become available for cementation in nearby sandstones.

Significant amounts of kaolinite are present in almost all samples. However, this mineral is absent in a few samples near the Cretaceous-Tertiary unconformity (near 1800 m in the B-08 well and 1500 m in the B-27 well). The abrupt disappearance of kaolinite in this interval most likely reflects a change in depositional environments and/or source or pore fluids compositions. Kaolinite (plus minor chlorite) decrease from an average of 35 wt.% (above 2000 m) to about 20 wt.% below 3950 m (Table 4.1). This change in kaolinite may be due to: (1) differential transportation and sedimentation, and/or (2) diagenetic degradation and transformation of kaolinite to illite or chlorite.

146

Differential sedimentation is an unlikely cause for the following reason. Kaolinite is generally a coarser-grained clay mineral and should increase in abundance with the transition from marine toward marine-deltaic to fluial environments that occurred in the Hibernia area with increasing geologic age during Cretaceous time (provided that the source area and the climate remained the same).

As subsurface temperatures and ionic strength of the pore fluids increase, kaolinite is tranformed to other clay minerals (Dunoyer de Segonzac, 1970; Foscolos and Powell, 1980). The observed increase in kaolinite crystallinity values (decrease of crystallinity, area/hight ratio; Schultz, 1964) with depth may be indirect evidence for a diagenetic degradation of kaolinite at temperatures above $90^{\circ}C$. Progressive destruction of kaolinite during burial diagenesis may begin near 80 $^{\circ}C$ (Dunoyer De Segonzac, 1970) and largely depends upon the pore-fluid compositions. Kaolinite may be converted to illite if the $[K^+]/[H^+]$ ratio in pore fluids is high (Hemley, 1959), or may form authigenic chlorite with the addition of Mg^{2+} and Fe^{2+} supplied by the breakdown of smectite layers (Boles and Franks, 1979). As mentioned earlier, chlorite decreases with increasing burial depth. This may be due to highly acidic pore waters (originating from the thermal decarboxylation of organic matter) which would have precluded chlorite precipitation and/or have caused dissolution of some of the detrital chlorite. The Mg^{2+} and Fe^{2+} ions released from smectite and detrital chlorite may then have been exported into nearby sandstone beds and have

been used in the precipitation of ferroan-dolomite, ferroan-calcite and late pyrite observed in many sandstone samples (see Chapters 3 and 6).

In summary, this study indicates the following mineralogical variations in shales with increasing burial depth.

(1) The amount of illite increases from approximately 40% (above 2000 m) to approximately 80% (below 3600 m).

(2) Discrete smectite (displaying the 17$\overset{\circ}{A}$ peak upon glycolation) is only present above 2000 m.

(3) Smectite in interstratified I/S decreases from 75% to less than 15% from 1000 to 5000 m subsurface depth.

(4) Kaolinite (plus minor chlorite) decreases from an average 35% (above 2000 m) to 20% below 3950 m. Its crystallinity (area/height ratio) decreases with depth and probably indicates degradation of kaolinite.

(5) Chlorite is present in small amounts and decreases below 3600m.

(6) An increase in illite crystallinity values (IC) below the Avalon Sandstone is probably due to an increase in organic matter content and percent mixed-layer I/S (and/or smectite) at that levels due to variations in composition of the sediment supplied to the basin.

(7) In the bulk shale samples, K-feldspar disappears below 3600m depth. Below 3500 m, calcite is absent in most samples.

148

CHAPTER V

EFFECTS OF DIAGENESIS ON POROSITY EVOLUTION

5.1   INTRODUCTION AND OBJECTIVES

The relationship of diagenesis to development and preservation of porosity in sedimentary rocks, particularly the origin of secondary porosity, has become a topic of major debate and concern for petroleum geologists. Evidence for the occurrence of secondary porosity in sandstones was first published in North America by Schmidt et al. (1977); Lindquist (1977); Hayes, 1979; and Schmidt and McDonald (1979 a,b), although it was first reported in USSR (Proshlyakov, 1960; Chepikov et al., 1961). The recognition of secondary porosity is significant because exploration for hydrocarbon reservoirs can be extended to much greater depths in sandstones that contain secondary porosity than it could be in sandstones only containing primary porosity (if not overpressured). The objectives of this chapter are to:

(1) recognize and describe the different types of porosity in reservoir sandstones;

(2) quantify these porosity types in different sandstone units;

(3) assess the effect of diagenesis (cementation, dissolution, and recementation) on reservoir quality;

(4) compare observed diagenetic sequences and evolution of secondary porosity with other quartz-rich sandstones from different sedimentary basins; and

149

(5) describe possible primary controls on sandstone diagenesis and porosity modification.

5.2   PRIMARY POROSITY TYPES

Primary pores form during deposition and may remain open for some time during mechanical compaction as long as no intergranular cement is introduced. Primary porosity is recognized by: (1) regular intergranular pores; (2) lack of oversized and elongated pores; (3) homogeneous compaction; (4) lack of grain margin corrosion and presence of uncorroded quartz overgrowths. Primary porosity is dominant in the Avalon Sandstone (Table 5.1). However, with increasing depth, secondary porosity develops. Secondary porosity is sometimes difficult to differentiate from primary porosity if both occur in the same thin section. Two types of primary porosity are recognized, intergranular and intraparticle porosity.

5.2.1 Intergranular Porosity

Intergranular pores are areas between detrital grains which remain uncemented (Plate 18A, 18B, and 18D). This is the dominant type of primary porosity. In the Avalon and "B" Sandstones much of the intergranular porosity was destroyed by early calcite cementation.

5.2.2 Intraparticle Porosity

Intraparticle porosity (mainly in fossil fragments) is observed in fossil-rich zones. It is a common porosity type

150

Table 5.1   Point-count analyses of selected samples showing
distribution of primary and secondary porosities.
Secondary porosity is further classified into four
genetic classes.

DC   = Dissolution of cement

DFG   = Dissolution of Framework Grains

DRC   = Dissolution of Replacive Cements

F   = Fracture Porosity

PP   = Primary Porosity

SP   = Secondary Porosity

TOL.P = Total thin section porosity

Depth (m)	Tol. P	SP	PP	DC	DFM	DRC	F

(A) AVALON SANDSTONE

Depth (m)	Tol. P	SP	PP	DC	DFM	DRC	F
2184.6	12.5	1.8	10.9	1.8	--	--	--
2185.8	9.2	1.2	8.0	1.2	--	--	--
2190.3	6.2	0.2	6.0	0.2	--	--	--
2190.8	9.2	0.8	8.4	0.8	--	--	--
2197.5	18.0	3.8	14.2	3.2	0.4	0.2	--
2197.9*	10.2	1.6	8.6	1.6	--	--	--
2578.8	21.2	6.0	15.2	3.2	2.8	--	--
2659.6	11.4	5.4	6.0	3.4	2.0	--	--
Av.	12.2	2.6	9.6	1.9	0.7		

(B) "B" SANDSTONE

Depth (m)	Tol. P	SP	PP	DC	DFM	DRC	F
3178.0	12.6	10.2	2.4	6.4	2.6	1.2	--
3179.1	10.8	6.7	4.7	3.0	1.6	1.5	--
3185.9	9.7	5.3	4.4	4.0	0.5	0.8	--
3131.5	9.6	5.0	4.6	--	--	--	--
Av.	10.7	6.7	4.0				

(C) HIBERNIA SANDSTONE

Depth (m)	Tol. P	SP	PP	DC	DFM	DRC	F
3481.3	8.9	4.1	4.8	2.6	1.2	0.3	--
3482.6	12.1	8.0	4.1	4.2	2.9	0.8	0.1
3483.4	6.3	3.6	2.7	1.2	0.8	1.6	--
3555.1	12.5	8.9	3.6	4.8	3.5	0.6	--
3606.2	3.4	1.8	1.6	0.1	1.7	0.0	--
3619.4	12.8	8.4	4.4	4.3	3.0	1.0	0.1
3622.4	9.8	6.9	2.9	5.5	1.0	0.4	--

3624.2	7.7	3.3	4.4	2.2	0.5	0.4	0.2
3845.8	10.7	8.8	1.9	1.7	1.3	5.8	--
3846.5	19.2	16.6	2.6	8.8	3.4	4.4	--
3849.75	16.9	15.0	1.9	7.5	2.2	5.1	0.2
3850.3	21.9	21.9	--	11.2	9.0	1.6	--
3850.7	25.0	25.0	--	16.0	6.6	2.4	--
3854.5	12.6	7.0	5.6	4.8	1.2	1.0	--
3879.0	16.0	16.0	-	10.3	4.4	1.3	--
3895.2	14.2	14.2	-	8.0	1.4	4.8	--
Av.	13.1	10.6	2.5	5.8	2.8	2.0	

PLATE 18

Primary porosity and geopetal structure.

(A) Intergranular primary porosity in a fine-grained sandstone. The lower half of photograph (stained red) is completely cemented with ferroan calcite. In the porous part, framework grains are coated with thin clay rims whereas the rims are absent in the lower cemented zone. Compared to lower cemented part, the porous part is slightly more compacted. Note uncorroded poikilotopic calcite crystal facing pore space. Avalon Sandstone, O-35, 2197.90 m. Plane-polarized light. Scale bar: 500 um.

(B) Intergranular primary porosity (blue) in a loosely compacted sandstone. Note pressure solution contacts (arrow) between fossil fragment and quartz grains. Bedding direction sub-horizontal. Avalon Sandstone, O-35, 2191.50 m. Plane-polarized light. Scale bar: 500 um.

(C) Geopetal structure in serpulid worm tube preserved due to early calcite cementation (C). The bedding direction is northsouth. Avalon Sandstone, O-35, 2185.60 m. Plane-polarized light. Scale bar: 500 um.

(D) Reduced intergranular primary porosity (blue) in one of the deeper reservoir sandstones of the Hibernia Field showing sub-triangular pores (P) with uncorroded framework grain margins. Hibernia Sandstone, C-96, 3928.60 m. Plane-polarized light. Scale bar: 100 um.
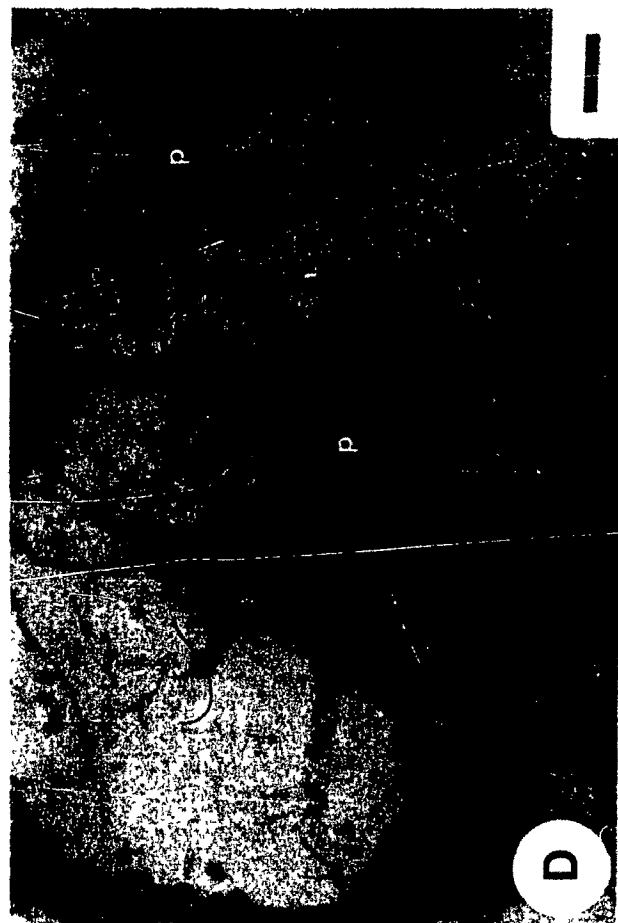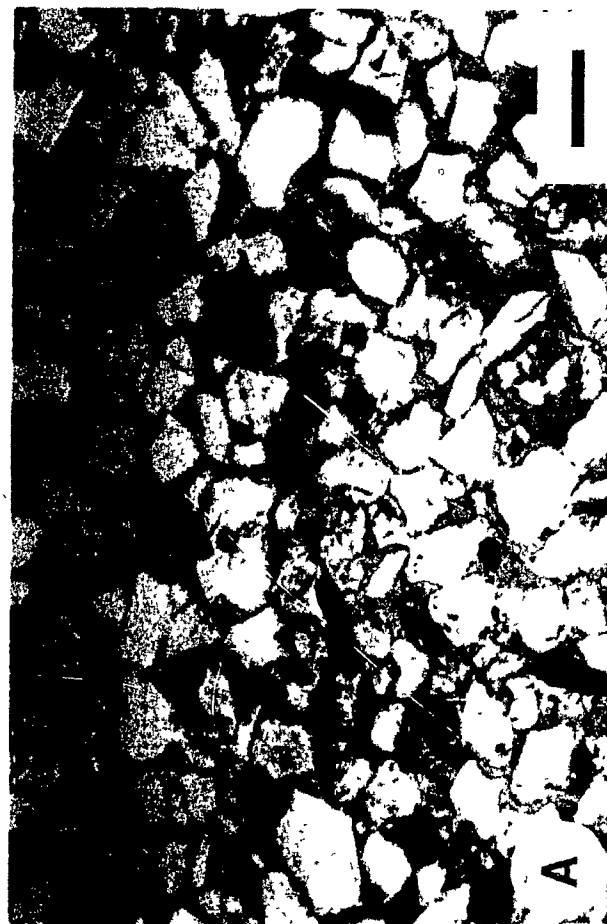
in the Avalon Sandstone, but its overall contribution to total porosity is not significant. A few intraparticle pores of primary origin were partially filled with geopetal sediments and then cemented by sparry calcite (Plate 18C).

5.3   SECONDARY POROSITY TYPES

All pore spaces which developed after deposition as a result of diagenetic processes are referred to as secondary pores. At intermediate depth levels secondary porosity increases with subsurface depth and may amount to as much as 25%. of the bulk volume in the Hibernia Sandstone (Table 5.1). The development of secondary porosity may either recover lost primary porosity or generate new porosity. Accordingly there are two categories of secondary porosity: (1) restored primary porosity that was lost by cementation but then recovered when the cements were dissolved. This process does not add any new porosity to the porosity present at the time of deposition/ cementation.   (2) Secondary porosity formed by the dissolution of framework grains and/or dissolution of replacive cements, which creates new porosity that was originally not present.

5.3.1 Intergranular Porosity

Most of the secondary porosity is intergranular and was formed as a result of dissolution of pore-filling and replacive cements (Plate 21C). Regular intergranular pores of secondary origin which mimic primary pores were observed in many sandstone samples from the Avalon and "B" Sandstones.

156

Enlarged intergranular pores of secondary origin are common in the Hibernia Sandstone. These pore spaces can be recognized by highly corroded detrital grain boundaries and their elongated shapes.

5.3.2 Moldic and Vuggy Porosity

Grain molds are pores which show outlines characteristic of their precursor framework grains. Moldic pores form by partial to complete dissolution of former framework constituents (e.g. chert, feldspar, shale clasts, fossils and other carbonate fragments), many of which are now unrecognizable. Moldic porosity was observed in all reservoir sandstones (Plate 19A, 19B, 19C, 19D, and 23D). It was also noticed mesoscopically during drill-core investigation as partly dissolved fossils (e.g., gastropods and pelecypods at 2581 m in B-27; see section 3.2.10.2). The size of individual moldic or vuggy pores depends on the size of the dissolved original constituents.

5.3.3 Oversized Pores Including Elongated and Irregularly Distributed Porosity

Oversized pores are those whose size exceeds the diameter of adjacent grains by a factor of at least 2 (Schmidt and McDonald, 1979b). They are commonly observed in the "B" and Hibernia Sandstones (Plate 20A, 20B, 21D, and 27D). Generally, these pores are formed through dissolution of large carbonate fragments, chert fragments, mud clasts and intergranular calcareous matrix. Choquette and Pray (1970) refer to this type of porosity as "fenestrate porosity".

157

PLATE 19

Moldic porosity in different reservoir sandstones.

(A) Large elongated moldic pore (MP) developed by the dissolution of shell fragment (probably pelecypod). Micrite lining of shell fragment dissolved at places, and partly broken and suspended within the pore. Ferroan calcite cement (stained blue, fc) also dissolved at a few places (arrow). This sample contains substantial amounts of mud-clast (brownish). Avalon Sandstone, B-27, 2555.25 m. Plane-polarized light. Scale bar: 100 um.

(B) A moldic pore (MP), lined with oil-stained dark calcite (arrow), produced by dissolution of a framework grain (most likely carbonate). Another moldic pore (left side) was subsequently filled by late ferroan dolomite (D). In the upper-right corner, a carbonate rock fragment is partly dissolved. "B" Sandstone, O-35, 3183.70 m. Plane-polarized light. Scale bar: 50 um.

(C) Moderately compacted sandstone showing isolated moldic pores (arrows) of secondary origin. Nature of the dissolved material is unknown. Hibernia Sandstone, B-O8, 3606.18 m. Plane-polarized light. Scale bar: 500 um.

(D) Large moldic pore formed by dissolution of a carbonate rock fragment. Prismatic crystals grown on the dissolved fragment are less affected by dissolution and partly preserved. Note variation of colour of calcite crystals as a function of varying Fe-content. Avalon Sandstone, B-27, 2578.84 m. Plane-polarized light. Scale bar: 50 um.
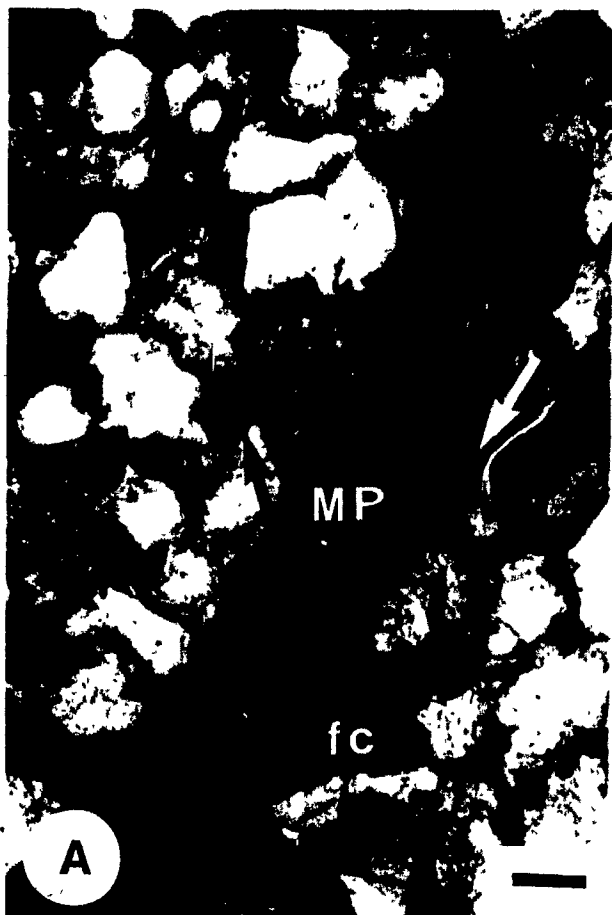
PLATE 20

Oversized and elongated pores. (Scale bar: 500 um.)

(A) Two oversized interconnected pores (P). Compare degree of mechanical compaction in the left and right sides of the photograph. Quartz overgrowth observed on a few detrital grains indicates corroded and replaced grain margins (arrows). Hibernia Sandstone, B-08, 3482.63 m. Plane-polarized light.

(B) Oversized pores and variable degree of compaction (compare arrows a and b) between different framework grains. Hibernia Sandstone, C-96, 3923.50 m. Plane-polarized light.

(C) Large calcite fragment (incompletely stained), deformed between rigid quartz grains, is partly dissolved forming secondary porosity. "B" Sandstone O-35, 3183.70 m. Plane-polarized light.

(D) In a well-compacted sandstone, large elongated pores suggest secondary origin after significant compaction. Hibernia Sandstone, B-08, 3706.18 m. Plane-polarized light.

Concentration of smaller dissolution-pores in patches or individual layers may also produce oversized pores. Elongated (Plate 20C, 20D) and irregularly distributed pores (Plate 21A, 21B, 21C) originated from dissolution of large fossil fragments and removal of irregularly distributed cements and/or replacive cements.

5.3.4 Intra-constituent Pores

Intraconstituent pores were formed by partial leaching within the following types of constituents: chert, feldspar grains, calcareous fossils, limestone rock fragments, and shale clasts (Plate 22A, 22B, 22C, 22D). This type of porosity is present in all reservoirs of the Hibernia field; however, it is most common in the "B" and Hibernia Sandstones.

5.3.5. Fracture Porosity

Fracture porosity is observed in many samples but is volumetrically insignificant. It is common in the "B" and Hibernia Sandstones and rarely observed in the Avalon Sandstone. Most of the fractures are confined to individual grains (e.g. quartz grains, fossil fragments, Plate 23A), but some of them pass through adjacent grains, including cement and matrix (rock fractures and joints). Rock fractures were also observed in the Hibernia Sandstone during core examination (Plate 23B). A few fractures are cemented with calcite and dolomite cements or with late pyrite. Although fractures do not significantly contribute to the development of porosity, they may significantly increase

PLATE 21

(A) Irregularly distributed secondary pores (blue). The lower part of the photograph indicates reduced intergranular porosity due to mechanical compaction. The middle part exhibits a loose fabric of framework grains with large secondary pores. Hibernia Sandstone, K-18, 3841.47 m. Plane-polarized light.

(B) Irregular and elongated pores (P) of secondary origin. In the lower right corner, porosity is completely eliminated by mechanical compaction and minor silica cementation, while the rest of the photograph shows enlarged intergranular porosity. Hibernia Sandstone, C-96, 3929.80 m. Plane-polarized light.

(C) Highly irregular shape of pores (P) as well as of quartz grains. The porosity is the result of dissolution of framework grains, calcite cements and replacive cements. Hibernia Sandstone, B-27, 3850.65 m. Plane-polarized light.

(D) Large irregular secondary pore. Note quartz overgrowth on framework grains with thick clay coating. Hibernia Sandstone, B-08, 3619.00 m. Plane-polarized light.
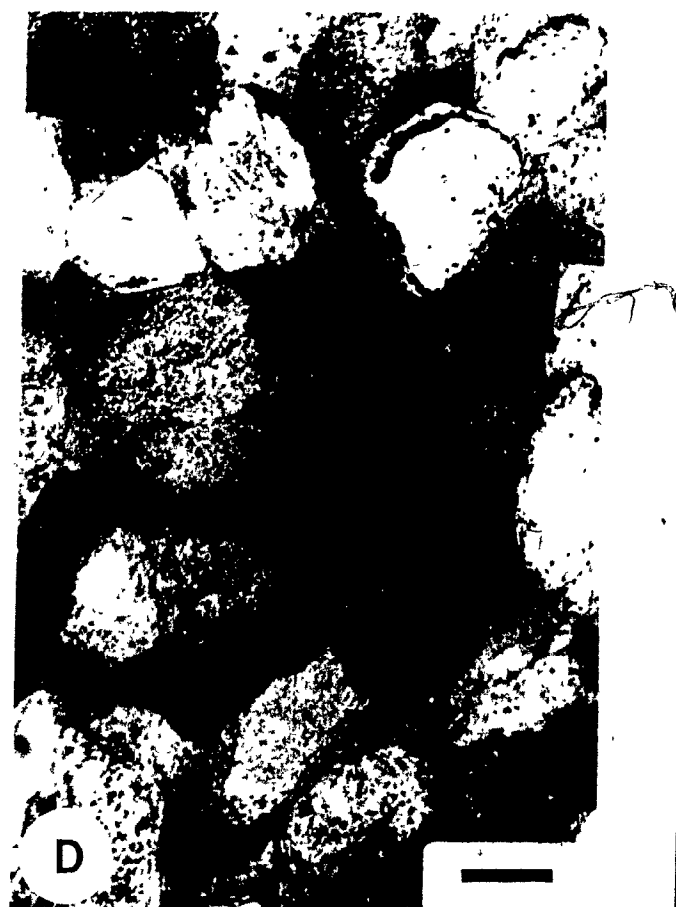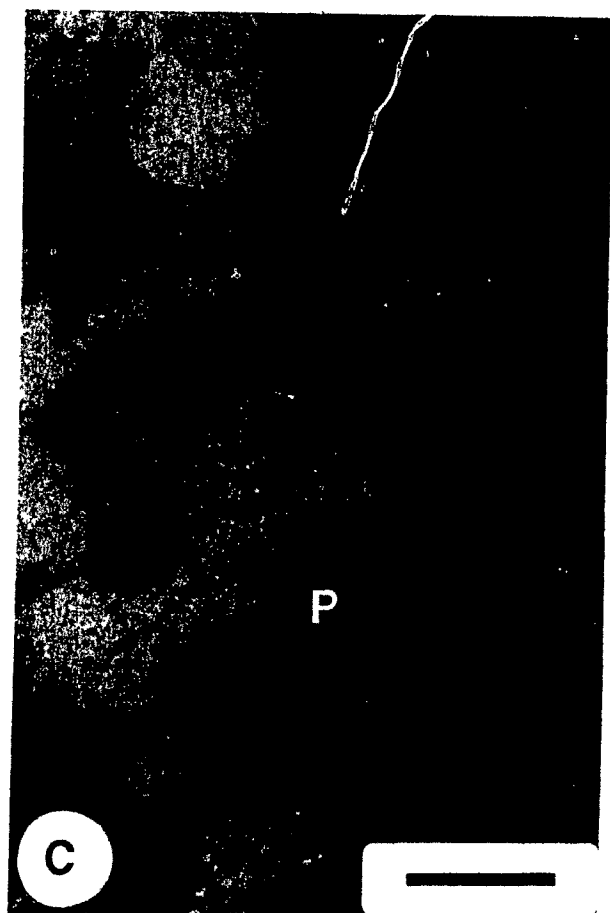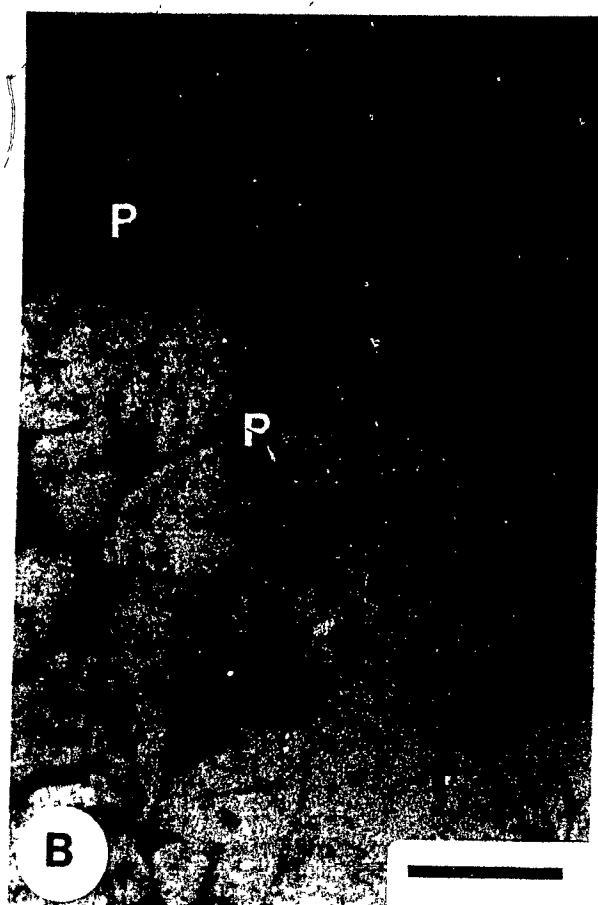
PLATE 22

Intra-constituent porosity in the Hibernia reservoir sandstones.

(A) Partial dissolution of a feldspar grain. Hibernia Sandstone, B-27, 3849.75 m. Plane-polarized light. Scale bar: 50 um.

(B) Advanced dissolution of feldspar grain (F) causing secondary porosity (SP). Quartz overgrowth produces well developed crystal faces. Hibernia Sandstone, B-08, 3481.28 m. Plane-polarized light. Scale bar: 50 um.

(C) Chert grain almost completely dissolved except at the rim. Hibernia Sandstone, B-27, 3850.27 m. Plane-polarized light. Scale bar: 100 um.

(D) Dissolution of a shale clast and surrounding calcite cement enhancing sandstone porosity. "B" Sandstone, O-35, 3176.00 m. Plane-polarized light. Scale bar; 50 um.
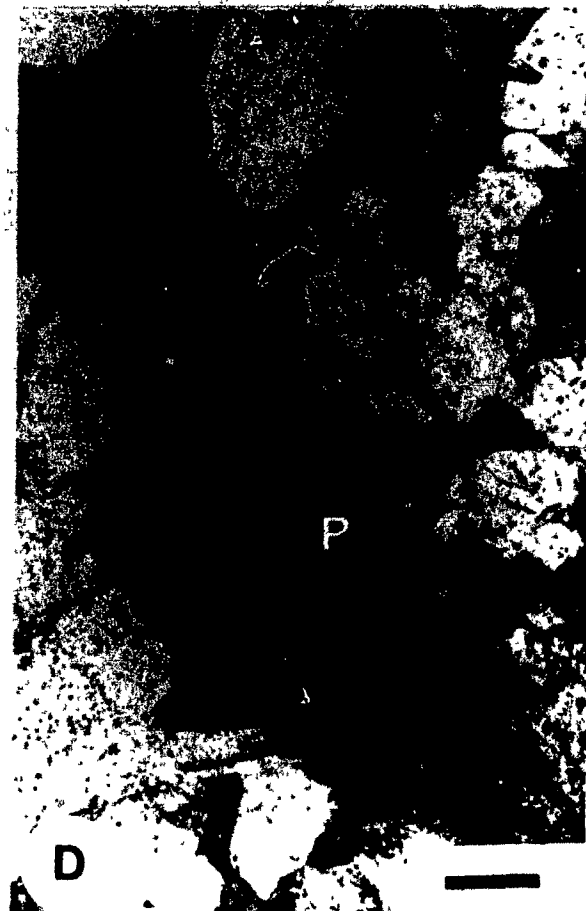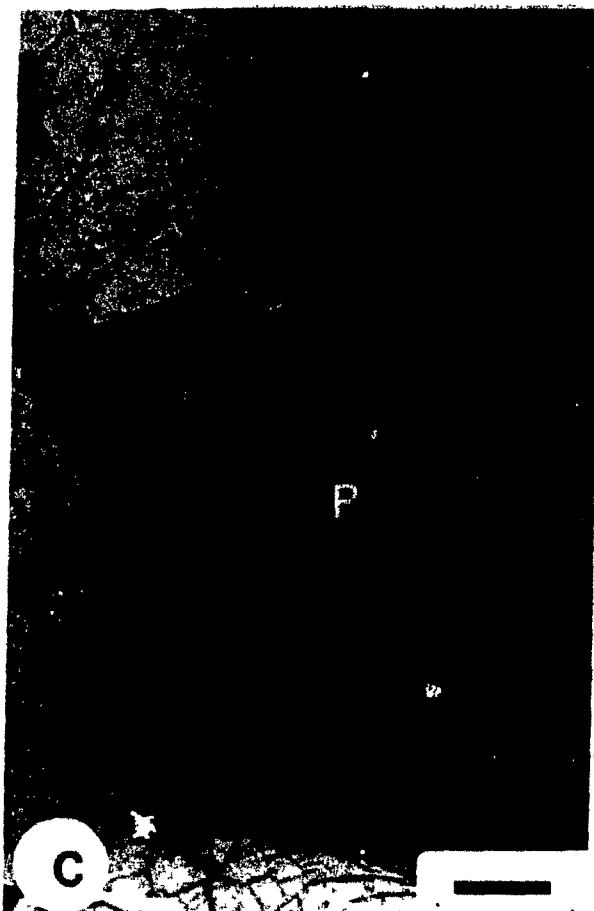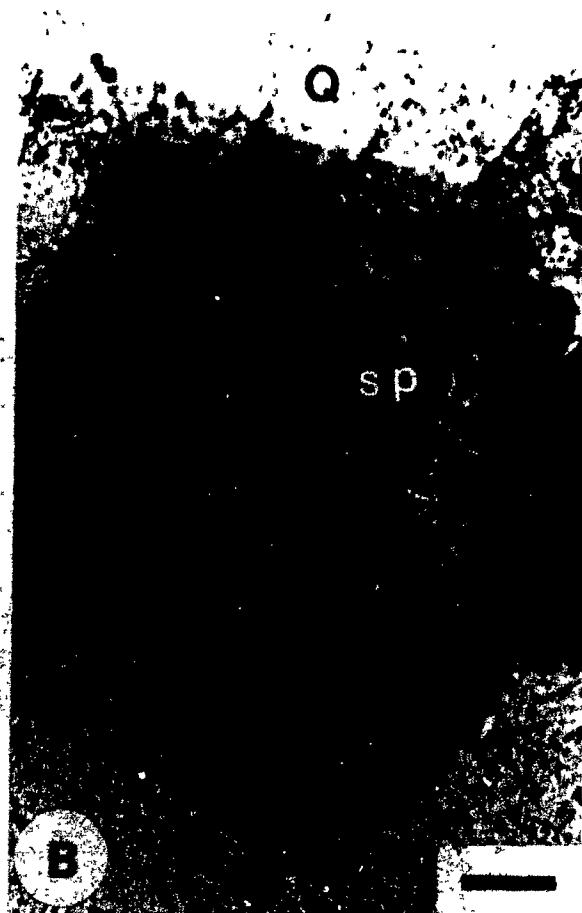
reservoir permeability.

5.3.6 Shrinkage Porosity

Shrinkage porosity was observed in a very few samples. For example, a thin rim of open pore space (revealed by blue-dyed epoxy) around a brownish fluorapatite (collophane) grain indicates shrinkage porosity (Plate 23C). Some observed fractures in glauconite grains may also result from shrinkage.

5.4 DIAGENETIC CONTROL ON RESERVOIR PROPERTIES

The effects of diagenesis (cementation, dissolution and recementation) on sandstone porosity will be discussed below for individual reservoirs. Table 5.2 summarizes average core porosities in hydrocarbon bearing zones in the Hibernia Oil Field.

5.4.1 Avalon Sandstone

In the Avalon Sandstone, the depositional environment has exerted significant control on subsequent diagenesis. The Avalon Sandstone consists mainly of fine-grained sandstone which was deposited in shallow water shoreline environments (Benteau and Sheppard, 1982). In places, both sandstones and interbedded shales are rich in limestone and fossil fragments. These readily available carbonate constituents may have served as an important source for early calcite cementation due to pressure solution (Plate 18B) in the Avalon Sandstone of the Hibernia Field.

PLATE 23

Fracture, shrinkage, and intraconstituent porosity.

(A) Intragranular fracture porosity (arrow) produced by mechanical compaction after quartz overgrowth. Note that isolated pores become interconnected by these fractures. Hibernia Sandstone, B-27, 3850.27 m. Plane-polarized light. Scale bar: 50 um.

(B) Drill-core photograph displaying numerous normal faults with small displacements. Hibernia Sandstone, B-27, 3878.6 m. Scale bar in cm.

(C) Thin rim of open pore space (arrow) around a fluorapatite (collophane) grain showing shrinkage porosity. Avalon Sandstone, O-35, 2190.81 m. Plane-polarized light. Scale bar: 50 um.

(D) Rhomb-shaped molds (M), in a silicified ooid suggesting the presence of a former carbonate phase which was leached after silicification. Avalon Sandstone, B-27, 2555.25 m. Plane-polarized light. Scale bar: 50 um.

3378.60
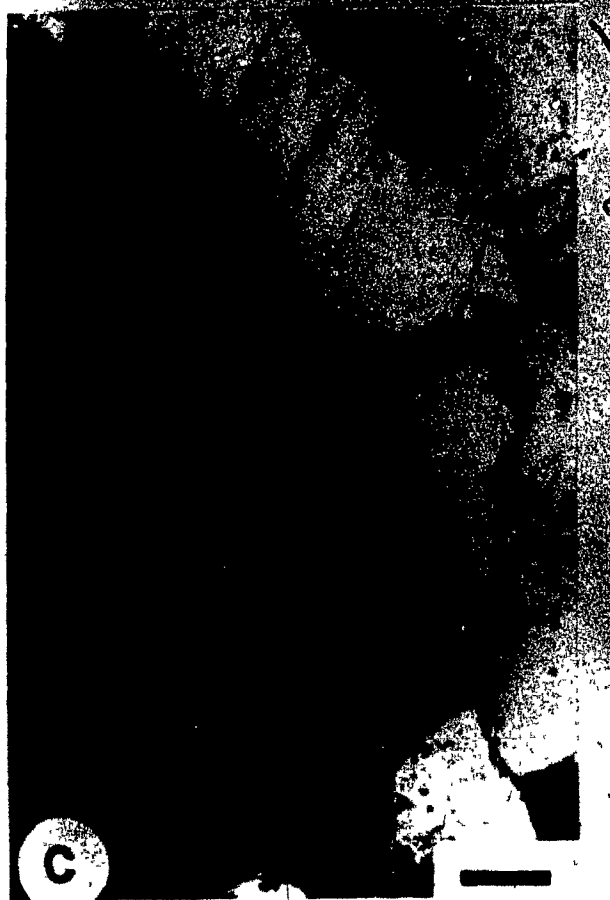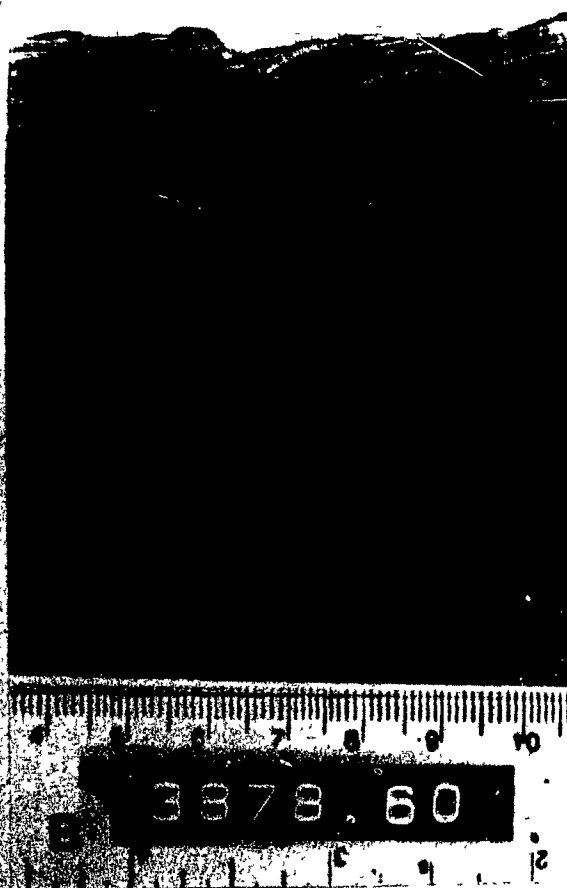
Table 5-2   Summary of average core porosities in hydrocarbon bearing zones with net pay zones in the Hibernia   area   (data from McMillan, 1982 and Handyside and Chipman, 1983).

Reservoir Zone	Gross interval tested (m)	Net Pay (m)	Average core porosity	Hydrocarbon bearing zones				
				P-15	O-35	B-08	G-55A	K-18
Avalon	2422-2443	17.1	18.0	oil	oil	oil	water	oil
"B" Sst	-	-	-	water	water	gas	water	oil
Hibernia	3752-3898	53.3	18.3	oil/ water	water	oil/ gas	water	oil
Jeanne d' Arc Member	4142-4159	18.3	10.13	oil	water	oil/ gas	water	oil

* well not studied

170

5.4.1.1 Porosity Loss by Cementation

The most important cementing mineral in the Avalon Sandstone is early ferroan calcite (8.4%). Porosity reduction by other authigenic minerals (quartz overgrowths, siderite, chlorite and pyrite) is comparatively less important (a total average of 4.9%). Thin chlorite coatings are common to the Avalon Sandstone and may reduce reservoir permeability. Dolomite and kaolinite were not observed.

The early calcite cementation, which affects zones less than 1.5 m thick, completely occludes available porosity ("tight—sandstone"). About 20% of the Avalon Sandstone drill-core (based on 5 wells studied) are completely cemented by calcite (Table 5.3). The tight-sandstone zones are abundant in wells B-27 and C-96, where 22% and 40% respectively of the sandstone cores are completely cemented by early calcite. The early calcite cementation has interrupted further mechanical compaction and precipitation of other cements which makes these sandstone excellent candidates for secondary porosity development at deeper levels.

5.4.1.2 Formation of Secondary Porosity
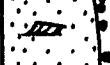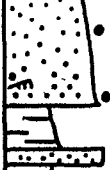
Although the porosity of the Avalon Sandstone is mainly primary in origin, some secondary porosity (an average of 2.6%) has been observed. Some calcite cements, as well as fossil and limestone fragments are partly dissolved (Fig. 5.1). This dissolution event was followed by the migration of hydrocarbons which stopped further dissolution (Plate 24A). In a few fossil fragments (i.e.pelecypods), the

Table 5.3 Distribution of tightly cemented zones (by calcite with minor dolomite) in different reservoir horizons in the Hibernia field (data based on drill cores from the B-08, O-35, B-27, K-18, and C-96 wells).

Well No	Avalon Sandstone		"B'" Sandstone		Hibernia Sandstone		Jeanne d'Arc Member		Total tight sst.
	Total sst. core (m)	Total tight sst. (m)	Total sst. core (m)	Total tight sst. (m)	Total sst. core (m)	Total tight sst. (m)	Total sst. core (m)	Total tight sst.	
O-35	10.0	1.5	7.0	3.2	-	-	2.9	0.3	5.0
B-27	22.0	5.0	-	-	32.5	2.0	-	-	7.0
K-18	6.0	0.0	9.7	1.7	41.0	2.5	-	-	4.2
C-96	9.0	3.6	-	-	42.0	0.8	-	-	4.4
B-08	3.2	0.4	6.2	0.2	17.0	0.0	-	-	0.6
Total	50.2	10.5	22.9	5.1	132.5	5.3	2.9	0.3	21.2

Fig. 5.1 Thin section and drill-core observations from a 17 m thic section
of the Avalon Sandstone in the B-27 well. Most of the porous hydrocar-
bon bearing zones which alternate with calcite cemented zones (tight-
sandstone) show dissolution features.

■ Tight-sandstone

⌒ Fossil-rich zone

▱ Cross bedding

➤ Mud clasts

● Location of samples

DEPTH (m)	LITHOLOGY	CORE OBSERVATIONS	DIAGENETIC FEATURES
2571		Sharp contact between porous (above) and tight-sandstone (facing black area).	Completely cemented by early ferroan calcite Few siderite crystals are also present.
		Tight-sandstone with rounded mud-clasts.	
		Sharp contact.	
		Oil stained sandstone with abundand fossil fragments.	Mainly primary porosity (18%).
		Gradded bedding.	
		Grey shale.	
2575		Medium- to fine-grained laminated sandstone.	Primary porosity.
		Erosional contact.	
		Porous and oil-stained sandstone.	Evidence of calcite dissolution.
		Sharp contact.	
		Vugs and moldic pores.	
		Porous and oil-stained sandstone.	Moldic pores with partly dissolved carbonate fragments.
		Porous and oil-stained sandstone.	Secondary pores present.
2580		Conglomerate.	
		Calcareous shale alternating with fine-grained sandstone. Fossil fragments are partly dissolved.	See Plate 13C.
		Porous and oil-stained sandstone with 10-15% porosity.	Small amounts of calcite cement.
2585			
		Fissil-rich shale.	
		Raddish-brown non-calcareous shale.	

dissolution is restricted to a particular layer in their wall structure, probably a former aragonite(?) layer. Some fossils are partly recrystallized and subsequently dissolved along cleavage planes in the recrystallized part (Plate 24B). In a few samples, micritic limestone fragments are partly to completely dissolved. "Dogtooth" calcite crystals which grew on them, however, are still present (Plate 19D). In the vicinity of contacts with shale beds, a limited number of samples with high secondary porosity (up to 20% by volume) has been observed. This secondary porosity mimics primary porosity and can easily be overlooked. Dissolution is more widespread in the Avalon Sandstone of wells B-27 and B-08 than in well O-35. Lack of significant chemical compaction (pressure solution) and abundance of primary porosity classify Avalon Sandstone as immature.

5.4.1.3 Recementation and Porosity Destruction

After this minor dissolution pulse no recementation occurred in the Avalon Sandstone, with one exception. In one sample, a small number of secondary pores that developed by dissolution of micritic limestone fragments were subsequently recemented, in part, with ferroan-calcite cement.

5.4.2 "B" Sandstone

5.4.2.1 Porosity Loss by Cementation

The only available drill-cores of the "B" Sandstone are from the O-35 and K-18 wells. This reservoir sandstone has an average porosity of 10.7% (excluding tight-sandstone

PLATE 24

Photomicrographs showing dissolution features.

(A) Partial dissolution of recrystallized fossil fragment. The undissolved remaining part is surrounded by hydrocarbons (arrow). Avalon Sandstone, O-35, 2185.60 m. Plane-polarized light. Scale bar: 500 um.

(B) Partly recrystallized fossil fragment (lower left) with microporosity (blue) due to irregular dissolution. In the recrystallized part, the fossil-wall structure has been obliterated. The arrows indicate uncorroded crystal faces of calcite. Avalon Sandstone, O-35, 2185.80 m. Plane-polarized light. Scale bar: 500 um.

(C) Partial dissolution of calcite cement (C) and formation of secondary porosity (SP). "B" Sandstone, O-35, 3179.09 m. Plane-polarized light. Scale bar: 100 um.

(D) Partial dissolution of carbonate rock fragments generating irregular secondary pores. The presences of hydrocarbon has stained the remaining material black. "B" Sandstone, O-35, 3185.90 m. Plane-polarized light. Scale bar: 500 um.

A   B

C Q SP Q   D
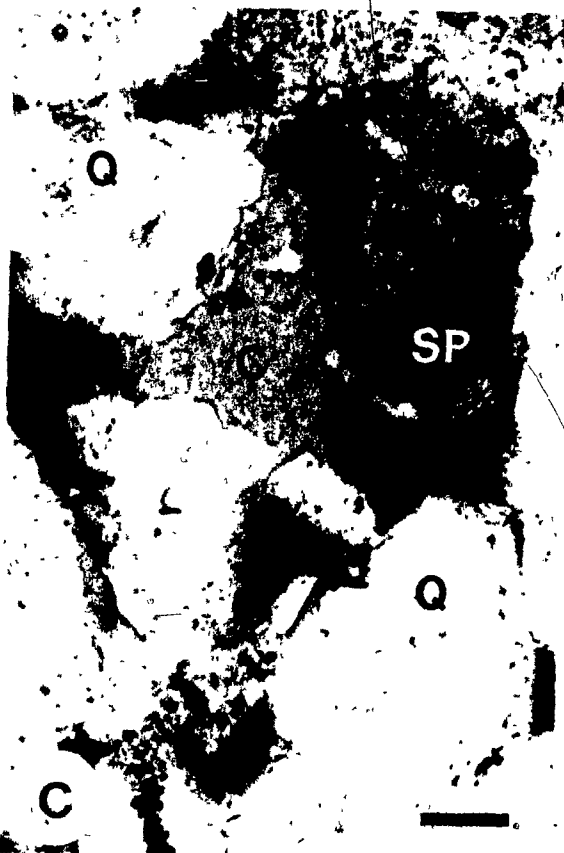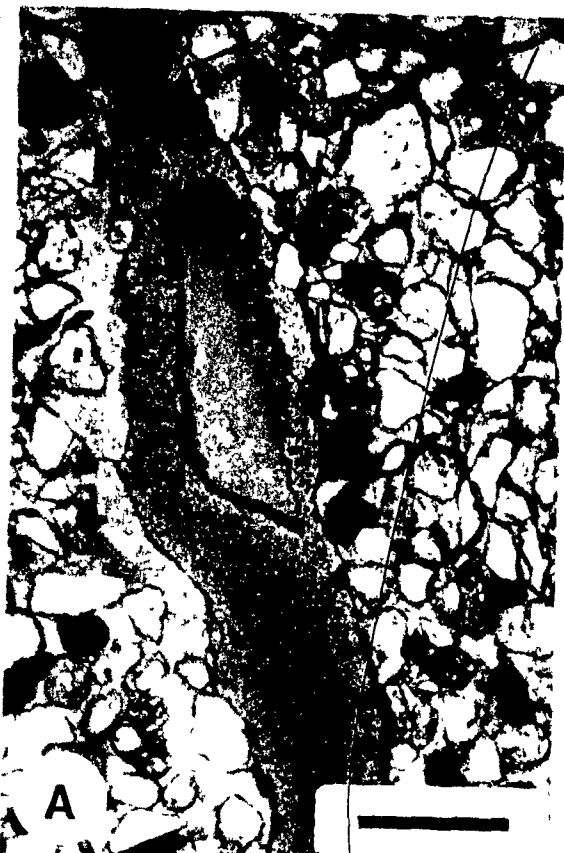
zones).   Out of 16.7 m of available sandstone core,   4.9 m
are completely cemented with early ferroan calcite (Table
5.3).   This cement is more abundant in the O-35 well than in
the K-18 well.   In the O-35 well,   45.7% of the available
sandstone cores are completely cemented by calcite,   compared
to 17.5% in the K-18 well (Table 5.3).   This difference may be
due to the fact that sandstone beds are thicker in the   K-18
than in the O-35 well.   In many of the horizons   where no
early calcite cement was precipitated, moderate compaction
together   with quartz overgrowths reduced   the   original
porosity considerably (Plate 7C).   In the K-18 well, the
"B" Sandstone shows less silica cementation because most of
the quartz grains are coated by a thin   micritic calcite
layer   (approximately 25um thick).   The   calcite   layer
inhibited quartz growth.

5.4.2.2   Formation of Secondary Porosity

Dissolution of calcite cement (Plate 24C),   and
carbonate fragments   (Plate 24D and 27D) has contributed   a
significant amount of porosity in the "B" Sandstone.   In the
O-35 well,   about 62% of the total porosity is interpreted as
secondary porosity.   Most of it occurs immediately above
shale beds.   In   contrast   to the O-35 well, the   "B"
Sandstone of the K-18 well shows only minor dissolution.
Porosity in K-18 is dominantly primary.   Diagehetically "B"
Sandstone is semi-mature.

5.4.2.3   Recementation and Porosity Destruction

The porosity which developed as a result of dissolution

178

(of calcite cement, and framework grains) together with the remaining primary porosity was locally reduced by late cements (ferroan dolomite, ferroan calcite, and kaolinite). The late ferroan dolomite is an important cement which precipitated after the dissolution event. It was observed in all porous sandstones of well O-35 where an average of 4.2% porosity (ranging from trace amounts to 20.3%) was lost due to this cement. Minor amounts of porosity are lost to late ferroan calcite cement. Porosity reduction by kaolinite is negligible. The common presence of ferroan dolomite and, at places highly fractured quartz grains in the O-35 well may indicate a fault zone at the "B" Sandstone interval that might have served as a conduit for the circulation of acidic fluids. Later on, the fluids may also have provided the cations (i.e. Mg^{2+}) necessary for dolomite formation. An east-west cross-section of the Hibernia Oil Fild shows a fault passing through the "B" Sandstone at the location of the O-35 well (Fig. 2.6).

5.4.3 Hibernia Sandstone

The Hibernia Sandstone is the main reservoir zone in the Hibernia Oil Field. As pointed out in Chapter 2, it was deposited in a fluvial-deltaic environment. The average core porosity is 18.3% (Table 5.2) and the average thin section porosity 13%. The most important diagenetic features in the Hibernia Sandstone include: the precipitation and dissolution of carbonate cements, and the dissolution of framework grains. These processes have markedly influenced the

179

porosity of the Hibernia Sandstone.

5.4.3.1   Porosity Loss by Cementation

Early ferroan calcite cement has filled significant pore space in the Hibernia Sandstone. This cementation at shallow depth has played an important role in preventing permanent porosity loss by quartz overgrowth and mechanical compaction.   At present   calcite-rich sandstones are not common, but most of them do contain remnants of calcite cements with numerous features indicative of secondary porosity.   Excluding calcite-rich zones (which comprise 4% of the studied sandstone cores), the Hibernia Sandstone presently contains 1% calcite cement. Late ferroan calcite cement has completely filled available pores at a few levels (i.e. at 3905.5 and 3906 m in B-27; 3939.0 m in C-96),   but total porosity loss by this cement is not significant.

The porosity loss by silica cementation averages 4.9% in the Hibernia Sandstone. About one third of the samples show more than 8% silica cement.   Sandstone samples with high secondary porosity generally contain less silica cement (Plate 21C).   This may reflect the fact that early calcite cementation prevented intense silica cementation. Samples lacking early calcite cementation generally contain more quartz overgrowths (i.e. at 3625.00 m in B-08; at 3860.80 m in K-18) or show advanced compaction causing permanent destruction of much of their porosity.   In two samples (at 3885.8 in the B-27 well), primary porosity was completely

180

occluded by intergranular precipition of siderite. However, volumetrically, such sandstones are negligible. Pyrite, generally a minor authigenic mineral, locally may reduce all available porosity.

5.4.3.2 Formation of Secondary Porosity

The Hibernia Sandstone shows a significant amount (80% of total porosity) of secondary porosity (Fig. 5.2). In B-27, the average thin section porosity is 17% (ranging from 10.7 to 25%) and more than 90% of it is interpreted as secondary. Characteristic features of secondary porosity observed in many samples of the Hibernia Sandstone include (see Plates 19,20, 21, and 22): (i) extensive grain margin corrosion; (ii) pitting and formation of embayments in quartz grains by dissolution of replacive cements (some embayments, however, may have been present at the time of deposition); (iii) inhomogeneous framework packing (e.g. at 3816.80 and 3841.47 m in K-18) and irregular porosity distribution; (iv) remnants of carbonate cements; (v) oversized and moldic pores; and (vi) elongated pores and grain fracturing.

— Many thick sandstones (6 to 15 m) were not completely cemented by early calcite and exhibit different porosity types (Plate 25). Where calcite cementation did not occur, either (1) silica cementation took place reducing ingnificant amounts of primary porosity (Plate 25E), or (2) mechanical compaction and squeezing of shale clasts into primary pores eliminated most of the primary porosity
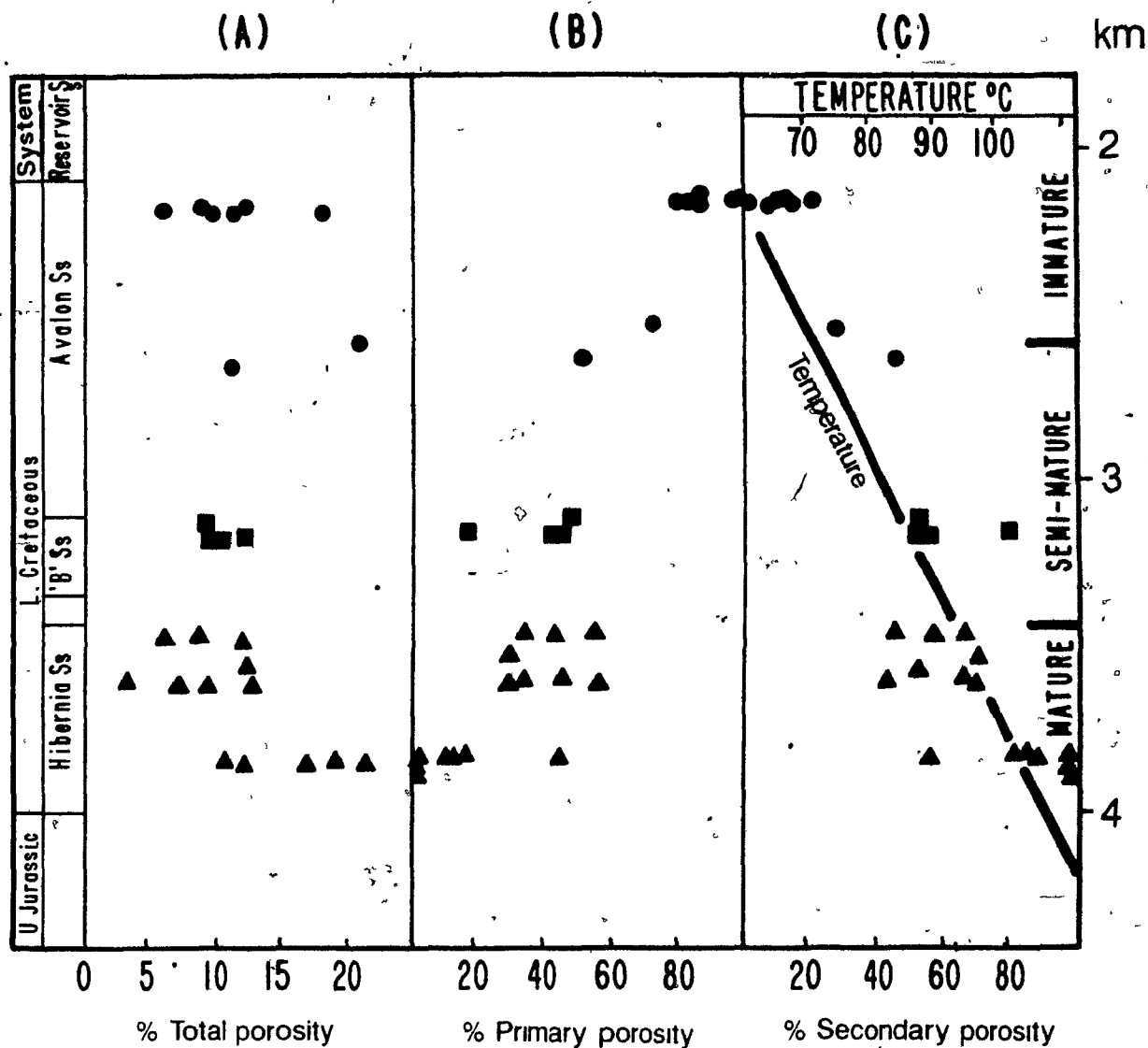
Fig. 5.2 (a) Percent total porosity, and percent (b) primary and (c) secondary porosity versus depth of burial, Hibernia Oil Field. In the Hibernia Sandstone more than 80 % porosity is interpreted as secondary.

Avalon Ss ● "B" Ss ■ Hibernia Ss ▲

PLATE 25

PLATE 25

Porosity types in thick sandstone beds from the Hibernia Sandstone. (Scale bar: 1000 um.)

Photomicrographs showing: (A) the presence of calcite rich zone; (B) secondary porosity with remnants of calcite cement; (C) irregularly distributed secondary porosity. Note lack of quartz overgrowths and corroded grain-margins; (D) oversized secondary pores; (E) reduced intergranular pores mainly of primary origin with large amounts of silica cement. Compare intergranular porosity types and silica cement in (D) and (E).

m C 96

3920

3925

3930

3935

3939

E

D

C

B

A

e

d

c

b

a
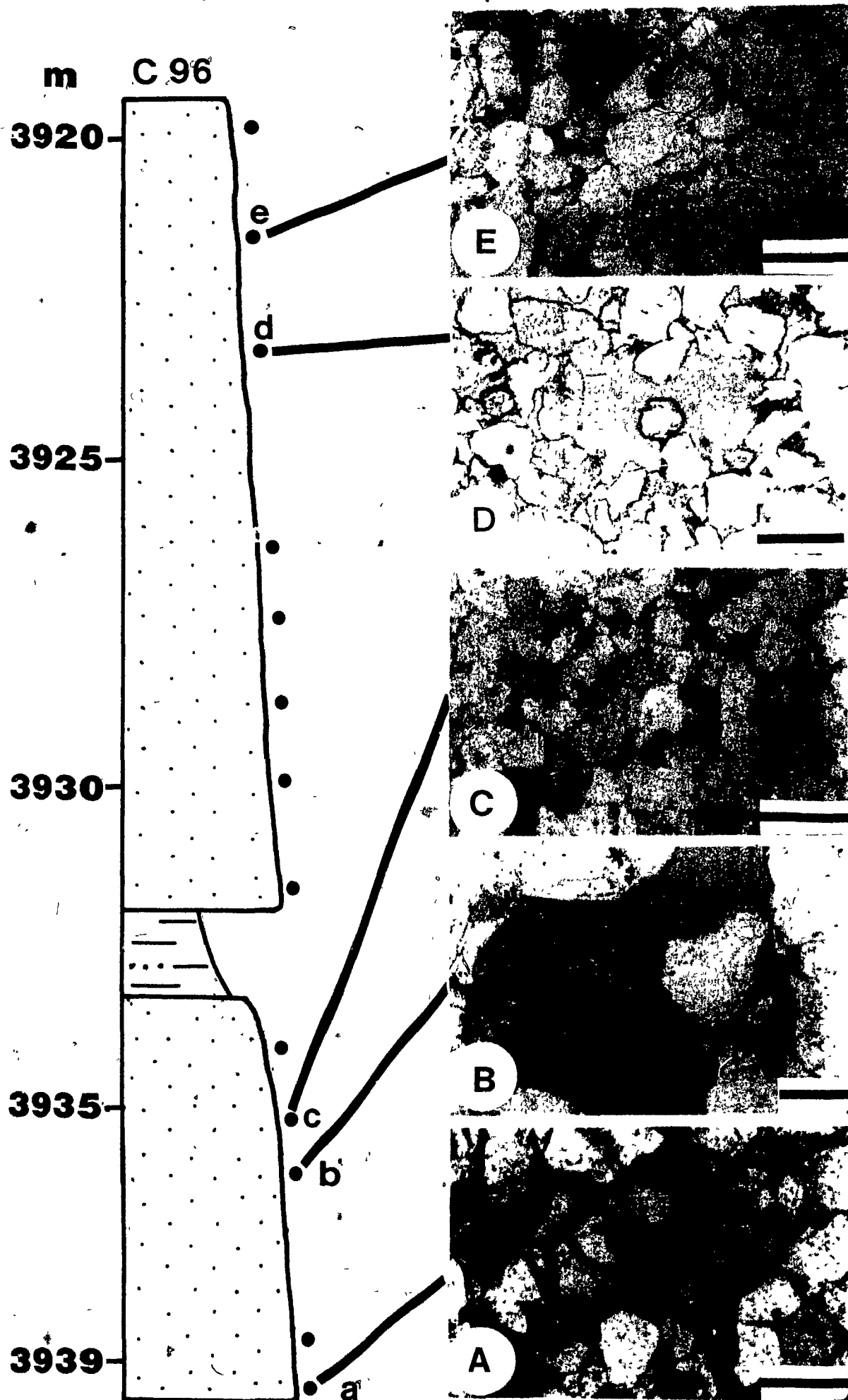
irreversibly. Sandstone samples, which escaped this porosity destruction still contain some primary porosity with variable amounts of secondary porosity resulting from the dissolution of framework grains and shale clasts. As pointed out earlier, thin sandstone beds (<3 m), on the other hand, were generally completely cemented by an early calcite which prevented mechanical compaction and other irreversible cementation. Later in the diagenetic history, the calcite cement was dissolved and most of the original porosity recovered. For example, in the B-27 well, many medium-grained sandstone beds are less than 3 m thick. These beds show a high proportion of secondary porosity (90 % of the total porosity). Diagenetically Hibernia is a mature Sandstone (abundant secondary porosity and chemical compaction).

The sandstone drill-cores examined from the Hibernia Sandstone contain only 4.0% calcite-rich zones (tight-zones), as compared to 20% in the Avalon Sandstone. One might argue that a significant portion of the Hibernia Sandstone throughout its diagenetic history may never have been cemented with carbonates. This is unlikely, however, in view of the fact that 48% of the thin sections studied from this zone still contain calcite remnants and a variety of other features characteristic of secondary porosity (Plate 26). Thus, it is assumed that a significant proportion of the porosity (80%, based on selected studied samples) in the Hibernia Sandstone is secondary in origin.

PLATE 26

Remnants of calcite cements and replacement of quartz overgrowths in the Hibernia Sandstone.

(A) Scanning electronmicrograph showing partial dissolution of quartz overgrowth (QOV). Dissolution associated with precipitation of replacive calcite which was dissolved later on. These groved and etched quartz grains (Q) are from a porous zone in the Hibernia Sandstone and suggest that it was once cemented with calcite. Hibernia Sandstone, C-96, 3892.35 m. Scale bar: 10 um.

(B) Partial dissolution of pore-filling carbonate cement (thin section not stained) forming secondary porosity (SP). Hibernia sandstone, C-96, 3935.79 m. Plane-polarized light. Scale bar: 100 um.

(C) Scanning electron photomicrograph of a quartz grain showing partial dissolution of quartz overgrowths (QOV) as in Plate 26A. Irregular pores produced by dissolution of replacive calcite are partly filled by late authigenic kaolinite (arrow). See also Plate 8A. Hibernia Sandstone, C-96, 3892.35 m. Scale bar: 10 um.

(D) Sandstone with high percentage of secondary porosity (SP), and remnants of ferroan calcite (rm, stained dark blue). Hibernia Sandstone, C-96, 3908.30 m. Plane-polarized light. Scale bar: 50 um.
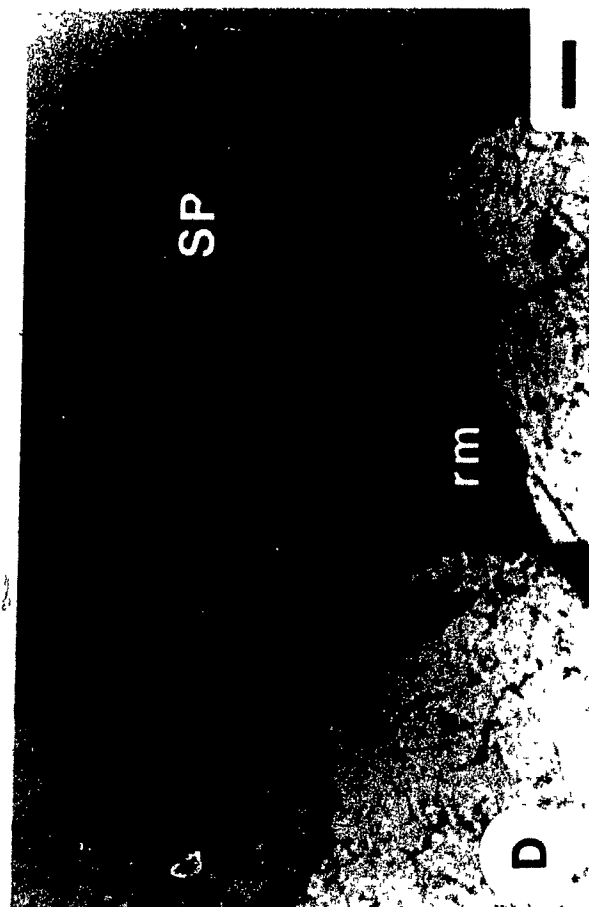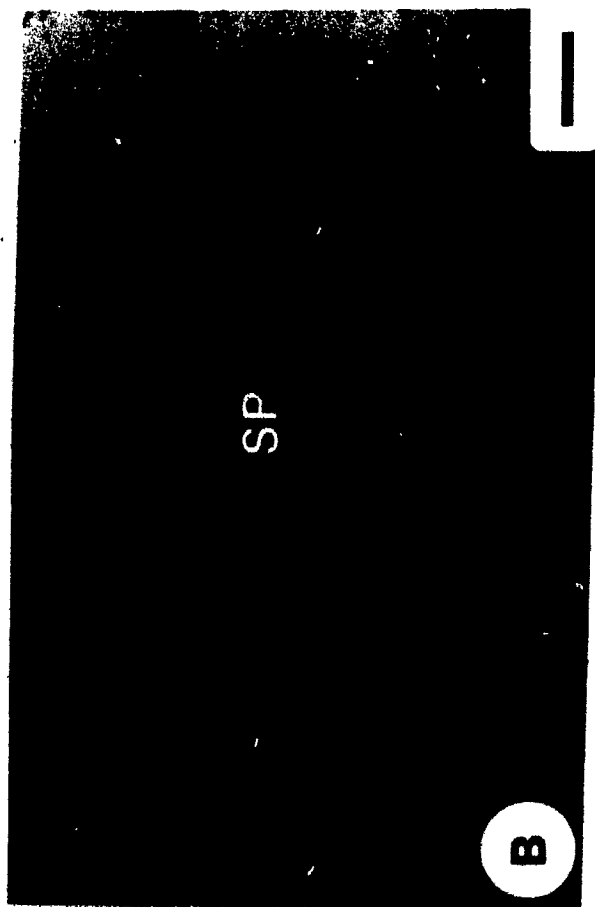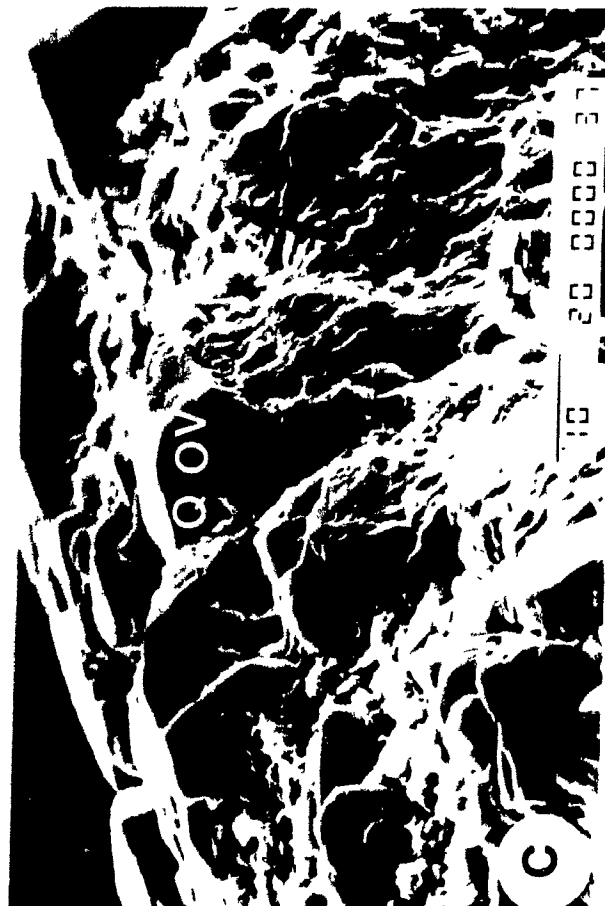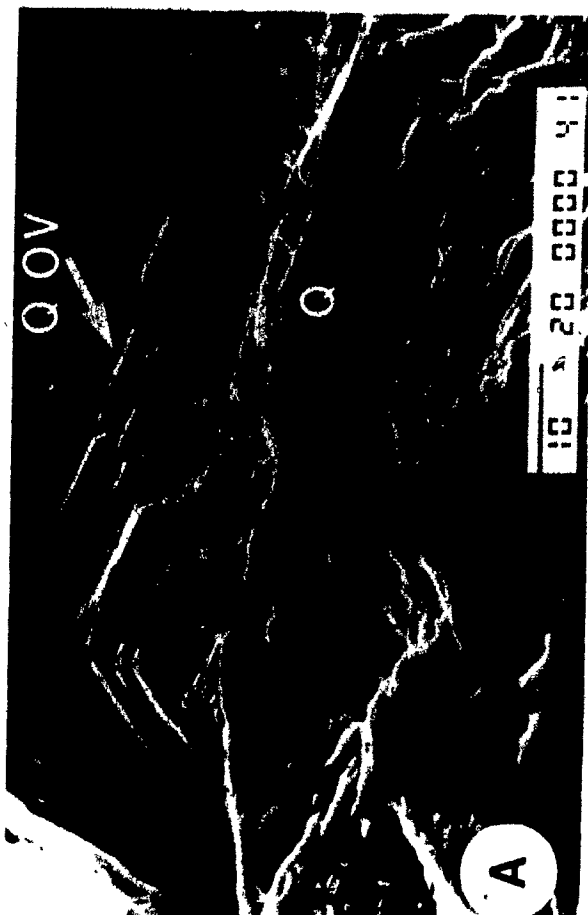
5.4.3.3   Recementation and Porosity Destruction

A stage (or stages) of recementation occurred after dissolution. This involved precipitation of kaolinite, quartz overgrowths, pyrite and minor amounts of ferroan-dolomite in recognizable secondary pores. Generally, the porosity loss due to these cements is small (1 to 2%). However, locally as much as 10% porosity has been destroyed by post-dissolution cements. Trace-amounts of kaolinite have been observed in numerous samples. Very few samples contain as much as 6% kaolinite (e.g. at 3906 m, in the C-96 well). Porosity loss by late quartz overgrowth is negligible. Late pyrite is noted in the B-27 well. In most of the samples pyrite amounts to less than 1%, however, at places it completly occludes all available pore space.

5.4.4   Jeanne d' Arc Member

Drill-cores from the Jeanne d'Arc Member were only available from well O-35 and consist of alternating sandstone and conglomerate beds. Thin sections from the available core indicate very low porosities (< 5.0%). Advanced mechanical compaction together with ferroan-dolomite cement, quartz overgrowths and deformed shale clasts have occluded most of the porosity.

In summary, diagenetic processes play a significant role in to modifying sandstone porosity. In the Hibernia Oil Field, calcite and quartz cementation alone, beside mechanical compaction, are the most important processes to reduce the primary porosity (9.5 % of total rock volume). With

increasing burial depth the porosity reduction is partly offset by dissolution of carbonates and detrital material (Fig. 5.2A and 5.2C). Depth versus porosity plot from the Scotian Shelf also shows a offset in porosity reduction trend with increasing burial depth (Fig. 5.3 ;Schmidt and Mcdinald, 1979). In Figure 5.4 the secondary porosity from different basins is plotted as percentage of total porosity and compared with the present data. The comparison shows that secondary porosity is the dominant type of porosity in many reservoir sandstones worldwide (Shanmugam, 1985).

5.5 DIAGENETIC SEQUENCES AND SECONDARY POROSITY

Diagenetic sequences observed in the Hibernia Field (discussed in Ch. 3) are summarized and compared with other quartz-rich sandstones from marine-deltaic environments (Table 5.4). Paragenetic sequences of authigenic minerals associated with secondary porosity, are similar for oil fields of very different regions and ages. Franks and Forster (1984) have first noted these similarities in diagenetic sequences. Pre-dissolution quartz overgrowth and early calcite (less commonly early ferroan-calcite) are volumetrically the most important cements in all cases (Table 5.4). Pre-dissolution authigenic chlorite, illite, pyrite, and siderite are usually volumetrically less important. Ferroan-carbonates and kaolinite are important post-dissolution minerals. Dissolution of early calcite cement and feldspar, rock fragments, and siderite is the

189

MOBIL-TEXACO CITNALTA I-59
(SCOTIAN SHELF)

PRESENT DEPTH

M   M
METERS   FT.

MAINLY
PRIMARY POROSITY

TEMPERATURE

SANDSTONES
CEMENTED
BY CARBONATE

PRIMARY &
SECONDARY
POROSITY

SECONDARY
POROSITY

IM-
MATURE

SEMI-
MATURE

MATURE
"A"

MATURE
"B"

TERTIARY   U.CR.   LOWER CRETACEOUS   JUR.

PERCENT POROSITY	30	20	10	0
TEMP. °F	100	200	300	400
TEMP. °C	38	93	149	204
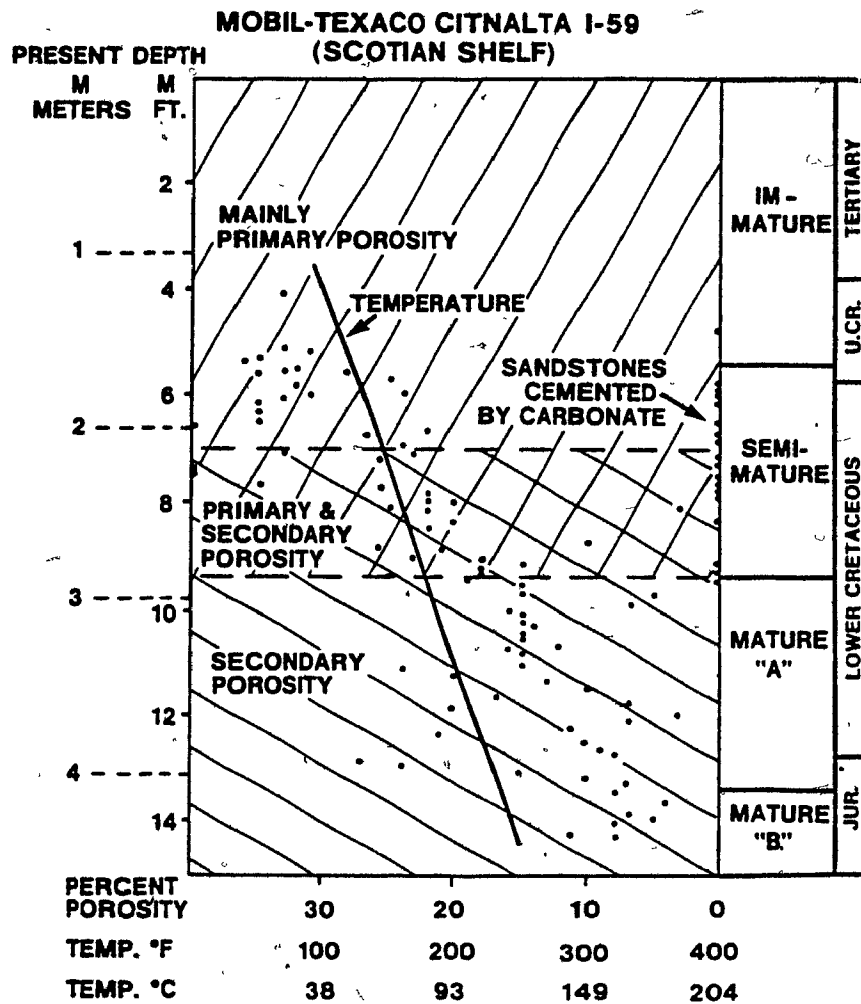
Fig. 5.3 Depth versus porosity plot from the Scotian Shelf. Note
a change in the porosity reduction trend where by secondary
porosity becomes a major porosity type (from Schmidt and
McDonald, 1979b).

190

SECONDARY POROSITY IN RESERVOIR SANDSTONES

RESERVOIR SANDSTONES	SECONDARY POROSITY AS PERCENTAGE OF TOTAL POROSITY (VISUAL ESTIMATION) 0 10 20 30 40 50 60
Avalon Ss	
"B" Ss	
Hibernia Ss	
PUENTE (California) (LATE MIOCENE)	
FRIO (Texas) (OLIGOCENE)	
CARDIUM (Alberta) (LATE CRETACEOUS)	
PARSONS (Mackenzie Delta) (EARLY CRETACEOUS)	
BRENT (North Sea) (MIDDLE JURASSIC)	
BERYL (North Sea) (EARLY TO MIDDLE JURASSIC)	
MIC MAC (Scotian Shelf) (JURASSIC)	
STATFJORD (North Sea) (LATE TRIASSIC TO EARLY JURASSIC)	
SADLEROCHIT (Alaska) (PERMIAN TO TRIASSIC)	
ROTLIEGENDES (North Sea) (PERMIAN)	
OLD FORT ISLAND (N.W. Territories) (CAMBRIAN)	

Fig. 5.4 Percentage of secondary porosity in reservoir sandstones from various oil fields (modified after Shanmugam, 1985).

1	2	3	4	5	6	7	8	9	10
Oligocene Frio, Gulf Coast	Eocene Wilcox, Gulf Coast	Pennsylvanian Gray, Texas	L.Jurassic Taylor, Louisiana	U. Jurassic Norphlet, Mississippi	L.Cretaceous Hosston, Mississippi	Triassic Ivishak, N.Alaska	Neogene Surma, Bengal	E.Jurassic Tromsi, N.Norway	This Study
Calcite		Chlorite-rims	Pyrite	Illite	Calcite		Chlorite		Chlorite-rims
				Feldspar overgrowths			Siderite Calcite		Siderite
Quartz overgrowths	Quartz overgrowths	Quartz overgrowths	Quartz overgrowths	Quartz overgrowths	Quartz overgrowths Fe-dolomite	Quartz overgrowths	Quartz overgrowths	Quartz overgrowths	Quartz overgrowths Pyrite
Calcite	Calcite	Calcite	Calcite	Calcite		Siderite	Fe-calcite	Calcite	Fe-calcite Fe-dolomite
									Quartz overgrowths
Dissolution	Dissolution	Dissolution	Dissolution	Dissolution	Dissolution	Dissolution	Dissolution	Dissolution	Dissolution
Kaolinite	Kaolinite	Fe-carbonates	Illite Illite Smectite	Pyrite	Kaolinite	Kaolinite	Kaolinite	Kaolinite	Kaolinite Late calcite
Fe-carbonates	Fe-carbonates	Kaolinite		Dolomite Illite Quartz overgrowths	Pyrite Barite Sphalerite	Fe-calcite		Fe-calcite	Fe-dolomite Pyrite
									Hydrocarbon Migration(?)

(1) Loucks et al. (1977); (2) Stanton (1977); (3) Land and Dutton (1978); (4) Trojan (1985); (5) McBride (1981); (6) Fielder et al.(1985); (7) Dutton (1977); (8) Imam and Shaw (1987); (9) Riches et al. (1986).

Table 5.4 Paragenetic sequences and dissolution event in quartz-rich sandstones from different sedimentary basins. Note difference in suites of authigenic minerals above and below the dissolution event (modified from Franks and Forester, 1984).

192

most important feature common to all sandstones listed in Table 5.4. The resulting secondary porosity forms at the base of the middle stage of diagenesis (3000-4000 m, depending upon geothermal gradient and pore water composition). This zone of major dissolution and well developed secondary porosity corresponds to a well temperature of above 80 $^{\circ}$C. In general, this interval is well within the liquid window of hydrocarbon generation. The importance of organic matter maturation in dissolution and post-dissolution cementation will be discussed in Chapter 6.

5.6 HYDROCARBON MIGRATION AND PRESERVATION OF SECONDARY POROSITY

It is a well established fact of oil exploration which also emerges from this study that the relative timing between secondary porosity generation and hydrocarbon migration is crucial for the occurrence of hydrocarbon reservoirs. If the time interval between the generation of secondary porosity and hydrocarbon migration was long, then cementation and compaction may have severely reduced the newly generated porosity. For example, some oil-filled samples of the Hibernia Sandstone show a very loose packing of framework grains, which resembles that of the Avalon Sandstone. Such samples indicate pervasive dissolution of an early calcite cement. This, in turn, suggests that calcite (and other) dissolution was followed shortly afterwards by hydrocarbon migration. In a few samples grain fracturing may have occurred after the dissolution of calcite cement. The

preservation of secondary porosity by means of overpressuring is less likely in the Hibernia Sandstone. In the Hibernia area the top of the overpressured zone generally occurs at or near the top of the Kimmeridgian shale, that is below the Hibernia Sandstone (Grant et al., 1986).

5.7 PRIMARY CONTROLS ON DIAGENESIS AND SANDSTONE POROSITY

5.7.1 Position of Sandstone in Sedimentary Basin and Thickness of Interbedded Shales

Sandstone beds in different parts of a sedimentary basin may undergo a somewhat different diagenetic history, depending on the amounts and composition of pore fluid available for diagenetic reactions. This point may be elaborated on by comparing marginal Avalon Sandstone, rapidly subsided along a growth fault (i.e. Avalon Sandstone in O-35 well), with basinal Avalon Sandstone (i.e. B-27 and C-96 wells). In contrast to the marginal sandstone (O-35 well), dissolution of early calcite cement is more common in the B-27 and C-96 wells. The more extensive dissolution in these wells may have been controlled, in part, by the presence of large volume of interbedded shales which would provides greater amounts of fluids for cementation and dissolution processes. Since all wells investigated in the present study are not widely spaced (<5 km), therefore, this aspect needs a further investigation on a regional scale in the Jeanne d'Arc Basin·

5.7.2 Thickness of Sandstone Beds

The thickness of sandstone beds plays an important role during diagenesis. In the Hibernia Field, sandstone thickness varies from a few centimeters to more than 14 m.

Well developed thick sandstone beds (Hibernia Sandstone, C-96) were not completely cemented by an early calcite cement and generally show advanced mechanical compaction compared to thiner sandstone beds. Relatively thin sandstones, on the other hand, were completely calcite cemented during early diagenesis and subsequent dissolution of calcite cements and framework grains recovered most of their primary porosity (up to 80% in the Hibernia Sandstone of the B-27 well).

5.7.3 Grain Size.

Grain size variation has an important effect on diagenesis. As a result of variable initial porosity and permeability (due to grain-size variation and detrital clay content) the extent and type of diagenesis may vary even on the thin-section scale (diagenetic scatter). For example in sample 3178.4 of the O-35 well, early calcite cementation has occluded all pores in a clay-free coarser part of the thin section. Due to the finer grain size and greater abundance of detrital clay, porosity and permeability were low in the remainder of the section. Consequently, no calcite was precipitated in this part. After all pores in the porous zone had been filled with calcite, the pore fluid subsequently moved through the less porous zone and precipitated minor silica (about 3%) and ferroan dolomite cement (about 2%). Thus considerable diagenetic variation, even on a microscopic scale, can be explained by initial grain size and clay control on porosity and permeability.

5.7.4 Geothermal Gradient (or Subsurface Temperature)

Temperature is a major controlling factor on diagenesis and hence porosity and permeability of sandstone reservoirs (Galloway, 1974). The initiation of diagenetic reactions in a sedimentary basin (e.g. transformation and precipitation of clay minerals, organic matter maturation and related generation of acidic fluids) are largely controlled by temperature. In 16 southern Californiua oil fields Dixon and Kirkland (1985) found a strong positive correlation between the thermal gradient (which ranged from 2.9 to 4.0 $^\circ$C / 100 m) and the porosity decline gradient (which ranged from 1.1 to 5.8% /100 m). Similarly, a small change in the geothermal gradient (0.47 $^\circ$C/100 m) from lower toward upper Texas in the Frio Formation of the Gulf Coast causes a change in the mean porosity from 18 to 27% at 3000 m depth (Loucks et al., 1984). The present geothermal gradient in the Hibernia field is 2.4 $^\circ$C/100m. The geothermal gradient from other fields of the Jeanne d' Arc Basin is not available. On a regional scale, the geothermal gradient may be variable in the Jeanne d' Arc Basin. Thus it would be important to establish the variation in geothermal gradients for predicting reservoir porosity in the Jeanne d'Arc Basin on a regional scale.

5.9 SUMMARY

Different reservoir zones in the Hibernia Field show distinct diagenetic features and porosity modification with increasing burial depth. Some important features observed

are:

(1) Porosity in the fine-grained, loosely packed Avalon Sandstone is mainly primary.

(2) Precipitation of early ferroan calcite cement is the most porosity-destructive authigenic mineral in these sandstones. This cementation phase has completely filled up to more than 20% of the sandstone core from the Avalon Sandstone.

(3) An average 2% porosity in the Avalon Sandstone was lost by quartz overgrowths. Porosity loss due to other cements (siderite, authigenic clay minerals) averages 2.9%. In this sandstone no dolomite or kaolinite were observed.

(4) A few samples from the Avalon Sandtone show secondary porosity (average 2.6%). Acidic pore water for dissolution (of calcite cement and rock fragments) was presumably derived from adjacent shales. Minor dissolution of carbonate rock fragments, prior to early ferroan calcite cement, may have occurred by meteoric waters invading the reservoir during the Mid-Cretaceous hiatus (Hutcheon et al., 1985).

(5) Fine-grained, moderately compacted "B" Sandstone exhibits 10.6% thin section porosity on average (excluding completely cemented sandstones).

(6) A large portion of the "B" Sandstone (23% of the sandstone core studied) is completely cemented with early calcite. In the remaining porous sandstone,

quartz overgrowths (4.7%) and late ferroan dolomite (3.6%) are other important authigenic minerals. Reduction of porosity by late ferroan calcite and kaolinite is not significant in the "B" Sandstone.

(7) On average 7% porosity in the "B" Sandstone of the O-35 well is secondary which originated mainly by dissolution of early calcite cement and carbonate fragments.

(8) The presence of high secondary porosity near the sandstone-shale contacts probably indicates that acidic fluids for dissolution were provided by adjacent shales.

(9) The medium-to coarse-grained Hibernia Sandstone shows on average 13.1% thin-section porosity.

(10) Out of 132.5 m sandstone core from the Hibernia Sandstone, only 4.0% are completely cemented with calcite. However, it appears that during early diagenesis a significant portion of the Hibernia Sandstone was completely cemented with calcite which was later dissolved.

(11) Quartz overgrowths reduce on average 4.9% porosity (ranging from 1 to 11%) in the Hibernia Sandstone. Siderite, late ferroan dolomite, kaolinite, and late pyrite cause a combined porosity reduction of about 1%.

(12) Secondary porosity formed by the dissolution of calcite is dominant in thin sandstone beds which were completely cemented during their early diagenetic history.

(13) Thick sandstone beds were partly cemented with calcite.

The lower part of thick sandstone beds is usually coarse-grained and contains a lot of shale-clast and chert fragments. Due to the high initial porosity, large amounts of fluid passed through these sandstones causing dissolution of chert fragments and shale clasts. The upper parts of thick sandstone beds generally still contain considerable primary porosity.

CHAPTER VI

SOURCE OF MAJOR AUTHIGENIC MINERALS AND ORIGIN OF SECONDARY POROSITY: DISCUSSION AND INTERPRETATIONS

6.1   INTRODUCTION

The diagenesis of sandstones and its effects on reservoir porosity have been discussed in Chapters 3 and 5, respectively. Mineralogical variations in the interbedded shales undergoing burial diagenesis were dealt with in Chapter 4. Using various observations obtained during this study the sources of authigenic minerals and the origin of secondary porosity in sandstone can now be discussed and their relationship with shale diagenesis as a function of burial depth be evaluated.

6.2   DISCUSSION AND SOURCE OF MAJOR AUTHIGENIC MINERALS

6.2.1   Calcite

Early non-ferroan and ferroan-calcite cements (precipitated above 2000 m burial depth) have been widely reported in the literature (Blatt, 1979; Almon and Davies, 1979; Loucks et al., 1984 and Imam and Shaw, 1987). Four major sources of early calcite have been suggested: (1) dissolution and reprecipitation of carbonate from fossil and limestone fragments in sandstones and nearby shales (Almon and Davies, 1979; Blatt, 1979); (2) percolating meteoric water supersaturated with calcite (Longstaffe, 1984); (3) upward migrating pore-water experiencing a decreasing P_{CO2} and,

200

consequently, decreasing calcite solubility; and (4) carbonate generated in the sulphate reduction and methane production zones. The precipitation of calcite is enhanced by high activities of Ca^{2+}, and CO_3^{2-}, alkaline pH, low PCO_2, and an increase in temperature. If the pH of the fluid is buffered by an external source (i.e. acetate which has a maximum buffering capacity at a pH of approximately 5) an increase in pCO_2 favours calcite precipitation (Surdam et al., 1984).

In the Hibernia field, early ferroan calcite cement was precipitated at relatively shallow burial depth, probably around 1000 to 1500 m. Petrographic arguments (minus cement porosity, fractured grains healed with calcite cement) have been previously discussed (section 3.2.3.7.2). Although calcite is abundant where fossil and limestone rock fragments are abundant, a considerable amount of calcite cement in sandstones of the Hibernia field is believed to have an external source (most likely from interbedded shales) or redistributed within the sandstone units. The presence of calcite cement in zones free of fossil or carbonate fragments (Plate 27A) and, its absence in some of the fossil-rich zones (Plate 27B), also suggest redistribution or an outside source. Meteoric water percolating downward from the Mid-Cretaceous (Albian) unconformity and/or along syndepositional faults (growth faults) may have provided some of the calcite by dissolving carbonate fragments on its way as discussed below. Upward moving trapped pore water from

201

PLATE 27

Cementation, dissolution and sandstone porosity

(A) Medium-grained sandstone completely cemented by early ferroan calcite cement (C). Note absence of fossil fragments. Quartz grain margins are partly replaced by calcite (arrows). This part of the thin section was stained with Alizarin-Red only. Avalon Sandstone, O-35, 2191.5 m. Plane-polarized light. Scale bar: 100 um.

(B) Loosely packed fine-grained sandstone with abundant fossil fragments and lack of calcite cement. Note pressure solution contacts (arrows) between quartz grains and fossil fragments. Bedding direction sub-vertical. Avalon Sandstone, O-35, 2195.4 m. Plane-polarized light. Scale bar: 500 um.

(C) Late dolomite (D) precipitated in a secondary pore (SP) that originated from the dissolution of a calcite fragment (stained red). "B" Sandstone, O-35, 3183.70 m. Plane-polarized light. Scale bar: 50 um.

(D) A large secondary pore (approximately 2.0 mm long) originated due to dissolution of a carbonate fragment. This sample still contains large (0.5-5.0 mm long) carbonate fragments. The dissolution event was followed by hydrocarbon migration (black grain coating). Note euhedral dolomite crystal (D) in lower right corner. "B" Sandstone, O-35, 3182.82 m. Plane-polarized light. Scale bar: 500 um.
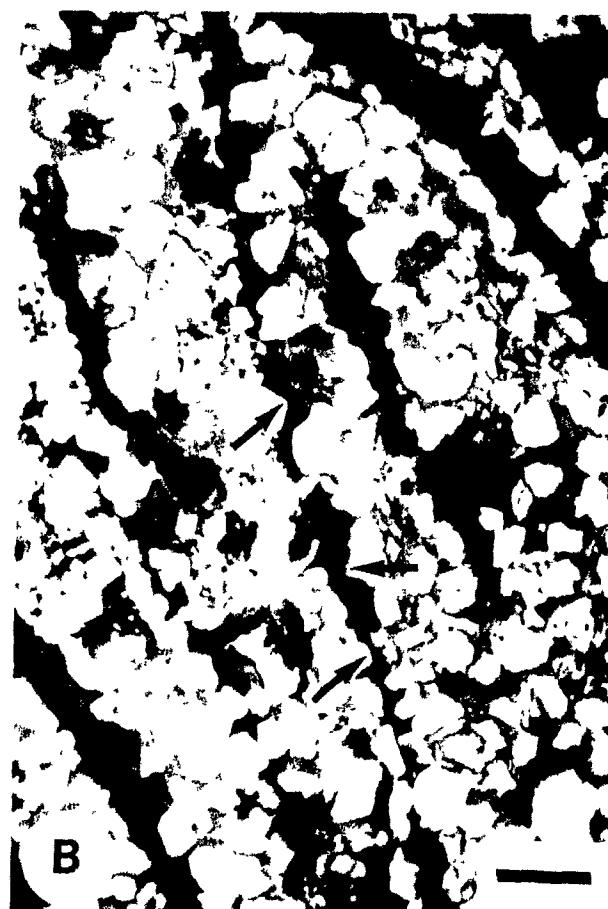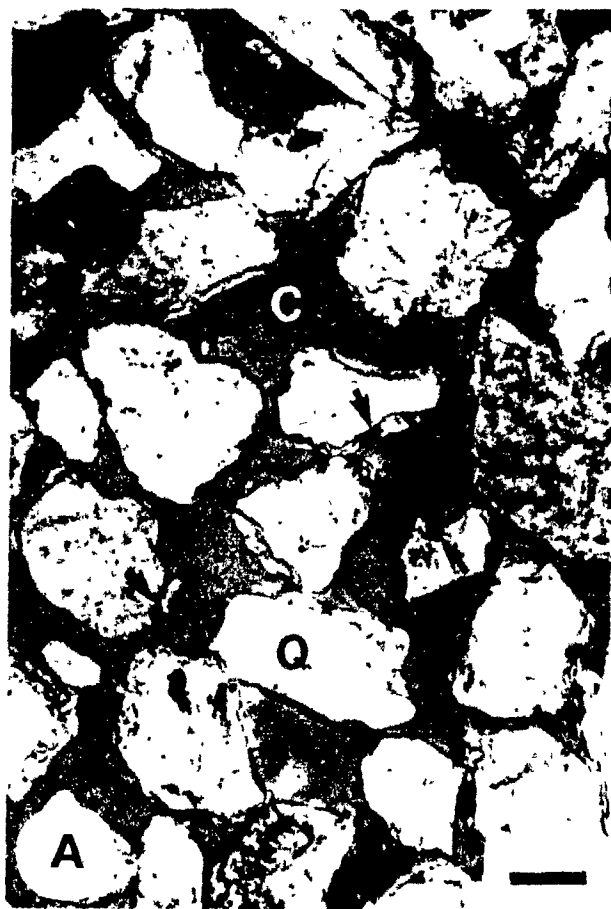
compacting fossil-rich interbedded and deeper shales (see below) may have supplied most of the $CaCO_3$. Calcite-rich sandstone zones are generally present above or near fossil-rich calcareous shales and tend to comprise a pebbly bed at the base and a bioturbated zone at the top. This indicates that initial porosity and permeability together with proximity of calcareous shales may have been important factors controlling the precipitation of early calcite.

A marine source for the early calcite cement is supported by isotopic data (Figure 3.7). $\delta^{13}C$ values restrain the possible sources of bicarbonate for the precipitation of calcite cements in the following way: (1) Sea water has an isotopic composition of $\delta^{13}C$ near 0 ‰ PDB; (2) on average calcareous fossils have a $\delta^{13}C$ of +2‰ PDB; (3) oxidation of marine organic matter by bacterial sulphate reduction produces bicarbonate with a $\delta^{13}C$ of -25‰ PDB; (4) methanogenesis produces CO_2 with $\delta^{13}C$ of up to +15‰ PDB; and (5) thermal decarboxlation of organic matter again generates CO_2 with lighter values of $\delta^{13}C$ (up to -25‰ PDB). The measured $\delta^{13}C$ value of early calcite in this study averages -1.64‰ PDB (ranging from +2 to -5.8‰). In the Avalon Sandstone, the average $\delta^{13}C$ of early calcite cements is close to zero (-0.87‰ PDB; Hutcheon et al., 1985; Fig. 3.7). The $\delta^{13}C$ values obtained in this study indicate that marine carbonate fragments (fossil and limestone fragments), rather than sulphate reduction and thermal decarboxylation, are the main sources of carbon for early calcite precipitation.

In Figure 6.1, the $\delta^{18}O$ values of both early and late calcite cements are plotted versus depth together with the $\delta^{18}O$ values for early calcite cements of Hutcheon et al. (1985). In the Avalon and "B" Sandstones, the early calcite cements show a wide range of $\delta^{18}O$ from -0.5‰ to -10‰ PDB. The $\delta^{18}O$ values of carbonate cements are controlled by the $\delta^{18}O$ of the pore water and temperature at the time of precipitation (McCrea, 1950; Epstein et al., 1953). The range of $\delta^{18}O$ of early calcite cement obtained for the 2400 m subsurface depth level is difficult to explain with variable burial temperature alone. Texturally, early ferroan calcite cement from various depths looks similar (i.e minus cement porosity ranges from 25 to 30%) and suggest a narrow depth interval (probably <500 m) for precipitation. This interval corresponds to a subsurface temperature range of not more than 15 ^{O}C (assuming a geothermal gradient of 24 ^{O}C/Km; Suie, COGLA personal communication). As mentioned earlier (section 2.3.4), the Avalon Sandstone was mainly deposited in a marine environment. Using a Cretaceous seawater $\delta^{18}O$ value of 0‰ SMOW (Veizer, 1983) and the equation of O'Neil et al. (1969) the range in $\delta^{18}O$ values (-0.5 to -10.0‰ PDB) would require a tempeature range of >36°C, if temperature was the only factor for the observed variation. This wide range, therefore, must reflect pore fluids with variable $\delta^{18}O$ values at the time of precipitation. Such variable isotopic composition of the pore fluids may be due to: (1) variable proportions of meteoric water input into different wells

System		Stage	Reservoir Zone
L. Cretaceous		Albian-Hauterivian	Avalon Ss
		Berriasian-Valanginian	'B' Ss
		Tithonian	Hibernia Ss
U. Jurassic		Kimmeridgian-Oxfordian	Jeanne d' Arc Member
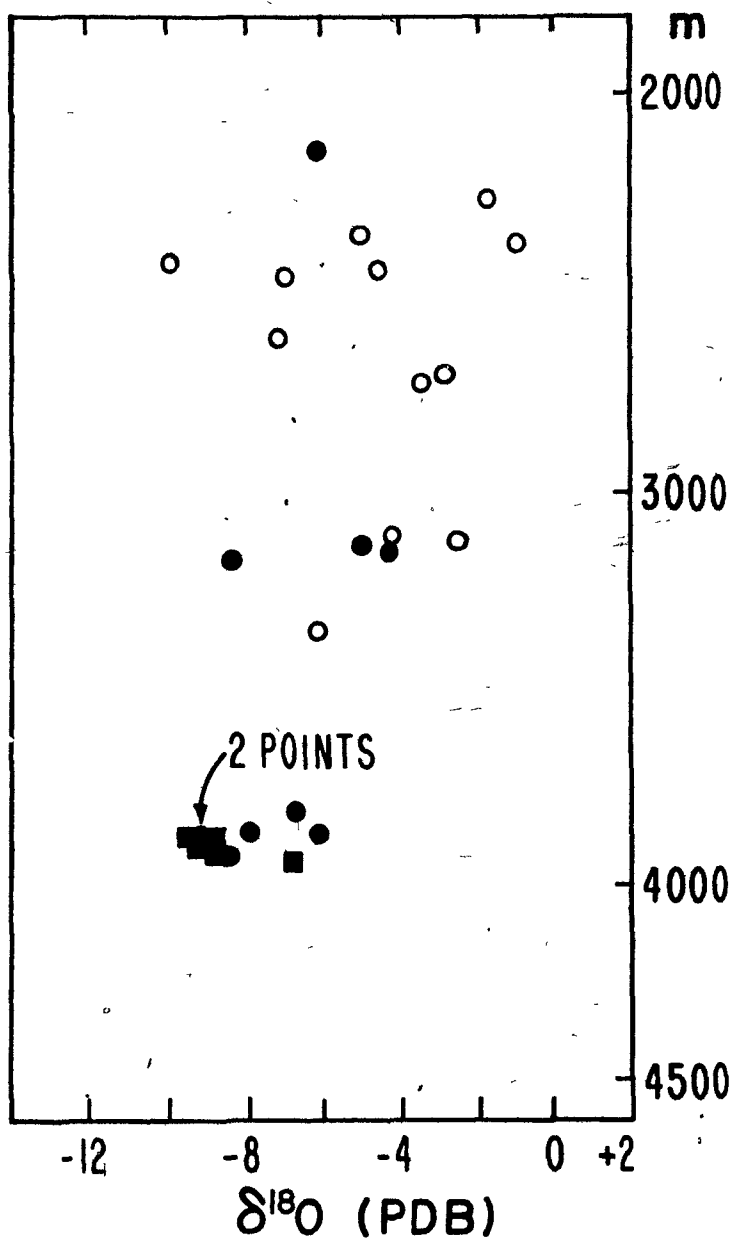
● Early calcite   O Early calcite (Hutcheon et al, 1985)

■ Late calcite

Fig. 6.1 δ^{18}o of early and late calcite cements versus subserface depths.

sites; (2) mixing with upward moving isotopically light hot fluids derived from deeper levels; or (3) a combination of these.

Trace element analyses (i.e Sr^{2+}, Mn^{2+}, Mg^{2+} etc.) on Avalon calcite cement (Hutcheon et al., 1985) show values between meteoric-water and sea-water calcite. This indicates mixing of meteoric with sea water. To evaluate the influence of meteoric water versus temperature on the geochemical composition, ratios of Sr/Ca and Mn/Ca were plotted versus $\delta^{18}O$ of these cements. If the light $\delta^{18}O$ values of early calcite cement were mainly due to the presence of meteoric water, there should be a decrease in the Sr/Ca and an increase in the Mn/Ca ratios with more negative $\delta^{18}O$ values.

Hutcheon et al. (1985) obtained no apparent relationship between the Sr/Ca and Mn/Ca ratios versus oxygen isotopic compositions. This may suggest that lighter oxygen isotopic values of early calcite cements are the result of upward moving shale water both from interbedded and deeper levels (hot fluids) mixed, at places, with meteoric water.

The isotopic composition of early calcite cements buried to deeper levels (in the Hibernia Sandstone) is less variable than at shallower levels and shows lighter isotopic values (average $\delta^{13}C$ = -3.4‰ and $\delta^{18}O$ = -7.4‰ PDB). This may reflect recrystallization of early calcite cement at higher temperatures and isotopic re-equilibration with somewhat different pore water compositions. Partially to completely recrystallized fossil fragments with obliterated microstructures were commonly observed (Plate 24B). Some

recrystallized fossil fragments and their surrounding poikilotopic calcite cements are in optical continuity probably indicating recrystallization of calcite cement. Where early calcite cement has been buried to a greater depth, it shows progressively lighter $\delta^{13}C$ values (Fig. 6.2). This may also reflect recrystallization at higher temperatures where some organically derived carbon was available.

Isotopic data from the late ferroan calcite cements lie close to Wilcox calcite of U. S Gulf Coast (Fig. 6.3) and are much less scattered than those for early ferroan calcites and show the lightest isotopic values (Fig. 6.1 and 6.2). The isotopic signature of this cement reflects generally similar temperatures and pore fluid compositions during precipitation between different wells.

The $\delta^{13}C$ values (average -10.9‰ PDB) indicate incorporation of substantial amounts of organically derived light carbon. The main processes for generating significant amounts of $\delta^{13}C$-depleted CO_2 or HCO_3^{2-} in a subsurface clastic system during burial have been discussed by Curtis (1978). Microbial oxidation of organic matter and SO_4^{2-} reduction generate CO_2 with negative $\delta^{13}C$ values. These processes usually occur in the upper few to few tens or hundreds of meters in the sediment column. Grain fabrics and other petrographic evidence, however, suggest precipitation of the late ferroan calcite cement below 2600 m, probably near 3000 m subsurface depth. The closely clustered $\delta^{18}O$ values on this cement (-8.85‰ PDB) also favour precipitation at

System	Stage	Reservoir Zone
	Albian–Hauterivian	Avalon Ss
L. Cretaceous		
	Berriasian–Valanginian	'B' Ss
	Tithonian	Hibernia Ss
U. Jurassic	Kimmeridgian–Oxfordian	Jeanne d' Arc Member

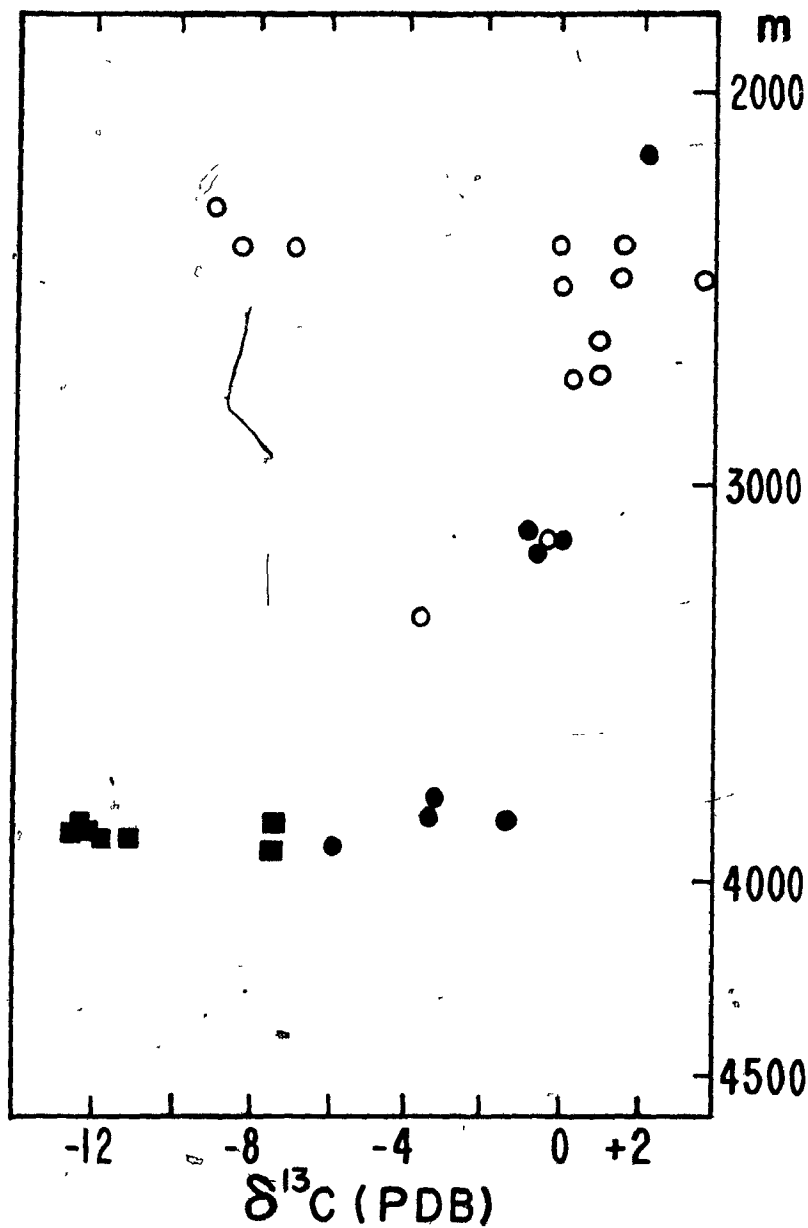● Early calcite   ○ Early calcite (Hutcheon et al, 1985)
■ Late calcite

Fig. 6.2 $\delta^{13}C$ of early and late calcite cements versus subserface depth.

somewhat elevated temperature. This type of evidence speaks against a significant input of carbon from surface and near-surface environments of microbial oxidation and sulphate reduction. From this, one has to conclude that thermal decarboxlation of organic matter of shales at greater depth provided significant amounts of carbon for the late calcite cement. Fig. 6.3 shows a covariation in the $\delta^{18}O$ and $\delta^{13}C$ composition of carbonate cements from the Hibernia and other sedimentary basins. This implies increasing contribution of organically derived carbon to marine carbonate carbon with increasing temperature and depth. Thermal breakdown of the carboxyl group of the organic material releases isotopically light CO_2 ($\delta^{13}C$ of about -25‰ PDB) to the pore water. This CO_2 may dissolve carbonates having comparatively heavier $\delta^{13}C$ values present in shales and sandstone beds. The resultant bicarbonate that forms from the mixture of this carbon dioxide and carbonate fragments (or cements) may be utilized in the precipitation of isotopically relatively light late calcite cements (provided that the pH is not buffered by the carbonate system). If the pH is controlled by the carbonate system, an increase in CO_2 will increase calcite solubility causing calcite dissolution instead of precipitation.

Early and late ferroan calcite cements contain variable amounts of iron (as observed in stained thin sections). Microprobe data for these cements (Avalon Sandstone, Hutcheon et al., 1985), also indicate variable iron contents (ranging from 1.5 to 4.39 wt.%). For the early calcite
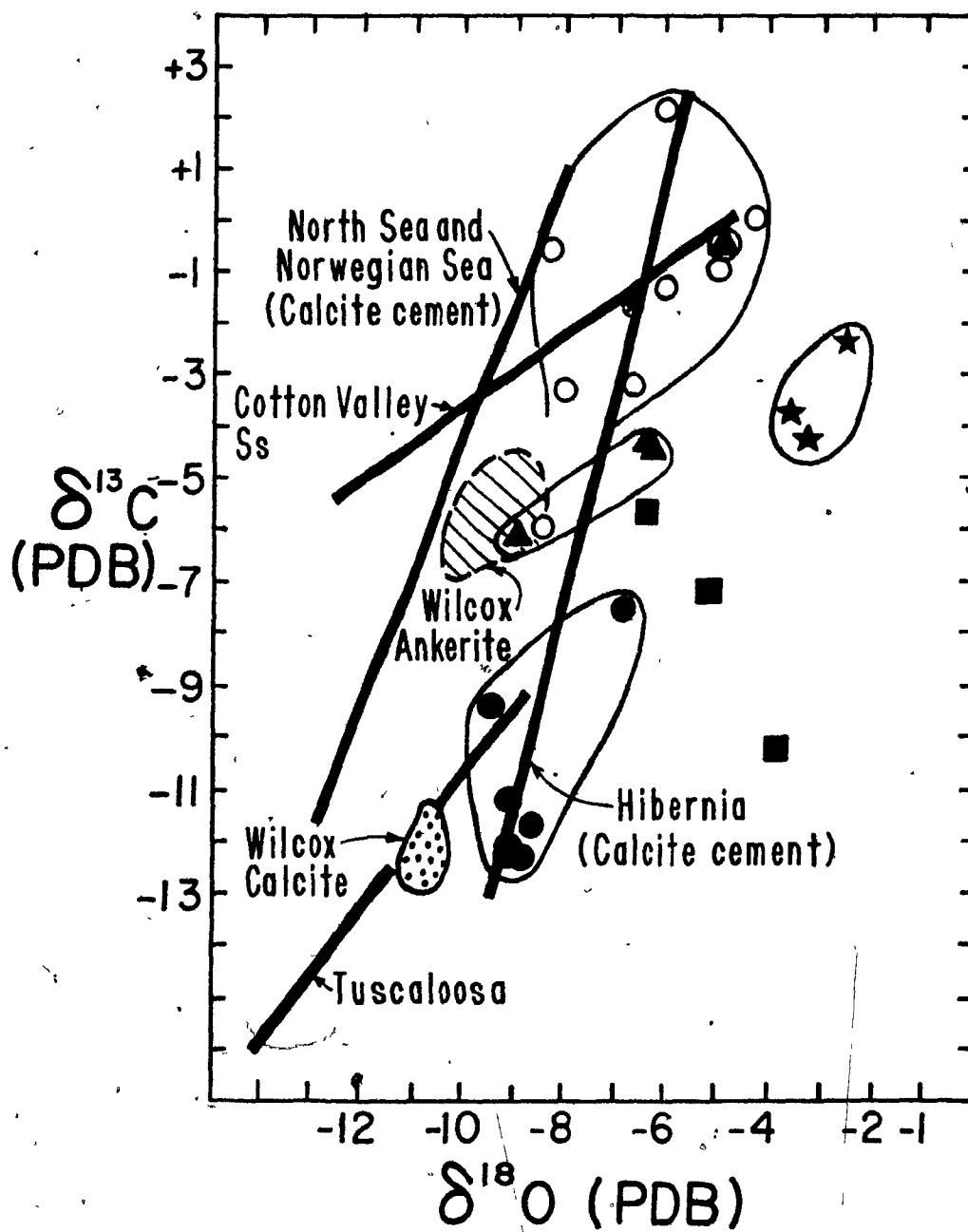
210

Fig. 6.3 A covariation in the carbon and oxygen isotopic composition of the carbonate cements in sandstones from different parts of the world. For symbols see Fig. 3.7.

(possibly precipitated below 50 $^{\circ}$C) a source of iron may be Fe-oxide and Fe-hydroxide coatings of clay minerals and other detrital grains. For early ferroan calcite, it is unlikely that the transformation of smectite to illite in the interbedded shales has served as a source of iron because this transformation usually occurs at temperature above 50 $^{\circ}$C. Beside the above mentioned sources, the diagenesis of interbedded shales (smectite /illite transformation), however, may have provided additional iron required for the precipitation of late ferroan calcite and late ferroan dolomite. Oldershaw and Scoffin (1967) also concluded that clay minerals are probably the main source of iron for late ferroan calcite cement in the Wenlock and Halkin Limestones.

6.2.2   Dolomite

On the ^{13}C/^{18}O diagram (Fig. 3.7) the early and late dolomite cements occupy distinct fields, demonstrating that the petrographic distinction of different types of dolomite cements does, in fact, reflect different temperatures and pore fluid compositions.

Petrographic evidence (see section 3.2.3.9.2) and relatively heavy δ^{18}O values (average of -3.1‰ PDB) of early ferroan dolomite (presently buried to > 3850 m subsurface depth, corresponding to temperatures above 90 $^{\circ}$C) suggest precipitation at shallower depths (above 2000 m). The average δ^{18}O of Cretaceous marine calcite cements is about -2‰ PDB (James and Choquette, 1983). Marine dolomite

212

precipitated at near surface temperatures (25 ^{o}C) would be enriched in $\delta^{18}O$ relative to co-precipitated calcite by 3‰ to 6‰ (Land 1980, 1983). If we assume that pore water responsible for the precipitation of early dolomite was similar to that of Early Cretaceous sea water, then the $\delta^{18}O$ value of the early dolomite should be +1.0‰ or heavier (assuming no late diagenetic change in isotopic composition). Early ferroan dolomite, however, shows $\delta^{18}O$ values of -3.1‰ PBD. This probably indicates precipitation and/or recrystallization at somewhat elevated temperatures (but still less than those of the late dolomite). Early ferroan dolomite was only observed in a thick (18 m) fine-grained sandstone unit which contains abundant plant fragments and organic-matter. During early diagenesis, the oxidation of organic matter and reduction of SO_4^{2-} (as indicated by abundant pyrite in the Hibernia Sandstone of the B-27 well) may have locally favoured ferroan-dolomite precipitation. The $\delta^{13}C$ values (-3.5‰ PDB) of early dolomite also indicate some organically derived carbon.

The late ferroan dolomite of the Hibernia field plotes close to the Wilcox ankerite of U. S. Gulf Coast (Fig. 6.3) The material required to precipitate late ferroan dolomite came, at least in part, from the dissolution of limestone and fossil fragments, and early calcite cements. This is supported by petrographic observations (see section 3.2.3.9.3) as well as carbon isotopes. This dolomite is commonly associated with partially dissolved carbonate fragments (Plate 16C and 27C) and early calcite cements. Late

ferroan dolomite only occurs at depths below 3000 m corresponding to well temperatures above 80 $^{\circ}C$ (Fig.6.4). At higher temperatures, iron-rich carbonates are thermodynamically more stable than calcite (Boles, 1978). The formation of ferroan dolomite from calcite in the presence of Fe^{2+} and Mg^{2+} can be expressed as;

$$4CaCO_3 + Fe^{2+} + Mg^{2+} ---> 2CaMg_{0.5}Fe_{0.5} +4CO_3 + 2Ca^{2+}$$
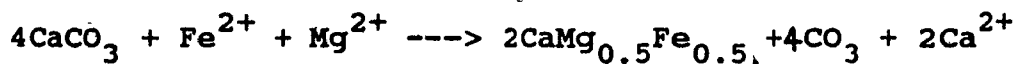
The carbon isotopes of late ferroan dolomite (average $\delta^{13}C$ = -5‰ PDB) also indicate that fossils and limestone fragments were the main source of carbon, and only a small amount of carbon was derived from an organic source. The diagenetic reactions in the interbedded shales below 3000 m (at temperatures above 80 $^{\circ}C$) may have provided Fe^{2+} and Mg^{2+} needed for this late dolomite. This is indirectly supported by the fact that late ferroan dolomite is more common when interbedded shales are common (i.e. in the "B" Sandstone of the O-35 well and the Upper Hibernia Sandstone of the B-08 well). Oldershaw and Scoffin (1967) also observed a close association between the distribution of late ferroan calcite cements and clay minerals in the Halkin and Wenlock Limestones. The presence of late pyrite, particularly in the Hibernia Sandstone of the B-27 well, also indicates that substantial amounts of reduced iron were available during "late" diagenesis in the Hibernia Oil Field.

6.2.3 Quartz

The solubility of silica increases rapidly above pH 9, but this pH is rarely encountered in natural environments
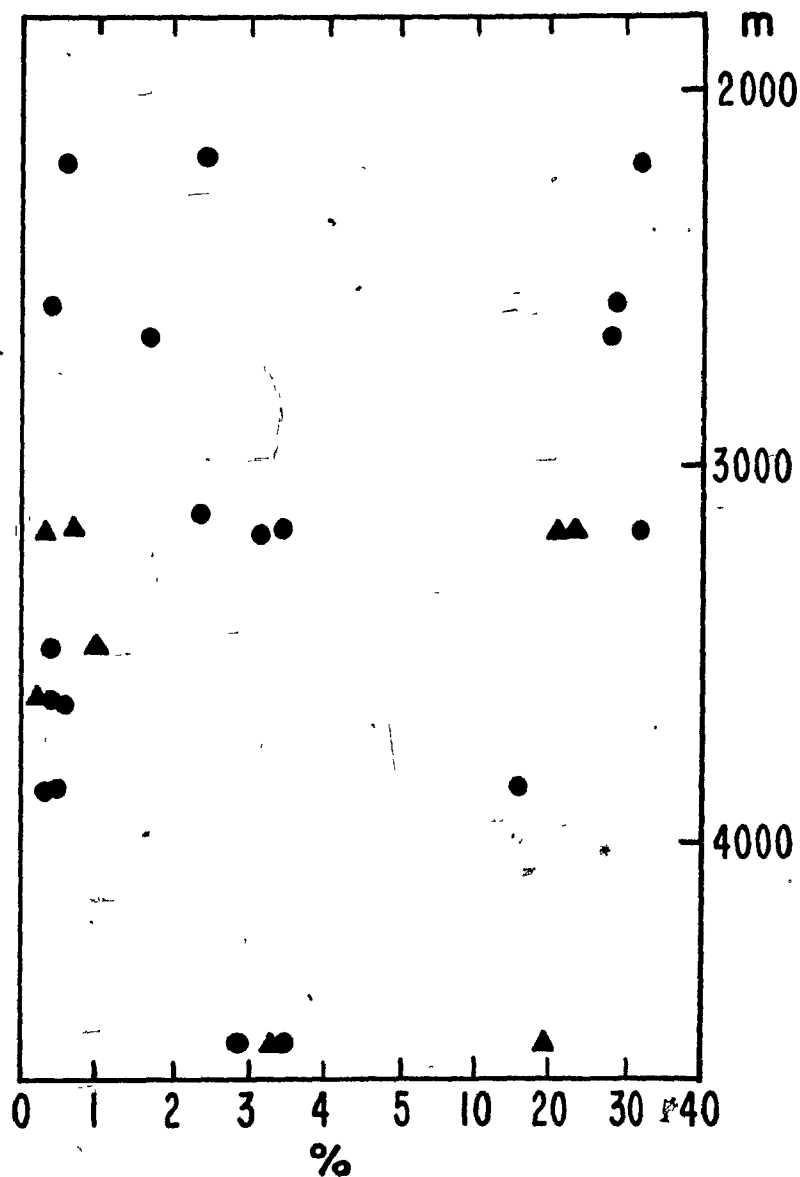
Fig. 6.4   Percent calcite and dolomite cements versus depth of burial.

215

(Berner, 1971). Quartz solubility is also dependent on temperature and hydrostatic pressure. At 100 $^{\circ}$C in oil field brines, its solubility may increase from less than 10ppm at surface conditions (25 $^{\circ}$C, near neutral pH) to about 62 ppm (Siever, 1962). When such pore water moves upward, its temperature and silica solubility decrease and as a result silica precipitation may occur.

Of the many postulated sources of silica cement (reviewed by McBride, 1977), only the following sources may have contributed to silica cementation in the Hibernia field sandstones: (i) the conversion of smectite to illite in interbedded shales, (ii) the dissolution of silica-bearing detrital grains including silicious shell fragments (fine-grained quartz, feldspar, chert, radiolaria, diatoms and sponge spicules), both in sandstones and shales, and (iii) the replacement of silica-bearing minerals (mainly quartz) by carbonates.

The Avalon Sandstone contains little quartz overgrowths. However, quartz is a common cement in the "B" and Hibernia Sandstones. Sandstone samples containing abundant quartz cement are generally from thin sandstone units present near thick shale beds. For instance, a sandstone bed above a 9 m thick shale (at 3483 m in the B-08 well) contains abundant silica cement (10.6%). Similarly, in the O-35 well between 3173 to 3185 m depth, thin sandstone beds alternating with relatively thick shales show high amounts of silica cement. Contrary to thin sandstone beds, many thick coarse-grained sandstones show only minor quartz

216

overgrowths (3920-3940 m, C-96). It seems that shale beds immediately adjacent to sandstone beds may have supplied significant amounts of the silica needed for quartz overgrowths.

The diagenesis of shales (i.e. the smectite/illite transformation) is considered an important source of silica for nearby sandstone cementation (Boles and Franks, 1979; Milliken et al., 1981; Land and Dutton, 1978; Franks and Forester, 1984). Füchtbauer (1967) also reported that in the Dogger Beta-Sandstone of northwest Germany silica cement increases toward the shaly margin of the sandstone beds. However, if one considers a possible mechanism to transfer diagenetically released silica from shales into nearby sandstones, this model faces problems. It has been shown that due to the low solubility of silica, the water content of shales (where smectite diagenesis occurs) is too low to account for the observed silica cements (Blatt, 1979; Bjorlykke, 1979). Diffusion of silica from shales into sandstones has been proposed (Jacka, 1970; Wood and Surdam, 1979), but this mechanism appears to be too slow to supply the volume of silica needed in the available geologic time.

To overcome this difficulty, Blatt (1979) proposed early silica cementation (during the first few 100 m of burial) by descending ground-waters. According to Blatt (1979), such circulation can provide a high flux of water through sandstones.

Table 6.1 Temperature of Si precipitation in quartz rich sandstones deduced from oxygen isotopic data in different sedimentary basins.

Reference	Temperature (°C)	Sedimentary basin and age
Mack (1984)	50	Noland County Texas (Pennsylvanian)
Land (1984)	60	Frio Formation, U.S. Gulf Coast (Tertiary)
Haszeldine et al. (1984)	>68	Beatrice Field of North Sea (Lower Jurassic)
Milliken et al. (1981)	75 to 80	Frio Formation, Brazoria County, Texas (Tertiary)
Land and Dutton (1978)	>75	Gray Sandstone, Taylor County, Texas (Pennsylvanian)

Petrographic observations from sandstones of the Hibernia Field do not support Blatt's model of extensive early silica cementation by meteoric water influx. In the Hibernia Field, most samples that contain abundant silica cement (>8%) are from medium-grained thin sandstone beds alternating with shales. If early meteoric water was indeed an important source of silica cement, cementation would have been more widespread in thick medium-grained sandstones rather than in thin sandstone beds alternating with shales. In addition, the Avalon Sandstone which was invaded by meteoric water during and/or after the hiatus corresponding to the Mid-Cretaceous (Albian) unconformity (Hutcheon et al., 1985), does not show abundant silica cements. Furthermore, isotopic data (Table 6.1) on quartz overgrowths from other sedimentary basins (Land and Dutton, 1978; Milliken et al., 1981; Haszeldine et al., 1984; Land, 1984; Mack, 1984) indicate the precipitation of quartz cement between 50 ^{o}C and 80 ^{o}C. At these temperatures and corresponding burial depths of 2000-3000 m (assuming average geothermal gradients on the order of 25-35 C^{o}/100 m), descending ground-water is unlikely to have high discharge rates, as needed by Blatt's model, unless the recharge of meteoric water countinues over long periods of time under special geological conditions (i.e. Western Canada Basin; Hitchon, 1969a,b). Moreover, sandstones in recent deltaic environments do not show significant amounts of silica cementation in zones of shallow meteoric groundwater circulation (Todd and Folk, 1957; Galloway, 1977). The foregoing discussion indicates some of

the problems faced with Blatt's (1979) model.

In an attempt to solve the problem of finding adequate volumes of water to carry sufficient amounts of silica from shales into nearby sandstones, Land (1984) and Haszeldine et al. (1984) suggested convective recycling of water. The source of the silica would be the smectite to illite transformation which takes place at subsurface temperatures between 60 to 120 ^{o}C. Wood and Hewlett (1982) showed that theoretically a gently dipping porous and permeable sandstone bed in a subsurface environment with a geothermal gradient as low as 25 ^{o}C/km, would experience gentle unicellular convection. Such convectional movement of fluid could transport dissolved solids over distances in the kilometer range much more rapidly than diffusive processes. However, so far, it is not known how important and effective this mechanism is and the origin and transport of silica causing widespread quartz cementation in sandstones remains an open question.

In the Hibernia Field, precipitation of silica cement occurred in different episodes, both before and after the development of secondary porosity. Although the transportation mechanism for silica is still unclear, it seems that most of it was derived from nearby shales. During early diagenesis, water expelled from shales due to mechanical compaction may have deposited small amounts of silica. This phase was followed by early calcite cementation. Where this calcite cement was missing, quartz cementation continued. Upward moving pore water may have transported some of the

silica from shales which were buried deep enough to undergo the smectite-illite transformation. Thermal maturation of organic matter within shales released carbonic and organic acids. These acids may have dissolved fine-grained feldspar present in shales, as well as feldspar and chert in sandstones (see Plates 22A, 22B, and 22C) to provide additional silica for cementation.

3.2.4 Pyrite

Pyrite forms in reducing environments in the presence of S^{2-} and Fe^{2+} (Berner, 1971). These conditions are commonly encountered in organic matter-rich marine sediments, a few centimetres to a few meters below the sediment-water interface (Curtis, 1978). Sulfide is mainly derived from the bacterial reduction of sulfate from sea water. The most likely source of iron for early pyrite is ferric oxides and hydroxides which were absorbed onto clays and other detrital grains (Carroll, 1958).

The formation of late pyrite probably occurred as a result of a reaction between iron and thermally decomposed organic sulphur compounds. It seems that enough Fe^{2+} is available in the pore waters during most of the diagenetic history. This is evident from iron-rich carbonate minerals, precipitated during different stages of diagenesis. The source of iron for late pyrite could be from shales undergoing transformation of smectite to illite and/or from the dissolution of iron-bearing early calcite. Markert (1982), and Markert and Al-Shaieb (1984) have reported the

formation of late pyrite by reduction of iron by hydrogen sulfide gas associated with hydrocarbons.

6.2.5   Siderite

Siderite has a relatively restricted stability field. Four conditions are necessary for its formation (Berner, 1971): (1) Low Eh; (2) high pCO_2 to ensure an adequate supply of the bicarbonate ion, with a pH buffer reaction other than that of the carbonate system; (3) low $[S^{2-}]$, otherwise the ferrous iron would be taken up by the precipitation of pyrite; and (4) a relatively high $[Fe^{2+}]/[Ca^{2+}]$ ratio (Fe^{2+} concentration of at least 10^{-7} mole/liter), or else calcite would form instead of siderite (Curtis, 1967). These conditions for siderite formation are commonly encountered in terrestrial sedimentary environments, particularly coal swamps where the content of dissolved Ca^{2+} and S^{2-} is low. However, in marine environments, favourable conditions for siderite precipitation may exist below the sulphate reduction zone (in the carbonate reduction and fermentation zones) during early diagenesis (0° to $75^{\circ}C$).

A clue for the origin of the HCO_3^- may be obtained from the carbon isotopic composition of siderite. Only three siderite samples from the Hibernia sandstone of the B-27 well were analysed for carbon and oxygen isotopes. At this subsurface interval, pyrite was commonly observed (see Appendix 1). The negative isotopic composition of carbon (-5.6 to -10.2‰ PDB) indicates that sulfate reduction contributed some bicarbonate. This was buffered with less

222

negative HCO_3^- derived from methanogenesis and/or sea water HCO_3^-. A contribution of HCO_3^- from methanogenesis is required by geochemical arguments, because siderite should not form until sulfate reduction ceases. As the values of $\delta^{13}C$ become less negative (from -10.2 to -5.6‰ PDB), the $\delta^{18}O$ becomes more negative (from -3.9 to -6.5‰ PDB). This indicates progressive burial as sediments move away from the SO_4^{2-} reduction zone into the carbonate reduction and the methane production zones. It is interesting to note that relatively thin sandstone beds containing dense bands of siderite are surrounded by thick organic-matter rich shales (i.e. 3910 m in the B-27 well). These shales may have provided favourable geochemical environments. The oxidation of organic matter in these shales provides strong reducing environments with high HCO_3^- and extremely low SO_4^{2-} concentration which favour siderite formation. If the pH of the pore fluid is buffered by reactions other than those of the carbonate system, precipitation of siderite in sandstones may occur when pore fluids move from the shales into nearby sandstones. The source of iron for the siderite may be the same as suggested for the early calcite cement. Siderite replacing early ferroan calcite (type 2) indicates a change in pore fluid composition. After ferroan calcite precipitation, the activity of Ca^{2+} was lowered relative to Fe^{2+} which favoured siderite precipitation. Dissiminated "wheatseed" siderite observed in the Avalon Sandstones was not analysed for isotopes.

6.2.6   Kaolinite

In the Hibernia field the authigenic kaolinite represents a relatively late phase of diagenesis. Formation of kaolinite requires a low pH with high $[Si^{4+}]$ and $[Al^{3+}]$, and low $[K^{+}]$ and $[Mg^{2+}]$ in the pore fluids. These conditions can be met during early diagenesis (by leaching of feldspar with meteoric waters) or at   moderate to greater burial depths. Early precipitation of kaolinite, in the presence of meteoric waters is less likely because (i) kaolinite frequently occurs in oversized and elongated pores of secondary origin with partly dissolved calcite remnants; (ii) it was precipitated after the formation of I/S coatings and quartz overgrowths;   (iii) delicate authigenic kaolinite crystals do not show any signs of compaction even at 4000 m depth.

As stated before, diagenesis of organic matter in shales can release acidic pore water. These pore fluids moved   through shale and sandstone beds dissolving calcite and feldspars. The dissolution of feldspar may have provided Al^{3+} and Si^{4+} required for kaolinite precipitation. Following calcite dissolution,   but before kaolinite formation, precipitation of late ferroan dolomite occurred. This will lower the Mg^{2+} and Ca^{2+} concentration and facilitate precipitation of kaolinite. Its precipitation after calcite dissolution has also been noted by other workers (e.g. Dutton, 1977; Loucks et al., 1977; Lindquist, 1977 and Curtis, 1983).

6.3   ORIGIN OF SECONDARY POROSITY

Significant amounts of porosity (up to 80% of the total porosity) in the Hibernia Oil Field are interpreted to be secondary in origin (see Chapter 5). It is, therefore, important to investigate the possible chemical processes which may have been involved in the dissolution of cements and detrital grains. Several processes have been suggested to produce aggressive pore fluids needed for dissolution; i.e. (1) meteoric water influx (Bjorlykke, 1979); (2) acidic pore fluids generated from CO_2, produced during thermal maturation of organic matter (Schmidt and McDonald, 1979); (3) organic acids formed during organic matter maturation (Surdam et al., 1984); (4) clay mineral transformation reactions (i.e. smectite K^+ + Al^{3+} ---> illite + quartz + H^+; Bjorlykke, 1981); (5) mixing corrosion (Bogli, 1964; Plummer, 1975); and (6) acidic fluids generated by reactions between clay minerals and carbonates (Hutcheon et al., 1980). Basically there are two major schools of thought:

(A) dissolution by meteoric water;

(B) dissolution by acidic fluids generated during maturation of organic-matter rich shales due to release of:

    (i) carbonic acid (thermal decarboxylation);

    (ii) organic plus carbonic acids.

6.3.1   Dissolution by Meteoric Waters

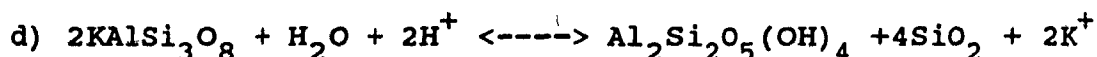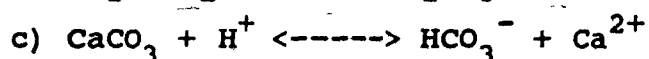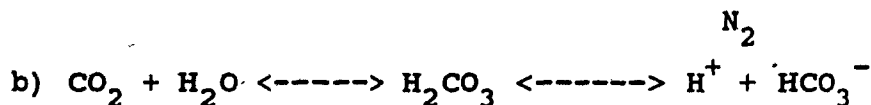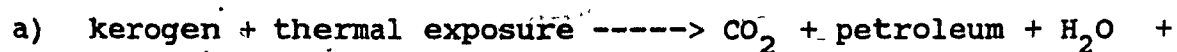In a sedimentary basin, secondary porosity may develop

due to dissolution caused by percolating meteoric waters. These waters should be undersaturated mainly with respect to calcite and feldspar and reside in the reservoir for longer periods of time. Such dissolution may occur at an early stage of diagenesis (Mathisen, 1984) and be preserved through the establishment of overpressures (Bjorlykke et al., 1979). However under special geological conditions, meteoric waters can penetrate to considerable depths (due to hydraulic-head driven flows i.e. 4000 m in case of Western Canada Basin; Hitchon, 1969ab) and distances (up to 120 km off the coast of Florida, Manheim, 1967). If meteoric waters pass slowly through a deep sedimentary basin, they are more likely to become saturated with respect to reactive minerals and therefore, would be unable to cause dissolution on a large scale.

6.3.2 Dissolution by Acidic Fluids

6.3.2.1 Carbonic Acid (thermal decarboxylation)

During organic-matter maturation significant amounts of CO_2 are generated prior to hydrocarbon generation and migration. Type III (woody) organic matter has a higher CO_2 generation potential than type II (herbaceous) organic matter (Tissot and Welte, 1978). If the pH of the pore fluid is controlled by the carbonate system (H_2CO_3, HCO_3^-, and CO_3^{2-}), an increase in pCO_2 will lower the pH thus increasing HCO_3^-. The resultant carbonic acid can dissolve carbonates. However, it will have a comparatively little effect on
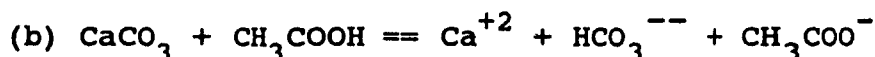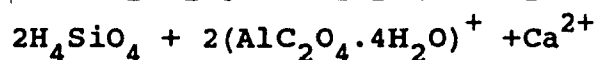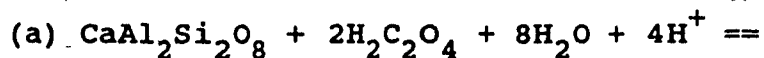
aluminosilicates present in sandstones. — Thermal degradation of kerogen and interrelated dissolution reactions can be written as:

a) kerogen + thermal exposure -----> CO_2 + petroleum + H_2O + N_2

b) $CO_2 + H_2O$ <------> H_2CO_3 <------> $H^+ + HCO_3^-$

c) $CaCO_3 + H^+$ <------> $HCO_3^- + Ca^{2+}$

d) $2KAlSi_3O_8 + H_2O + 2H^+$ <----> $Al_2Si_2O_5(OH)_4 + 4SiO_2 + 2K^+$

6.3.2.2 Organic plus Carbonic Acids

During thermal maturation of organic matter, carboxyl groups (-COOH) bonded to the kerogen core are cleaved. This process probably occurs before the generation of liquid hydrocarbons. Experimental results confirm the formation of carboxylic acids (i.e. acetic, oxalic, formic, and succinic acids) during the maturation of organic matter (Surdam et al., 1984). Carothers and Kharaka (1978, 1980) reported consibderable concentrations of these acids (up to 5000 ppm) in brines of several oil fields in California and Texas. Surdam et al. (1984) also pointed out that organic acids together with the carbonic acid have a higher dissolution potential than carbonic acid alone, particularly for feldspars. The development of secondary porosity in many sandstones is the result of aluminosilicate dissolution. The dissolution of aluminosilicate minerals, however, faces the problem of aluminium mobility as aluminium is the least mobile element in natural systems (with a solubility of 1 ppm in aqueous solution at a pH between 4 and 8). This problem can

227

be partly resolved if organic acids are considered, at temperatures where they still do not undergo thermal decarboxylation (i.e. below 120 $^{\circ}$C; Surdam et al., 1984). Experimental results indicate that aluminosilicates can be destabilized readily in the presence of organic acids. Organic acids (i.e. acetic and oxalic acids) form complexes with aluminium (i.e. $AlC_2O_4 \cdot 4H_2O$) and these complexes are soluble in water and can be transported in aqueous solution. Some dissolution reactions with organic acids can be written as:

(a) $CaAl_2Si_2O_8 + 2H_2C_2O_4 + 8H_2O + 4H^+ ==$
$2H_4SiO_4 + 2(AlC_2O_4 \cdot 4H_2O)^+ + Ca^{2+}$

(b) $CaCO_3 + CH_3COOH == Ca^{+2} + HCO_3^{--} + CH_3COO^-$

The carbonic and organic acids formed in shales are carried into nearby sandstone by the pore water, which includes water released by clay mineral reactions (i.e. the smectite/illite transformation). The development of maximum acidity in organic-matter rich shales is broadly coincident with the onset of ordering in the I/S mixed-layers (near 100 $^{\circ}$C; Pearson et al., 1983; Dypvik, 1983). The transformation of smectite to illite is probably the result of K-feldspar dissolution and is generally associated with a major dehydration reaction which releases considerable volumes of fresh water (Powers, 1967; Burst, 1959 and 1969; Perry and Hower, 1972) capable of flushing acids from the shales.

In many deltaic sequences, high sedimentation rates can prevent normal compaction causing overpressured zones (Magara,

1975 and Bruce, 1984). In these zones the expulsion of pore water is slowed down considerably. In such cases, larger volumes of water would be available at deeper levels (> 2500 m) than would be expected under normal compaction. These trapped waters may be released in different episodes of fracturing subsequently causing dissolution in sandstones. Distribution of secondary porosity above and within the geopressured zones have been reported from other sedimentary basins (Parker, 1974; Loucks et al., 1984)

Possible sources of acidic fluids for dissolution in the reservoir sandstones are discussed below in the light of available information .

6.3.3 Avalon Sandstone

The Avalon Sandstone mainly shows intergranular primary porosity. In the B-27 well, dissolution of calcite cement and carbonate fragments has occurred above a 11 m thick shale bed. The interbedded shales contain 0.8 wt % organic carbon (based on 4 samples). The Avalon Sandstone is presently buried to depths of between 2100 to 2600 m, where temperatures of 60-70 $^{\circ}$C are encountered. At 60-70 $^{\circ}$C, the organic-matter contained with shales may have started to release minor amounts of acids (Hunt, 1979). Most of the Avalon shales are calcareous so that much of the acidity generated would have been consumed locally and only small amounts of acids would have been able to reach nearby sandstones. The isotopic data (large variation of $\delta^{18}O$) and the trace element composition of calcite cements

229

indicate the involment of meteoric waters during the precipitation and recrystallization of early calcite cements (Hutcheon et al., 1985). This meteoric water which penetrated the reservoir along the Mid-Cretaceous (Albian) unconformity may have been involved in some of the dissolution.

6.3.4 "B" Sandstone

In contrast to the Avalon Sandstone, in the "B" Sandstone evidence for secondary porosity is widespread. Secondary porosity in the O-35 well is closely associated with shale-sandstone contacts (Fig. 6.5). Feldspar grains are commonly corroded in zones with secondary porosity compared to nearby early calcite-cemented zones. This may reflect an interaction with organic acids. At the present burial depth of about 3000 m (corresponding to a subsurface temperature of 80-85 ^{o}C) thermal maturation of organic matter in adjacent shales may have provided sufficient amounts of acids needed to cause the dissolution of calcite cement near sandstone-shale contacts.

6.3.5 Hibernia Sandstone

As discussed in section 5.4.3.2 the proportion of secondary porosity increases with depth from 20% to 80% of the total porosity. In the Hibernia Sandstone, extensive dissolution of carbonates, chert, feldspar, and mud clasts has generated significant secondary porosity which now exceeds the amount of primary porosity. The origin of
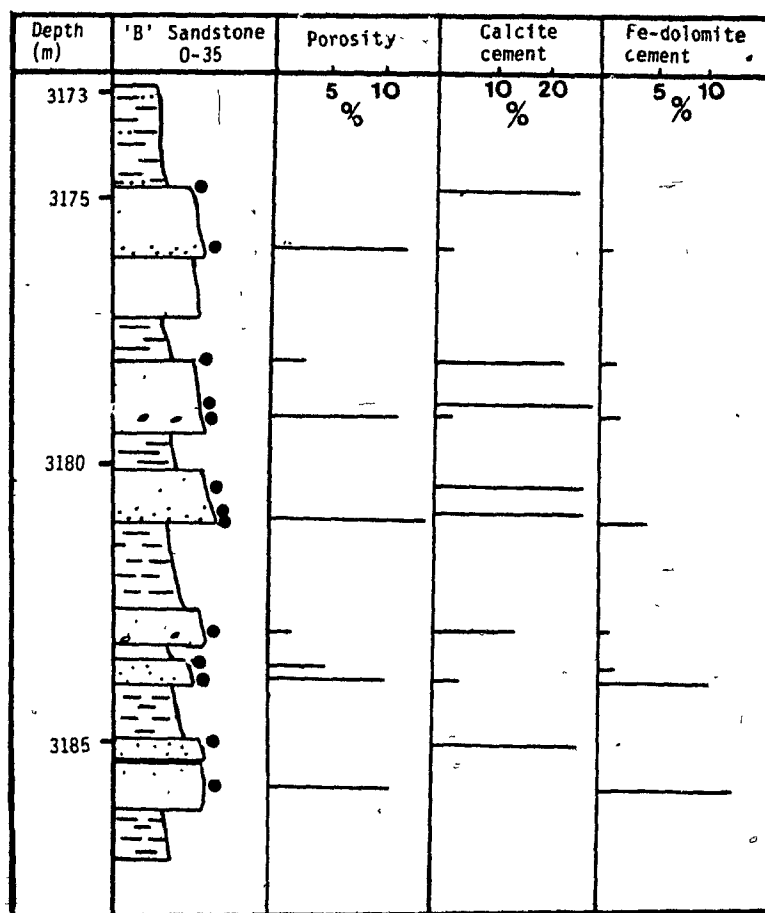
Depth (m)	'B' Sandstone 0-35	Porosity	Calcite cement	Fe-dolomite cement
		5 10 %	10 20 %	5 10 %

Fig. 6.5 A stratigraphic section from the "B" Sandstone of the O-35 well showing distribution of porosity and carbonate cements. Most of the sandstone beds alternating with shales are cemented with early calcite except a few centimeters above the shale beds where dissolution of calcite has generated secondary porosity.

231

secondary porosity due to the dissolution caused by descending meteoric waters is an attractive process at a shallow stage of diagenesis (up to a few hundred meters burial; Bjorlykke, 1979) but becomes increasingly more difficult at greater depths. Petrographic observations (i.e. heterogeneous packing, partly dissolved undeformed skeletal grains, the lack of other cements in samples of high secondary porosity) in the Hibernia Sandstone indicate a relatively deep origin of the secondary porosity. If secondary porosity had originated close to the surface, it is difficult to conceive how it could have been preserved with subsequent compaction at subsurface-depths down to 4000 m. The preservation of secondary porosity by means of overpressuring is a possibility (Bjorlykke, 1979) but is unlikely in the Hibernia Sandstone, because in the Hibernia area, the top of the overpressured (Fig. 6.6) zone generally occurs below the Hibernia Sandstone (at or near the top of Kimmeridgian shales of the Verrill Canyon Formation; Grant et al., 1986).

For secondary porosity originating at greater burial depths, the sources of aggressive pore waters are related to the thermal maturation of organic matter (Schmidt and McDonald, 1979; Surdam et al., 1984). The similarity in the paragenetic sequences of authigenic minerals associated with secondary porosity in various oil fields from different regions (see Table 5.4) is considered to result from organic matter-rich shales undergoing burial diagenesis (Curtis, 1978; Land and Dutton, 1978; Franks and Forester,
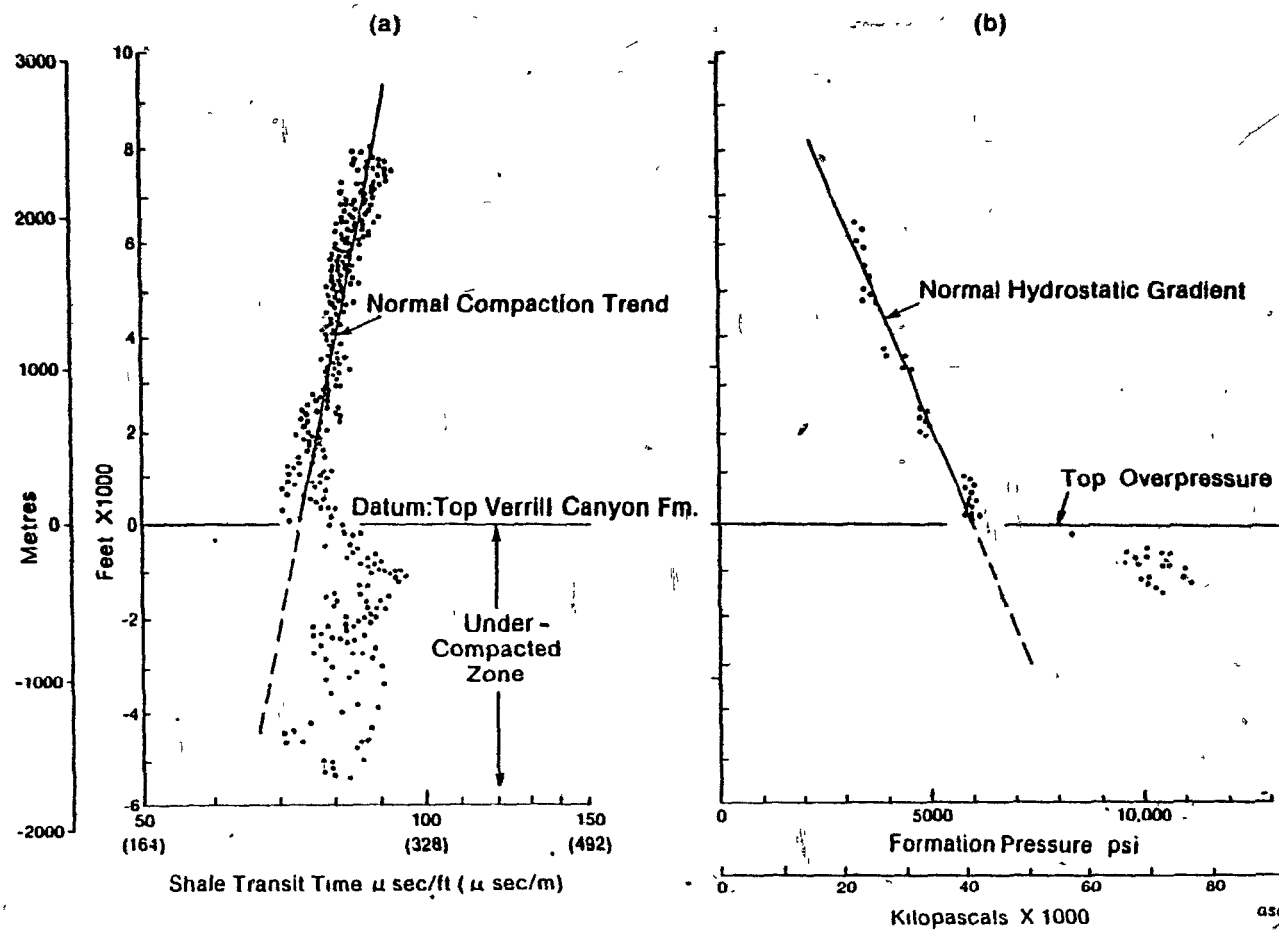
232

Fig. 6.6 Computer-generated plot of (a) shale transit time, and (b) measured formation pressure in porous rocks of the Hibernia field (B-08, K-18, O-35, and P-15 wells). The Kimmeridgian shale of the Verrill Canyon Formation is overpressured (Grant et al., 1986).

1984). Interbedded shales in the Hibernia Sandstone of the
Avalon Sub-Basin contain 0.6 wt.% terrestrial organic matter
(Swift and Williams, 1980). As mentioned before, terrestial
organic matter (Type III) has the highest CO_2-generating
capacity   (Tissot and Welte,1978). However, the potential to
generate CO_2 is dependent not only on type and abundance of
organic matter but also on the thickness of the shales. For
the Jeanne d' Arc Basin in general, shale/sandstone ratios
have   not yet been; published. In the Hibernia area (K-18
and   B-27 wells), however, the shale/sandstone ratio is
approximately 2.0 (Brown,   1985).   As a result of the
proximity   of source areas   near the basin boundary fault
(i.e. the Murre Fault),   these wells contain a   higher
percentage of sandstones.   Towards the basin centre   the
shale/sandstone ratio would be higher. In the Avalon
Subbasin, the Kimmeridgian shales   (< 300 m below the Hibernia
Sandstone) contain up to 8 wt.%   (average > 2 wt.%) organic
carbon   (mainly Type II,   and Type III) and their average
thickness   exceeds   200 m (Creaney and Allison, 1987).
Organic-matter rich Kimmeridgian shales are presently buried
to more than 4000 m corresponding to subsurface temperature
>100 ^{O}C (Fig. 6.7). They are considered the main source of
hydrocarbons in the Hibernia area (Powell, 1985; Creaney and
Allison,   1987). These shales, which presently   are
overpressured, may have provided acids and water during shale
diagenesis. Aggressive pore fluids migrating upward   from
organic-matter rich shales may have moved into the   nearby
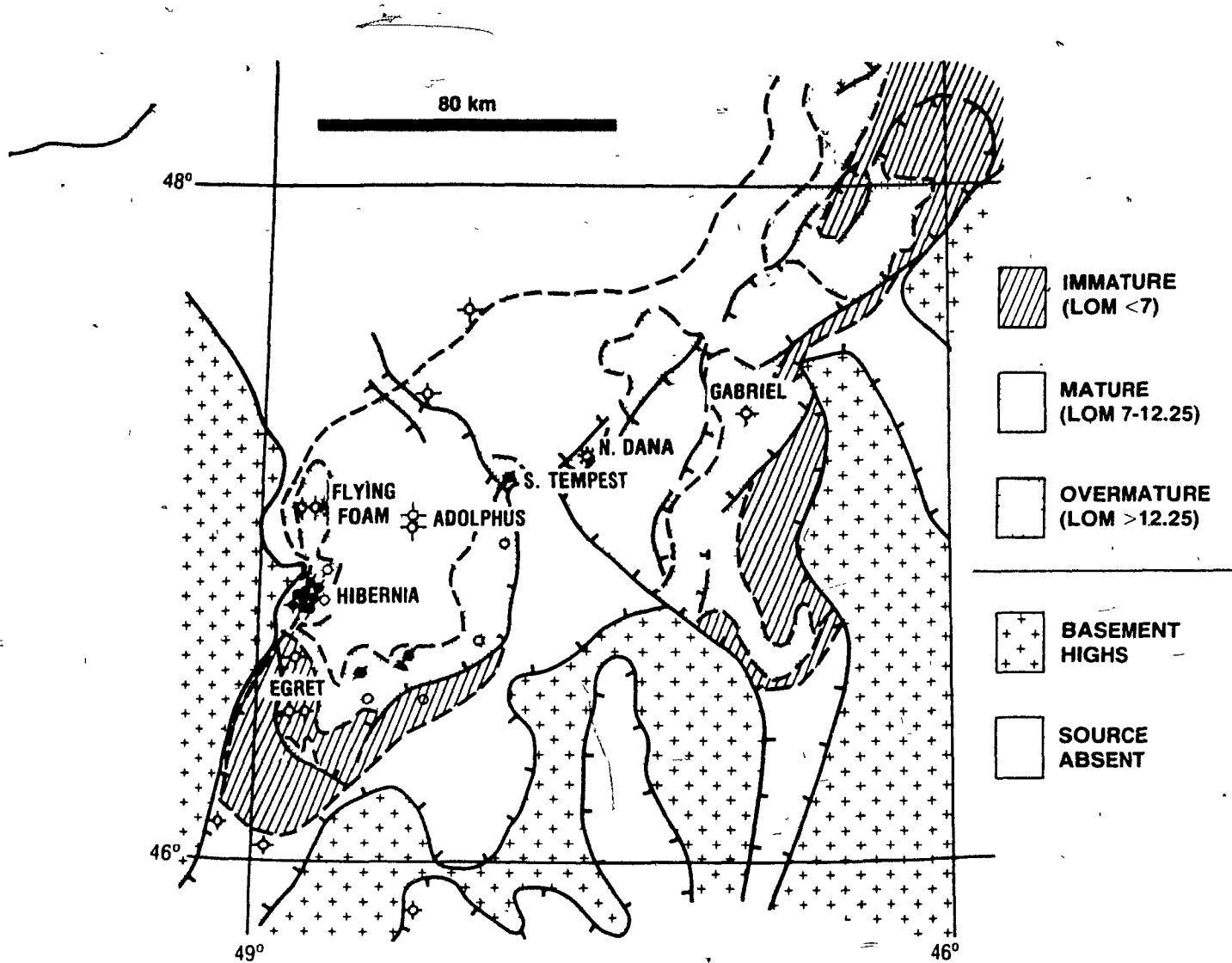Hibernia   Sandstone causing dissolution and   porosity

Fig. 6.7 Present day maturity of the Kimmeridgian source rock
in the Avalon and Flemish Pass sub-basins (from Creaney and
Allison, 1987).

enhancement. The presence of high secondary porosity near overpressured zones is also reported from the lower Gulf Coast, Texas (Loucks et al., 1984).

The Hibernia Sandstone is highly dissected by minor faults. Most of these faults have served as conduits for fluids (Meneley, 1986). This is evident from the distribution of oil fields in the Jeanne d' Arc Basin (Fig. 2.7). These oil fields are closely related to transbasin faults which appear to be an important controlling factor for transportation and accumulation of hydrocarbons. A geochemical analysis of oil and gas in the Avalon Subbasin indicates the migration of hydrocarbons from a deeper source into the Hibernia Sandstone (Creaney and Allison, 1987). A linkage between the Kimmeridgian shales and the Hibernia Sandstone may have developed some time before the peak hydrocarbon generation. Acidic pore water expelled from the compacting shales (Kimmeridgian shales as well as interbedded Hibernia shales) may have been carried into adjacent permeable conduits (fractures and faults). These aggressive subsurface fluids subsequently gained access to the carbonate-cemented sandstones via more permeable flow paths (i.e: non-calcite cemented porous zones), creating large amounts of secondary porosity by dissolving framework grains and intergranular cements, especially carbonate cements. Partly corroded chlorite inclusions within quartz grains also hint at the acidic nature of the fluids. The absence of chlorite grain-coatings in the Hibernia Sandstone, in contrast to the Avalon Sandstone, is further indirect evidence for the

presence of acidic pore waters.

It can be argued that the solubility of CO_2 will decrease as pore water migrates upwards several hundred meters (i.e. from Kimmeridgian shales to the Hibernia Sandstone), favouring carbonate precipitation rather than dissolution. This, however, may not be the case if some of the carbonate dissolution occurs by organic acids. As outlined before, organic acids are an important maturation product of organic matter. When some of the carbonates are dissolved in acetic acid the resultant calcium acetate has a higher solubility in water (by 3 orders of magnitude higher) compared to calcium carbonate (Meshri, 1986). This higher solubility will keep calcium ions in solution and prevent immediate reprecipitation of calcium as calcium carbonate. Thus the presence of organic acids would aid in the preservation of secondary porosity.

Some problems have been raised in the literature concerning the organic-matter maturation and origin of secondary porosity (Bjorlykke, 1983; Land, 1984; Lundegard et al., 1984, 1986). Mass balance calculations by these authors indicate that: (1) thermal maturation of organic matter alone cannot account for all the secondary porosity observed in sandstone reservoir rocks of the Frio Formation (Oligocene), Texas Gulf Coast, (2) some of the acidity will be neutralized within the source rocks depending upon the amount of reactive substances (e.g. carbonate) present. The total organic carbon content of the Frio Formation at present is

237

quite low (<0.28 wt. %). Assuming an original concentration of 0.5 wt % organic matter (type III with 25 wt % oxygen, 25 % of the oxygen being in the carboxyl group), a shale density of 2.6 g/cm^3, a shale/ sandstone ratio of 4.4, no dissolution in the source rocks, and the dissolution reaction $CaCO_3 + H_2O + CO_2 ---> Ca^{2+} + 2HCO_3^-$, Lundegard et al. (1984) calculated that decarboxylation of organic matter can only account for 1 to 2 vol % secondary porosity, whereas, on average the Frio Formation has 10 % secondary porosity. The Hibernia Sandstone, on average, has 9.2 % secondary porosity. The present organic carbon content in the shales of the Hibernia Zone (0.6 wt.%) and in the Kimmeridgian shales (> 2 wt. %) is significantly higher than that in the Frio Formation of the Gulf Coast. The loss of organic-carbon during early and middle stages of diagenesis have been discussed (Claypool and Kaplan, 1974; Curtis, 1978; Hesse, 1986). In the Hibernia area, Hibernia shales may have originally started with an organic-carbon content of 1 to 3 wt %. and the Kimmeridgian shales even much higher. Taking an average 2 wt % organic matter (Type III) with 25 wt. % oxygen and assuming similar conditions as Lundegard and Land did for the Frio Formation, decarboxylation of organic matter can account for 4 to 8% secondary porosity in the Hibernia Sandstone. As not all the organic matter in shales is of Type III, the actual amount of secondary porosity generated by this prosess may be less. But this doesn't take into account organic acids.

The CO_2 produced by simple decarboxylation or oxidation

of organic matter will have about the same $\delta^{13}C$ as the organic matter from which it is derived (i. e. about $-24‰$. PDB; Claypool and Kaplan, 1974). If this organically derived CO_2 is in fact used to dissolve early calcite cement (with an average $\delta^{13}C$ of $-1.6‰$ PDB) and/or calcareous fossil fragments (with an average $\delta^{13}C$ of about $+2‰$ PDB) the resultant isotopic composition of the total dissolved carbon should reflect the contribution from the various sources. The resulting $\delta^{13}C$ values will depend upon the relative proportions of carbon input from the organic and the inorganic pool, respectively. The late calcite cement in the Hibernia Sandstone has an average $\delta^{13}C$ of $-11‰$ PDB which indicates that oxidation and decarboxylation of organic matter were probably involved to mobilize the carbonates. Although decarboxylation or oxidation of organic matter seem to have played an important role in the formation of secondary porosity in the Hibernia Sandstone, they cannot account for all the observed secondary porosity (i.e. 9.0%). Organic acids can produce secondary porosity by dissolving mainly carbonates and feldspars. The dissociation and hydrogen ion donor capacity of organic acids are much higher than those of carbonic acid (3 to 350 times; Meshri, 1986). However, this mechanism faces the same material balance problem (amount of acids) because the oxygen content of kerogen is a limiting factor (Lundegard and Land, 1986).

The acid potential of organic-matter rich shales may be increased if, besides decarboxylation, other reactions are

considered, such as:

(1) Hydrous pyrolysis reaction (Kerogen + H_2O ----> CO_2 + CH_4): In this case the organic matter reacts with an external oxidant (e.g. H_2O; Lundegard et al., 1984). At present there is no direct evidence that such a "hydrous pyrolysis" reaction occurs, although Hoering (1982) has demonstrated extensive exchange of hydrogen between organic matter and H_2O during simulated maturation experiments.

(2) Mineral oxidants: During clay mineral diagenesis (smectite/illite transformation) Fe^{3+} is released together with other cations (Mg^{2+}, Si^{4+}, Ca^{2+} etc.). The Fe^{3+} is reduced to Fe^{2+} by combined associated oxidation reactions in the organic matter (Eslinger et al., 1979) which may be written as

$$CH_2O + 4Fe^{3+} + H_2O ----> CO_2 + 4Fe^{2+} + 4H^+$$

An external source of oxydant must be available for this reaction. This reaction can provide large amounts of acidic fluids as one mole of protons is produced for every mole of iron reduced. However, the quantitative significance of the reaction has not yet been confirmed. It is important to note that most of the Fe^{3+} is released from clay minerals when mixed-layer illite/smectite (I/S) acquire ordering at temperatures of about 90 to 100°C (Surdam and Crossey, 1985) and that this level corresponds to maximum organic acid generation (Surdam et al., 1984).

(3) In Lundegard et al. (1984) mass balance calculations it

was assumed that only the carboxyl group (-COOH) could be converted into CO_2 by decarboxylation. Besides the carboxyl group, other functional groups of organic matter (e.g. phenol, ester, ether, and carbonyl groups) may also produce CO_2 and H_2O at higher temperatures (Lundegard and Land, 1986).

The present study suggests that significant amounts of secondary porosity in the Hibernia Sandstone developed at deeper levels rather in near-surface environments (by meteoric water influx). The acidic pore fluid required for dissolution was most probably derived from shales undergoing burial diagenesis. The organic matter and clay minerals of shales undergo multiple complex chemical reactions capable of producing acids during burial diagenesis. As a result, the acids required for the generation of secondary porosity may be produced by more than one process. The quantitative evaluation of individual processes is a complex matter. However, some quantitative data are available on the acidic potentials of decarboxylation and organic acids in the Frio Formation of U. S. Gulf Coast. Using the same assumptions and taking 2 wt.% organic matter (Type III) decarboxylation and organic acids can account for a minimum 4% out of 9% secondary porosity in the Hibernia Sandstone. Additional acidity may have been provided by various pyrolysis and mineral oxidant reactions which need further evaluation.

241

CHAPTER VII

CONCLUSIONS AND SUGGESTIONS FOR FUTURE STUDY

7.1 CONCLUSIONS

This thesis presents the first comprehensive investigation of the burial diagenesis of reservoir sandstones, and interbedded and deeper shales from the Upper Jurassic to the top of the Lower Cretaceous in the Hibernia oil field. The main conclusions from this study are:

(1) The average framework grain composition of the reservoir sandstone is $Q_{87.9}$, $R_{8.5}$, $F_{3.6}$. Rock fragments are mainly of sedimentary origin (i.e. mud clast, sandstone, chert, and carbonate) and varies from 1 to 18%. On average there is 10.6% rock fragments in the Avalon Sandstone which decreases to 3.3% in the Hibernia Sandstone. With depth, feldspar content also decreases from 5.3% in the Avalon Sandstone to 1.9% in the Hibernia Sandstone. This decrease is in part due to dissolution of feldspar with increasing burial depth.

(2) Ten authigenic minerals were identified, comprising 1.6 to 47.7% (average 13%) of the bulk rock volume. Only 6 of them are commonly present (quartz overgrowth, calcite, dolomite, siderite, pyrite, and kaolinite). Major early to later diagenetic sequences are summarized as: thin chlorite rims--> siderite-->quartz-->early pyrite-->early ferroan calcite-->quartz-->dissolution (dominantly of calcite) and generation of secondary porosity-->minor

grain fracturing-->precipitation of late ferroan calcite/late ferroan dolomibte-->late quartz-->kaolinite-->late pyrite and migration of hydrocarbons.

(3) Late ferroan dolomite with curved cleavages and sweeping extinction resembles saddle dolomite and has not previously been reported from sandstones.

(4) Relative location in the sedimentary basin appears to influence the diagenesis of sandstones (i.e. dissolution of calcite appears to be more common basinward).

(5) X-ray mineralogy of shales (< 2.0 um) from the Hibernia and West Ben Nevis oil fields shows the following variations with increasing burial depth:

   (a) Illite generally constitutes a significant part of the clay fraction. The amount of illite increases from approximately 40% (above 2000 m) to approximately 80% (below 3600 m).

   (b) Except for a few samples near the Cretaceous/Tertiary unconformity, kaolinite is present throughout the wells B-08, B-27 (Hibernia) and B-75 (West Ben Nevis). Kaolinite (plus minor chlorite) decreases from an average 35% (above 2000 m) to 20% below 3950 m. Its crystallinity (area/height ratio) decreases with depth and probably indicates degradation of kaolinite.

   (c) The 17 $\overset{\circ}{A}$ peak (upon glycolation) is only present above 2000 m and disappears below 2000 m.

   (d) Interstratified I/S is present in all samples below 1500 m subsurface depth. Over a depth range of 1000

243

to 5000 m, expandable smectite layers in I/S mixed-layers decrease from about 75% S to < 15% S, with most rapid decrease occurring above 2500 m subsurface depth.

(e) The mixed-layered I/S is randomly interstratified above 2500 m. Below 2500 m, where illite exceeds 65% in the mixed-layers, the I/S is regularly interstratified.

(f) In the Hibernia and West Ben Nevis fields, the width of the (001) illite peak below the Avalon Sandstone increases slightly with increasing burial depth indicating poorer crystallinity. This reversal (compared to the usual trend of illite crystallinity) is probably due to an increase in organic matter content and percent mixed-layer I/S (and/or smectite) in the original sediments supplied during deposition.

(g) The use of IC as an indicator of maturation in organic-matter rich source rocks, therefore, requires considerable caution, particularly during the middle (and probably also the late) stages of diagenesis.

(h) In the bulk shale samples, K-feldspar disappears below 3600 m depth. Below 3500 m, calcite is absent in most samples.

(6) Assuming 40% original porosity in sands at the time of deposition, an average 17% porosity were lost mainly due to mechanical compaction, and 13% due to cementation,

244

leaving an average of 10% total porosity in thin sections.

(7) Porosity in the fine-grained, loosely packed diagenetically immature, Hauterivian-Albian Avalon Sandstone (2100 to 2660 m) is mainly primary. In the Avalon sandstone, early ferroan calcite cement destroys most of the primary porosity. This cement has completely filled the pores in more than 20% of the sandstone drill-core from the Avalon Sandstone. An average 4.9% porosity were lost by other cementing minerals (quartz overgrowth, siderite, pyrite etc.). In the Avalon Sandstone, no dolomite or kaolinite were observed. Dissolution features were only observed in the Avalon Sandstone of the B-08 the and B-27 wells situated basinward from well O-35 where no dissolution was observed.

(8) With increasing burial depth, the percentage of secondary porosity increases and in the diagenetically semi-mature Berriasian-Valanginian "B" Sandstone (3150 to 3360 m, O-35 well), 62% of the porosity are secondary. This secondary porosity originated mainly by dissolution of early calcite cement and carbonate fragments. A large portion of the "B" Sandstone (23% of the sandstone drill-core studied) is completely cemented with early calcite. Quartz overgrowth (4.7%) and late ferroan dolomite (3.6%) are other important authigenic minerals. Reduction of porosity by late ferroan calcite and kaolinite is insignificant.

(9) Below the Avalon and "B" Sandstones, porosity in the medium-to coarse-grained diagenetically mature Tithonian Hibernia Sandstone (3480 to 4100 m) is mainly secondary (> 80% of the total porosity). At present only 4% sandstone drill-core are completely cemented mainly with calcite. However, it appears that during early diagenesis a significant portion of the Hibernia Sandstone was completely cemented with early calcite thus conserving original intergranular porosity for later recovery by dissolution at depth. Porosity reduction due to quartz overgrowths in the Hibernia sandstone averages 4.9%. Porosity reduction by other cementing minerals (siderite, late ferroan dolomite, kaolinite, and late pyrite) is about 1%. It should be emphasized that these estimates are based on selected samples that may not necessarily represent the entire reservoir zone.

(10) Based on isotopic data obtained during this study and that by Hutcheon et al. (1985), the early calcite cement is tentatively interpreted as the result of upward moving shale waters mixed, at places, with meteoric waters. The shale waters are assumed to have came both from interbedded and deeper level shales (hot fluids with lighter $\delta^{18}O$) Marine carbonate fragments are the main source of Ca and C for these early calcite cements.

(11) Isotopic data and petrographic observations on late ferroan calcite cement suggest that its precipitation occurred at elevated temperatures. Thermal maturation

246

of organic matter of shales at deeper levels provided significant amounts of carbon for this cement.

(12) The material required to precipitate late ferroan dolomite came, at least in part, from the dissolution of limestone and fossil fragments, and early calcite cements. Interbedded shales may have provided the Fe^{2+} and Mg^{2+} needed for this cement. Indirect support for this assumption comes from the fact that late ferroan dolomite is more common where interbedded shales are abundant (i.e. in the "B" Sandstone of the O-35 well and in the upper Hibernia Sandstone of the B-08 well). The presence of late pyrite also indicates that substantial amounts of reduced iron were available during "later" diagenesis.

(13) In the Hibernia field, precipitation of silica cement occurred in different episodes, both before and after the development of secondary porosity. It seems that most of the silica was derived from nearby shales. During early diagenesis, water expelled from shales due to mechanical compaction deposited small amounts of silica. This phase was followed by early ferroan calcite cementation. Where this calcite cement was missing, quartz cementation continued. Upward moving pore water may have transported some of the silica from shales which were buried deep enough to undergo the smectite-illite transformation. Thermal maturation of organic matter within shales released carbonic and organic acids. These acids may have dissolved fine-grained feldspar present in shales, as well as feldspar and chert in sandstones, to provide

247

additional silica for cementation.

(14) Minor amounts of siderite is commonly observed in different reservoir sandstones. However, siderite-rich zones (> 30%) were only observed in relatively thin sandstone beds surrounded by thick organic-matter rich shales. These sandstone beds may mark the zones of greatest pore fluid circulation expelled from compacting shales which may have provided favourable geochemical environments needed for siderite precipitation.

(15) The results of this study suggest that dissolution and development of secondary porosity occurred at greater burial depths. Acidic pore water needed for dissolution was probably generated by maturation of organic matter in interbedded and deeper organic-matter rich Kimmeridgian shales. Taking an average 2 wt % organic matter (Type III) and assuming similar conditions as Lundegard et al. (1984) did for the Frio Formation in the U. S. Gulf Coast, thermal maturation of organic matter can account for 4 to 8% secondary porosity in the Hibernia Sandstone. As not all the organic matter in shales is of type III, the actual amount of secondary porosity generated by this processes may be less. Organic matter and clay minerals of shales undergo multiple complex chemical reactions capable of producing acids during burial diagenesis. As a result, the acids required for the generation of secondary porosity may be produced by more than one process, such as various pyrolysis and mineral

oxidation reactions.

7.2 SUGGESTION FOR FUTURE STUDY

This study is only the first step to understand trends of diagenesis and their effects on reservoir porosity both vertically and laterally in the Jeanne d'Arc Basin. An important area for future study is to obtain fluid inclusion data on carbonate cements and quartz overgrowths. This, together with isotopic and petrographic information, will provide an additional control to reconstruct depths of precipitation for major authigenic minerals. Secondly, analysis and interpretation of carefully obtained formation waters data is an urgently needed source of information to study fluid/rock interaction during diagenesis. Such information can be used to prepare subsurface saturation/undersaturation maps for different solid species which may help to predict zones of enhanced porosity. Thirdly, a detailed regional study is needed which includes the investigation of lateral variation in burial diagenesis from the centre toward the margin of the basin. This would include an evaluation of the type and extent of diagenesis, correlation of overpressured zones with distribution of secondary porosity, and the control of depositional lithofacies on sandstone porosity. Such studies would help to refine our understanding of migration and accumulation of hydrocarbons within the Jeanne d'Arc Basin.

REFERENCES

AHN, J. H., AND PEACOR, D. R.,1986. Transmission and analytical electron microscopy of the smectite-to-illite transition. Clays and Clay Minerals, **34,** 165-179.

ALMON, W. R., AND DAVIES, D. K., 1979. Regional diagenetic trends in the Lower Cretaceous Muddy Sandstone, Powder River Basin. In: Scholle, P. A., and Schluger, P. R. (Eds.): Aspects of diagenesis, Soc. Econ. Mineral. Paleont., Spec. Publ., **26,** 379-400.

AMOCO AND IMPERIAL, 1973. Regional geology of the Grand Banks. Bull. Canadian Petrol. Geol., **21,** 479-503.

ARTHUR, K. R., COLE, D. R., HENDERSON, G. G. L., AND KUSHNIR, D. W., 1982. Geology of the Hibernia discovery. In: Halbouty, M. T. (Ed.): The deliberate search for the subtle trap, Amer. Assoc. Petrol. Geol. Memoir, **32,** 181-195.

ASSERETO, R., AND FOLK, R. L., 1980. Diagenetic fabrics of aragonite, calcite, and dolomite in an ancient peritidal-spelean environment: Triassic Calcare Rosso, Lombardia, Italy. Jour. Sediment. Petrol., **50,** 371-394.

BARSS, M. S., BUJAK, J. P., AND WILLIAMS, G. L., 1979. Palynological zonation and correlation of sixty-seven wells, eastern Canada, Geol. Surv. Canada, Paper 78-24, 118-125.

BASU, A., YOUNG, S. W., SUTTNER, L. J., JAMES, W. C., AND MACK, G. H., 1975. Re-evaluation of the use of undulatory extinction and polycrystallinity in detrital quartz for provenance interpretation. Jour. Sediment. Petrol., **45,** 873-882.

BATHURST, R.G.C., 1958. Diagenetic fabrics in some British Dinantian limestones. Liverpool Manchester Geol. J., **2,** 11-36.

BELL, T. E., 1986. Microstructure in mixed-layer illite/smectite and its relationship to the reaction of smectite to illite. Clays and Clay Minerals, **34,** 146-154.

BENTEAU, R. I. AND SHEPPARD, M. G., 1982. Hibernia-a petrophysical and geological review. Jour. Canadian. Petrol. Technology, **21,** 59-72.

BERNER, R. A., 1971. Principles of chemical sedimentology. McGraw-Hill, New York, 240pp.

BISCAYS, P. E., 1965. Mineralogy and sedimentation of recent deep-sea clay in the Atlantic Ocean and adjacent seas and

oceans. Geol. Soc. Amer. Bull., **76**, 803-832.

BJORLYKKE, K., 1979. Cementation of sandstones. Jour. Sediment. Petrol., **49**, 1358-1359.

--------, 1981. Diagenetic reactions in sandstones. In: Parker, A., and Sellwood, B. W. (Eds.): Sediment diagenesis. Proceedings of a NATO advanced study conference at Reading University UK.

--------, 1983. Diagenetic reactions in sandstones. In Parker, A., and Shellwood, B. W. (Eds): Sediment diagenesis, Reidel Publishing Co., Dordecht, 169-213.

--------, MALM, K. O., AND ELVERHOI, A., 1979. Diagenesis in the Mesozoic sandstones from Spitsbergen and the North Sea. Geologisches Rundschau, **68**, 1151-1171.

BLATT, H., 1979. Diagenetic processes in sandstones. In: Scholle, P. A., and Schluger (Eds.): Aspects of Diagenesis, Soc. Econ. Paleontol. Mineral., Spec. Publ., **26**, 141-157.

BOGLI, A., 1964. Mischungskorrosion; ein Beitrag zum Verkarstungsproblem, Erdkunde, **18**, 165-180.

BOLES, J. R., 1978. Active ankerite cementation in the subsurface Eocene of southwest Texas. Contrib. Mineral. Petrol., **68**, 13-22.

--------, AND FRANKS, S. G., 1979. Clay diagenesis in Wilcox sandstones of Southwest Texas: Implication of smectite diagenesis on sandstone cementation. Jour. Sediment. Petrol., **49**, 55-70.

BROWN, D. M., 1985. Sedimentology of the Upper Jurassic-Lower Cretaceous Hibernia Member of the Missisauga Formation in the Hibernia Oil Field, Jeanne d' Arc Basin. Unpubl. M. Sc. thesis, Carleton Univ., Ottawa, Ontario, 157pp.

BRUCE, C. H., 1984. Smectite dehydration and its relation to structural development and hydrocarbon accumulation in Northern Gulf of Mexico Basin. Amer. Assoc. Petrol. Geol. Bull., **68**, 673-683.

BUJAK, J. P., BARSS, M. S., AND WILLIAMS, G. L., 1977a. Offshore eastern Canada- Part I, Organic type and colour and hydrocarbon potential. Oil Gas Jour., **75** (14), 198-202.

--------,--------,--------, 1977b. Offshore eastern Canada-Part II, Organic type and colour and hydrocarbon potential. Oil Gas Jour., **75** (15), 96-100.

BURLEY, S. D., AND KANTOROWICZ, J. D., 1986. Textural criteria for the recognition of cement-dissolution

251

porosity. Sedimentology, **33**, 587–605.

BURST, J. F., 1959. Post-diagenetic clay mineral-environmental relationships in the Gulf Coast Eocene in clays and clay minerals. Clays and Clay Minerals, **6**, 327–341.

————, 1969. Diagenesis of Gulf Coast clayey sediments and its possible relation to petroleum migration. Amer. Assoc. Petrol. Geol. Bull., **53**, 73–93.

CAROTHERS, W. W., AND KHARAKA, Y. K., 1978. Aliphatic acid anions in oil-field waters: implication for origin of natural gas. Amer. Assoc. Petrol. Geol. Bull., **62**, 2441–2453.

————,————, 1980. Stable carbon isotopes of HCO_3 in oil field waters: implication for the origin of CO_2. Geochim. Cosmochim. Acta, **44**, 323–332.

CARROLL, D., 1958. Role of clay minerals in the transportation of iron. Geochim. Cosmochim. Acta, **14**, 1–27.

CHEPIKOV, K. P., YERMOLOVA, Y. P., AND ORLOVA, N. A., 1961. Corrosion of quartz grains and examples of the possible effect of oil on the reservoir properties of sandy rocks. Doklady, Acad. Sci., USSR, Earth Science Sections, **140**, 1111–1113 (in English).

CHOQUETTE, P. W., AND PRAY, L. C., 1970. Geologic nomenclature and classification of porosity in sedimentary carbonates. Amer. Assoc. Petrol. Geol. Bull., **54**, 107–250.

CLAYPOOL, G. E., AND KAPLAN, I. R., 1974. The origin and distribution of methane in marine sediments. In: Kaplan, I. R. (Ed.): Natural gases in marine sediments, New York, Plenum Press, 99–139.

CRAIG, H., 1957. Isotopic standards for carbon and oxygen and correction factors for mass-spectrometric analysis of carbon dioxide. Geochim. Cosmochim Acta, **12**, 272–374.

CREANEY, S., AND ALLISON, B. H., 1987. An organic geochemical model of oil generation in the Avalon/ Flemish Pass sub-basins, East Coast Canada. Bull. Canadian Petrol. Geol., **35**, 12–23.

CURTIS, C. D., 1967. Diagenetic iron minerals in some British carboniferous sediments. Geochim. Cosmochim. Acta, **31**, 2109–2123.

————, 1978. Possible links between sandstone diagenesis and depth-related geochemical reactions occurring in enclosing mudstones. Jour. Geol. Soc. London, **135**, 107–117.

————, 1983. Link between aluminium mobility and the

destruction of secondary porosity. Amer. Assoc. Petrol. Geol. Bull., **67,** 380-384.

DICKSON, J. A. D., 1965. A modified staining technique for carbonates in thin section. Nature, **205,** 587

DIXON, S. A., AND KIRKLAND, W. D., 1985. Relationship of temperature to reservoir quality for feldspathic sandstone of southern California. Amer. Assoc. Petrol. Geol., Southwest Section Transactions, 82-99.

DUNOYER DE SEGONZAC, G., 1970. The transformation of clay minerals during diagenesis and lower grade metamorphism: a review. Sedimentology, **15,** 281-396.

DUTTON, S. P., 1977. Diagenesis and porosity distribution in deltaic sandstone, Strawn series, Pennsylvania, North Central Texas. Trans. Gulf Coast Assoc. Geol. Soc., **27,** 272-277.

DYPVIK, H., 1983. Clay mineral transformations in Tertiary and Mesozoic sediments from the North Sea. Amer. Assoc. Petrol. Geol. Bull., **67,** 160-165.

EBERL, D., 1978a. The reaction of montmorillonite to mixed-layer clay: the effect of interlayer alkali and alkaline earth cations. Geochim. Cosmochim. Acta, **42,** 1-7.

--------, 1978b. Reaction series of dioctahedral smectites. Clays and Clay Minerals, **26,** 327-340.

--------, AND HOWER, J., 1976. The kinetics of illite formation. Bull. Geol. Soc. Amer., **87,** 1326-1330.

EMERY, K. O., UCHUPI, E., PHILLIPS J. D., BOWIN, C. O., BURNE, E. T., AND KNOTT, S. T., 1970. Continental rise off eastern North America. Amer. Assoc. Petrol. Geol. Bull., **54,** 44-108.

EPSTEIN, S., BUCHSBAUM, R., LOWENSTEM, H. A., AND UREY, H. C., 1953. Revised carbonate water isotopic temperature scale. Geol. Soc. Amer. Bull., **64,** 1315-1326.

ESLINGER, E., HIGHSMITH, P., ALBERS, D., AND DEMAYO, B., 1979. Role of iron reduction in the conversion of smectite, to illite in bentonites in the disturbed belt, Montana. Clay and Clay Minerals, **27,** 327-338.

FIELDER, G. W., DISTEFANO, M. P., AND SHEARER, J. N., 1985. Depositional influences in sandstone diagenesis of the Lower Cretaceous Hosston Formation, Marion and Walthall Counties, Mississippi. Trans. Gulf Coast Assoc. Geol. Socs., **35,** 367-371.

FOLK, R. L., 1974. Petrolpgy of Sedimentary Rocks. Hemphill

Publ. Co. Austin, Texas. 182pp.

FOSCOLOS, A. E., AND KODAMA. H., 1974. Diagenesis of clay
minerals from Lower Cretaceous shales of north eastern
British Columbia. Clays and Clay Minerals, **22**, 319-335.

--------, AND STOTT, D. F., 1975. Degree of diagenesis,
stratigraphic correlations and potential sediment sources
of Lower Cretaceous shale of northeastern British Columbia.
Geol. Survey Canada Bull., 250, 1-46.

--------, AND POWELL, T. G., 1980. Mineralogical and geochemical
transformation of clays during burial catagenesis and their
relation to oil generation. Canadian Soci. Petrol. Geol.,
Memoir, **6**, 153-172.

FRANKS, S. G., AND FORESTER, R. W., 1984. Relationships among
secondary porosity, pore-fluid chemistry and carbon
dioxide, Texas Gulf Coast. In: McDonald, D. A., and Surdam,
R. C. (Eds): Clastic diagenesis, Amer. Assoc. Petrol. Geol,
Memoir, **37**, 63-80

FREED, R. L., 1981. Shale mineralogy and burial diagenesis of
Frio and Vicksburg Formations in two geopressured wells,
Mcallen Range area, Hidalgo County, Texas. Trans. Gulf
Coast Asso. Geol. Soc., **31**, 289-293.

FUCHTBAUER, H., 1967. Influence of different types of
diagenesis on sandstone porosity. 7th World Petrol. Congr.
Proc., **2**, 353-369.

GALLOWAY, W. E., 1974. Deposition and diagenetic alteration of
sandstone in northeast Pacific arc-related basins.
Implication for graywacke genesis. Geol. Soc. Amer. Bull.,
85, 379-390.

--------, 1977. Catahoula Formation of the Texas Coastal Plain.
Depositional systems, composition, structural development,
groundwater flow history and uranium distribution. Bur.
Econ. Geol., Univ. of Texas, N87.

GEOLOGICAL SURVEY OF CANADA, 1977. Basement structure, Eastern
Canada and adjacent areas map 1400A (SE).

GONZALEZ, L. A., AND LOHMANN, K.C., 1985. Carbon and oxygen
isotopic composition of Holocene reefal carbonates.
Geology, **13**, 811-814

GRADSTEIN, F. M. AND WILLIAMS, G. L., 1981. Stratigraphic
charts of the Labrador and Newfoundland shelves, Geol.
Surv. Canada, Open File Report **826**.

GRANT, A. C., McALPINE, K. D., AND WADE, J. A., 1986. The
continental margin of eastern Canada- geological framework
and petroleum potential. In: Halbouty, M.T. (Ed.): Future

petroleum provinces of the world. Amer. Asso. Petrol. Geol. Memoir, 40, 177-205.

HANDYSIDE, D. D., AND CHIPMAN, W. I., 1983. A preliminary study of the Hibernia field. Jour. Canadian Petrol. Technol, 22, 67-78.

HASZELDINE, R. S., SAMSON, I. M., AND CORNFORD, C., 1984. Quartz diagenesis and convective fluid movement: Beatrice oil field, U. K. North Sea. Clay Minerals, 19, 391-402.

HAYES, J. B., 1979. Sandstone diagenesis- the hole truth. In: Scholle, P. A., and Schluger, P. A. (Eds): Aspects of diagenesis, Soc. Econ. Paleont. Mineral. Specl. Publ., 26, 127-139.

HEMLEY, J.J., 1959. Some mineralogical equilibria in the system ($K_2O-Al_2O_3-SiO_2-H_2$). Amer. Jour. Science, 257, 241-270.

HÉROUX, Y., BERTRAND, R., AND CHAGNON, A., 1981. Evolution thermique et potential petroligene par li etude des kérogenes, des extraits organiques, des gaz adsorbes, des argiles, du sondage Karlsefni H-13 (offshore Labrador, Canada). Canadian Jour. Earth Sciences, 18, 1856-1877.

HESSE, R., 1986. Diagenesis No. 11. Early diagenetic pore water/sediment interaction: Modern offshore basins. Geoscience Canada, 13, 165-196.

HISCOTT, R. N., 1984. Clay mineralogy and clay-mineral provenance of Cretaceous and paleogene strata, Labrador and Baffin shelfs. Bull Canadian. Petrol. Geol., 32, 272-280.

HITCHON, B., 1969a. Fluid flow in the Western Canada sedimentary basin: 1. Effect of topography. Water Resour. Research, 5, 186-195.

--------, 1969b. Fluid flow in the Western Canada sedimentary basin: 2. Effect of geology. Water Resour. Research, 5, 460-469.

HOERING, T. C., 1982. Thermal reactions of kerogen with added water, heavy water, and pure organic substances. Carnegie Institution, Geophys. Lab., Ann. Report, 1981-1982, p.397-402.

HOWER, J., ESLINGER, E. V., HOWER, M. E., AND PERRY E. A., 1976. Mechanism of burial metamorphism of argillaceous sediment: 1. Mineralogical and chemical evidence. Geol. Soc. Amer. Bull., 87, 725-737.

HUNT, J. M., 1979. Petroleum geochemistry and geology. W. H. Freeman and Co. San Francisco, 617pp.

HUTCHEON, I., OLDERSHAW, A., AND GHENT, E. D., 1980. Diagenesis of Cretaceous sandstones of the Kootenay Formation at Elk Vally (southeastern British Columbia) and Mt. Allan (southwestern Alberta). Geochim. Cosmochim. Acta, **44**, 1425-1435.

--------, NAHNYBIDA, C. G., AND KROUSE, H. R., 1985. The geochemistry of carbonate cements in the Avalon sand, Grand Banks of Newfoundland. Mineral. Magazine, **49**, 457-467.

IMAM, M. B., AND SHAW, H. F., 1987. Diagenetic controls on the reservoir properties of gas bearing Neogene Surma Group sandstones in the Bengal Basin, Bangladesh. Marine & Petroleum Geol., **4**, 103-111.

JACKA, A. D., 1970. Principles of cementation and porosity occlusion in Upper Cretaceous sandstones, Rocky Mountain region. In: Wyoming Geol. Assoc. Guigebook, 22nd, 265-285.

JAMES, N. P., AND CHOQUETTE, P. W., 1983. Diagenesis 6. Limestone-The sea floor diagenetic environment. Geoscience Canada, **10**, 162-180.

JANSA, L. F., AND WADE, J. A., 1975. Geology of the continental margin off Nova Scotia and Newfoundland, Geol. Surv. Canada Paper **74-30**, 51-105.

--------, GRADSTEIN, F. M., HARRIS, I. M., JENKINS, W. A., AND WILLIAMS, G. L., 1976. Stratigraphy of the Amoco-IOE Murre G-67 well, Grand Banks of Newfoundland, Geol. Surver of Canada Paper 75-30, p. 14.

KLITGORD, K. D., AND SCHOUTEN, H., 1986. Plate kinematics of the central Atlantic. In: Vogt, P. R., and Tucholke, B. E. (Eds.): The geology of North America, Volume M, The Western North Atlantic region: Geol. Soc. Amer., 351-378.

KÜBLER, B., 1967. La cristallinite de l' illite et les zones tout a fait superieures du metamorphisme. In: Etages tectoniques, Colloque de Neuchatel (Suisse), 105-122.

LAHANN, R. W., AND ROBERSON, H. E., 1980. Dissolution of silica from montmorillonite: effect of solution chemistry. Geochim. Cosmochim. Acta, **44**, 1937-1943.

LAND, L. S., 1980. The isotopic and trace element geochemistry of dolomite: The state of the art. Soc. Econ. Paleont. Mineral. Specl. Publ., **28**, 87-110.

--------, 1983. The application of stable isotopes to studies of the origin of dolomite and to problems of diagenesis of clastic sediments. In: Arthur, M. A. (Ed.): Stable isotopes in sedimentary geology, Soc. Econ. Paleont. Mineral. Short

Course 10, p. 4-1--4-22.

--------, 1984. Frio Sandstone diagenesis, Texas Gulf Coast: A regional isotopic study. Amer. Assoc. Petrol. Geol. Memoir, 37, 47-62.

--------, AND DUTTON, S. P., 1978. Cementation of a Pennsylvanian deltaic sandstone: Isotopic data. Jour. Sediment. Petrol., 48, 1167-1176.

--------, AND MILLIKEN, K. L., 1981. Feldspar diagenesis in the Frio Formation, Brazoria County, Texas Gulf Coast. Geology, 9, 314-318.

LINDQUIST, S. J., 1977. Secondary porosity development and subsequent reduction, overpressured Frio Formation sandstone (Oligocene), South Texas. Trans. Gulf Coast Assoc. Geol. Soc., 27, 99-107.

LONGSTAFFE, F. J., 1984. The role of meteoric water in diagenebsis of shallow sandstone: stable isotope studies of the Milk River Aquifer and Gas Pool, southeastern Alberta. Amer. Assoc. Petrol. Geol. Memoir, 37, 81-98.

LOUCKS, R. G., BEBOUT. D. G., AND GALLOWAY, W. E., 1977. Relationship of porosity formation and preservation to sandstone consolidation history, Gulf Coast Lower Tertiary Frio Formation. Trans. Gulf Coast Assoc. Geol. Soc., 27, 109-120.

--------, DODGE, M. M., AND GALLOWAY, W. E., 1979. Importance of secondary leached porosity in Lower Tertiary sandstone reservoirs along the Texas Gulf Coast. Trans. Gulf Coast Assoc. Geol. Socs., 34, 164-171

--------,--------, AND --------, 1984. Regional controls on diagenesis and reservoir quality in Lower Tertiary sandstones along the Texas Gulf Coast. Amer. Asso. Petrol. Geol. Memoir, 37, 15-45.

LUNDEGARD, P. D., AND LAND, L. S., 1986. Carbon dioxide and organic acids: Their role in porosity enhancement and cementation, Paleogene of the Texas Gulf Coast. In: Gautier, D. L. (Ed.): Roles of organic matter in sediment diagenesis, Soc. Econ. Paleont. Mineral. Spec. Publ., 38, 129-146.

--------,--------, AND GALLOWAY, W. E., 1984. Problem of secondary porosity: Frio Formation Texas Gulf Coast. Geology, 12, 399-402.

MACHEL, H.-G., 1987. Saddle dolomite as a by-product of chemical compaction and thermochemical sulfate reduction. Geology, 15, 936-940.

MACK, L. E., 1984. Petrography and diagenesis of a submarine fan sandstone, Cisco Group (Pennsylcanian), Nolan. Unpubl., M.S. thesis, Univ. Texas, Austin, 154pp.

MAGARA, K., 1975. Importance of aquathermal pressuring effect in Gulf Coast. Amer. Assoc. Petrol. Geol. Bull., **59,** 2037-2045.

MANHEIM, F. T., 1967. Evidence for submarine discharge of water on the Atlantic continental slope of the Southern United States, and suggestions for further research. Trans. New York Acad. Sci., **11,** 839-853.

MARKERT, J. C., 1982. Mineralogical, geochemical, and isotopic evidence of diagenetic alteration, attributable to hydrocarbon migration, Raven Creek and Reel fields, Wyoming. Unpubl., M.Sc. thesis, Oklahoma State Univ., 126 pp.

MARKERT, J. C., AND AL-SHAIEB, Z., 1984. Diagenesis and evolution of secondary porosity in Upper Minnelusa Sandstone, Power River Basin, Wyoming. Amer. Assoc. Petrol. Geol. Memoir, **37,** 367-389.

MASSON, D. G., AND MILES, P. R., 1984. Mesozoic sea-floor spreading between Iberia, Europe and North America. Marine Geology, **56,** 279-287.

------,-------, 1986. Development and hydrocarbon potential of Mesozoic sedimendary basins around margins of North Atlantic. Amer. Assoc. Petrol. Geol. Bull., **70,** 721-729.

MATHISEN, M. E., 1984. Diagenesis of Plio- Pleistocene nonmarine sandstone, Cagayan Basin, Philippines: Early development of secondary porosity in volcanic sandstone. Amer. Assoc. Petrol. Geol. Memoir, **37,** 177-193.

MATTES, B. W., AND MOUNTJOY, E. W., 1980. Burial dolomitization of the Upper Devonian Miette Buildup, Jasper National Park, Alberta. Soc. Econ. Paleont. Mineral. Specl Publ., **28,** 259-297.

McBRIDE, E. F., 1977. Secondary porosity-importance in sandstone reservoirs in Texas . Trans. Gulf Coast Assoc. Geol. Soc., **17,** 121-122.

-------, 1981. Diagenetic history of Norphlet Formation (Upper Jurassic), Rankin County, Mississippi. Trans. Gulf Coast Assoc. Geol. Socs., 31 347-351.

McIVER, N. L., 1972. Cenozoic-Mesozoic stratigraphy of the Nova Scotia shelf. Canadian Jour. Earth Sci., **9,** 54-70.

McMILLAN, N. J., 1982. Canada's east coast; the new super petroleum province. Jour. Petrol. Technology, **21,** 1-15.

MENELEY, R. A., 1986. Oil and gas fields in the east coast and Arctic Basins of Canada. In: Halbouty, M. T. (Ed.): Future petroleum provinces of the world. Amer. Assoc. Petrol. Geol. Memoir, **40,** 143-176.

MESHRI, I. D., 1986. On the reactivity of carbonic and organic acids and generation of secondary porosity. In: Gautier, D. L. (Ed.): Roles of organic matter in sediment diagenesis. Soc. Econ. Paleont. Mineral. Spec. Publ., **38,** 123-128.

MILLIKEN, K. L., LAND, L. S., AND LOUCKS, R. G., 1981. History of burial diagenesis determined from isotopic geochemistry, Frio Formation, Brazoria County, Texas. Amer. Assoc. Petrol. Geol. Bull., **65,** 1397-1413.

--------, **GOLD, P. B., AND LAND, L. S.,** 1985. Feldspar diagenesis in Neogene sediments, northern Gulf of Mexico (abs.). Amer. Assoc. Petrol. Geol. Bull., **69,** 288.

MORROW, D. W., CUMMING, G. L., AND KOEPNICK, R. B., 1986. Manetoe facies- A gas bearing, megacrystalline, Devonian dolomite, Yukon and North west territories, Canada. Amer. Assoc. Petrol. Geol. Bull., **70,** 702-720.

OGUNYOMI, O., HESSE, R., AND HEROUX, Y., 1980. Pre- and synorogenic diagenesis and anchimetamorphism in Lower Paleozoic continental margin sequences of the Northern Appalachians in and around Quebec City, Canada. Bull. Canadian Petrol. Geol., **28,** 559-577.

OLDERSHAW, A. E., AND SCOFFIN, T. P. 1967. The source of ferroan and non-ferroan calcite cements in the Halkin and Wenlock Limestone. Geol. Jour., **5,** 309-320.

O'NEIL, J. R., CLAYTON, R. N., AND MAYEDA, T. K., 1969. Oxygen isotope fractionation factors in divalent metal carbonates. Jour. Chem. Physics, **51,** 5547-5558.

PARKER, C. A., 1974. Geopressures and secondary porosity in the deep Jurassic of Mississippi. Trans. Gulf Coast Assoc. Geol. Socs., **24,** 69-80.

PEARSON, M. J., WATKINS, D., PITTION, J.-L., CASTON, D., AND SMALL, J.S., 1983. Diagenesis, organic maturation and paleothermal history of an area in the South Viking Graben, North Sea. In: Brooks, J. (Ed.): Petroleum geochemistry and exploration of Europe, Geol. Soc. London, Spec. Publ., **12,** 161-174.

PERRY, E. A., AND HOWER, J., 1970. Burial diagenesis in Gulf Coast pelitic sediments. Clays and Clay Minerals, **18,** 165-177.

--------, **AND** --------, 1972. Late stage dehydration in deeply

buried pelitic sediments. Amer. Assoc. Petrol. Geol. Bull., **56**, 2013-2021.

PLUMMER, L. N., 1975. Mixing of sea water with calcium carbonate ground water. Geol. Soci. Amer. Memoir, **142**, 219-236.

POWELL, T. G., 1982. Petroleum geochemistry of the Verrill Canyon Formation; a source for Scotian Shelf hydrocarbons. Bull. Canadian Petrol. Geol, **30**, 167-179.

—————, 1985. Paleogeographic implications for the distribution of Upper Jurassic source beds, Offshore Eastern Canada. Bull. Canadian Petrol. Geol., **33**, 116-119.

POWERS, M. C., 1967. Fluid release mechanisms in compacting marine mudrocks and their importance in oil exploration. Amer. Assoc. Petrol. Geol. Bull., **51**, 1240-1253.

PROSHLYAKOV, B. K., 1960. Reservoir properties of rocks as a function of their depths and lithology. Geol. Nefti i Gaza, v. **4**, No.12, 24-29. Assoc. Tech. Sercices Translation RJ 3421.

PURCELL, L. P., RASHID, M. A. AND HARDY, I. A., 1979. Geochemical characteristics of sedimentary rocks in Scotian Basin. Amer. Assoc. Petrol. Geol. Bull., **63**, 87-105.

RADKE, B. M., AND MATHIS, R. L., 1980. On the formation and occurrence of saddle dolomite. Jour. Sediment. Petrol., **50**, 1149-1168.

RASHID, M. A., PURCELL, L. P., AND HARDY, I. A., 1980. Source rock potential for oil and gas of the East Newfoundland and Labrador Shelf areas. In: Miall, A. D., (Ed): Facts and principles of world petroleum occurrence, Canadian Soc. Petrol Geol. Memoir, **6**, 589-608.

REYNOLDS, R. C., AND HOWER, J., 1970. The nature of interlayering in mixed-layer illite-montmorillonites. Clays and Clay Minerals, **18**, 23-56.

RICHES, P., TRAUB-SOBOTT, I., ZIMMERLE, W., AND ZINKERNAGEL, U., 1986. Diagenetic peculiarities of potential Lower Jurassic reservoir sandstones, Troms area, Off Northern Norway, and their tectonic significance. Clay Minerals, **21**, 565-584.

SCHMIDT, V., AND McDONALD, D. A., 1979a. The role of secondary porosity in the course of sandstone diagenesis. In: Scholle P. A., and Schluger, P. A. (Eds): Aspect of diagenesis, Soc. Econ. Paleont. Mineral. Spec. Publ., **26**, 175-207.

—————,—————, 1979b. Texture and recognition of secondary

porosity in sandstones. In: Scholle, P. A., and Schluger, P. A. (Eds): Aspects of diagenesis, Soc. Econ. Paleont. Mineral. Spec. Publ., **26**, 209-225.

————,————, AND PLATT, R. L., 1977. Pore geometry and reservoir aspects of secondary porosity in sandstones. Bull. Canadian Petrol. Geol., **25**, 271-290.

SCHULTZ, L. G., 1964. Quantitative interpretation of mineralogical composition from x-ray and chemical data for the Pierre Shale. U. S. Geol. Survey Prof. Paper, 391-C, C1-C31pp.

SHANMUGAM, G., 1985. Significance of secondary porosity in interpreting sandstone composition. Amer. Assoc. Petrol. Geol. Bull., **69**, 378-384.

SHERWIN, D. F., 1973. Scotian Shelf and Grand Banks. In McCrossan, R. G. (Ed.): The future petroleum provinces of Canada. Canadian. Soc. Petrol. Geol., Memoir, **1**, 519-559.

SIBLEY, D. F., AND BLATT, H., 1976. Intergranular pressure solution and cementation in the Tuscarora orthoquartzite. Jour. Sediment. Petrol., **46**, 881-891.

SIEVER, R., 1962. Silica solubility, 0-200 $^{\circ}$C, and the diagenesis of siliceous sediments. Jour. Geology, **70**, 127-150.

SRIVASTAVA, S. P., 1978. Evolution of the Labrador Sea and its bearing on the early evolution of the North Atlantic. Geophys. Jour. Royal Astron. Soc., **52**, 313-357.

ŚRODOŃ, J., 1981. X-ray identification of randomly interstratified illite-smectite in mixtures with discrete illite. Clay Mineral, **16**, 297-304.

————, 1984. Mixed-layer illite-smectite in low temperature diagenesis: data from the Miocene of the Carpathian Foredeep. Clay Minerals, **19**, 205-215.

SURDAM, R. C., BOESE, S. W., AND CROSSEY, L. J., 1984. The chemistry of secondary porosity. In: McDonald, D. A., and Surdam, R. C. (Eds.): Clastic diagenesis. Amer. Assoc. Petrol. Geol. Memoir, **37**, 127-151.

SURDAM, R. C., AND CROSSEY, L. J., 1985. Mechanisms of organic/inorganic interactions in sandstone/shale sequences. In: Gautier, D. L., Kharaka, Y. K., and Surdam, R. C. (EDS.): Relationship of organic matter and mineral diagenesis. Soc. Econ. Paleont. Mineral., Short Course **17**, 177-232.

STANTON, G. D., 1977. Secondary porosity in sandstones of the lower Wilcox (Eocene), Karnes County, Texas. Trans. Gulf

Coast Assoc. Geol. Soc., **27**, 147-207.

SWIFT, J. H., AND WILLIAMS, J. A., 1980. Petroleum source rocks, Grand Banks area. In: Miall, A. D. (Ed.): Facts and principles of world petroleum occurrence, Canadian. Soc. Petrol. Geol. Memoir, **6**, 167-188.

--------, **SWITZER, R. W., AND TURNBULL, W. F.**, 1975. The Cretaceous Petrel Limestone of the Grand Banks, Newfoundland. In: Yorath, C. J., Parker,E. R., and Glass, D. J. (Eds.): Canada's continental margins and offshore petroleum exploration. Canadian. Soc. Petrol. Geol. Memoir, **4**, 181-194.

TANKARD, A. J., AND WELSINK, H. J., 1987. Extensional tectonics and stratigraphy of Hibernia Oil Field, Grand Banks, Newfoundland. Amer. Assoc. Petrol. Geol. Bull., **71**, 1210-1232.

TANKARD, A. J., AND WELSINK, H. J., (in press). Extensional tectonics, structural styles and stratigraphy of the Mesozoic Grand Banks of Newfoundland. In: Manspeizer, W. (Ed.): Triassic-Jurassic rifting and opening of the Atlantic Ocean, Elsevier, Amsterdam.

TILLMAN, R. W., AND ALMON, R. W., 1979. Diagenesis of Frontier Formation offshore bar sandstones, Spearhead Ranch field, Wyoming. In: Scholle, P. A. and Schluger, P. R. (Eds.): Aspects of diagenesis. Spec. Publ. Soc. Econ. Paleont. Mineral., **26**, 337-378.

TISSOT, B. P., AND WELTE, D. H., 1978. Petroleum formation and occurrence. New York: Springer-Verlag, 538pp.

TODD, T. W., AND FOLK, R. L., 1957. Basal Claiborne of Texas, record of Appalachian tectonism during Eocene. Amer. Assoc. Petrol. Geol. Bull., **41**, 2545-2566.

TROJAN, M., 1985. Effects of diagenesis on reservoir properties and log response, Upper Jurassic Taylor Sandstone, Cotton Valley Group, Lincoln Parish, Louisiana. Trans. Gulf Coast Assoc. Geol. Socs., **35**, 367-371.

UPSHAW, C. F., ARMSTRONG, W. E., CREATH, W. B., KIDSON, E. J., AND SANDERSON, G. A., 1974. Biostratigraphic framework of the Grand Banks. Amer. Assoc. Petrol. Geol. Bull., **58**, 1124-1132.

VEIZER, J., 1983. Trace elements and isotopes in sedimentary carbonates. In: Reeder, R. J. (Ed.): Carbonates: Mineralogy and Chemistry. Mineral. Soc. Amer. Reviews in Mineralogy, **11**, 265-299.

WILLIAMS, G. L., AND BRIDEAUX, W. W., 1975. Palynological analysis of Late Mesozoic-Cenozoic rocks of the Grand Banks

of Newfoundland, Geol. Surv. Canada. Bull., **236**, 162pp.

WOLFE, K. H., AND CONOLLY, J. R., 1965. Petrogenesis and paleoenvironment of limestone lenses in Upper Devonian Red Beds of New South Wales. Paleo., **1**, 69-111.

WOOD, J. R, AND HEWLETT, T. A., 1982. Fluid convection and mass transfer in porous sandstones-a theoretical model. Geochim. Cosmochim. Acta, **46**, 1707-1713.

WOOD, J. R., AND SURDAM, R. C., 1979. Application of convective-diffusion models to diagenetic processes. In: Scholle, P. A., and Schluger, R. P. (Eds.): Aspects of diagenesis, Soc. Econ. Paleont. Mineral., Spec. Publ., **26**, 243-250.
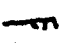
APPENDIX 1

Detailed core logs from the B-27, O-35, B-08, C-96, and K-18 wells of the Hibernia Oil Field. Location of sandstone and shale samples studied during this project are indicated by dots. For lithological and other symbols see next page.

(Thickness in meters)

LEGEND FOR STRATIGRAPHIC SECTIONS

Fine-grained sandstone

Siltstone

Medium-grained sandstone

Shale

Coarse-grained sandstone
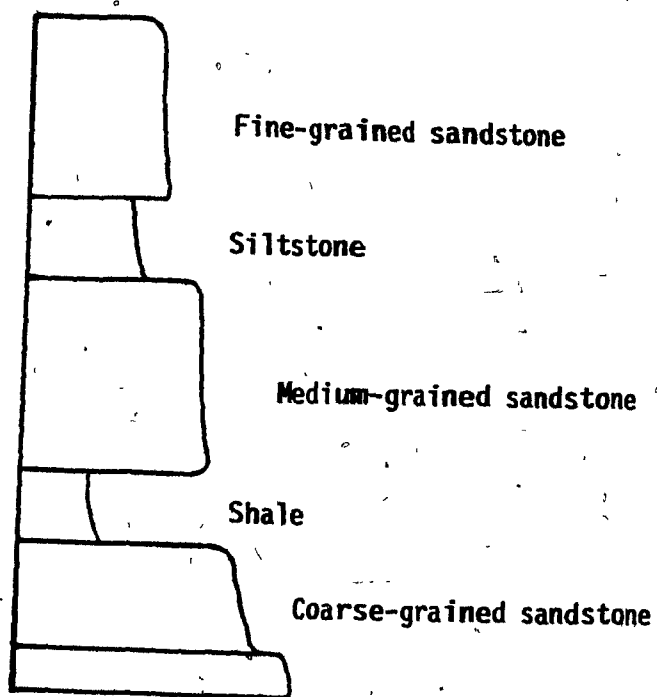
⌷	Bioturbation
∿	Carbonaceous stringer
⧫	Convoluted-laminated
⬚	Cross-bedding
╲	Fining-upward cycle
╱	Fining-downward cycle
⬮	Irregular sandstone lense
⬮	Mud clast
▮	Pyrite
⌒	Ripple
●	Sample location
⬬	Sandstone clast
∿	Scoured surface
⌢	Shell fragment
⬭	Siderite nodule
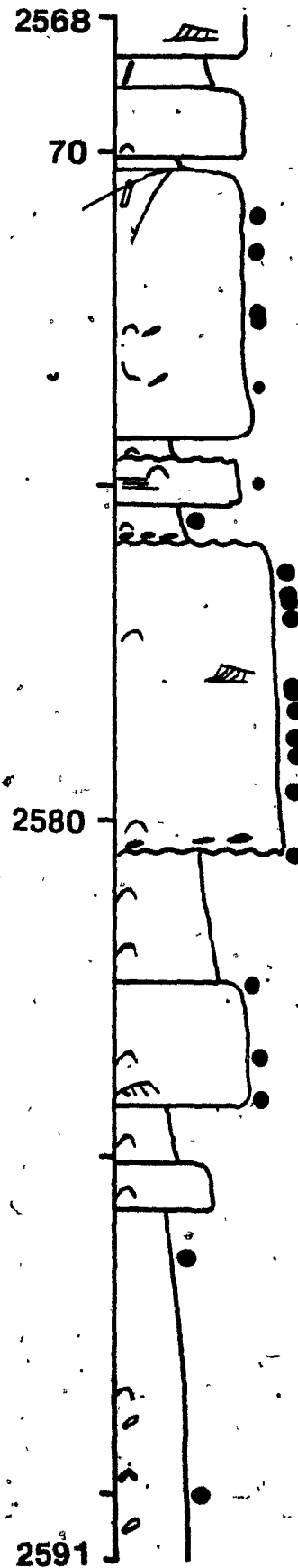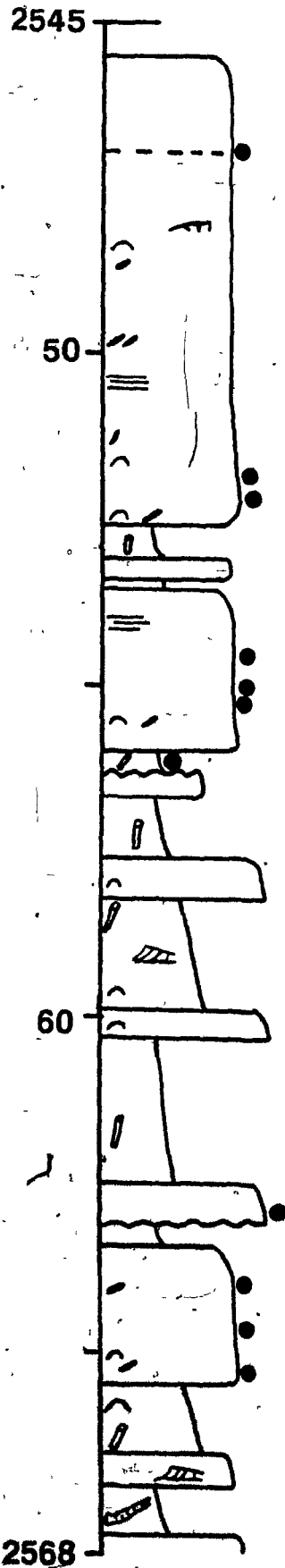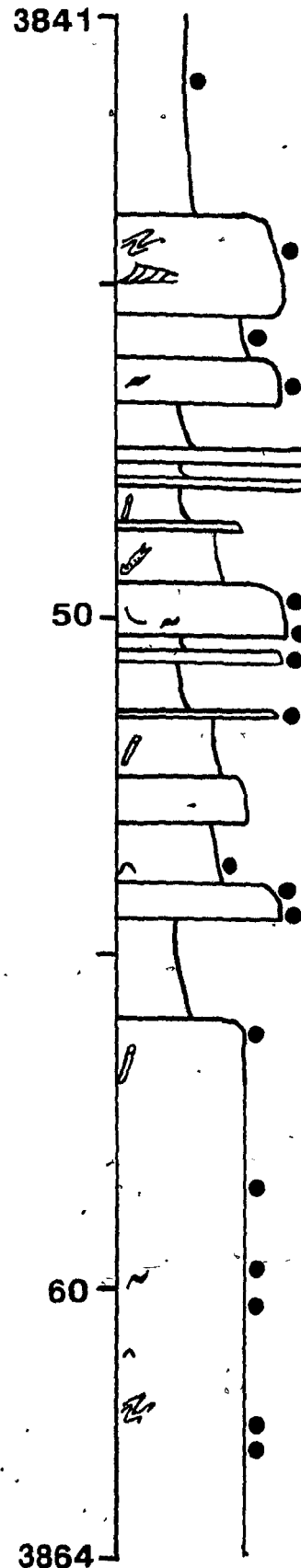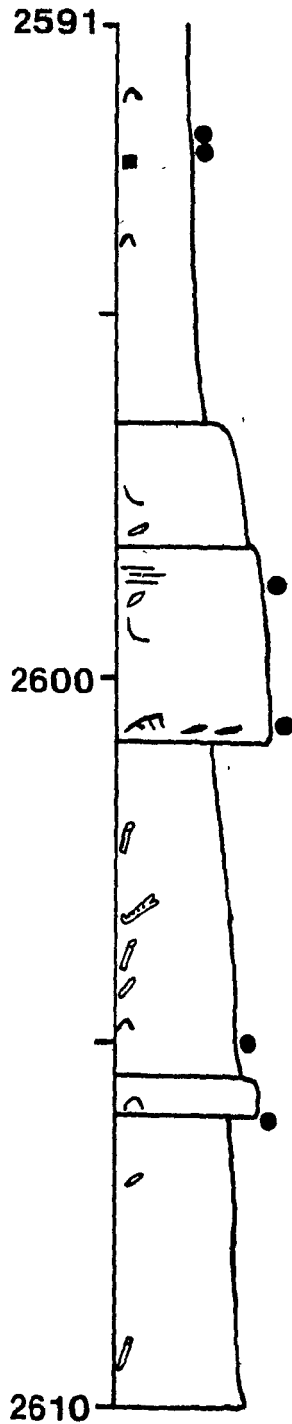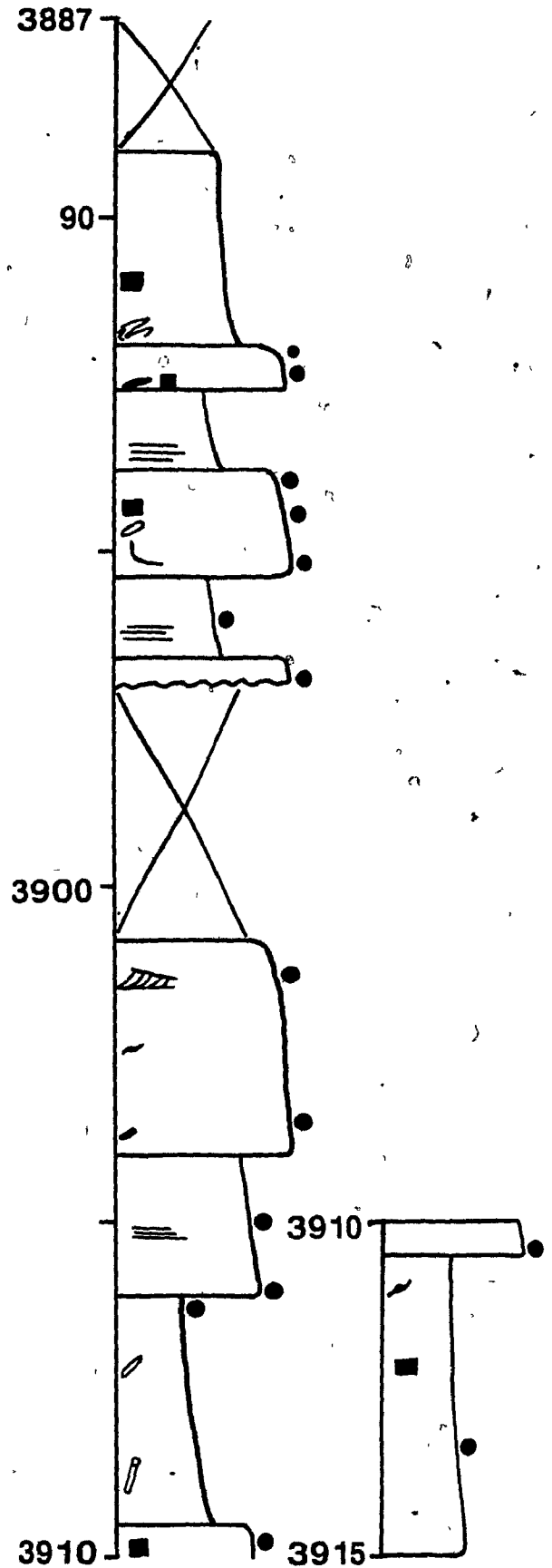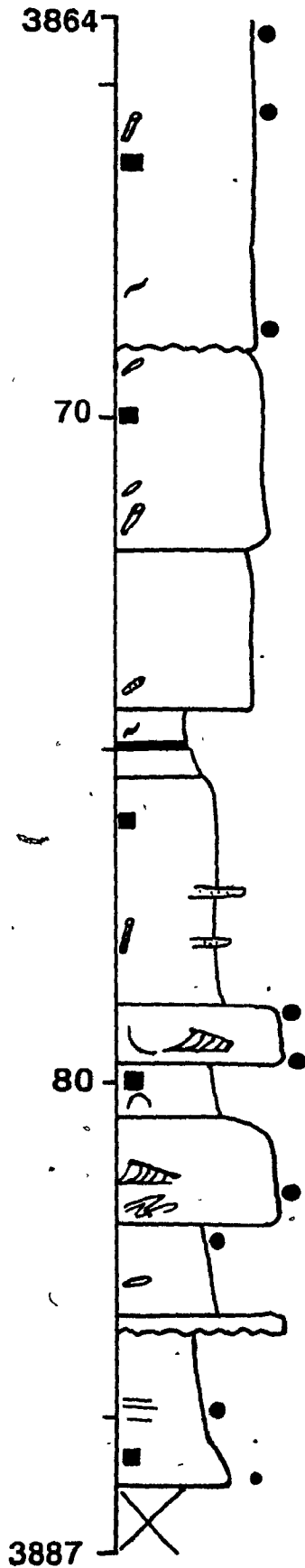
285

B-27

2545

2568

50

70

60

2580

2568

2591

266

B-27

2591

2600

2610

3841

50

60

3864

267

B-27

O-35

B-O8

2658

60

65

3480

90

3494

3494

97

3554

60

64

3606

10

270

B-O8

3611

20

25

C-96

1670
72

2302

10

2319

2319
20

30

33

272

C-96

3869
70
3892
3900
80
10
90
15
92
273

C-96

3915

20

30

38

3938

40

50

59

274

K-18

K-18

276

K-18

3841

5021

30

50

40

60

277
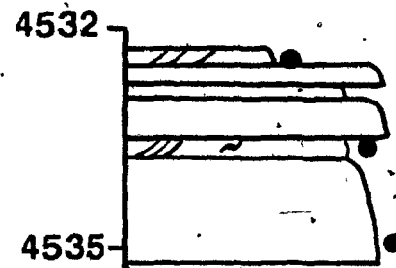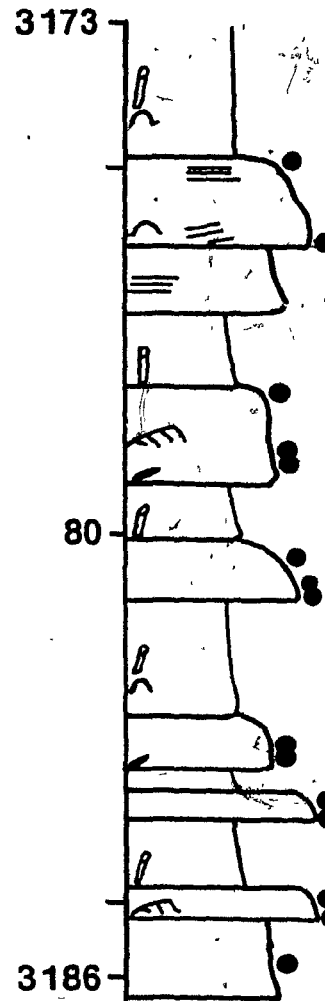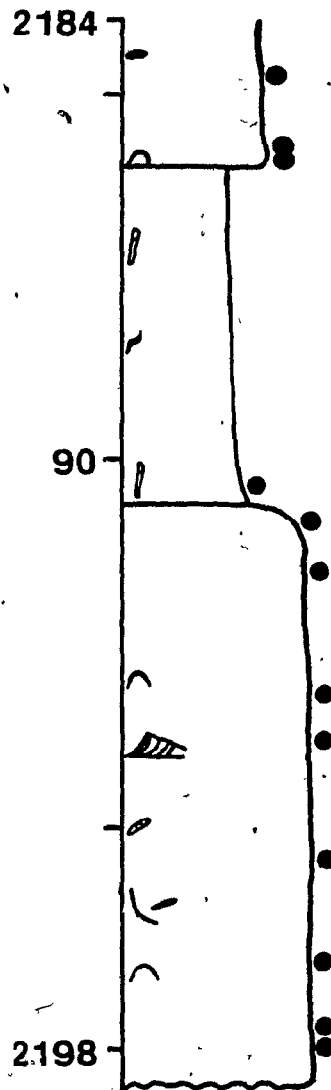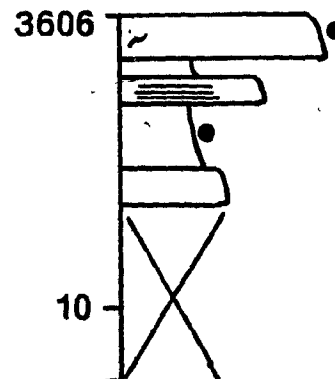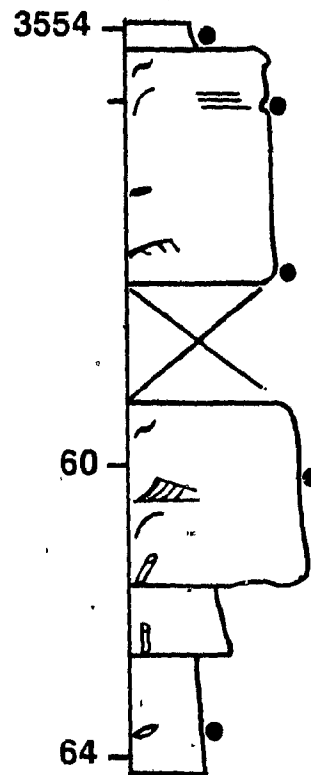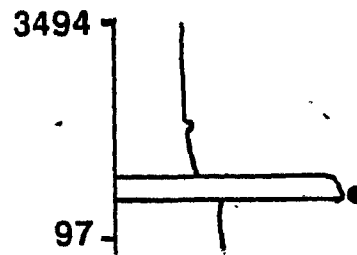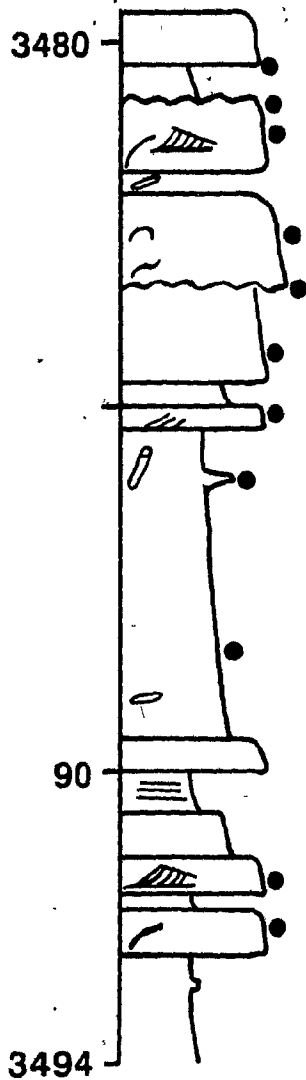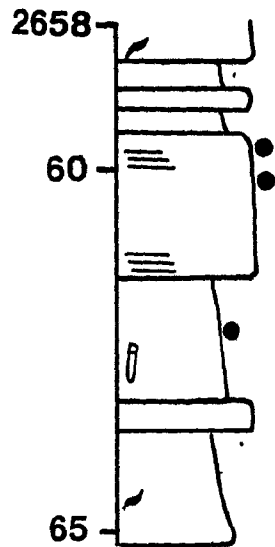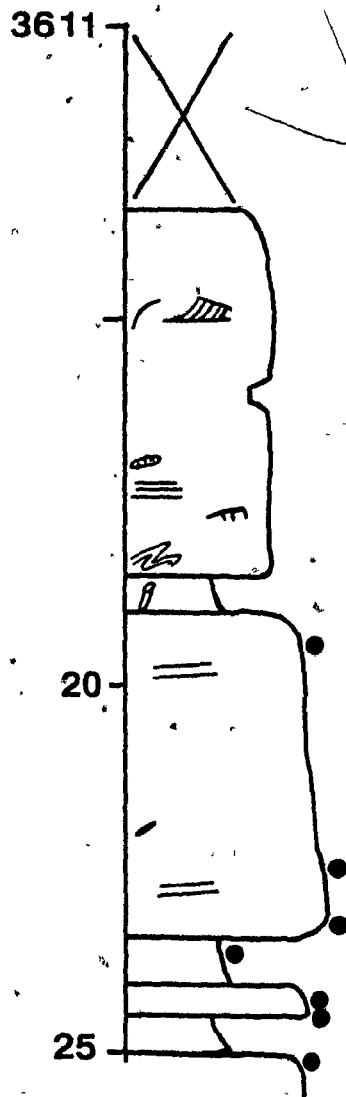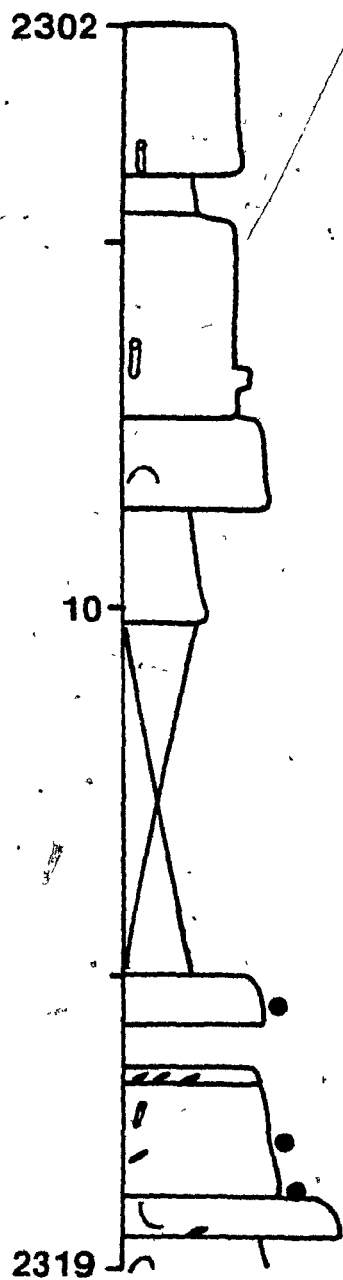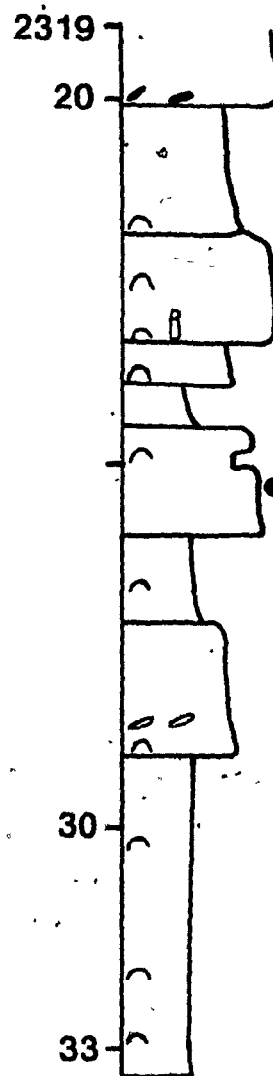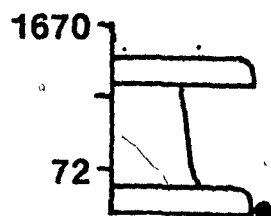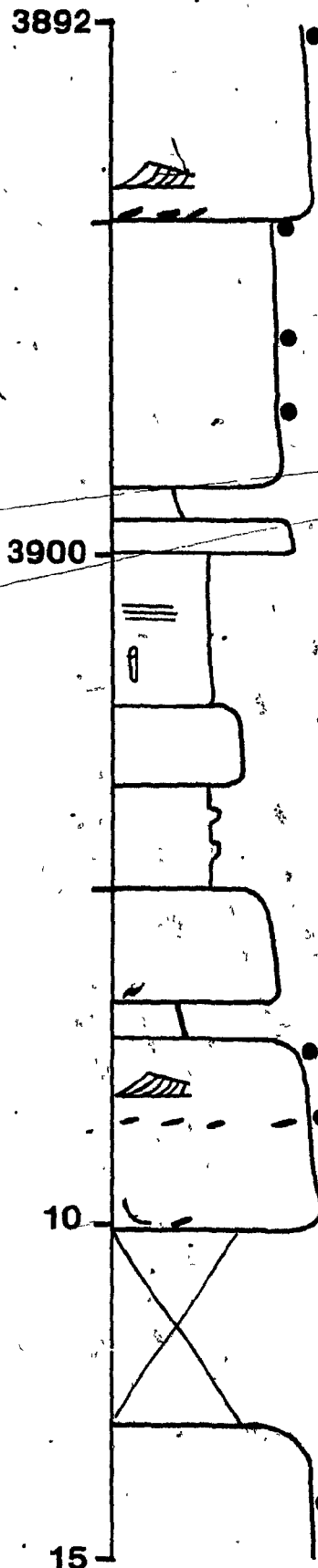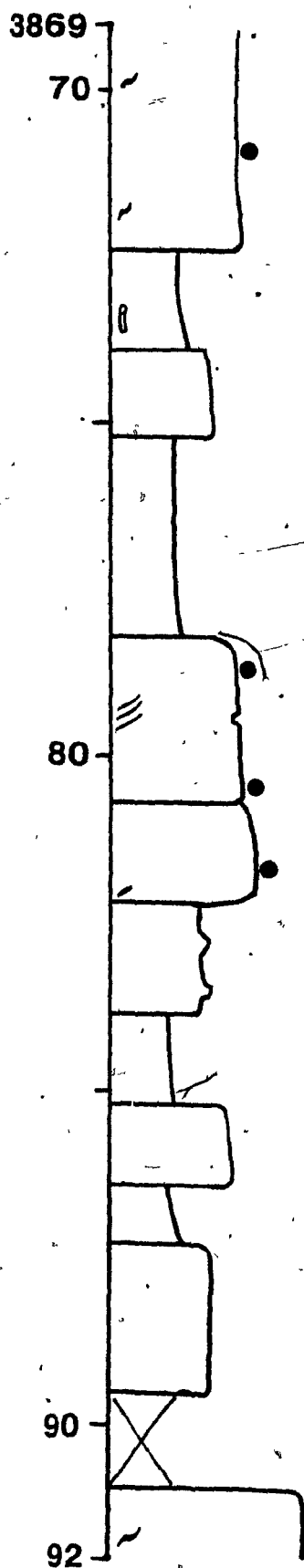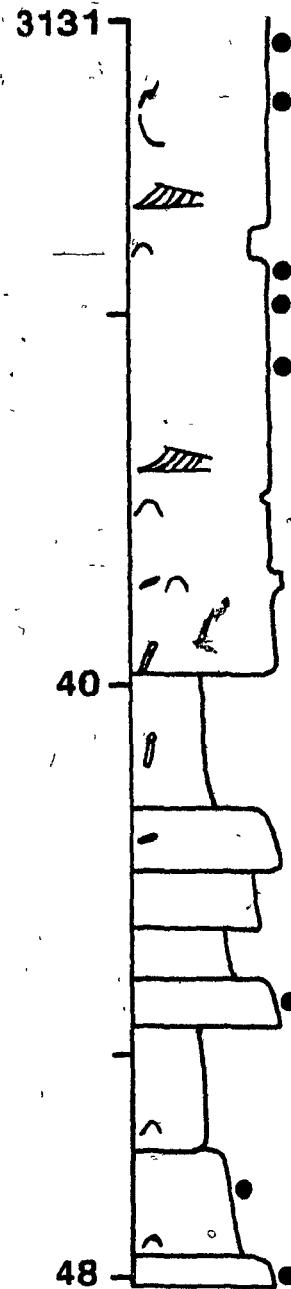
APPENDIX 2

Organic carbon content and IC values of selected shale samples from the B-08, B-27 (Hibernia) and B-75 (West Ben Nevis).

B-27 HIBERNIA

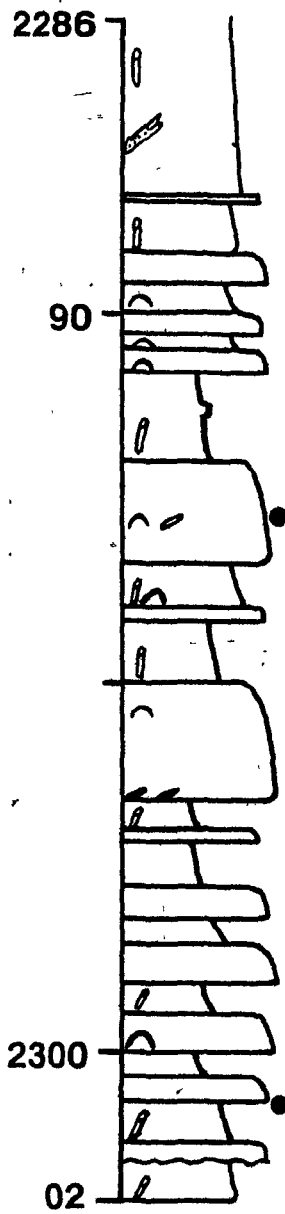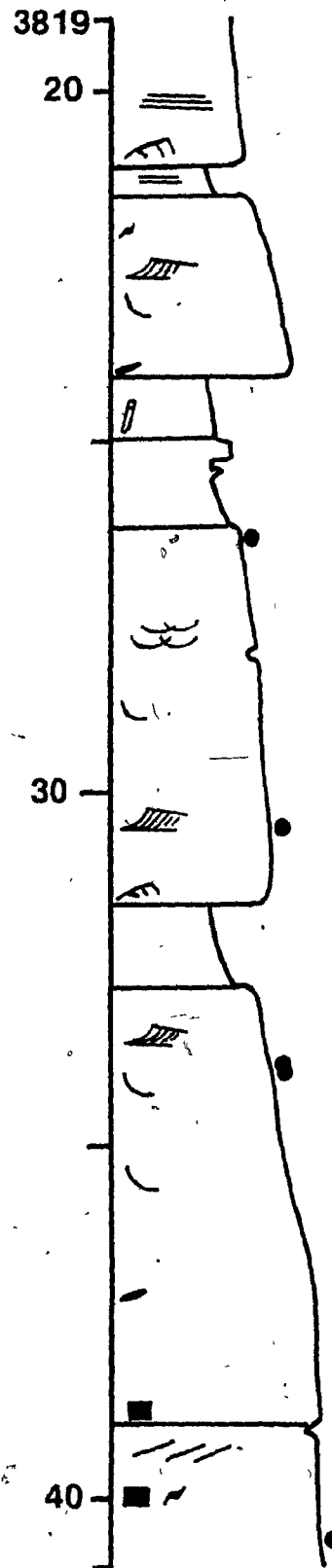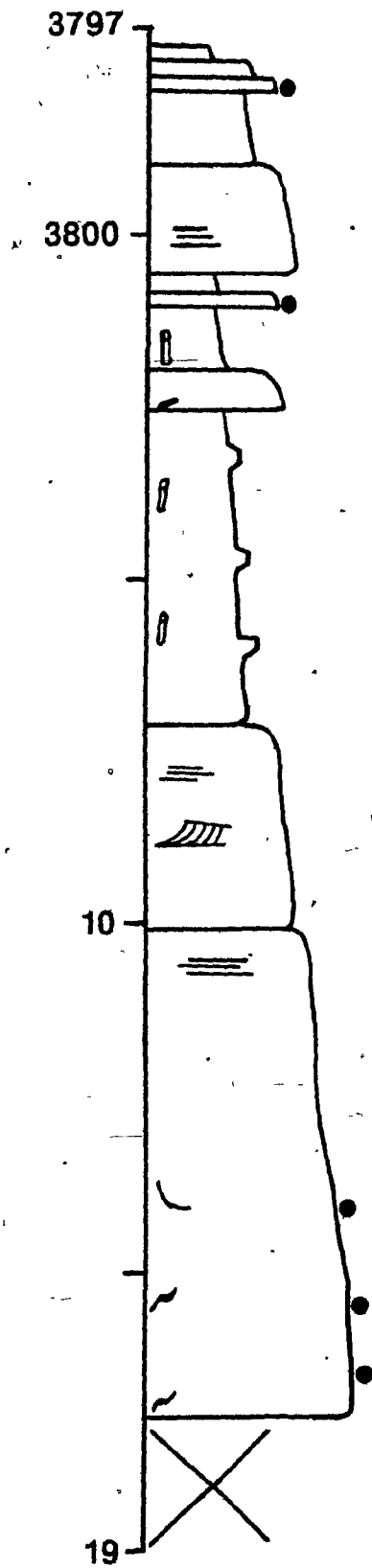| #	Depth (m)	C_{org} wt%	C_{inorg} wt%	IC $°\Delta2\theta$
1	2575	0.49	0.90	0.89
2	2590	0.98	0.33	0.8
3	3842	0.17	0.10	1.57
4	3853	0.23	0.10	0.94
5	3882	0.25	0.41	1.17
6	3896	0.38	0.28	1.19
7	3906	1.01	0.22	N D
8	3913	0.72	0.04	1.26
9	4060	0.97	0.71	1.18
10	4175	1.63	0.65	1.25
11	4290	2.43	0.23	1.16
12	4345	2.02	0.43	N D
13	4370	1.71	0.69	1.14

* N D = not determined

279

B-08 HIBERNIA

#	Depth (m)	C_{org} wt%	C_{inorg} wt%	IC $^{\circ}\triangle 2\theta$
1	2662	0.74	0.14	0.97
2	2673	1.00	0.42	1.09
3	3400	0.68	0.20	1.41
4	3550	0.31	0.16	1.25
5	3607	0.31	0.10	1.13
6	3623	0.63	0.14	1.27
7	3700	0.57	0.22	1.51
8	4000	1.31	1.31	1.43
9	4120	1.76	0.02	1.46
10	4210	1.43	0.15	1.47

B-75 WEST BEN NEVIS

#	Depth(m)	$C_{org.}$ wt%	$C_{inorg.}$ wt%	IC $^{\circ}\triangle 2\theta$
1	4315	1.40	0.54	1.34
2	4435	2.47	0.1	1.44